UNIVERSITY OF LIVERPOOL

Microwave Synthesis of Hierarchical H-ZSM-5, H-Beta and H-Y and Their Catalytic Applications in Alkylation and Diels-Alder Cycloaddition

Thesis submitted in accordance with the requirements of the University of Liverpool for the degree of Doctor of Philosophy

By

Joel McGlone

October 2016

Acknowledgments

First and foremost, I would like to express my sincere gratitude to my PhD supervisor, Professor Tony-Lopez Sanchez for giving me the opportunity to carry out research in his group. Over the last 4 years he has provided continued support and guidance, of which I am truly grateful. A special thanks goes to Dr Peter Priecel for being on hand for his continued guidance, support and being there to help solve all my technical problems, no matter how trivial there were!. Thank you so much! Another special thanks goes to Dr Tom Davies for all his support and for always being on hand on to help solve all problems I have encountered throughout the PhD.

A big thanks goes to Dr Luigi Da Via who was there to welcome me on my first day and helping to make the last 4 years really enjoyable! I hope we will continue to have "quaffable drinks" for many years to come! I would like to thank the MBR crew for their valuable help throughout my studies. A big thanks to Piera for the many coffee breaks we had!

I would like to thank past members of the group such as Thalita, Thiago and Estevao who provided much entertainment during the early stages of my PhD. I promise I will visit you all in Brazil soon! I would like to thank Olivia and Emma who were my first students. I wish you all the success.

I would like to wish all the current members of the group in G30 and 1.87 all the best. Ali, David, Romen, Monica, Javier, Hammed, Liqaa, Nadiah, Aldo, Edgar and Azam; you have all made the last 4 years a really enjoyable experience and have made coming into work every day all the worthwhile! Thank you so much! I wish you all the success throughout the remainder of your PhD studies and subsequent careers!

I would like to thank my friends outside the University "The Lads" for their constant support and general amusing antics throughout. I never expected anything less!

Last, but by no means least. I would like to thank my Mum, Dad, Daniel and Laura for generally being there for me throughout. Without your support I would never have got through the last four years! Thank you so much!

Abstract

In this thesis, new methodologies in zeolite synthesis have been explored to enhance mesoporosity and, their catalytic performance in alkylation, but also in the production of bulky bio-derived aromatics via Diels-Alder cycloaddition of ethylene to 2,5-dimethylfuran.

There is a growing amount of interest in the synthesis of hierarchical zeolites in catalytic transformations, with the aim of improving diffusion within pores and catalytic performance. Typically, the formation of hierarchical zeolites can be achieved by using top-down or bottom-up approaches. In this thesis, a top-down approach was first studied, whereby the post synthesis treatment of commercial and in-house prepared zeolites are carried out using alkaline conditions to remove silicon and therefore, enhance mesoporosity. Furthermore, a bottom-up approach was also explored and a hard template used to generate mesoporosity during the synthesis of the zeolite. In both approaches, we have studied and optimised synthetic conditions with the utilisation of microwave reactors.

Firstly, the optimum conditions used for the alkaline treatment for H-ZSM-5 were applied to commercial and home-made H-ZSM-5, H-Beta and H-Y with varying SiO_2/Al_2O_3 molar ratios. We report the microwave synthesis of H-ZSM-5, H-Beta and H-Y zeolites with a synthesis time of 14 hours or less. We found that desilication was effective at increasing pore size at the mesoporous range as measured by nitrogen adsorption-desorption, although the higher the desilication the higher the loss in crystallinity. Desilication resulted in an increased acid site density in H-ZSM-5, whereas a reduction of acid site density was observed for desilicated H-Beta and H-Y, as determined by temperature programmed desorption. Hierarchical H-ZSM-5, H-Beta and H-Y prepared by post synthesis treatment were tested in the Friedel-Crafts alkylation of benzyl alcohol. Interestingly, at the range of reaction conditions studied, not all of the zeolites showed enhanced activity after desilication and this is discussed on the basis of changes in the acid site density. However, with alkaline treated H-Y nearly 20% greater catalytic activity was attained.

On the templating approach, we utilised polystyrene as we could carry out our own polymerisations and so control the size of the templating agent. Prior work showing enhanced porosity of ZSM-5 using polystyrene as a hard templating agent is scarce and limited to the utilisation of > 280 nm polystyrene nanoparticles. In this work, it is shown that polystyrene nanoparticles of around 30-60 nm are required to enhance the mesoporosity profile and catalytic activity. Furthermore, this works in the first example of synthesis of hierarchical H-ZSM-5 by microwave assisted heating using polystyrene as a template, and highlights that this is a very effective method to obtain very high surface area materials in the range of 302-620 $m^2 g^{-1}$ with extraordinary external pore volumes in the range of 0.08-0.44 $cm^3 g^{-1}$ in one single step, in just 12 hours or less compared to 72 hours when using conventional heating

Finally, this study demonstrates the generation of mesoporosity in microporous zeolites results in higher conversions and higher yields of aromatics in the Diels-Alder cycloaddition reaction between 2,5-dimethylfuran and ethylene. In some instances, conversion trebled and yield to *p*-xylene doubled. Reaction conditions, zeolite structure, templating procedure and catalyst preparation method were all determinant in whether an enhancement in activity was observed. We conclude, that the generation of mesoporosity, crystallinity and catalyst acid properties all play a role in the catalytic performance.

List of Tables

List of Figures

List of Schemes

List of Equations

Contents

Chapter 1

Literature Overview

1 Literature Overview

1.1 Introduction to Biomass

Fossil fuels from non-renewable resources provide nearly three-quarters of the world's energy.[1] Unfortunately, increased demand comes at a time when non-renewable feed stocks are diminishing. It is estimated that oil reserves will have run out by the middle of the 21st Century.[2] Production of energy from biomass could prove to be an attractive alternative as it has the potential to reduce carbon emissions and it is not only a renewable carbon source, but also carbon neutral. Global production of cellulosic biomass is estimated to be approximately 200 billion metric tonnes[3], with less than 5% used for food applications. Approximately three-quarters of cellulosic biomass consists of the carbohydrates starch and sucrose, polysaccharides such as cellulose and hemicellulose. The remaining proportion of biomass consists of lignin and triglycerides, waxes, proteins and terpenes.[4, 5] An advantage of lignocellulose is that it is not used to compete with the food industry. However, there are many challenges to depolymerise lignocellulose into platform chemicals. The depolymerisation of cellulose is a slow process due its crystallinity and requires more hostile treatments.[6] In contrast, hemicellulose is an amorphous structure and is easily hydrolysed in diluted acids. Glucose from biomass is predominately used as a sweetener. However, the production of glucose is attracting significant interest as a precursor for the production HMF which can be upgraded to *p*-xylene as shown in Scheme 1.1 (below).

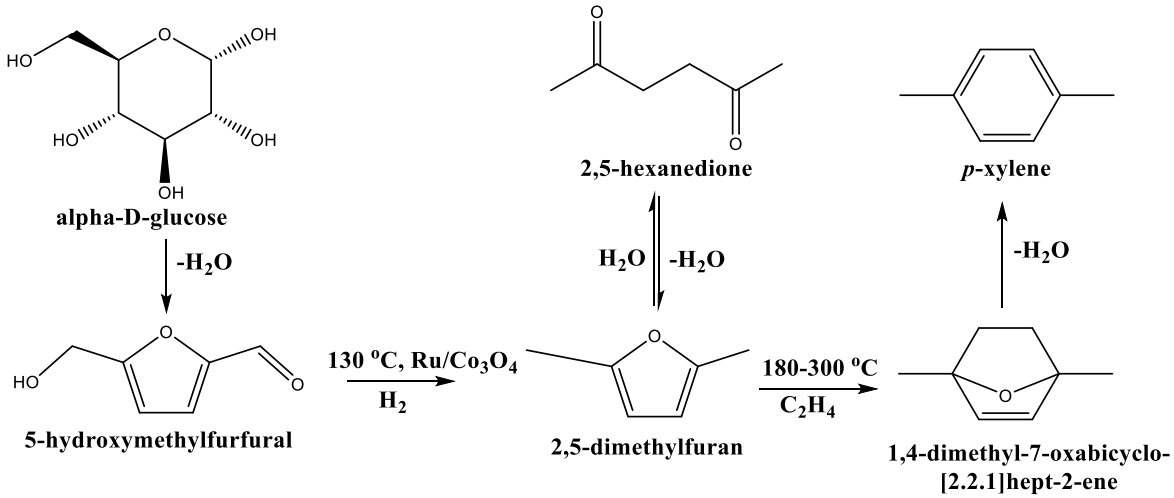

Scheme 1.1 Proposed reaction for the conversion of glucose to *p*-xylene.

1.2 Production of 5-Hydroxymethylfurfural (HMF)

An extensive review detailing the production of HMF was written by Mukherjee et al.[7] in 2015. (HMF) is a very versatile chemical that can be used as a precursor for the production of platform chemicals such as 2,5-furandicarboxylic acid (FDCA), 2-furancarboxaldehyde, 2,5-bis(aminomethyl)furan which can be used as precursors for the production of polyesters, Schiff bases and polyamides respectively.[8] Industrially, HMF is produced in a homogeneous system using sulfuric acid as a catalyst.[9] The use of homogeneous catalysts has not yielded an optimum amount of HMF and there is still on-going research to selectively synthesise HMF. HMF is produced by the removal of 50% of oxygen by water elimination from sugars such as hexoses which can be obtained from cellulose, hemicellulose or starch[10] using relatively cheap acids such as hydrochloric acid (HCl), sulfuric acid (H_2SO_4) or phosphoric acid (H_3PO_4).[11-13] However, the use of mineral and organic acids has many disadvantages; the difficulties in separating the acid catalyst from the reaction mixture upon completion and the employment of expensive reactors that are resistant to corrosion. D-fructose is a particularly useful precursor for the production of HMF. Antal et al.[14] studied the dehydration of D-fructose using sulfuric acid (2 mM) as a catalyst and water as a solvent at 250 ^{o}C with a total reaction pressure of 345 bar. It was found that during the first ten seconds of the reaction approximately 60% of fructose had been converted to form a mixture which contained a 20% yield of 5-HMF. Upon increasing the concentration of sulfuric acid to 3 mM a maximum yield of approximately 55% of HMF was obtained. This could be attributed to the acidic conditions of water under supercritical conditions. Bicker et al.[15] studied the dehydration of D-fructose in sub-critical and super-critical acetone-water mixtures. It was found that fructose solubility in pure acetone was poor. The authors compromised using a 90:10 acetone/water solution (v/v). The influence of temperature, pressure, catalyst concentration on the effect of dehydration of D-fructose were studied. A temperature range of 180-300 ^{o}C using a sulfuric acid (3 mM) at 200 bar demonstrated that higher 5-HMF selectivities were obtained at lower temperatures when longer residence times were used. There appeared to be no direct correlation between pressure and selectivity towards HMF. It was found that an optimum yield of 77% of HMF could be obtained when the reaction was carried out at 180 ^{o}C at 200 bar. The main by-product formed was fufural with trace amounts of glucose and levulinic acid. No solid by-products were formed such as humic acids, which were found when the reaction was carried out in supercritical water. Despite the fact that water is a cheap and ecologically friendly solvent there are limitations with using water

as a solvent since it cannot prevent the formation of side products such as levulinic acid and formic acid formed by the rehydration of HMF. More recently, Roman-Leshkov et al.[16] studied the effect of organic solvents on the effect of 5-HMF production from the dehydration of D-fructose in a two-phase reactor system. Their synthesis setup is shown in Figure 1.1.

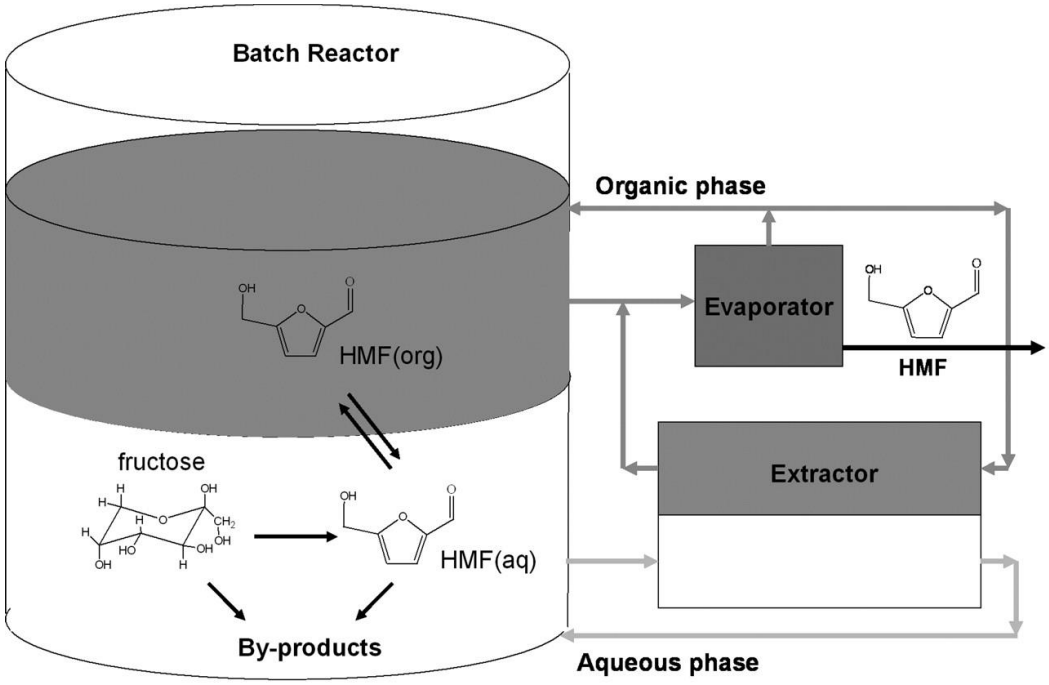

Figure 1.1 The synthesis and extraction of HMF from fructose. Taken from Roman-Leshkov et al.[16]

In a typical procedure an aqueous phase of water or water plus an organic solvent such as poly(1-vinly-2-pyrrolidinone) (PV) or dimethylsulfoxide (DMSO) was added to an aqueous mixture of fructose (30-50 % wt). The reaction was carried out at 180 ºC for 3 minutes using hydrochloric acid (0.25 M) as a catalyst under autogenous pressure conditions. 5-HMF was separated by continuous extraction into the organic phase using methylisobutylketone (MIBK). The addition of 2-butanol helped to enhance the partitioning of HMF relative to pure MIBK. When a 30% wt fructose concentration was used, an optimum selectivity of 83% for 5-HMF at 82% conversion was found. It was found that selectivity towards 5-HMF decreased when the concentration of fructose increase to 50% wt. This result was attributed to increased rates of condensation reactions as described previously.[17, 18] Increasing the amount of MIBK/2-butanol mixture dramatically increased selectivity towards HMF to 77% at 92% conversion.

Solid acid catalysts are generally more favourable than liquid acid catalysts for this reaction as they are easier to separate from the reaction products and can be recycled. Rivalier et al.[19] studied the effect of solid acid catalysts such as H-Beta, H-ZSM-5 and H-Y and H-mordenite. The reactions were carried out using 1-7 g of catalyst in a mixture of water (35 mL) and MIBK (175 mL) as an organic solvent to extract HMF. The reactions were carried out using inert conditions at 165 ^{o}C for 30-60 minutes. It was found that without the presence of a catalyst, selectivity towards HMF was 40% at 15% conversion of fructose, and it was reported upon the addition of zeolite catalysts H-beta and H-ZSM-5 with medium Si/Al ratios, conversion of fructose increased dramatically to 85% and 90% respectively. H-Beta appeared to be just as selective towards HMF as without the addition of a catalyst. However, selectivity towards HMF increased by nearly 47% when the zeolite H-ZSM-5 was used. The authors studied the effects of Si/Al ratios on the effects of fructose dehydration by using HY and H-mordenite with varying Si/Al ratios. There were clear differences between the zeolites, even when the Si/Al ratio was similar. H-mordenite with a higher Si/Al ratio equal to 7.5 gave the optimum selectivity towards HMF at shorter reaction times; however, this came at the expense of conversion which was lower with shorter reaction times.

1.3 Production of 2, 5-Dimethylfuran (DMF)

An extensive review was written by Qian et al.[20] in 2015 showing the formation of DMF from bio-derived feedstocks. (DMF) is an attractive material as a second generation biofuel. The United States Department of Energy (DOE) in 2010 targeted that by the middle of the next decade nearly 36 billion gallons of second generation biofuels will be produced, of which 45% would be derived from cellulosic feedstocks.[21] It is particularly interesting due to its ideal physical and chemical properties such as; its boiling point (92-94 ^{o}C), high octane number (RON = 119)[22] compared to ethanol (RON = 110) which improves anti-knocking properties and a low oxygen content (O/C = 0.17).[23] In addition, DMF has a 40% higher energy density than bioethanol (30 kj cm^{-3})[24] but lower than gasoline and is insoluble in water. However, the precise toxicity and environmental effect of DMF is still relatively unknown and further studies are required.[25] The two main approaches for the production of DMF from biomass is (a) hydrogenolysis of HMF derived from fructose, (b) hydrogenolysis of 5-choromethylfurfural (CMF) derived from dehydration of glucose as shown in Scheme 1.2

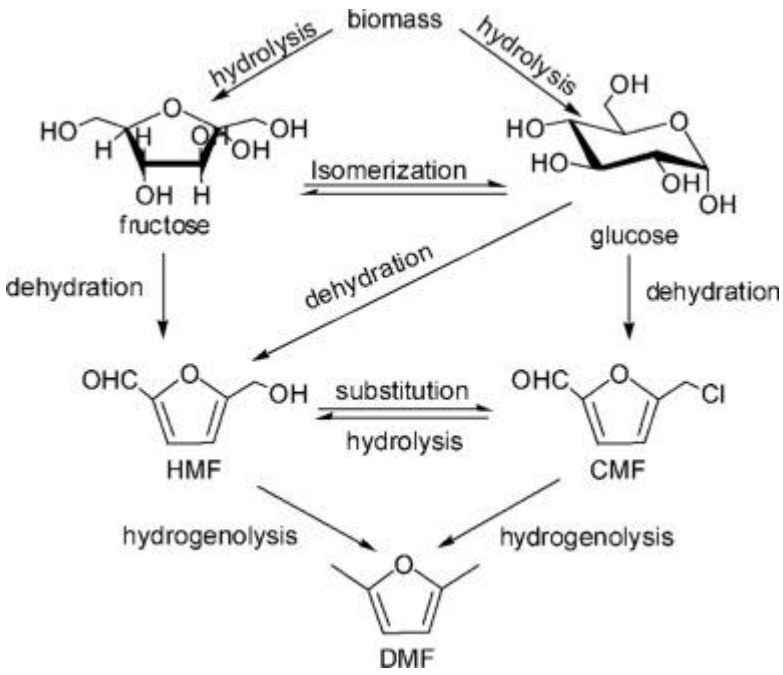

Scheme 1.2 The production of 2,5-dimethylfuran from raw biomass.[20]

Roman-Leshkov et al.[26] expanded their prior work in the synthesis of HMF[16] to DMF using D-fructose as a precursor in a biphasic reaction system. Firstly, HMF was produced using hydrochloric acid as a catalyst in an aqueous solution containing sodium chloride. HMF was extracted into the organic phase using 1-butanol, which is advantageous since it is inert to hydrogenolysis. The investigators found that when 1-butanol was used the concentration of hydrochloric acid appeared to have no effect on the selectivity towards HMF. The solvent containing HMF was extracted and converted into DMF using carbon-supported copper-ruthenium (CuRu/C) catalyst. The addition of copper to ruthenium prevented the formation of 2,5- dimethyltetrahydrofuran which was the case when carbon-ruthenium (Cu/C) was used. The authors argued that the addition of copper to ruthenium created a biphasic system where copper coated the ruthenium surface therefore giving the catalyst hydrogenolysis properties from copper and chloride-resistance properties from ruthenium. Two catalysts were investigated; CuCrO which was promoted using barium and Cu-Ru/C. Typically, both catalysts were active for hydrogenolysis of HMF to DMF. CuCrO showed 100% conversion and 61% DMF selectivity. Similarly, 3:1 Ru-Cu/C showed 100% conversion and 71% selectivity. Thananatthanachon et al.[27] studied the one pot synthesis of DMF using formic acid as a catalyst to act as a hydrogen donor for the hydrogenation of HMF to bis(hydroxymethyl)-furan (BHMF) and to act as a deoxygenating agent for furanylmethanol. The reaction gave DMF yields of 95%. Further

analysis of by the mixture by NMR revealed the presence of 2-hydroxymethyl-5-methylfuran (HMMF) as an intermediate product, likely caused by the hydrogenolysis of BHMF. Additionally, the authors investigated the one pot dehydration of D-fructose to produce DMF using DMSO as a solvent and sulfuric acid as an additive at 100 ^{o}C for 5 hours under reflux conditions. The Pd/C catalyst was recovered by filtration and DMF was recovered by extraction using diethyl ether to give a 95% yield of DMF which was confirmed by NMR.

1.4 Production of aromatics from the cycloaddition of furanics with olefins in the gas phase over zeolites

A review showing the formation of aromatics from renewable sources was written by Maneffa et al.[28] Extensive work has been carried out by George Huber showing the formation of aromatics from bio-derived feedstocks such as wood and furanics.[29, 30,31, 32] This subsection will focus on studies carried out in 2012 which focused primarily on the cycloaddtion of furanics with olefins to form aromatics in the gas phase using H-ZSM-5 and Ga/H-ZSM-5. Firstly, the conversion of furan over olefins (ethylene and propylene) and 2-methylfuran over propylene. The catalyst used in this study was H-ZSM-5, with a SiO_2/Al_2O_3 molar ratio of 30.

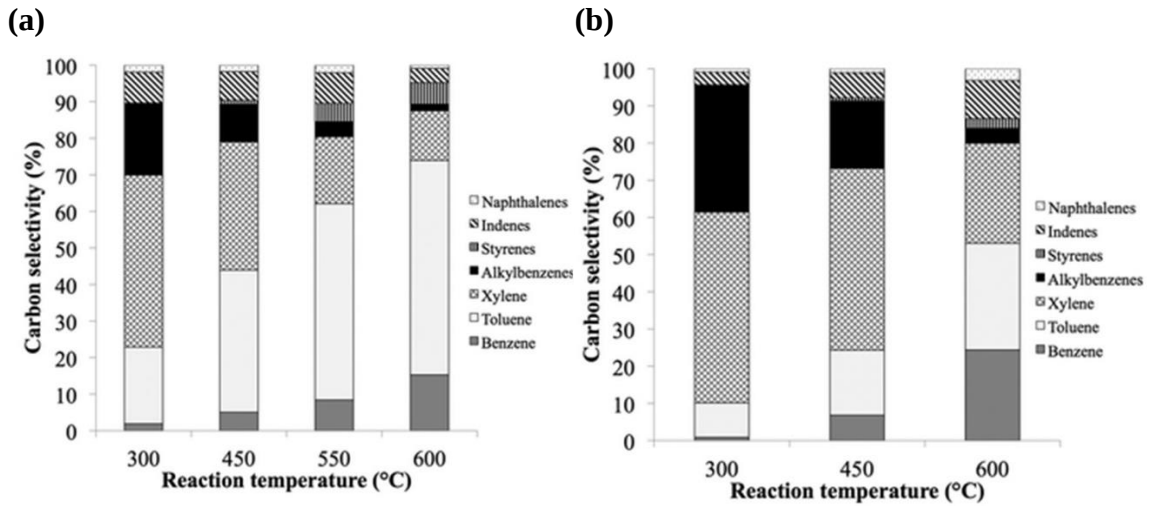

Figure 1.2 Aromatics distribution for (a) Furan and (b) 2-methylfuran as a function of temperature with propylene over H-ZSM-5. Taken from Cheng et al.[33]

The authors showed that furan and 2-methyl furan were active in the cycloaddition reaction with propylene using H-ZSM-5 as a catalyst. At 600 ^{o}C without co-feeding of

propylene, furan showed 48% conversion, with a total selectivity of 29.2% to aromatics. The formation of benzene, toluene and *p*-xylene from furanics were due to decarbonylation of furan followed by allene dimerisation. Analysis of the aromatic products showed low selectivity to xylenes, with the major aromatics consisting of benzene, toluene, indenes and naphthalenes. Introducing propylene as a co-feed showed increasing furan conversion with increasing temperature, with an optimum conversion of 65% at 600 ^{o}C. Selectivity to total aromatics generally increased with increasing temperature, with BTX being the major aromatic products. Toluene was the major aromatic product at higher temperature. However, selectivity to xylenes was higher at lower reaction temperatures. This was due to the dealkylation reaction being less favourable at lower reaction temperatures. Exchanging the diene to 2-methylfuran showed much higher levels of conversion. Even without the addition of propylene, conversion was 98% at 600 ^{o}C with 47.3% selectivity to aromatics. Xylenes consisted nearly 10% of the total aromatics produced. Optimum selectivity to aromatics was achieved at 450 ^{o}C with the reaction showing 66.1% selectivity to aromatics, with *p*-xylene consisting of 43% of the total xylenes. This was achieved with 92% conversion of 2-methylfuran.

After this study, the authors investigated the optimisation of *p*-xylene by comparing conventional H-ZSM-5 with H-ZSM-5 doped with gallium.[34] The SiO_2/Al_2O_3 molar ratio was 30. Ga/H-ZSM-5 was prepared by ion exchange under reflux conditions to give a final weight loading of 3.8% Ga/H-ZSM-5. 2-methylfuran was tested over naked H-ZSM-5 and 3.8% Ga/H-ZSM-5 at 600 ^{o}C. Of these, 3.8% Ga/H-ZSM-5 was the most selective at iso-conversion with a *p*-xylene selectivity at 58% of the xylene products at ca. 99% conversion. It was suggested that this was due to the reduced pore opening size of the zeolitic structure. Both studies have shown that the gas phase reaction is highly active in the cycloaddition of furanics with olefins. Selectivity to aromatics can be tuned depending on the reaction parameters, with higher temperatures favouring benzene compared to *p*-xylene. It was suggested by the authors that higher temperatures promote dealkylation of toluene/*p*-xylene. Despite this, studies have shown that gas phase reactions produce a broad range of products with separation of individual aromatics being very complex and in need of further study.

1.5 Production of renewable *p*-xylene from 2,5-dimethylfuran (DMF) via Diels-Alder cycloaddition with ethylene in the liquid phase.

1.5.1 Introduction

The chemical *p*-xylene is an aromatic hydrocarbon with methyl groups in the *para* position. Industrially, it is more attractive than *m*-xylene and *o*-xylene. *P*-xylene is used as a precursor for terepthalic acid used for the synthesis of polyethylene terephthalic acid (PET), which is used in the manufacture of fibres, films and plastic bottles.[35] Pepsi Cola have successfully synthesised bottles from bio-terephtallic acid from hexoses.[4] Global consumption of PET in 2016 is predicted to be 100 million metric tonnes and growing at a rate of 4% per annum.[36] It is produced on an industrial scale from the catalytic reforming of naphtha. However, the separation of *p*-xylene from its isomers is a difficult and expensive process due to their similar boiling points. Therefore, there is growing interest in alternative strategies for the synthesis of *p*-xylene, especially from a bio-derived route. On a laboratory scale, *p*-xylene is usually synthesised from the alkylation of toluene with methanol using the solid acid catalyst H-ZSM-5. It has been reported that *p*-xylene has a 1000 times higher diffusion coefficient than *m*-xylene and 100 times larger than *o*-xylene at temperatures above 250 ^{o}C. After *p*-xylene has diffused out of the pores the remaining ortho and meta xylene will isomerise to produce *p*-xylene. The Diels-Alder reaction was first discovered by Kurt Diels and Otto Alder in 1927 to describe the [4+2] cycloaddition of an electron rich diene containing 4 π-electrons and an electron poor dienophile containing 2 π-electrons to form the more stable 6-membered rings containing new σ-bonds.[37] They were eventually awarded the Nobel Prize in Chemistry in 1950 for their pioneering work. It wasn't until 1982 when Brion[38] proposed the cycloaddtion of furan derivatives to form substituted cyclohexenol and cyclohexanediol in the presence of the Lewis acid ZnI_2. Brion hypothesised that furan would be a poor diene due to the higher energy gap of the highest occupied molecular orbital (HOMO), and therefore, would require a dienophile that would lower the energy barrier difference between the HOMO and the lowest unoccupied molecular orbital (LUMO). Typically, the reaction between furan and an olefin involves the formation of a cycloadduct, an oxa-norbornene which then undergoes β-elimination of the heteroatom bridge to form the major product. The mechanism of this reaction is described in more detail in section 1.5.2

1.5.2 Mechanism for the acid catalysed production of renewable *p*-xylene from 2,5-dimethylfuran via Diels-Alder cycloaddition with ethylene

Nikbin et al.[39] studied a comprehensive mechanism for the production of *p*-xylene from the conversion of DMF and ethylene using DFT electronic calculations based on Brønsted and Lewis acid catalysed reactions. This was then compared to an uncatalysed reaction. DFT calculations were compared to experimental data carried out using H-Y with a low Si/Al ratio. To produce experimental evidence of the nature of the active sites, the catalyst was washed with sodium hydrogen carbonate to remove the Brønsted acid sites. The authors found H-Y had a 60% higher turnover frequency to *p*-xylene at iso-conversion than Na-Y at ca. 10% conversion. It was assumed by the authors that in order to promote the cycloaddition, the HOMO-LUMO gap must be minimised by addition of electron-donating groups to the electron rich diene and electron-withdrawing groups to the electron poor dienophile. Gas phase calculations are illustrated in Scheme 1.3 (below).

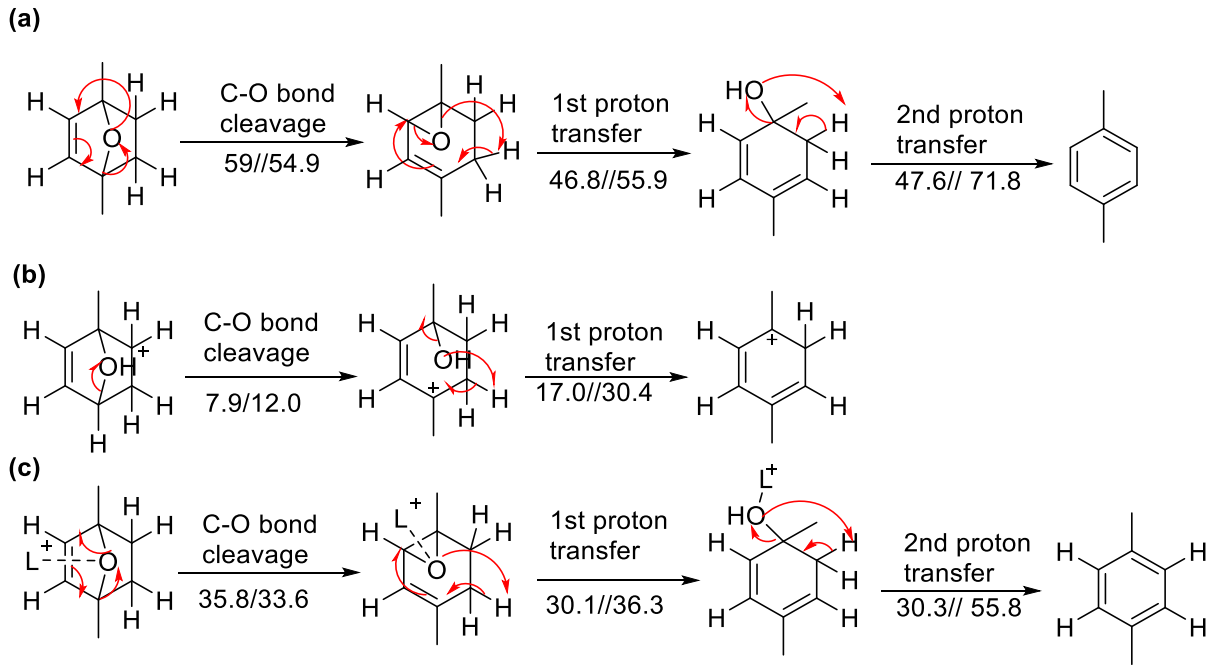

Scheme 1.3 Reaction mechanism and energetics for the production of *p*-xylene by the dehydration of 1,4-dimethyl-7-oxabicyclo[2.2.1]hept-2-ene by (a) No catalyst, (b) Brønsted acid and (c) Lewis acid catalyst. Redrawn from Nikbin et al.[40]

DFT calculations showed that in the absence of a catalyst the activation energy to break the C-O bond is as high as 59 kcal mol^{-1} which would indicate that the reaction would proceed slowly. This was confirmed by the reaction carried out without a catalyst, which

produced no *p*-xylene. When a catalyst was used, the Brønsted acid sites catalysed the dehydration reaction, which occurs in just two steps; the first being protonation of the oxygen atom followed by C-O cleavage. This step requires an activation energy of just 7.9 kcal $mol^{-1.}$ Experimentally, the authors found that the turnover frequency for the Brønsted acid catalyst was higher than the Lewis acid catalyst.

1.5.3 Parameters affecting the production of renewable *p*-xylene from furanic feedstocks in liquid phase reactions

1.5.3.1 Effect of catalyst

There have been a few studies that have investigated the effect of solid acid catalyst on the [4+2] cycloaddition between DMF and ethylene.[41-46] Williams et al.[41] studied the production of renewable *p*-xylene in the liquid phase using a range of different solid acid catalysts. This can be observed in Figure 1.3.

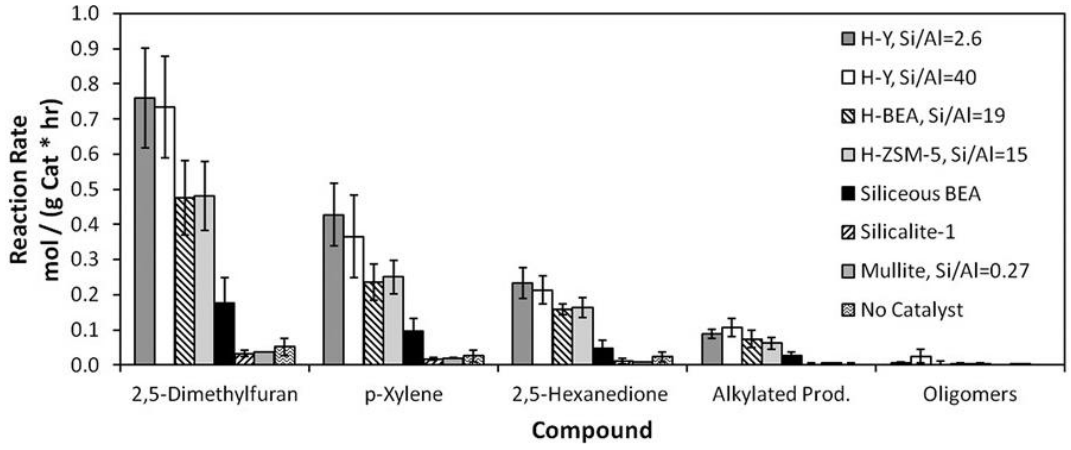

Figure 1.3 Initial catalytic rates of reaction of 2,5-dimethylfuran with ethylene. Taken from Williams et al.[41]

H-BEA, H-ZSM-5, H-Y showed enhanced rates of reaction, which possess Brønsted acidity. The authors found that although H-ZSM-5 possessed the largest quantity of Brønsted acidity it was less active than the H-Y zeolite which showed 52% selectivity to *p*-xylene at 10% conversion for initial catalytic rate experiments. It was assumed by the authors that this was due to the cage structure of H-Y, in contrast to the channel structure of H-Beta and H-ZSM-5. This strongly indicates the effect of pore morphology and mass

diffusion effect. Without the addition of a solvent H-Y showed 90% conversion with approximately 50% selectivity to *p*-xylene. Calculations showing how selectivity was calculated was not shown. Therefore, it remains unclear whether their selectivity values are based on the total of known products or the number of moles of DMF converted. The authors confirmed the presence of by-products such as 2,5-hexanedione (HDO), formed by hydrolysis of DMF which can undergo polymerisation to form oligomers and 1-ethyl-2,5-dimethylbenzene, which is formed by the alkylation of *p*-xylene with ethylene. Interestingly, the authors found only trace amounts of *m*-xylene which strongly indicates that *p*-xylene was stable and did not undergo isomerisation reactions. This is advantageous because separation of xylene isomers can be expensive. The spent catalyst was tested for its recyclability. XRD of the spent catalyst showed a decrease in the intensity of the peaks, which indicated the catalyst was largely deactivated due to pore blocking. The spent catalyst was then calcined at 500 ^{o}C and crystallinity measurements confirmed that the peak intensity was restored. The regenerated H-Y catalyst was retested and showed excellent recyclability properties for at least the first three cycles. Kinetic studies confirmed that the cycloaddition reaction was first order. Mass transfer experiments were carried out using only H-Y catalyst at 300 ^{o}C. The measurement was calculated based on the rate of reaction taken by kinetic studies, relative to the diffusive mass transfer rate which was measured as a function of pressure versus time. The authors found no significant mass transfer limitations. Kinetic studies on other zeolites such as H-ZSM-5 were not reported.

In a separate study by the same research group, Chang et al.[45] studied the effect of the production of *p*-xylene using numerous solid acid catalysts in an aliphatic solvent at 250 ^{o}C at total pressure of 62 bar. The authors found that at 20% conversion, selectivity to *p*-xylene was 60%. The remaining products were found to be HDO, alkylated products and oligomers. As conversion exceeded 80%, selectivity to *p*-xylene increased. It was found that although H-Beta and H-ZSM-5 possessed a similar number of Brønsted acid sites it was unclear as to whether this was due to a porosity effect or acidity effect since porosity measurements were not reported. The optimum level of selectivity towards *p*-xylene was 90% at 99% conversion levels. Unlike in their previous study,[41] selectivity to products was calculated based only on the number of known products. Therefore, their reported value is not a true representation of the real selectivity. The authors hypothesised that this behaviour was due to the hydrolysis of the initial product, DMF. They believed that HDO

reformed to produce DMF to maintain equilibrium and then reacted with ethylene to form the thermodynamically stable *p*-xylene. This hypothesis was tested experimentally. The reaction involved HDO (0.12 M) dissolved in water and heptane and 0.5 g of H-Beta (Si/Al = 12.5) catalyst. The reaction was carried out at 250 ^{o}C without the addition of ethylene until after 4 hours. The results showed that prior to the addition of ethylene HDO was cyclised back to DMF. The product *p*-xylene was not present prior to the addition of ethylene. Interestingly, alkylated products were present which confirms that oligomers can be formed due to the polymerisation of the diketone. Once ethylene was added to the reactor, DMF was consumed and underwent cycloaddition to produce *p*-xylene. The concentration of alkylated products was largely unaffected after the addition of ethylene.

Wijaya et al.[42] investigated the production of *p*-xylene using silica-alumina aerogels (SAA) and compared this with zeolites H-ZSM-5 (Si/Al = 15), H-Y (Si/Al=30) and H-Beta (Si/Al =12.5-19). Characterisation results showed that SAA had surface areas comparable to H-Beta, H-Y and H-ZSM-5 zeolites. Unlike the zeolites, SAA were predominately mesoporous and showed smaller amounts of microporosity. FTIR-pyridine confirmed the presence of both Brønsted and Lewis acid sites. Typically, the reaction method differed slightly from Williams and Fan[41, 45] as ethylene was added at room temperature. Typically, the reaction was carried out in the liquid phase using heptane as a solvent for 4 hours at 250 ^{o}C and 20 bar. As expected, the commercial zeolites showed high catalytic activity, with H-Beta showing the highest conversion (55%) and selectivity to *p*-xylene, compared to H-ZSM-5 and H-Y which showed conversion levels of 6% and 23% respectively. The rate of *p*-xylene production increased in the order: H-ZSM-5 > H-Y > H-Beta. The catalyst H-ZSM-5 showed lower conversion of DMF due to the narrower channels compared to H-Beta and H-Y. Meanwhile, the SAA catalyst with a Si/Al ratio of 1 displayed a remarkable high rate of conversion with selectivity to *p*-xylene comparable to the catalyst H-Beta. It could be assumed that the high levels of conversion and selectivity to *p*-xylene could be due to the presence of Brønsted acidity. Additionally, the catalyst displayed significant mesoporosity, with an average mesopore pore diameter of 28 nm compared the commercial zeolites which displayed an average mesopore diameter less than 10 nm despite showing comparable number of acid sites.

In the same study, the authors investigated the effect of Si/Al ratios on the rate of conversion in reactions carried out in dioxane as a solvent for 6 hours. Silica-alumina aerogels with Si/Al ratios from 0.5-9 were synthesised and characterised. As expected,

the total acidity was proportional to the amount of aluminium added, which translated to the number of Brønsted acid sites generated. The authors found that the silica aerogel catalyst without the presence of aluminium displayed less than 10% conversion of DMF, but surprisingly showed approximately 50% selectivity to *p*-xylene. Once again, the calculation showing how selectivity was not reported. Upon the addition of aluminium conversion of DMF dramatically increased optimising for the SAA with a Si/Al ratio of 1 with a conversion of 90% with a 60% yield of *p*-xylene. The authors found there was a linear relationship between acidity and conversion and the formation of *p*-xylene increased with Brønsted acid concentration. 3-methyl-2-cyclopentenone was formed, presumably by the acid catalyst intramolecular aldol reaction, and 1-methyl-4-propylbenzene, by the acid catalyst alkylation of *p*-xylene. After the reaction the catalyst SAA (Si/Al =1) was recovered and regenerated by centrifugation, washed with 2-propanol and dried and reused. In a separate experiment, the catalyst was treated similarly but was calcined after the drying step. The authors found that without the calcination step, conversion dramatically decreased with a significantly lower yield of *p*-xylene. The catalyst was calcined displayed similar activity as the fresh catalyst, which strongly implies the formation of heavy organic oligomers on the external surface of the catalyst. The authors concluded that SAA catalysts display excellent reusability properties.

1.5.3.2 Effect of solvent

The effect of polar solvents on the Diels-Alder reaction is well defined.[47, 48] Solvents such as water have been extensively used due to the enhanced effect due to the hydrophobic effect and the interaction between the hydrogen bonds that is disrupted by the non-polar reactants. Williams et al. [41] investigated the effect of the aliphatic solvent n-heptane on the [4+2] cycloaddition reaction. The reaction was carried out using a commercial H-Y catalyst (Si/Al = 30) and a total pressure of 62 bar. The amount of solvent varied from 0% to 75% of the total volume. In the absence of n-heptane, conversion of DMF was 95% and the selectivity to *p*-xylene was 51%. When the amount of solvent was increased to 75% of the total mixture, conversion of DMF remained largely unchanged but selectivity to *p*-xylene increased to 75% due to the suppression of DMF hydrolysis, reducing selectivity to HDO.

Wijaya et al.[42] studied the effect of polar solvents such as dioxane, tetrahydrofuran and isopropanol and studied their effect versus non-polar solvents such as heptane. Typically, a 150 mL Parr reactor containing 35 mmol DMF was mixed in a solution containing the catalysts H-Beta or SAA with the appropriate solvent, and the vessel was purged before being pressurised at room temperature to <30 bar ethylene. The reaction was carried out at 250 ^{o}C for 6 hours. When isopropyl alcohol was used as a solvent conversion of DMF was <45% with selectivity to *p*-xylene was around 30% when the catalyst SAA was used. Interestingly, selectivity to HDO was high for both the SAA and H-Beta catalyst. It was assumed that under acidic conditions isopropyl alcohol can dehydrate to either propene or 2-isopropoxypropane, which produces water and can hydrolyse DMF to HDO. The polar aprotic solvents dioxane and THF showed high conversions with relatively high selectivity to *p*-xylene. The authors argued that due to the positive Gibbs free energy for the formation of the cycloadduct at high temperature, it would not be possible to measure the rate of formation of the cycloadduct intermediate in various solvents. The authors hypothesised that the high yields of *p*-xylene in polar aprotic solvent could be attributed to improved rate of dehydration. The authors decided to test this hypothesis experimentally by varying the concentration of acid sites in dioxane, THF and heptane for *p*-xylene formation at low conversion. It was found that increasing the concentration of acid sites had a positive effect on the rate of *p*-xylene formation. However, at high concentration levels of acid sites the rates of formation of *p*-xylene were similar, which suggests that the solvent effect becomes insignificant when there is an abundant amount of Brønsted acid sites available. At low levels of acid concentration, the rate of *p*-xylene formation was higher in the polar aprotic solvents than in the non-polar aliphatic solvent which confirmed the superiority of dehydration in polar aprotic solvents which would support the theory that polar solvents stabilise the charged intermediate in the dehydration step.[47-49]

1.5.3.3 Effect of temperature

Although there have been numerous studies that have investigated the direct effect of temperature on the Diels-Alder reaction[50-52] the number of studies that have been carried out investigating the direct effect of temperature on the cycloaddition of DMF and ethylene is limited. Williams et al.[41] studied the effect of temperature on the [4+2] cycloaddition reaction of DMF with ethylene without the presence of a solvent. A

temperature range of 200-300 ºC was used at 62 bar. The catalyst chosen was H-Y zeolite with a Si/Al equal to 30.

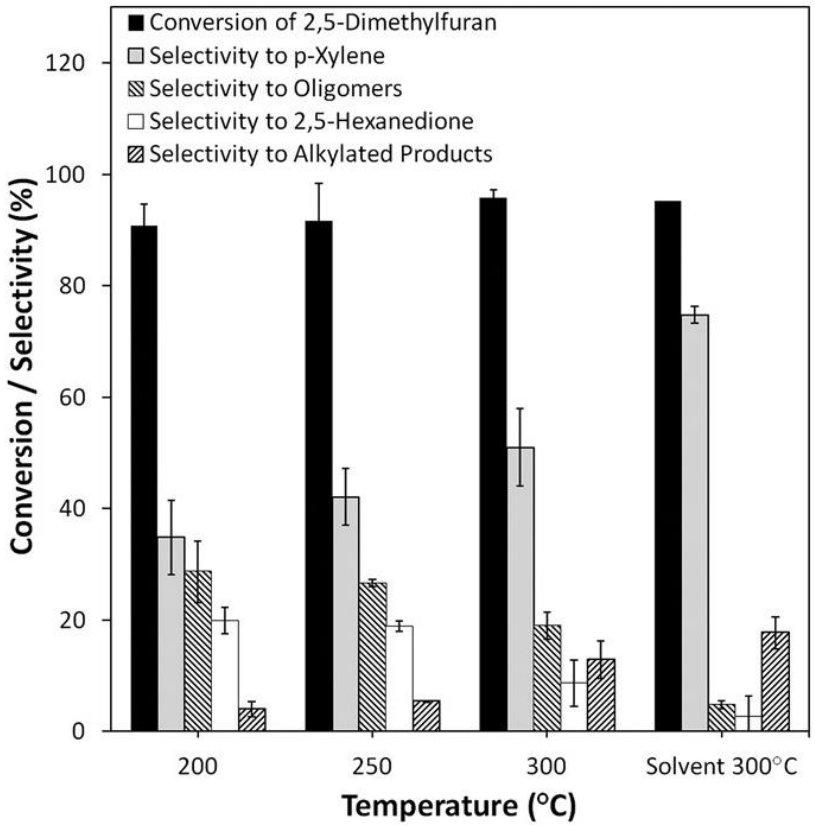

Figure 1.4 The effect of an aliphatic solvent and temperature on selectivity to *p*-xylene. Taken from Williams et al.[41]

Increasing the temperature from 200-300 ºC had no impact on DMF conversion, however selectivity towards *p*-xylene increased from <40% to 51% at the same level of conversion. This could be attributed by the suppression of HDO formation due to hydrolysis of DMF.

1.6 Zeolites

As seen from previous sections, zeolites have shown to be very active in the production of renewable *p*-xylene in the cycloadditon reaction of DMF with ethylene in the liquid phase. However, there appears to be no study that has shown the effect of post synthesis treatment of zeolites has on the production of renewable *p*-xylene from DMF with ethylene in the liquid phase. Hence, the following subsections gives a brief introduction

of zeolites. This will include the physical and chemical properties of H-ZSM-5, H-Beta and H-Y.

1.6.1 Introduction to zeolites

The first zeolites were discovered by the Swedish mineralogist Frederik Cronstedt in 1756.[53] Zeolites have a wide range of applications in the petrochemical industry. Zeolites are used for such applications as the conversion of methanol to gasoline [54] , fluid catalytic cracking [55] and xylene isomerisation[56] etc. As of 2012 there are 206 zeolites that have been identified with over 40 zeolites that are naturally occurring.[57] Global consumption of zeolites is estimated at approximately 1.7-2 million metric tonnes per year for synthetic zeolites[58, 59] while consumption for natural zeolites is about 2.5 million metric tonnes per year.[59] The market demand for synthetic zeolites is estimated at around $2 billion per year.[59] According to the US Department of the Interior China produced nearly 2 million metric tonnes in 2010 which accounted for 72% of the zeolite production for that year.[60] It has been estimated that 95% of zeolite consumption is used for the application of Fluid Catalytic Cracking (FCC) using zeolite Y. This process involves the cracking of high boiling point alkanes at 500 ^{o}C at a pressures 15-40 bar in a fluidised fixed bed reactor to produce gasoline and light olefins (predominately propylene). Nearly 30% of gasoline is produced. Recently, Brønsted sites have been replaced with rare earth metals such as lanthanum and cerium as an alternative to HY due to its increased activity and stability.[61] Zeolites are microporous (pore diameter $\leq$ 2 nm) aluminosilicate compounds with the general formula:

$$(M_{2/n}O)_x{:}Al_2O_3(SiO_2)_y{:}(H_2O)_z$$

where M represents a monovalent metal, a divalent metal or hydrogen, *n* represents the valence of M, *z* represents the amount of water molecules per unit cell. [62] All zeolite frameworks are built by linking a structural building unit (SBU); the tetrahedron. At the very centre of the tetrahedron are atoms with low electronegativities such as Si^{4+}, Al^{3+},P^{5+}, Zn^{2+} with the corner consisting of oxygen anions (O^{2-}). Zeolites consist of primary structural units $[AlO_4]^-$ and $[SiO_4]$ which can be summarised as $[TO_4]$, or more precisely $[TO_{4/2}]$ to emphasise that each oxygen atom is coordinated between two tetrahedral atoms. The O-T-O angle is 109^{o} whereas the T-O-T angle is around 140-165^{o}. However, bond angles lower than this has been reported previously.[63] The T-O bond length is dependent

on the cation present at the centre of the tetrahedron. For instance, the bond length between Si-O is between 0.159-0.165 nm[64, 65] compared to the bond length between Al-O which has been reported as 0.173 nm.[66, 67] Unlike the rigid O-T-O angle the flexibility of the T-O-T angle allows the formation of a variety of zeolitic frameworks. In the case of the Si-O tetrahedral site the silicon constitutes a charge of +4. Therefore, in the Si-O tetrahedral site the net charge is zero. In the case of the $[AlO_4]^-$ tetrahedral aluminium consists of a charge of +3. Therefore, in the case of the aluminium tetrahedral the net charge is -1. This can be counterbalanced by the presence of a proton which has an effect on the acid strength of the catalyst. It can be concluded that the acid strength value is inversely proportional to the Si/Al ratio. Synthetic zeolites are usually prepared using sodium aluminate[68-72] which contains Na^+ ions which can easily be ion exchanged using an NH_4^+ ion which readily turns into H^+ upon calcination. It is important to note that upon calcination temperatures above 550 ^oC results in dehydroxylation with the formation of Lewis acidic sites.[73]

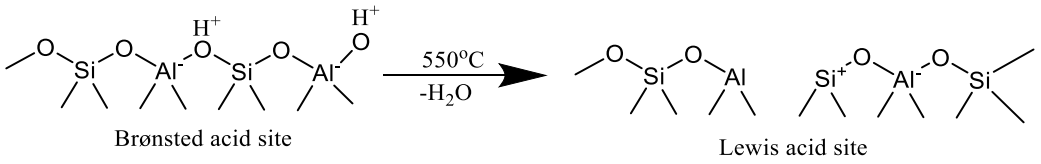

Scheme 1.4 Formation of Lewis acid sites from Brønsted acid sites by thermal treatment.[74]

Frilette and Weisz were the first authors to describe the hypothesis of shape selectivity.[75] Shape selectivity is based on the formation of a desired product. Shape selectivity can be divided into three main categories as shown in Figure 1.5 [76, 77]

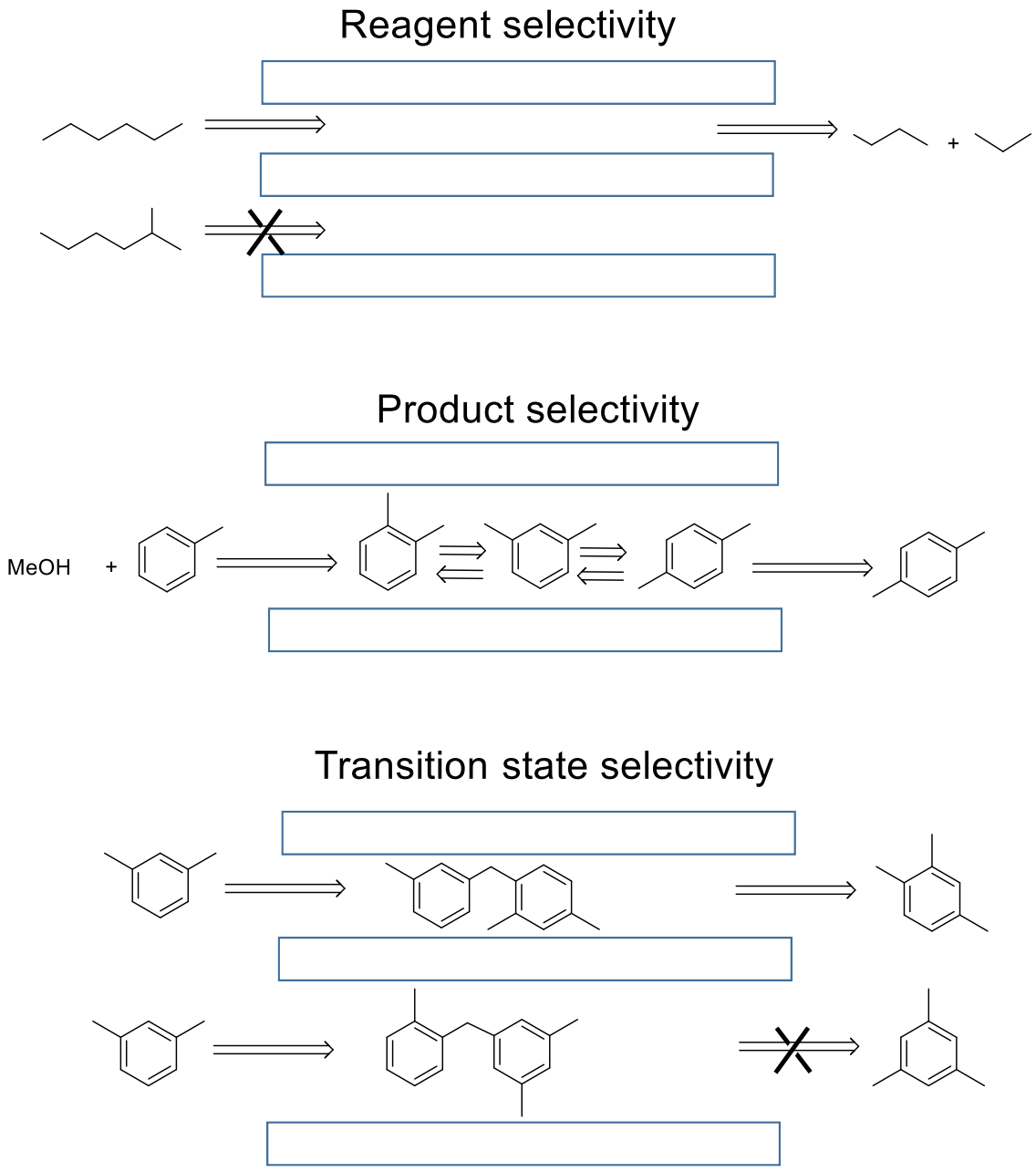

Figure 1.5 Examples of three types of shape selectivity in zeolites. Adapted from Rinaldi et al.[76]

(1) Reagent shape selectivity occurs when only the reactant molecules which have a similar pore size dimension as the catalyst pore can diffuse through the structure while molecules with larger size dimensions are prohibited (cracking of larger alkanes).

(2) Product shape selectivity occurs when products which are formed are too bulky to diffuse through the catalyst pore. They are converted to less bulky products (by equilibrium) or will block the catalyst pore and cause deactivation (para-selective alkylation of toluene by methanol).

(3) Restricted transition state shape selectivity occurs when some specific reactions such as parallel or consecutive are inhibited due to the corresponding transition state requires more space than is available inside the cavities. Reactions that require smaller transition states proceed without hindrance (transalkylation of meta-xylene).

1.6.2 Zeolite H-ZSM-5 (MFI)

Zeolite H-ZSM-5 (MFI) was first synthesised by the company Mobil in the 1960's and patented in 1972[78]. MFI zeolite is one of the most used solid acid catalysts in many petrochemical processes and is the second most commonly used zeolite catalyst after zeolite Y. The framework of MFI possesses a 10-membered ring with 8 of the rings being 5-membered. MFI consists of 2 distinct 10 ring channels; a straight channel of elliptical shape (0.53 x 0.56 nm) running along the [100] direction and a sinusoidal channel of almost oval shape (0.51 x 0.55 nm) running along the [010] direction.[79]

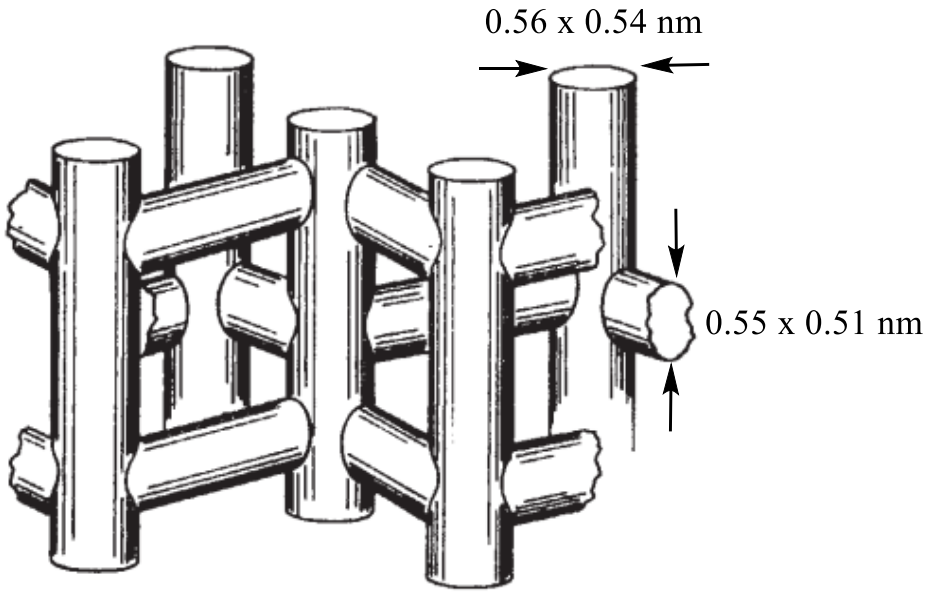

Figure 1.6 The channel structure of H-ZSM-5 showing the elliptical and straight channels. Adapted from Kokotailo. [79]

MFI can be divided into two different structures. Firstly, there is silicalite-1 which is strictly siliceous or has negligible amounts of aluminium and therefore lacks Brønsted acid sites. Secondly, there is Zeolite Socony Mobil-5 (H-ZSM-5) which has a considerable amount of aluminium present and, unlike silicalite-1, contains Brønsted acid site centres.

H-ZSM-5 zeolites usually have Si/Al ratios >10 MFI is formed of 5 rings that are connected to each other. MFI belongs to the orthorhombic crystal system P*nma* (a = 20.1, b= 19.9, c = 13.4 Å)[79] which can reversibly form the monoclinic crystal system as observed by XRD. This phase can be identified in the 2θ range 24-25º. The presence of a single peak in this area is caused by orthorhombic symmetry whereas if there are two peaks observed the unit cell is monoclinic. For Silicalite-1 (SiO_2/Al_2O_3 molar ratios > 3000) the peak angles at 25 ºC were monoclinic ($P2_1/n$) whilst at 52 ºC the peak angles matched orthorhombic crystal symmetry.[80]

1.6.2.1 Preparation and post synthesis treatment of H-ZSM-5

There is an extensive amount of literature regarding the synthesis of H-ZSM-5. The first reported synthesis of H-ZSM-5 was carried out by Landolt et al.[78] A mixture of silica (SiO_2), n-tetrapropylammonium hydroxide (TPAOH), sodium aluminate and water was placed in a pyrex autoclave and heated at 150 ºC for six days before being allowed to cool to ambient temperature. The resultant solid was filtered and washed with an excess amount of water and dried at 110 ºC before being calcined at 537 ºC for 16 hours in air. The resulting H-ZSM-5 zeolite had a SiO_2/Al_2O_3 ratio equal to 32.5. Mohamed et al.[81] studied the effects on different silica sources on the crystallinity of H-ZSM-5; tetraethoxysilane (TEOS), colloidal silica, sodium metasilicate and fumed silica dissolved into a mixture containing TPAOH, sodium hydroxide, sodium aluminate and water and treated under hydrothermal conditions at 230 ºC for 45 hours. It was found that sodium metasilicate was a poor silicon source for H-ZSM-5 synthesis due to the formation of quartz silica. TEOS and fumed silica produced a very crystalline H-ZSM-5 phase whereas colloidal silica gave a less crystalline H-ZSM-5 phase. Ismail et al. [82] also studied the effect of different aluminium sources such as sodium aluminate, aluminium sulfate, alumina and aluminium hydroxide on the formation of nanosized H-ZSM-5 crystals. The reaction conditions were the same as described previously.[81] It was reported that sodium aluminate and aluminium sulfate produced a highly crystalline structure with large surface areas; in contrast aluminium hydroxide and alumina produced a low crystalline phase with smaller surface areas. Quite surprisingly, there appears to be a limited amount of literature regarding the effect of aluminium sources on the effect of H-ZSM-5 properties.

Lu et al.[83] studied the effect of calcination temperature on the acidity and structural stability on H-ZSM-5 with a Si/Al ratio of 32. Calcination temperatures ranging from 500-800 ^{o}C in air were chosen. The catalyst was characterised by XRD to determine its crystallinity and TPD-NH_3 and FTIR-pyridine measurements were used to determine the total number of acid sites and the nature of the acid sites respectively. It was found that at temperatures as high as 80 ^{o}C the zeolite remained crystalline which indicates that it has excellent thermal stability. XRD revealed that at high calcination temperatures there was a phase change from orthorhombic to monoclinic. TPD-NH_3 revealed that at high calcination temperatures the total number of acid sites decreased, presumably due to dehydroxylation. Additionally, the authors found that there was a peak shift, especially for the strong sites were there was a phase shift by <100 ^{o}C, which strongly indicates that the strength of both weak and strong acid sites increased upon calcination. This was confirmed by FTIR-pyridine measurements which showed that the intensity of the band at 1540 cm^{-1} which suggests that the amount of Brønsted acid sites decreased.

1.6.3 Zeolite Beta (BEA)

Zeolite beta was first patented by Mobil in 1967 and was the first zeolite to be prepared using organic species. [84] Zeolite Beta is widely used in industry for processes involving hydrocarbons such as cracking,[85] hydrocracking,[86] dewaxing.[87] Beta zeolites are highly disordered siliceous zeolites and are synthesised with Si/Al ratios from 5 to infinity.

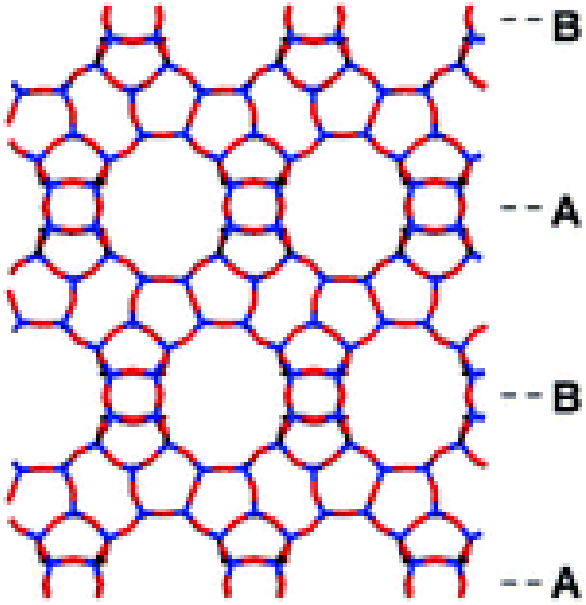

Figure 1.7 Framework structures of Beta zeolite (polymorph A). Taken from Corma et al. [88]

Beta zeolites can be classed into three main polymorphs; A, B and C which can summarised as BEA, BEB and BEC respectively.[88] Polymorph A or BEA has the tetragonal crystal space group $P4_122$ (a=12.63 and c =26.186 Å). Zeolite beta is part of the ABC-6 family which is described as the stacking of 6-rings; firstly a layer of 6-membered rings (layer A) is presented. A second layer (layer B) can either be superimposed onto layer A or can form a separate new layer leading to an AB system as shown in Figure 1.7. This layer is stacked with rotations of ±90^o and translations of ±33% along *a* or *b* to form the zeolite. If the translations are stacked in a left or right hand fashion; i.e LLL or RRR which are enantiomers of each other then polymorph A is formed. However, if the layers are stacking fashion is irregular; i.e RLRLR fashion then polymorph B is formed.[89] Regardless of the stacking arrangement both polymorph A and B form a three-dimensional 12-ring channel system (0. 67 x 0.66 nm) x (0.67 x 0.66 nm) x (0.56 x 0.56 nm)[90] which makes zeolite beta a very attractive option in heterogeneous catalysis.

1.6.4 Zeolite Faujasite (FAU)

Commercial zeolite Y was first claimed to have been discovered by Breck in 1964[91] and after the industrial manufacturer Union Carbide patented the Faujasite material X in

1959.[92] Zeolites X, Y and USY are large pore zeolites that belong to the structural type Faujasite (FAU) but are different in terms of their framework and properties. Zeolite X is normally synthesised with a Si/Al ratio approximately 1.25, zeolite Y with a Si/Al ratio of around 2.3 and USY with a Si/Al ratio at least 5.6. These catalysts are important in industry; zeolite X is used as a carbon dioxide absorbent from gas streams.[93] Zeolite Y and USY are the most commonly used solid acid catalysts in industry; over 100,000 metric tonnes are used in the industrial process Fluid Catalytic Cracking (FCC) which produces the overwhelming majority of the world's gasoline; with a higher octane rating compared to thermal cracking.[94, 95]

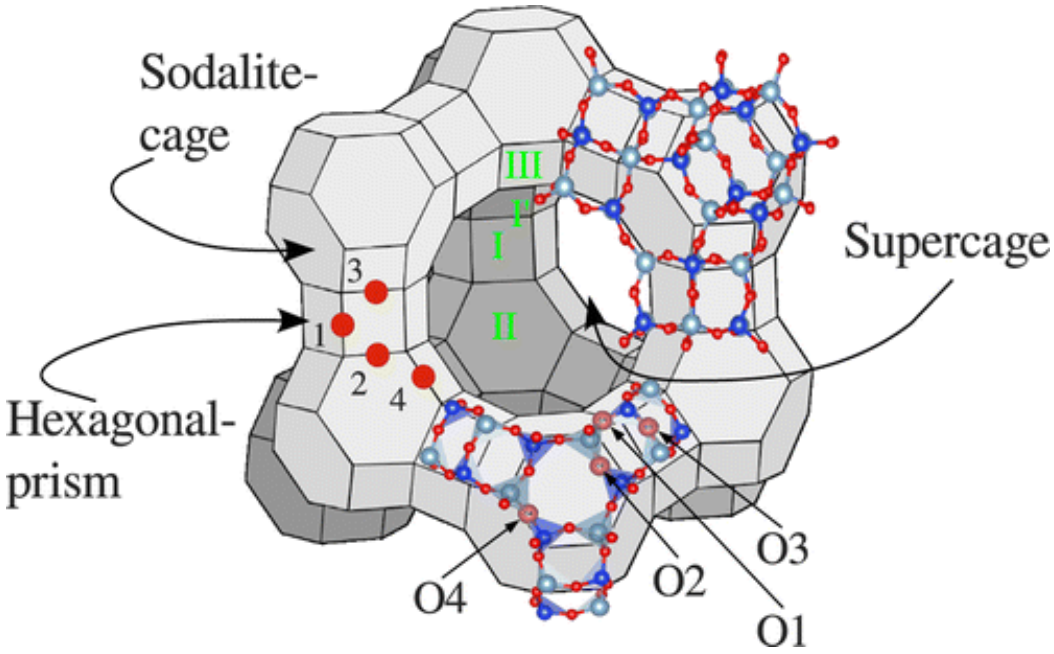

Figure 1.8 Structure of the Faujasite zeolite. Taken from Blondki et al. [96]

FAU consists of a double 6-membered ring, the sodalite cage; where approximately half of the cations are located bonded to three framework oxygen atoms and, a large cavity of tetrahedral symmetry containing 4 x 12-ring windows. It is known as the "supercage". This is where the remaining cations and water molecules are located. In addition, this is where all reactions take place. This connectivity allows the facile diffusion of molecules in three dimensions the interior. FAU zeolites Y and USY belong to the crystal system Fd3m (a= 24.74, b= 24.74, c = 24.74 Å) whereas X has the space group Fd3.[97] The 12-membered ring has a diameter of 0.74 nm and is perpendicular to the [111] direction but

there is no straight channels running along this direction due to the tetrahedral symmetry of the cavity.

1.7 Microwave synthesis of zeolites

In the following subsections, synthesis of zeolites using microwave assisted heating will be described, with a brief history and general principles will be presented. The final subsection will introduce the synthesis of H-ZSM-5 using microwave assisted heating.

1.7.1 Introduction

Microwave technology is proving to be an exciting prospect for the synthesis of nanomaterials. The utilisation of materials using microwave assisted heating could have many applications in industry and research. The company Mobil first patented the process of synthesising H-ZSM-5 in 1988.[98] The first open literature regarding microwave assisted synthesis of zeolites appeared in 1993 when Arafat et al. [99] reported the synthesis of zeolites H-ZSM-5 and Y. Studies have demonstrated that microwave syntheses can take considerably less time compared to conventional heating methods.[99-102] It has been suggested that microwaves can increase the synthesis rate of zeolites by:

(a) Increased uniform heating[103]
(b) Enhancing the dissolution of the precursor gel mixture[104, 105]
(c) Creating hot spots[106]

1.7.2 Principles of microwave heating

Microwaves have wavelengths ranging from 1 millimetre to 1 metre and operate at frequencies 0.3-300 GHz.[107] In the laboratory most microwave experiments are conducted at 2.45 GHz due to the maximum absorption of energy by water at this frequency. It has been suggested that the mechanism of microwave heating is the interaction of dielectric materials and ionic conduction in an oscillating field. However, due to inter-particle interaction this may resist the field and will generate heat. Materials can be divided into three main sections in terms of their interaction with microwave irradiation:

(a) Materials that will reflect microwave irradiation

(b) Materials that are transparent to microwave irradiation

(c) Materials that will absorb microwave irradiation

Generally, precursor solutions which contain a high pH and ions have a large dissipation factor, tan δ, which is a measurement of the gel's ability to convert microwave energy into heat energy. Therefore, precursor gels can heat quickly at low levels of microwave energy.

1.7.3 Microwave synthesis of zeolites

1.7.3.1 Microwave synthesis of H-ZSM-5 (MFI)

There have been more articles on the microwave synthesis of H-ZSM-5 than any other zeolite. An extensive review detailing the synthesis of various zeolites was written by Li et al.[107] in 2008. Arafat et al.[99] reported the synthesis of H-ZSM-5 using microwave heating using tetrapropylammonium bromide as a structure directing agent. The mixture was placed in a Teflon vessel and heated to 140 ^{o}C for 30 minutes. The resulting mixture had a SiO_2/Al_2O_3 molar ratio of 12. After heating, the mixture was cooled to ambient temperature and the solid was filtered, washed and dried. The resulting zeolite was characterised by XRD to determine its crystallinity. The morphology of H-ZSM-5 was determined by FE-SEM. XRD revealed that H-ZSM-5 had been successfully synthesised. Interestingly, FE-SEM revealed that H-ZSM-5 had formed prismatic shapes. The authors carried out the same synthesis using conventional heating in an oven with the same precursor solution for days at 180 ^{o}C. The authors found that the crystals were cubic in shape compared to the elongated prismatic shapes formed during microwave heating. The authors could not explain the reasoning behind this phenomenon. When the authors carried out the same synthesis procedure at 180 ^{o}C using microwave irradiation it was found that amorphous phases were formed. The authors hypothesised that microwave irradiation caused thermal degradation of the structure directing agent due to Hoffman elimination.

Jin et al.[108] studied the synthesis of mesoporous H-ZSM-5 by microwave induced assembly method of acid functionalised MFI and cationic surfactants. The synthesis procedure compared the physical properties to hydrothermally synthesised H-ZSM-5. The zeolite was synthesised using tetraethoxysilane as a silicon source, aluminium

isoporopoxide as an aluminium source and tetrapropylammonium hydroxide as the structure directing agent. The final mixture was crystallised at 165 ºC under microwave irradiation for 0.5 hours and under conventional heating at the same temperature for 72 hours. XRD measurements confirmed a highly crystalline H-ZSM-5 zeolite had been synthesised. Surface area and porosity measurements showed that the templated H-ZSM-5 catalyst that underwent microwave treatment had a much larger surface area compared to the conventionally synthesised templated H-ZSM-5 catalyst (529 vs 388 m^2 g^{-1}).

Hasan et al.[109] studied the effect of desillication of H-ZSM-5 using microwave heating and conventional heating. Prior to treatment the catalyst was pre-heated at 550 ºC for 5 hours to produce the proton form. A highly siliceous H-ZSM-5 was treated under alkaline conditions using sodium hydroxide (0.05-0.5 M), NH_3 (aq) (0.5-0.9 M) or ethylenediamine (1.5-7.5 M). Due to the fact that ethylendiamine or NH_3 (aq) had no significant impact on the structure of H-ZSM-5 using conventional heating, this section will focus primarily on the alkaline treatment using sodium hydroxide. Treatment of H-ZSM-5 using sodium hydroxide led to a structural decrease in using conventional or microwave assisted heating methods. For the conventional method it took 4 hours to to increase the external surface area to 155 m^2 g^{-1} compared to just 20 minutes under microwave under the same conditions.

1.8 Hierarchical zeolites

The following subsections will outline a brief introduction to hierarchical zeolites, documenting their physical and chemical properties, with a particular focus on synthesis strategies.

1.8.1 Introduction to hierarchical zeolites

Interest in the synthesis of hierarchical zeolites is increasing, with a comprehensive review written by Serrano et al.[110] in 2013. Microporous zeolites contain pore sizes less than 2 nm. Hierarchical (mesoporous) zeolites contain pore sizes in the range of 2-50 nm. Hierarchical zeolites can be synthesised by a different number of ways such as desilication[111], dealumination [112], the use of templating agents such as surfactants [113] hard templates such as polymers or carbon.[114, 115]

The creation of at least two levels of porosity has attracted particular attention due to the limitations of mass diffusion in the micropore region, due to the pore size. This can become more pronounced if the reactant/ product in question are approximately the same size as the cavity pores. Therefore, in the case of microporous zeolites diffusion can become the rate determining step.[116] The creation of mesopores shows the diffusion mechanism becomes more consistent with that of Knudsen diffusion than the classic configurational diffusion model. [117] In the case of Knudsen diffusion mechanism the molecules will collide more frequently with the wall than with each other due a reduction in the mean free path of diffusion. Since the rate of diffusion is inversely proportional to the mean free path of diffusion value, it would be expected that diffusion rate in the new levels of porosity would be enhanced at least 2-3 times. [116] The formation of coke inside the porous cavities is also a limitation involved in chemical reactions involving microporous zeolites. The formation of coke can block access to the active microporous sites and therefore deactivate the catalyst. It has been argued that secondary porosity could also be used for coke storage and therefore not block access to the active micropore sites.[110] Despite the fact that more coke might form in the mesopores, the catalyst will not deactivate. Coke formation can be typically reversed by calcining the zeolite without damaging the structure. [33]

Top down strategies for the creation of mesoporous involves the removal of either Si or Al as shown in Scheme 1.5

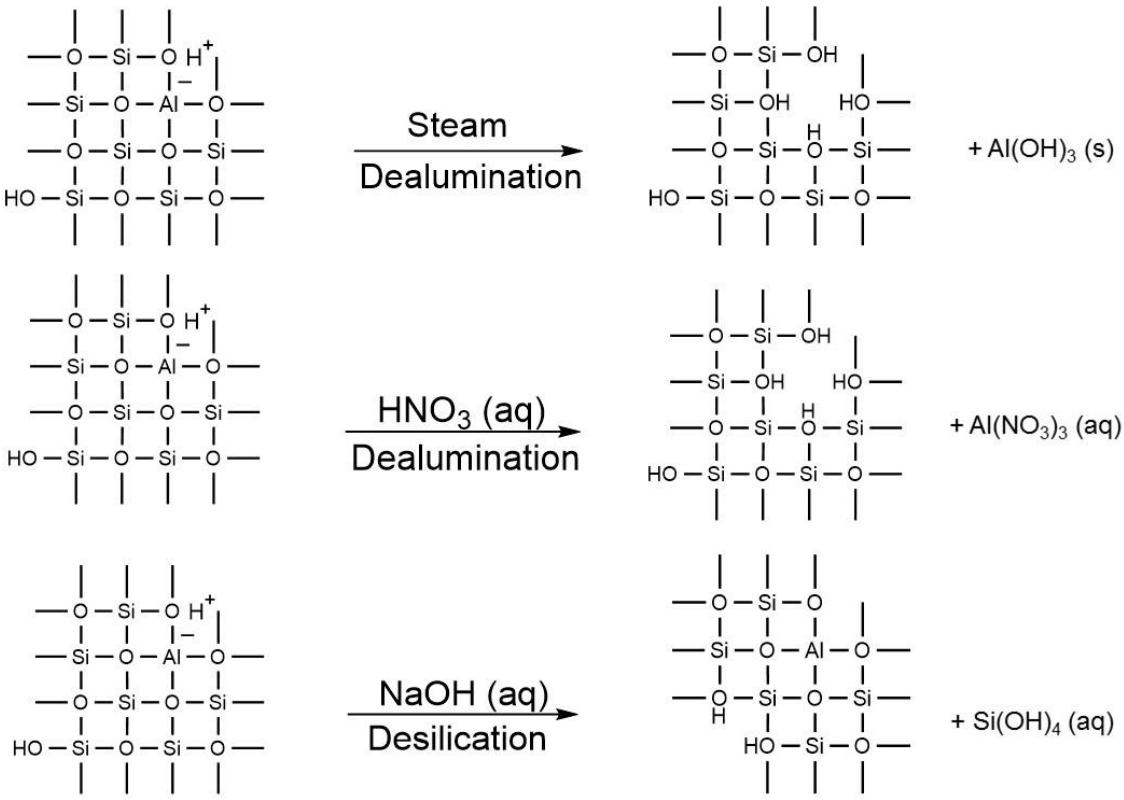

Scheme 1.5 Top down strategies to generate mesoporosity: steaming, acid leaching or alkaline treatment. Taken from Groen et al.[118]

Since acid strength is proportional to the amount of aluminium in the framework it would be expected that treatment of conventional zeolites by dealumination of framework aluminium would increase the Si/Al ratio and therefore, decrease the acid strength of the zeolite catalyst. This would reduce Brønsted acidity and activity. Dealumination can be achieved by acid treatment of the zeolite.[112] In this scenario the Si-O-Al bond is hydrolysed and aluminium is removed from the framework.

1.8.2 Preparation of hierarchical zeolites

1.8.2.1 Desillication

Dean Arthur Young was first to realise the potential of base treatment towards mordenite to enhance catalytic performance in the gas-oil reaction. [119] A SiO_2/Al_2O_3 ratio of 9-10 was chosen. In a typical reaction, sodium hydroxide (20% wt in water) was mixed with

mordenite (0.5 mL g^{-1}) which created a thick paste. The paste was mixed for 30 minutes at room temperature and then filtered and washed to remove the excess ions. Mordenite was brought into the proton form by ion exchange with ammonium chloride (20% wt in water) before being calcined for 16 hours at 540 ºC. Crystallinity slightly increased in the alkaline treated mordenite which suggests that amorphous silica was removed. The untreated and alkaline treated mordenite zeolites were tested for benzene adsorption. They reported that the alkaline treated mordenite improved the capacity of benzene adsorption. Although porosity and surface area measurements were not carried out it was suggested by Young that the improved performance of the modified catalyst was directly linked to increased access to the micropores.

During the 1970's patents were disclosed which demonstrated the superior performance of zeolites when treated by a base. Rosback and Neuzil[120] demonstrated the superior properties of desilicated X and Y zeolite as olefin absorbents using aqueous sodium hydroxide solution. Rein et al.[121] performed an alkaline treatment of zeolite of class A with a pore size range 0.3-0.5 nm. An aqueous solution of NaOH (0.1-0.5 M) for molecular sieves with a pore size of 0.4 nm and KOH with concentrations identical as for NaOH for molecular sieves with a pore size of 0.3 nm were used. The mixture was heated to 70-100 ºC for 15 minutes to 1 hr. The pH was kept within the range of 10-11. The slurry was filtered and washed and dried in a muffle furnace at 300 ºC. The alkaline washed molecular sieves showed enhanced acid scavenging ability. After some promising patents regarding extraction of silicon from zeolites using alkaline treatment it took until nearly 25 years after the patent by Young in the 1960's before the open literature regarding zeolite modification became available. One of the first publications was the work carried out by Dessau et al.[122] by synthesising H-ZSM-5 crystals of approximately 1 μm in size with SiO_2/Al_2O_3 ratios between 70-230 and then subjecting the H-ZSM-5 catalyst with Na_2CO_3 (0.5 M) and separately NaOH (1 M) at room temperature under reflux for 16-20 hrs. In the case of treatment with Na_2CO_3 for 15 minutes total dissolution had occurred whereas partial dissolution occurred when using sodium hydroxide. The remaining zeolite was enriched with aluminium with trace amounts being found in the filtrate which suggests that aluminium was not removed with silica being preferentially extracted instead. It was suggested that tetrahedral aluminium centres were inert of hydroxide attack due to the negative charge associated with the centre. Despite the dissolution of the silica from the structure, the channel structure of residual H-ZSM-5 remained largely intact

despite base treatment. Scanning electron microscopy (SEM) revealed dissolution of the interior crystals. The exterior surface remained largely unaffected by base treatment as shown in Figure 1.9 (below).

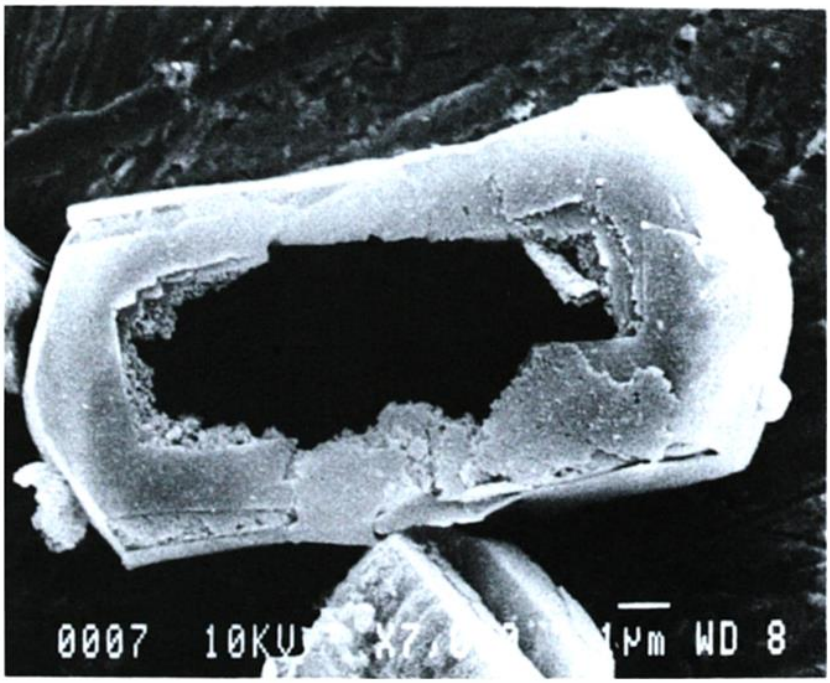

Figure 1.9 SEM image of alkaline treated ZSM-5.[122]

Cizmek et al.[123] studied the effect of dissolution of silicalite-1 and H-ZSM-5 in aqueous NaOH (5 M) solution. Firstly, silicalie-1 and H-ZSM-5 with varying SiO_2/Al_2O_3 ratios were synthesised hydrothermally at 170 ^oC. The synthesised powders were heated in a steam of nitrogen at 600 ^oC for 4 hours to remove the structure directing agent TPA^+ from the zeolite. In a typical dissolution process, the catalyst (12 g) was poured into a stainless steel vessel containing 250 mL of aqueous NaOH (2.5-5 M) at 60 ^oC and stirred. Aliquots were taken at times 0-420 mins. XRD of treated samples showed a transformation of H-ZSM-5 into an amorphous material. Fourier transform infrared spectroscopy showed a decrease in the band at 550 cm^{-1}, which is assigned to asymmetric stretching mode of the double five- membered ring in the zeolite structure. There was an increase in the band at 440 cm^{-1}. In addition, there was a shift in the band at 1100 cm^{-1} to a lower wavenumber. It was suggested that the amorphous phase was amorphous silica. The proposed mechanism suggested by Cizmek et al.[123] was that alkaline treatment hydrolysed Si-O-Si and Si-O-Al bonds leading to the formation of soluble silicate, aluminate and aluminosilicate, which leaves the surface of the dissolving zeolite. Le Van Mao et al.[124]

studied the effect of pH sodium carbonate/sodium hydroxide mixtures for desllication of zeolite materials FAU and H-ZSM-5. Typically zeolite (5 g) was placed into a Teflon beaker containing 150 mL solution of sodium carbonate with varying concentrations of NaOH (0.005-0.5 M) were added. The suspension was heated to 80 ^{o}C and stirred for 4 hrs. The liquid was removed and a fresh amount of solution was added to the mixture and stirred under the same conditions for another 4 hours. This procedure was repeated again before being collected for analysis. Crystallinity was measured by X-ray powder diffraction. A summary of their findings is shown in Table 1.1

Table 1.1 Influence of pH of Na_2CO_3 on the chemical and crystalline proprties on Y and MFI.[124]

Sample	NaOH (M)	pH	Recovery (%)	Crystallinity	Si/Al
Y	0	-	100	100	2.5
Y1	0.1	12.5	67	93	2.2
Y2	0.2	12.9	67	91	2.0
Y3	0.5	13.1	52	90	1.6
H-ZSM-5	0	-	100	100	19.5
H-ZSM-5	0.005	11.7	68	84	12.7
H-ZSM-5	0.01	11.9	68	84	12.2
H-ZSM-5	0.02	12.1	66	89	11.6

Le Van Mao et al.[124] appeared to find a direct correlation between sodium hydroxide content and the physical and chemical properties of treated zeolites. The effect of desillication upon H-ZSM-5 and Y appeared show similar trends. In the case of Y zeolites it was found that when the pH was adjusted to 12.5 crystallinity decreased to 93% of the untreated parent. In the more extreme cases when a higher pH was used >30% of the original mass was lost which strongly suggests that silicon was extracted from the zeolite surface. In addition, it can be seen that desilication had an effect on the Si/Al ratio. In the case of zeolite Y, Si/Al ratio decreased from 2.5 to 1.6 when a 0.5 M solution of sodium hydroxide was used. Interestingly, there appeared to be a more significant effect on H-ZSM-5 which had a higher starting Si/Al ratio than the Y zeolite. In the case of H-ZSM-5, Si/Al ratio decreased from 19.5 to 11.6 which is accounts for 40% decrease. Chemical absorption appears to show that zeolites with a lower Si/Al ratio show more resistivity towards desillication. Le Van Mao et al[124] studied the effect of desillication on surface area and porosity. Surface area measurements were carried out using nitrogen adsorption.

The surface area was calculated using the Brunauer–Emmett–Teller (BET) method. Micropore sizes were calculated by according to Horváth-Kawazoe (HK) method.

Table 1.2 Influence of pH of Na_2CO_3 on the surface area and porosity on Y and MFI. [124]

Sample	NaOH (M)	S_{BET} (m^2 g^{-1})	V_{total} (cm^3 g^{-1})	V_{micro} (cm^3 g^{-1})
H-Y	-	742	0.36	0.30
H-Y	0.1	765	0.41	0.33
H-Y	0.2	678	0.34	0.25
H-Y	0.5	731	0.39	0.32
H-ZSM-5	-	255	0.34	0.11
H-ZSM-5	0.005	194	0.59	0.09
H-ZSM-5	0.01	250	0.54	0.11
H-ZSM-5	0.02	241	0.62	0.11

Desilication had an effect on the surface area and porosity on both Y and H-ZSM-5 zeolites. The textural properties of zeolite Y did not change significantly upon desillication. The uptake of nitrogen adsorbed for H-ZSM-5 increased for desillicated samples which suggested that porosity had increase with alkaline treatment. This work found that alkaline treatment led to increased aluminium content and with increased ion exchange capability. However, the role of mesoporosity regarding intracrystalline diffusion was not discussed.

The first authors to realise that alkaline treatment led to mesoporosity was Ogura et al.[111] in 2000. H-ZSM-5 was subjected to alkaline treatment using sodium hydroxide as a base (0.05-0.2 M) for 65 or 85 ^{o}C. ICP-OES measurements confirmed that Si was predominately extracted from the zeolite during alkaline treatment. There was negligible aluminium content in the filtrate, suggesting most of the aluminium was located in the tetrahedral position. During alkaline treatment it was found that 2.6 Si atoms unit $cell^{-1}min^{-1}$ were extracted. In contrast, only 0.1 Al atoms unit $cell^{-1}min^{-1}$ were extracted. Nitrogen isotherms showed an increase uptake of nitrogen at higher relative pressures at longer reaction times which indicated enhanced porosity. The presence of a hysteresis showed the formation of ink-bottle type mesopores. FE-SEM showed cracks on the surface of H-ZSM-5 after alkaline treatment. The cracks became much more pronounced and deeper after longer reaction times as shown in Figure 1.10 (below).

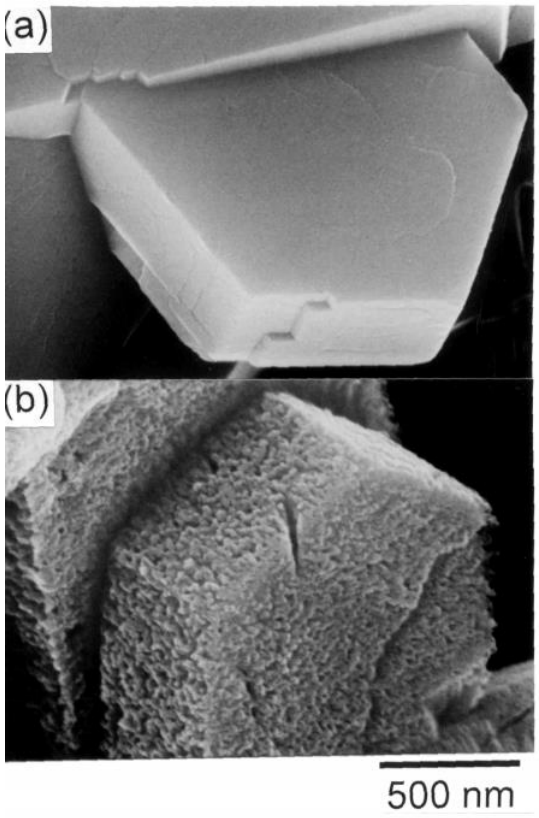

Figure 1.10 SEM image of (a) Parent H-ZSM-5 and (b) alkalined treated H-ZSM-5. Taken from Ogura et al.[111]

Under severe reaction conditions dissolved silica could precipitate onto the surface of H-ZSM-5 crystals forming an amorphous layer of silica which could cause blocking of the pores. XRD showed the [051] and [-501] reflections which are assigned to 2θ angles 23.1 and 23.3º respectively were split after alkaline treatment. This indicates that poor crystallinity parts of H-ZSM-5 were dissolved. It was concluded that alkaline treatment led to a structural change on the micrometre scale and not on the molecular scale. The effect of desilication on acidity was reported for the first time using NH_3-TPD. The amounts of acid sites was calculated based on desorption at higher temperature (230-480 ºC) It was found that the commercially received H-ZSM-5 had higher acid site density (704 μmol g^{-1}) compared to alkaline treated H-ZSM-5 at various times. There was an inverse proportional relationship between times of reaction versus acidity. Interestingly, desorption at lower temperatures (~110-230 ºC) was not taken into account when the determination of acidity was made. There appears to be a trend regarding alkaline treatment of the desorption peak at lower temperature. Upon alkaline treatment the intensity of this peak increases at the expense of the peak at higher temperature. Infrared

spectroscopic measurement was used to distinguish between Brønsted and Lewis acid sites using pyridine as a probe molecule. ^{27}Al MAS-NMR confirmed that only tetrahedral remained after alkaline treatment. ICP-OES showed the Si/Al ratio remained largely unchanged (32.8 to 28.9). The catalytic properties of alkaline treated H-ZSM-5 zeolites against the commercially available unmodified H-ZSM-5 were tested in the catalytic cracking of cumene., with the alkaline treated H-ZSM-5 showing 100% greater catalytic activity than the untreated H-ZSM-5 zeolite.

Despite the change in morphology XRD showed alkaline treated H-ZSM-5 maintained its crystallinity. The intensities between the parent and its alkaline treated counterpart remained similar which suggests that alkaline treatment did not have a significant effect on the crystallinity on H-ZSM-5. Nitrogen sorption measurements showed a decrease in micropore volume (from 0.17 to 0.13 $cm^3\ g^{-1}$) with regard to the parent H-ZSM-5. Interestingly, alkaline treatment had an effect of mesopore volume. The mesopore volume increased from 0.07 to 0.28 $cm^3\ g^{-1}$ which was due to dissolution of ~40% of the zeolite crystal. It was claimed that when compared to the mesoporous material M41S alkaline treated H-ZSM-5 showed a sharp increase around $P/P_o = 0.5$ which strongly indicates the creation of mesopores of ca 4 nm which was formed by the dissolution of Si at the boundaries of the crystal which resulted in intercrystalline voids.

Groen et al.[125] however, challenged this claim. A commercial ZSM-5 catalyst with SiO_2/Al_2O_3 ratio of 75 was treated in an identical manner described by Oguara et al.[111] Similarly, X-ray diffratograms showed crystallinity was largely unaffected. Nitrogen adsorption isotherm of alkaline treated H-ZSM-5 showed increased uptake relative to the commercial H-ZSM-5 which was associated by newly created mesoporosity. S_{BET} increased slightly upon alkaline treatment (440 to 450 m^2g^{-1}). The t-plot calculation showed that S_{ext} increased to 130 $m^2\ g^{-1}$ for the alkaline treated H-ZSM-5 from 40 $m^2\ g^{-1}$ for the commercially received zeolite. It was suggested that this comes at the expense of microporosity which decreased from 0.17 to 0.13 $cm^3\ g^{-1}$ as measured by the t-plot.

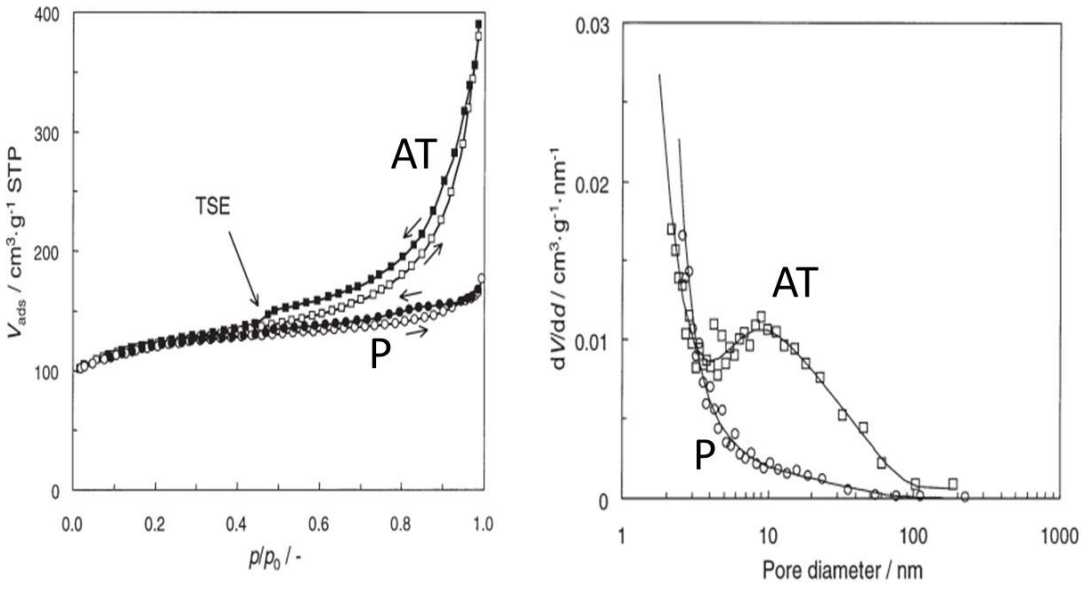

Figure 1.11 Surface area and porosity measurements for H-ZSM-5 treated with (left) N_2 adsorption-desorption and (right) BJH adsorption plots of parent and alkaline treated H-ZSM-5. (P = parent and AT = alkaline treated). Adapted from Groen et al.[125]

As shown in Figure 1.11, both the adsorption and desorption branch at $P/P_o > 0.5$ show a similar trend. A different behaviour is observed at $P/P_o = 0.45$. The adsorption branch showed a progressive increase in volume adsorbed but the desorption branch showed a pronounced step at $P/P_o = 0.45$ resulting in the closure of the hysteresis loop. Groen et al.[126] argued that rather than being due to an increase in pore size ~4 nm the closure of the hysteresis loop was typical of N_2 at -196 ^oC which is independent of the porous properties of the sample and always appears at the same position for different adsorbents. This phenomenon is called the Tensile Strength Effect (TSE).

Suzuki et al.[127] investigated the effects of low concentration of sodium hydroxide on the effects on physiochemical properties on H-ZSM-5 ($SiO_2/Al_2O_3 = 74$). A 0.05 M solution was used in the treatment for 0.5-30 hours at temperatures 50-70 ^oC. Supermicropores in the region of 1.8 nm were detected after alkaline treatment. It was found that the supermicropore volume increased in the initial stage but was unchanged as a function of longer times. Su et al.[128] studied the effect of alkaline treatment of the performance of methane dehydroaromatisation. Desillication was performed on H-ZSM-5 with a Si/Al ratio of 25 using sodium hydroxide (0.05-0.2 M). ^{27}Al-MAS NMR confirmed aluminium was located mainly in the tetrahedral positions of the framework. Upon alkaline treatment using harsher conditions the peak intensity at δ=55 ppm decreased slightly while the peak

at δ=0 ppm increased which suggests that aluminium was extracted from the tetrahedral position corresponding to the Brønsted acid sites and migrated to the extra-framework position. In moderate conditions ^{27}Al MAS-NMR showed that tetrahedral aluminium is largely unaffected. ^{29}Si MAS-NMR showed dramatic changes after alkaline treatment. The intensity of the peak δ=-114 ppm which corresponds $Si(OAl)_0$ decreased. In contrast the δ=-107 ppm which corresponds to $Si(OAl)_1$ remained unchanged except when harsher conditions were used. This confirmed that silicon was preferentially extracted. This confirms that except under harsh conditions that alkaline treatment preferentially extracts silicon. ^{1}H MAS-NMR found the band associated with Si-OH-Al (δ=3.7 ppm) increased slightly under moderate conditions but decreased when harsher alkaline treatments were applied. Due to the partial collapse of the zeolite structure groups associated with Al-OH and silanol groups were formed. The authors concluded that alkaline treatment did not affect the Brønsted acidity or the strength. Since this process preferentially extracts silicon under alkaline conditions, this type of top down approach has adopted the name "desillication".

Around four years after the word carried out by Ogura et al.[111] there was strong interest in this procedure by Perez-Ramirez. He sought to the find key of role of Si/Al ratio and fully understand the mechanism and effect of base treatment (i.e. creation of secondary porosity) [111]. H-ZSM-5 with a wide range of Si/Al ratios were used (15-1000). The standard desillication method was applied. Mesopore surface area reached an optimum for Si/Al ratios 25-50 with mesopores in the range 5-20 nm formed as shown in Figure 1.12.

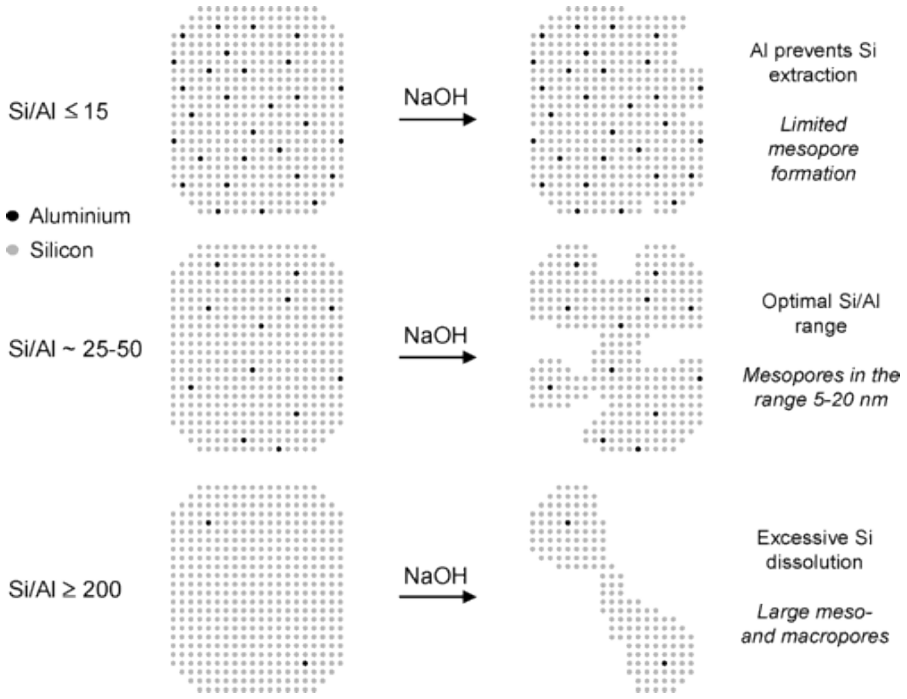

Figure 1.12 Influence of Si/Al molar ratio on desilication of H-ZSM-5. Taken from Groen et al.[129]

In contrast, zeolites with Si/Al ratio <15 there was limited mesopore formation due to the presence of tetrahedral aluminium. Excessive and uncontrolled dissolution of Si was found with Si/Al ratios >200 with large meso and macropores formed in the region of 20-100 nm. There was little effect on H-ZSM-5 with Si/Al ratio <25 whereas with more siliceous zeolites Si/Al ratio decreased dramatically. [129] This effect was confirmed by analysis of the filtrate which showed only a small amount of silicon present in the filtrate for zeolites with low Si/Al initially. The preferential dissolution of silicon increased with time and temperature (600-4800 mg L^{-1}) which led to lower Si/Al molar ratios (37-23). It has been claimed that the reproducibility of silicon extraction is excellent (up to 3% difference) providing the framework Si/Al ratio is taken into account. The presence of extra-framework aluminium which impacts the bulk Si/Al ratio can have an effect on the efficiency of the treatment. Clearly, parameters such as time, temperature and concentration can be modified to optimise the mesoporosity while maintaining the surface area. Optimum conditions for desilication of H-ZSM-5 (Si/Al = 37) were 65 ^{o}C for 30 minutes. Temperatures <65 ^{o}C led to only a small increase in the formation in mesoporosty at the expense of microporosity (017-0.13 cm^3 g^{-1}). This has opened up new approaches for the development of micro- and mesoporous zeolite catalysts. Other inorganic bases have been tested previously to determine whether stronger bases can have

a greater effect of enhancing mesoporosity than sodium hydroxide. These were found to be less effective than sodium hydroxide. Mesopore surface area increased in the order ammonium hydroxide < lithium hydroxide < potassium hydroxide < sodium hydroxide. The efficiency of the use of sodium hydroxide was attributed the stabilising effect of Na^+ of silicate anions which would prevent reinsertion back into the zeolite structure. The desillication of zeolites has proven to be one of the most versatile techniques and has attracted so much interest due to the simplicity and tune ability of the method.

1.8.2.2 Templation with solids

The assembly method approach involves the direct synthesis of zeolites with a porous or hollow solid for the generation of meso- and/ or macropores. This method has attracted much attention for the synthesis of hierarchical zeolites. The procedure involves three main steps:

(1) Infiltration of a solution using the templating agent
(2) Zeolite crystallisation
(3) Removal of the template

The removal of the template can be achieved by burning (for organics) or by dissolution (for inorganics). Secondary porosity can be generated due to intra and/or interparticle cavities. Pore sizes are usually generated in the mesoporous (2-50 nm) range. The synthesis conditions must be chosen as to avoid damage to the zeolite. Svelle et al. [130] found templating with carbon black particles with an average particle diameter of 12 nm led to the formation of complex hydroxyl silanol groups due the excessive combustion temperature. This was confirmed by FTIR which showed a more intense peak at 3740 cm^{-1} which is indicative of terminal Si-OH groups. Templating can be categorised into the following sections:

(1) Hard templating
(2) Soft templating[113, 131-136]

This section will focus mainly on hard templating methods. During the last 15 years there have been various solid materials that have been investigated as potential hard templates for the generation of mesoporosity. Carbonaceous species have attracted the most interest. In 1999 Madsen et al[114] reported for the first time a procedure to generate mesoporosity

in H-ZSM-5 using two types of carbon species; Black Pearls 2000 (d_{pore} = 45.6 nm) and Black Pearls 700 (d_{pore} = 21.2 nm). Black Pearl 700 had a smaller S_{BET} than Black Pearl 2000 (170 m^2 g^{-1} *vs* 520 m^2 g^{-1}). In a typical synthesis the carbon template was impregnated via the incipient wetness impregnation with a gel of molar composition:

$$xAl_2O_3 : 9\ TPA_2O : 0.15\ Na_2O : 50\ SiO_2 : 390\ H_2O : 200\ EtOH\ (0 \leq x \leq 0.5)$$

The precursor solution was aged for 3 hours at ambient temperature and steamed under hydrothermal conditions at 180 ^oC for 48 hours. The product was washed with ethanol and dried. The carbon template was removed under pyrolysis conditions at 550 ^oC for 6 hours. Crystal size was proportional the amount of aluminium added to the synthesis gel. X-ray diffraction revealed that a highly crystalline phase pattern typical of the H-ZSM-5 structure had been synthesised. Particle sizes was generated in the range of 8-30 nm with S_{BET} of 412 m^2 g^{-1} with little inter-growth when Black Pearl 700 was used. The total pore volume was found to be 0.58 cm^3 g^{-1} with a mean pore radius of 15 nm. The t-plot measurement revealed a bimodal pore size distribution. After this study, the authors applied the same method to zeolites Beta, X and A.[137] Black Pearl 2000 was used for the synthesis of zeolite beta. X-Ray diffraction of beta zeolite after calcination displayed a crystalline phase. Crystal sizes measured by the Scherrer equation showed a slight increase in crystal size distribution after calcination. One theory was that the exothermic nature of carbon combustion caused sintering. However, it was accepted by the authors that this increase in crystal size distribution was due to convolution of the XRD patterns between carbon and the zeolite crystalline phases. Therefore there was not a dramatic effect on crystal size as previously thought. The authors studied the effect of carbon (Black Pearl 2000 vs Black Pearl 700) templation on acidity of H-ZSM-5 by NH_3-TPD.[138] As expected, NH_3-TPD showed that there was an inverse relationship between the total number of acid sites and Si/Al ratio. Si/Al ratios were calculated based on the assumption that a zeolite followed the stoichiometric formula; $H_nAl_nSi(1-_n)O_2$ with one ammonia molecule corresponding to one framework aluminium atom. In all cases this was higher than the bulk Si/Al ratio but was similar to the values calculated based on ^{27}Al MAS-NMR. Interestingly, the zeolite with the lowest Si/Al ratio using $NaAlO_2$ as an aluminium source demonstrated only a peak at δ=60 ppm which suggests that only tetrahedral aluminium was present. When aluminium isoproxide was used as an aluminium source ^{27}Al MAS-NMR showed the presence of aluminium in extra-framework positions. A limitation of using mesoporous carbon templates is the cost efficiency of the synthesis of

the template. Alternatively, templating using polymers as solid templates is attracting interest due to cost efficiency. Polystyrene is relatively less expensive to synthesise than carbon templates.

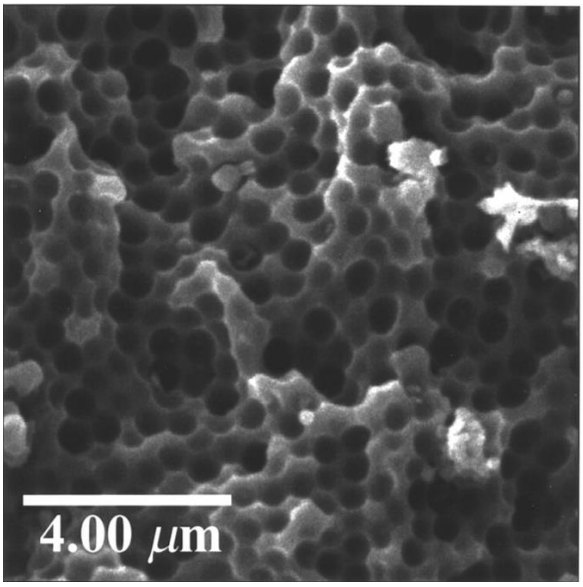

Figure 1.13 SEM image of silicalie showing the porous structure formed after the removal of the polystyrene template. Taken from Holland et al.[139]

Holland et al.[139, 140] synthesised silicalite-1 using polystyrene (PS) as a templating agent. In a typical synthesis PS monosopheres (526 nm) were centrifuged to form close packed arrays of spheres. A precursor solution containing TEOS, TPAOH was added to a polyethylene bottle containing the dried PS spheres (2 g) and shaken physically. The mixture was left overnight to harden. The resulting solid was heated under hydrothermal conditions at 130 ^{o}C for 40 hours. The PS template removed by calcination at 525 ^{o}C for 7 hours. X-ray diffraction confirmed a highly crystalline silicalite material without the presence of another crystalline phase. Silicalite-1 demonstrated two types of porosity; straight channels along [010] plane and sinusoidal channels along the [100] plane. In addition, silicalite-1 consisted of a 10 membered ring of range 0.55 x 0.51 nm. Silicalite-1 was tested to measure its hydrothermal stability. The zeolite was subjected to reflux using water for 13 hours. X-ray diffraction showed the reflections remained unaffected which indicates the hydrothermal stability of silicalite-1 compared to mesoporous MCM-41. Fourier transform infrared spectroscopy showed after calcination stretching associated with PS was absent which suggests that PS was fully removed after calcination. Absorptions around 1224 cm^{-1} were found which is associated to external Si-O

asymmetric stretching found in zeolites with five membered rings[141]. Scanning electron microscopy showed uniform macropores (250 nm). The wall thickness was estimated in the range of 20-220 nm. Nitrogen porosity and surface area measurements showed a type I N_2 isotherm with a S_{BET} of 421 $m^2\ g^{-1}$ with an S_{EXT} of approximately 206 $m^2\ g^{-1}$. The total pore volume was calculated as 0.39 $cm^3\ g^{-1}$ based on a single point measurement. Mesoporosity was calculated using the BJH model and measured 0.30 $cm^3\ g^{-1}$ which represented nearly 76% of the total porosity. An untemplated zeolite was not prepared in this study.

Xu et al.[115] studied the effect of templating H-ZSM-5 with PS on the catalytic activity of alkylation of phenol. PS (580 nm) was centrifuged to form a close packed array of spheres and added in a 1:10 PS/precursor solution (wt/wt) with the precursor solution having the following molar composition:

$$1.0\ Al_2O_3:\ 100\ SiO_2:\ 8TPAOH:\ 120\ C_2H_5OH:1500\ H_2O$$

The mixture was subjected to hydrothermal conditions at 100 ^oC for 16 hours. The PS spheres were removed by calcination in air at 550 ^oC for 5 hours. X-ray diffraction of the hierarchical H-ZSM-5 zeolites showed smaller peaks compared to the conventional H-ZSM-5 zeolite. This was attributed to amorphous aluminosilicate macroporous walls not being crystallised to the same extent. The authors argued that crystallisation can inhibit the mass transport due to the stronger effect of pore connectivity. The N_2 isotherm of the templated H-ZSM-5 zeolite clearly showed a type IV isotherm with a H1 hysteresis loop which strongly indicated the presence of mesopores. Pore size distribution showed a narrow peak at 11 nm for the hierarchical H-ZSM-5 zeolite. Microporosity in both the conventional and hierarchical zeolite appeared to be similar. The conventional zeolite lacked mesoporosity. In contrast, the hierarchical zeolite showed a large mesopore pore volume (0.78 $cm^3\ g^{-1}$). The authors argued that the increase in meso-/macroporosity was due to the interstitial voids and/or the formation of cracks during the calcination process.

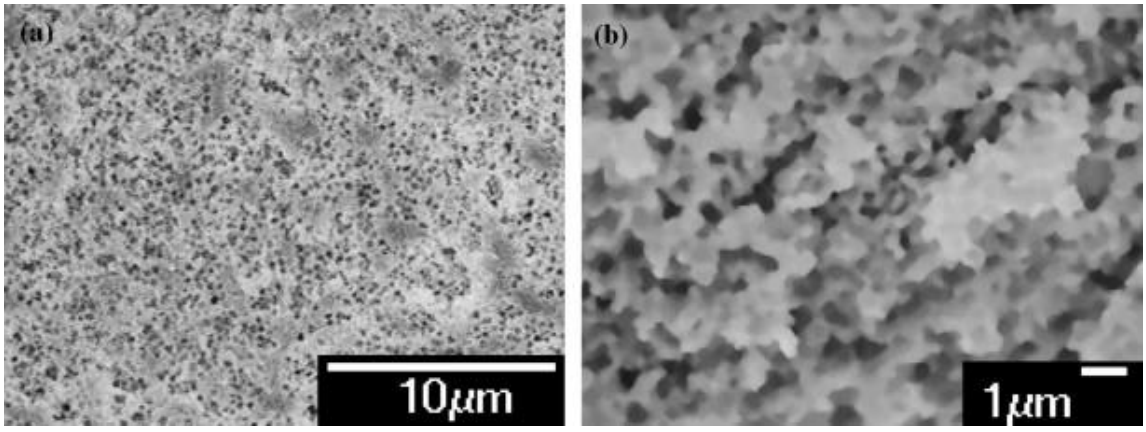

Figure 1.14 SEM image of hierarchical H-ZSM-5 synthesised by Xu et al.[115] (a) at 10 μm and (b) 1μm magnification.

NH_3-TPD confirmed that the acid site density of the hierarchical zeolite was lower than the conventional zeolite. This was likely caused by the presence of more amorphous alumosilicate the hierarchical zeolite than the conventional zeolite. The performance of the conventional and hierarchical zeolite was assessed by alkylation of phenol with tert-butanol at 145 ^oC for 2 hours. The conventional zeolite converted 16% of phenol whereas the hierarchical zeolite converted 81% of phenol which is approximately 5 times more active than the conventional zeolite. A mixture of 2-tert-butyl-phenol (2-TBP), 4-tert-butyl-phenol (4-TBP) and 2, 4-di-tert-butyl-phenol (2, 4-di-TBP) was produced with the conventional and hierarchical zeolite. 2-TBP was more selective with the hierarchical zeolite than the conventional zeolite but selectivity towards 2, 4-di-TBP was enhanced with the hierarchical zeolite. Selectivity towards 4-TBP was similar in the conventional and hierarchical zeolite. The authors assumed that the reaction occurred on the external surface of the zeolite as reported by Anand et al.[142]. Additionally, the hierarchical zeolite showed some selectivity towards 2, 4, 6-tri-TBP whereas none was detected with the conventional zeolite. The higher selectivity towards 2, 4-di-TBP in the hierarchical zeolite was associated as a direct consequence of increased meso-/macroporosity. The authors argued that the presence of both meso- and macropores facilitated the diffusion of the bulky products. The authors compared this result to the mesoporous Al-MCM-41and found that the hierarchical zeolite was more active. Al-MCM-41 was selective mainly to the product 4-TBP. The product 2, 4, 6-tri-TBP was not detected with Al-MCM-41. The authors assumed the lower activity of Al-MCM-41 was due to the weaker acidity of the amorphous walls compared to the acidic crystalline walls of hierarchical H-ZSM-5.

1.9 Reactions comparing catalytic activity of conventional and hierarchical zeolites studied in this thesis

Since the development of hierarchical zeolites there have been numerous reviews showing superior catalytic activity of hierarchical zeolites.[143-146] Here, reactions that will be presented throughout this thesis are discussed with selected studies shown, with a focus on reactions carried out using zeolites.

1.9.1 Friedel-Crafts alkylation of benzyl alcohol with benzene

Here, we focus on the Friedel-Crafts alkylation of benzyl alcohol with benzene as a probe reaction to compare catalytic activity of conventional with hierarchical zeolites. The main observation of alkylation reactions using hierarchical zeolites is the activity due to increased active site accessibility. The modification of zeolites by alkaline treatment provides an excellent opportunity to demonstrate increased intracrystalline diffusion. There have been numerous studies that have investigated the superior catalytic activity of hierarchical zeolites using the Friedel-Crafts alkylation of benzyl alcohol.[147-149] The alkylation of benzyl alcohol with benzene mechanism is illustrated in Scheme 1.6.

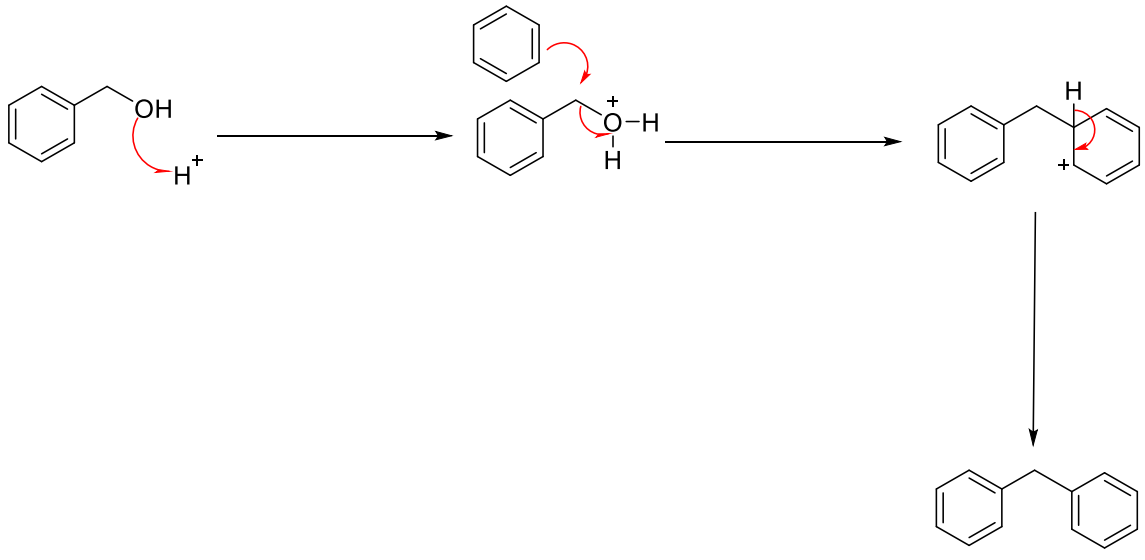

Scheme 1.6 Proposed mechanism of Friedel-Crafts alkylation of benzyl alcohol with benzene.

Sun et al.[147] compared hierarchical H-ZSM-5 prepared using an amphiphilic organosilane as a mesoporous directing agent. The hierarchical zeolite showed a larger uptake at higher relative pressure which suggests increased porosity. The hierarchical zeolite exhibited a type IV N_2 isotherm which confirmed the creation of mesoporosity with capillary condensation at relative pressure 0.3-0.6. In contrast, the conventional zeolite showed a type I isotherm which indicates a purely microporous material. Surface area measurements showed that the hierarchical zeolite was considerably larger than the conventional zeolite. Pore size distributions showed a large peak based around 4 nm. This is likely due to the tensile strength effect. Solid state NMR suggested that the aluminium environments were similar in both zeolites, consisting of mainly tetrahedral coordination with a smaller amount of extra-framework aluminium. The catalysts were calcined in air prior to the reaction. Typically, benzene (381 mmol) was added to a three-necked flask and heated to 80 ^{o}C and then benzyl alcohol (0.7 mmol) was added to the mixture and stirred for 3 hours. The conventional zeolite showed only 10% benzyl alcohol conversion after 10 hours. Remarkably, the hierarchical zeolite demonstrated >90% conversion using identical reaction conditions. The authors concluded that this was a direct consequence of increased mesoporosity in conjunction with strong acidity. Interestingly, the catalysts showed remarkably similar levels of conversion after 3 cycles which demonstrates excellent levels of reusability. These findings show the Friedel-Crafts alkylation of benzyl alcohol with benzene is an excellent probe reaction to show the formation of larger molecules. Also, this reaction is an excellent probe reaction to test the reusability properties of the solid acid catalyst.

1.9.2 The production renewable *p*-xylene by the Diels-Alder cycloaddition of furanics with olefins

Their unique physical and chemical properties have led to increased interest in the production of renewable *p*-xylene from bio-derived feedstocks. To the best of our knowledge, hierarchical zeolites prepared by top-down or bottom-up approaches have not been used to produce renewable *p*-xylene from the cycloaddition of DMF with ethylene. Studies showing the production of renewable *p*-xylene from DMF with ethylene in the liquid was discussed in section 1.5.3 with various solid acid catalysts (including conventional zeolites). However, to the best of our knowledge, there have been no prior

studies comparing the effect of conventional with hierarchical zeolites in the liquid or gas phase in the cycloaddition reaction of DMF with ethylene. Therefore, we believe this presents an exciting opportunity to study the effect of hierarchical zeolites on the cycloaddition of DMF, with a primary focus on the production of renewable *p*-xylene.

1.10 Objectives and thesis organisation

Chapter 1 provides a general introduction to biomass outlining the steps required to produce *p*-xylene from a second generation biofuel feedstock. Solid acid catalysts are discussed, particularly with a focus on the physical properties of H-ZSM-5, H-Beta and H-Y. Recent literature regarding the modification of zeolites to improve catalytic performance such as desillication and templating is discussed. In addition, alternative synthesis routes are presented, and the applications of mircrowave synthesis is highlighted.

Chapter 2 describes the experimental techniques, such as the characterisation of all zeolites that that have been used in this thesis. More in depth description of experimental work is separated into Chapters 3-5.

Chapter 3 reports the synthesis of hierarchical zeolites by a top down approach such as alkaline treatment. The physical and chemical properties are examined and tested in a Friedel-Crafts alkylation reaction to determine their catalytic activity. Our objective was to show desilication primarily leads to increased mesoporosity which would translate into higher catalytic activity. Future studies are reported to improve understanding of the effects of desilication on the physical and chemical properties of zeolites.

Chapter 4 reports the synthesis of conventional synthesis of H-ZSM-5 zeolites using microwave assisted heating. A hard templating agent was used to synthesise a hierarchical H-ZSM-5 by varying the synthesis parameters to optimise physical and chemical properties. The physical and chemical properties of the conventional and hierarchical zeolites were studied. The catalytic activities of the catalysts were compared using a Friedel-Crafts alkylation reaction with the objective of showing enhanced catalytic activity of the hierarchical zeolite due to enhanced mesoporosity. Future studies are discussed which could lead to enhance the physical and chemical properties of hierarchical H-ZSM-5 synthesised by microwave assisted heating.

Chapter 5 is focused on the study cycloaddition reaction of DMF with ethylene in the gas/liquid phase using hierarchical zeolites prepared in Chapters 3 and 4, and 5 by microwave assisted heating and conventional heating. The results are compared to a conventional zeolite with the objective of showing higher yields to aromatics, especially *p*-xylene for the hierarchical zeolite compared to the conventional zeolite. Reaction parameters were modified to attempt to optimise conversion and *p*-xylene yield. Preliminary investigations detailing the synthesis and characterisation of hierarchical ZSM-5 using conventional heating is discussed. Future studies discussed which could lead to improved yields of renewable *p*-xylene and improved understanding of product distribution.

Chapter 6 provides a summary of the findings from Chapters 3, 4 and 5 and some comments are given about future work.

Chapter 2

Experimental: Materials and Methods

2 Experimental: Materials and methods

2.1 Introduction

This chapter details the experimental techniques that were used for the zeolite synthesis, characterisation and testing of zeolite materials for the Friedel-Crafts alkylation of benzene with benzyl alcohol and the Diels-Alder cycloaddition of 2,5-dimethylfuran with ethylene in the liquid phase using a high pressure system. The supplier and purity of the materials used for this thesis will be detailed. Commercial zeolites were modified by alkaline treatment and compared to its untreated parent. Laboratory synthesised zeolites were synthesised using conventional or microwave assisted heating. Laboratory synthesised zeolites were modified and compared to its parent. Each zeolite was characterised to measure its physical and chemical properties such as crystallinity, acidity, thermal stability, surface area, porosity and morphology. The Brønsted (B) or Lewis (L) acid sites were identified and quantified. The silicon and aluminium content was measured and used to determine the SiO_2/Al_2O_3 molar ratio. This chapter also describes in detail the reaction procedures and details the reactor specifications used to carry out catalytic testing. The procedure used to quantify products will be discussed.

2.2 Chemicals and solvents

The following section describes the chemicals and solvents used for the synthesis of zeolites, followed by the post synthesis treatment using sodium hydroxide and ion exchange. After this, this section details the chemicals used for the synthesis of the hard templating agent and for reactions used for this thesis to test the catalytic activity.

2.2.1 Commercially unmodified zeolites

Commercial ZSM-5 zeolites were obtained in the ammonium form (CBV 3024E, SiO_2/Al_2O_3 = 30 and CBV 8014, SiO_2/Al_2O_3 = 80) from Zeolyst International. Commercial beta zeolite (CP814E SiO_2/Al_2O_3 = 25) was obtained from Zeolyst. Commercial beta zeolite (45874 SiO_2/Al_2O_3 = 38) was obtained from Alfa Aesar in the ammonium form. Commercial beta (45875 SiO_2/Al_2O_3 = 360) was obtained from Alfa

Aesar in the hydrogen form. Commercial Y zeolites were obtained from Alfa Aesar in the hydrogen form (45869, SiO_2/Al_2O_3 = 12 and 45872, SiO_2/Al_2O_3 = 80).

2.2.2 Chemicals used for desilication and ion exchange

Sodium hydroxide pellets were used for desilication of zeolites (Chapter 3) and were obtained from Fisher Scientific. Ammonium nitrate was used for ion exchange of zeolites (Chapters 3-5) and was purchased from Sigma Aldrich.

2.2.3 Chemicals used for the laboratory synthesises zeolites

In this subsection, the chemicals used for the synthesis of individual zeolites (Chapters 3-5) are described.

2.2.3.1 H-ZSM-5

The synthesis of H-ZSM-5 (Chapters 4-5) was carried out using the following chemicals: Tetraethoxysilane (98%) was purchased from Alfa Aesar. Tetra-propylammonium hydroxide (25% in water) was obtained from Fisher Scientific. Aluminium isopropoxide was obtained from Sigma Aldrich. All chemicals used for the synthesis of H-ZSM-5 were used without further purification.

2.2.3.2 H-Beta

The synthesis of H-Beta (Chapter 3) was carried out using the following chemicals: Colloidal silica (40% in water) was purchased from Sigma Aldrich. Tetra-ethylammonium hydroxide (25% in water) was purchased from Fisher Scientific. Sodium Aluminate (50-55% Al_2O_3) was obtained from Sigma Aldrich. All chemicals were used as received.

2.2.3.3 H-Y

The synthesis of H-Y (Chapter 3) was carried out using the following chemicals: Sodium hydroxide pellets were purchased from Fisher Scientific. Sodium Aluminate (50-55%

Al_2O_3) was obtained from Sigma Aldrich. Colloidal silica (40% in water) was purchased from Sigma Aldrich. All chemicals were used as received.

2.2.3.4 Chemicals used for the synthesis of polystyrene nanospheres

The synthesis of polystyrene (Chapters 4-5) was carried out using the following chemicals: Sodium hydroxide pellets were purchased from Fisher Scientific. Styrene (99%) was obtained from Sigma Aldrich. Ammonium persulfate (98%) and sodium dodecyl sulfate (General purpose grade) were obtained from Fischer Scientific. With the exception of styrene, all chemicals were used without further purification.

2.2.4 Chemicals used for Friedel-Crafts alkylation of benzyl alcohol with benzene

The Friedel-Crafts alkylation of benzyl alcohol with benzene (Chapters 3-4) was carried out using the following chemicals: beznene (99%) was obtained from Alfa Aesar and was used as a solvent. Benzyl alcohol (99%) was obtained from Alfa Aesar and used as a substrate. Tridecane (≥99%) was used an internal standard and purchased from Sigma-Aldrich. All chemicals were used as received.

2.2.4.1 Calibration standards used for the Friedel-Crafts alkylation of benzyl alcohol with benzene

Diphenylmethane (99%) and dibenzyl ether (98%) were purchased from Alfa Aesar. Tridecane (≥99%) was used an internal standard and purchased from Sigma-Aldrich. Both of these standards were used without further purification.

2.2.5 Chemicals used for the cycloaddition of 2,-5-dimethylfuran with ethylene

2,5-dimethylfuran (99%) was obtained from Sigma-Aldrich. The diene (brown liquid) was distilled using a rotary evaporatory (40 torr, 45^{o}C) to separate DMF from the heavy contaminants. A transparent liquid was obtained and used for subsequent reactions. Hexane (HPLC grade Fisher Scientific), octane (98%) and dodecane (99%) were used as

solvents and obtained from Alfa Aesar. Tridecane (≥99%) was used an internal standard and purchased from Sigma-Aldrich. Ethylene (CP grade N3.0) was obtained from The BOC Group. All chemicals with the exception of 2,5-dimethylfuran in this section were used as received

2.2.5.1 Calibration standards used for cycloaddition of 2,-5-dimethylfuran with ethylene

p-xylene (99%) was obtained from Alfa Aesar. 2,5-hexanedione (≥98.5%) was obtained from Sigma-Aldrich. 1,4-dimethyl-2-(4-methylbenzyl)benzene (CPR) was used as a calibration standard for alkylated aromatics. 3-methyl-2-cyclopentenone (97%) was obtained from Sigma-Aldrich.

2.3 Characterisation techniques

In the following subsections, the techniques used to characterise the hard templating and agent and zeolite structures are described. The particle size of polystyrene was used using dynamic light scattering. Our zeolite structures were characterised using a wide range of techniques. Firstly, XRD measurements were carried out to determine the effect of alkaline treatment on the parent zeolite in Chapter 3 on the relative intensity of the peaks compared to their untreated parent. The relative intensity of the peaks were used to measure semi-quantitatively the zeolite crystallinity. For our laboratory zeolites in Chapters 4 and 5, XRD was used to compare our structure to a zeolite reference from the International Zeolite Association (IZA). Surface area and porosity measurements were used to determine the specific surface surface areas for; commercially unmodified (Chapter 4), alkaline treated using sodium hydroxide (Chapter 4) and laboratory synthesised zeolites (Chapters 4 and 5). Temperature programme desorption used to determine the acid site density of all commercial, commercially modified and laboratory synthesised zeolites. Fourier Transform Infrared Spectroscopy (FT-IR) was used to measure qualitatively the polystyrene nanospheres (Chapter 5) and our laboratory synthesised H-ZSM-5 (Chapter 5). Diffuse reflectance infrared Fourier transform (DRIFT) was used to distinguish between Brønsted (B) and Lewis (L) sites for commercially unmodified and alkaline treated H-ZSM-5 (Chapter 3). Solid state NMR

studies were used to determine the coordination of the silicon and aluminium species for commercially unmodified zeolites (Chapter 4), alkaline treated using sodium hydroxide (Chapter 4) and laboratory synthesised zeolites (Chapters 4 and 5). Scanning Electron Microscopy (SEM) was used to show the effect of alkaline treatment of morphology of H-ZSM-5 (Chapter 3) and to the morphology and particle size of our laboratory synthesised zeolites (Chapter 4). In addition, SEM was used to demonstrate the shape of the hard templating agent (Chapter 5). Inductively coupled plasma optical emission spectroscopy (ICP-OES) was used to measure the SiO_2/Al_2O_3 molar ratio for commercial, alkaline treated and laboratory synthesised zeolites (Chapters 3-5). Thermogravimetric analysis (TGA) was used to determine the thermal stability of all zeolitic materials (Chapters 3-5) and to determine the thermal stability of the hard templating agent PS) up to 550 ^oC.

2.3.1 Dynamic light scattering (DLS)

All DLS measurements were performed using a Malvern Instrument Zetasizer Nano Series ZSP (Malvern Instruments, Westborough, MA, USA). Typically, 1 mL of particle suspensions were placed in a 10 mm × 10 mm and measured 3 times, using the average as the final measurement. All samples were analysed by the author.

2.3.2 X-Ray diffraction (XRD)

X-ray diffraction was carried out using Panalytical X'Pert PRO HTS X-ray diffractometer equipped with Ge monochromator giving Cu Kα radiation ($\lambda = 0.154$ nm). In a typical procedure the catalyst was ground to a very fine powder and placed in a sample holder. Data were recorded in the 2θ range of 5-50^o at room temperature by transmission. This service was provided by the Centre of Materials Discovery which is available in the Department of Chemistry at Liverpool University. Samples were submitted by the author and ran by Mr Rob Clowes.

2.3.3 Surface area and porosity measurements

Nitrogen sorption isotherms were measured using a Micromeritics ASAP 2020 at 77 K. Approximately 100 mg of sample was used for analysis and degassed under vacuum overnight at 300 ^{o}C. The specific surface area was determined using the BET equation by 5 point measurements between relative pressures (P/P_o) of 0.05-0.3. Single point adsorption taken at P/P_o equal to 0.99 was used to determine the total pore volume. The micropore volume was calculated using Hovarth-Kawazoe (Saito-Foley) model up to 2 nm pore size. Pore size distributions were measured using the Barrett-Joyner-Halenda (BJH) adsorption method. The external pore volume was calculated as the difference between the micropore volume measured using the Saito-Foley model and total pore volume measured using a single point adsorption measurement.

Figure 2.1 Image of Micromeritics ASAP 2020 used for specific surface area and porosity measurements.

2.3.4 Temperature programmed desorption studies using ammonia

Temperature desorption of ammonia (NH_3-TPD) was carried out using Micromeritics Autochem II 2920 equipped with a thermal conductivity detector. The sample (50 mg) was pre-treated in air at 550 °C at a rate of 5 °C min^{-1} and held for 60 minutes. The gas

flow was then changed from air to helium and flowed at a rate of 20 cm^3 min^{-1} for 20 minutes. The sample was then cooled to 150 °C. 5 % NH_3/He mixture was flowed at a rate of 20 cm^3 min^{-1} for 30 minutes. The gas was changed to helium and flowed at a rate of 20 cm^3 min^{-1} for 30 minutes. The sample was then heated to 700 °C at a rate of 10 ^oC min^{-1}. The author ran the measurements.

Figure 2.2 Image of Micromeritics Autochem II 2920 used to determine total acid strength.

2.3.5 Fourier Transform Infrared Spectroscopy (FT-IR)

FT-IR spectra were performed using FT/IR-4100 typeA (Jasco). Measurements were recorded in the range 4000-600 cm^{-1} (resolution 4 cm^{-1}) and 150 accumulations were recorded for each sample. Measurements were carried out by the author.

Figure 2.3 Image of Nicolet NEXUS FTIR spectrometer used to distinguish between Brønsted (B) and Lewis (L) sites.

2.3.6 Diffuse reflectance infrared Fourier transform (DRIFT)

Diffuse reflectance infrared Fourier transform (DRIFT) spectra of catalysts were taken on a Nicolet NEXUS FTIR spectrometer using powdered catalyst mixtures with KBr. H-ZSM-5 was mixed with KBr in a 4:1 weight ratio. The powder was pre-treated at 150 ^{o}C / 0.01 kPa for 60 minutes under vacuum. The sample was dried under a flow of nitrogen. Pyridine was dropped onto the sample. The samples were exposed to pyridine under an atmosphere of nitrogen for 60 minutes and then degassed at 150 ^{o}C to remove physisorbed pyridine. The Brønsted (B) and Lewis (L) sites were determined using peak intensities at 1540 cm^{-1} and 1450 cm^{-1} respectively. These measurements was carried out by the author in Professor Ivan Kozehnikov's laboratory at the Department of Chemistry in Liverpool University with the assistance of Dr Hossein Bayahia.

2.3.7 Solid state NMR

NMR spectra were obtained at the EPSRC UK National Solid-state NMR service at Durham University. ^{27}Al and ^{29}Si MAS-NMR spectra were recorded using Varian 4000 VNMRS spectrometer at 104.2 MHz, room temperature, in 4 mm rotor with spinning rate of 14 kHz for aluminium and 6.8 kHz for silicon with "onepul" pulse sequence, direct excitation, 1 us pulse duration, 10 ms acquisition time, 200 ms recycle time, collected 7000 transients, spectral width 416.7 kHz. Neat tetramethylsilane and 1M aqueous aluminium nitrate were used as references.

2.3.8 Scanning Electron Microscopy (SEM)

The morphology of the samples was measured using Scanning Electron Microscopy (SEM). SEM was carried out using Hitachi S-4800 Field Emission Scanning Electron Microscope. Samples were placed on carbon tabs and coated with gold to prevent charge build up. Drs Luigi Via or Peter Priecel ran the measurements.

Figure 2.4 Image of Hitachi S-4800 Field Emission Scanning Electron Microscope used to determine morphology and particle size.

2.3.9 Inductively coupled plasma atomic emission spectroscopy (ICP-OES)

For ICP-OES measurements, approximately 10 mg of zeolite was dissolved in 1 M NaOH (10 mL) in a polypropylene beaker and stirred under ambient conditions overnight. The amount of Si and Al in the suspension was measured and used to calculate Si/Al ratios. Each value of Si and Al was measured three times and averaged. ICP measurements were performed by the Analytical services within the Department of Chemistry by Mr George Miller or Dr Konstantin Luzyanin using instrument ICP-OES-SoP, Spectro Ciros CCD.

2.3.10 Thermogravimetric analysis (TGA)

Thermogravimetric analysis (TGA) was carried out using TA Instruments Q5000IR TGA equipped with a 25 position integrated sample holder. This service was provided by the Centre of Materials Discovery at the Department of Chemistry in Liverpool University. Typically, <10 mg of sample was placed in an aluminium pan. The sample was heated under air at a heating rate of 20 ^{o}C min^{-1} to 550 ^{o}C with a flow rate of 10 ml min^{-1}. The author ran the measurements.

Figure 2.5 Image of TA Instruments Q5000IR TGA used to measure thermal stability.

2.4 Synthesis of zeolites using conventional and microwave assisted heating

In this section, the reactors used to synthesise H-ZSM-5 using conventional heating methods (Chapter 5) is shown. In addition, the reactors used to synthesise H-ZSM-5, H-Beta and H-Y using microwave assisted heating methods (Chapters 3-4) are shown.

2.4.1 Synthesis of zeolites using conventional heating methods

The synthesis of H-ZSM-5 using conventional heating was carried out using a General Purpose Oven (Genlab, Model number PRO/50) as shown in Figure 2.6.

Figure 2.6 Image of oven used to synthesis H-ZSM-5 using conventional heating.

2.4.2 Synthesis of zeolites using microwave assisted heating

The microwave synthesis of H-ZSM-5 (Chapters 3-5), H-Beta (Chapter 3) and H-Y (Chapter 3) was carried using microwave assisted heating (CEM Discover SP) with a maximum power of 300 W.

Figure 2.7 Image of CEM Discover SP used to synthesise various zeolites and the Friedel-Crafts alkylation of benzyl alcohol with benzene.

2.5 Catalytic testing techniques

This section provides information regarding the catalytic testing reactors used in this thesis. In Chapters 3 and 4, we tested the Friedel-Crafts alkylation of benzyl alcohol with

benzene with microwave assisted heating in the liquid phase. In Chapter 5, the liquid phase cycloaddition of DMF with ethylene was carried out with varying temperatures and pressures. In this section, the experimental setups for both reactions are described here.

2.5.1 Friedel-Crafts alkylation of benzyl alcohol with benzene

The Friedel-Crafts alkylation of benzyl alcohol with benzene out (Chapters 3 and 4) was carried using microwave assisted heating (CEM Discover SP) with a maximum power of 300 W as shown in section 2.4.2.

2.5.2 Production of renewable *p*-xylene by the Diels-Alder cycloaddition of 2,5-dimethylfuran (DMF) with ethylene

In this subsection, the experimental setup detailing the Diels-Alder cycloadditon of DMF with ethylene using various temperatures and pressures (Chapter 5) is presented. Firstly, preliminary experiments were carried out to determine whether zeolites were active using our experimental setup. Then, extensive studies were carried out using a high throughput system. Separately, time online studies were performed to quantify products formed after specific reaction times.

2.5.2.1 Preliminary experimental setup

Preliminary experiments were carried out using a 45 mL closed Parr model 4717 pressure reactor. The set-up is shown in Figure 2.8.

Figure 2.8 Image of the reactor setup used for preliminary experiments in Diels-Alder cycloaddition of 2,5-dimethylfuran (DMF) with ethylene.

2.5.2.2 Catalytic testing setup

After preliminary experiments had been carried out as shown in section 2.5.2.1, H-ZSM-5, H-Beta and H-Y zeolites were tested over a range of temperatures and pressures. The reactions were carried out using a multiple reactor system (Parr series 5000). The reactor setup is shown below.

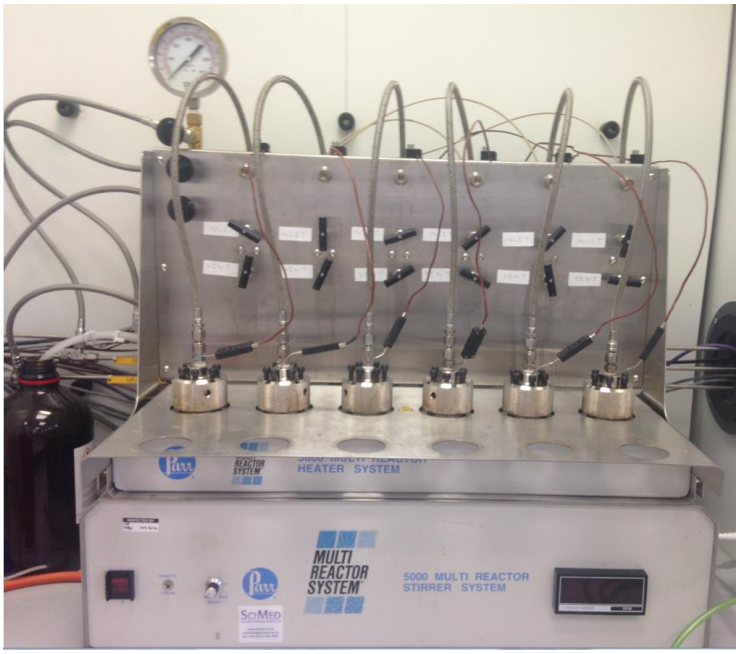

Figure 2.9 Image of the reactor used for the Diels-Alder cycloaddition of 2,5-dimethylfuran (DMF) with ethylene.

2.5.2.3 Time online experimental setup

Time online studies (Chapter 5) were carried out using a 50 mL Parr Micro Stirred reactor (series 4590) equipped with a 4848 temperature controller equipped with a temperature and pressure display. The reactor setup is shown in Figure 2.10.

Figure 2.10 Image of the reactor used for time online experiments.

2.6 Product analysis by Gas Chromatography-Flame ionisation Detector (GC-FID)

GC (Agilent series 7820A, HP-5 capillary column, 30 m, 0.32 mm, 0.25 μm) using flame ionisation detector was used to perform quantitative measurement of reaction products. 3 Measurements were taken for each sample (automatic liquid sampler) and averaged. The inlet port was held at a temperature of 280 ^{o}C and pressure of 20.4 psi with a split of 30:1. The flow in the column was kept at 0.5 mL min^{-1} with an average column velocity of 10.3 cm s^{-1} through the oven ramp cycle. The cycle started with an initial oven temperature of 50 ^{o}C and held at this temperature for 1 minute before ramping to 90 ^{o}C at a heating ramp rate of 20 ^{o}C min^{-1} before instantly ramping to 250 ^{o}C with a ramp rate of 30 ^{o}C min^{-1}. This was held for 2 minutes.

2.7 Product concentration determination

The method used to calibrate reaction products in this thesis was the internal standard method. A concentration of a known standard was injected into the GC using tridecane an internal standard, which concentration was constant throughout. The ratio of the peak

areas against the tridecane was used to determine the product concentration of the products. A summary of the results obtained for each reaction can be found in the subsequent subsections.

2.7.1 Friedel-Crafts alkylation of benzyl alcohol with benzene

This subsection provides information on the calibration of chemicals used in the Friedel-Crafts alkylation of benzyl alcohol with benzene. Typically, 5 volumetric flasks of known concentrations were prepared. Each sample was injected into the GC 3 times (1µL each), with the area of the product divided by the area of the internal standard. The final concentration was measured as an average of the 3 injections. A plot of $Concentration_{product}$ versus $Area_{product}/Area_{tridecane}$ was made for each standard. After the separation of the products at the end of the reaction, the concentration of the products were calculated based on the calibration plot. The calibration plots showed a linear response between $Concentration_{product}$ versus $Area_{product}/Area_{tridecane}$, with a linear regression coefficient $R^2 > 0.95$ were obtained for all the products. The calibration profiles of all products can be found in the appendix. To save space, the results are presented in tabular form here and can be found in Table 2.1.

Table 2.1 Calibration curve and retention times obtained for standards used in Friedel-Crafts alkylation of benzyl alcohol with benzene.

Chemical	Range (M)	Retention time (mins)	Equation	R^2
Benzene	-	1.09	-	-
Benzyl alcohol	$1x10^{-2}$ - 0.24	3.49	y = 0.0569x + 0.0012	0.99664
Tridecane	-	5.02	-	-
Diphenylmethane	6×10^{-3} -0.15	5.69	y = 0.0276x + 0.0064	0.95355
Dibenzyl ether	$1x10^{-2}$ -0.20	6.85	y = 0.03035x – 0.0034	0.99714

2.7.2 Diels-Alder cycloaddition of 2,5-dimethylfuran (DMF) with ethylene

The method used to quantify the products for the Diels-Alder cycloaddition of 2,5-dimethylfuran (DMF) with ethylene was identical to the method shown in section 2.7.1. The alkylated products were quantified using the calibration curve of 2-ethyl-*p*-xylene. The higher aromatics were analysed semi-quantitatively using a single point measurement, by separating the final mixture by silica gel chromatography using petroleum ether and ethyl acetate. Since the resulting chromatogram showed traces of other products apart from higher aromatics, it was acknowledged that there would be experimental error. The molecular weight of the higher aromatics was assumed to be 209 based on the study by Do et al.[150] A summary of the results obtained for the calibration plots are shown in Table 2.2.

Table 2.2 Calibration curve and retention times obtained for standards used in the Diels-Alder cycloaddition of 2,5-dimethylfuran (DMF) with ethylene.

Chemical	Range (M)	Retention time (mins)	Equation	R^2
Hexane	-	0.89	-	-
Octane	-	1.78	-	-
Dodecane	-	4.70	-	-
2,5-dimethylfuran	5×10^{-2} -3.12	1.20	y = 0.2828x + 0.0301	0.99878
p-xylene	2×10^{-3} -2.35	2.00	y = 0.18557x – 0.0204	0.9991
2,5-hexanedione	8×10^{-3}-0.06	2.62	y = 0.3205x + 0.0012	0.99424
3-methyl-2-cyclopentenone	1×10^{-2} -0.10	2.92	y = 0.3116x + 0.0019	0.99959
2-ethyl-*p*-xylene	1×10^{-2} -0.50	3.81	y = 0.15839 x – 0.0055	0.99816
Tridecane	-	5.02	-	-

Chapter 3

Microwave Synthesis of H-ZSM-5, H-Beta and H-Y and their Desilication to Hierarchical structures for Friedel-Crafts Alkylation

3 Microwave synthesis of H-ZSM-5, H-Beta and H-Y and their desilication to hierarchical structures for Friedel-Crafts alkylation

3.1 Introduction

The Friedel-Crafts alkylation reaction is an electrophilic aromatic substitution reaction developed by Charles Friedel and James Crafts in 1877 and is an important reaction in organic chemistry.[151] Liquid phase alkylation reactions have been carried out using Lewis acid catalysts such as iron (III) chloride and aluminium chloride.[152, 153] However, there are many limitations with these homogeneous catalysts; firstly, they are corrosive, separation is difficult and involves costly and time consuming processes. Additionally, they are moisture sensitive and require an inert atmosphere. Hence, great efforts have been made to overcome these problems by using heterogeneous solid acid catalysts. Zeolites are widely used, particularly in the petrochemical industry. They have received particular attention due to their high thermal stability, tuneable acidity and regular pore structure. The liquid phase benzylation of benzyl alcohol (BA) is a key reaction for the production of diphenylmethane (DPM), which is used in the pharmaceutical and fine chemical industry. There have been numerous studies that investigated the Friedel-Crafts alkylation of benzyl alcohol using benzene with zeolites as a solid acid catalyst.[147-149] However, poor catalytic activity was obtained due to diffusion limitations. Alkaline treatment of zeolites has shown to be an excellent strategy for the generation of mesoporosity, reducing diffusion limitations.[154] Studies that have been carried out using alkaline treatment are based H-ZSM-5, with an extensive review written by Verboekend et al.[155] in 2011. Work led by Perez-Ramirez has investigated the effect of alkaline treatment on the physical and chemical properties of H-ZSM-5.[129, 154, 156] This is not limited to H-ZSM-5. Previous work has demonstrated enhanced porosity for H-Beta and H-Y after alkaline treatment.[157,158] In this study, we report alkaline treatment of commercial H-ZSM-5, H-Beta and H-Y, increasing mesoporosity. Synthesis of zeolites using microwave assisted heating is proving to be a highly efficient alternative method for the synthesis of zeolites due its shorter synthesis times. Microwave synthesis of H-ZSM-5 has been widely reported in the literature as shown in the review by Li et al.[107] However, the number of studies showing synthesis of H-Beta and H-Y using microwave assisted heating is limited. In this study, we report the synthesis of H-ZSM-5, H-Beta and H-Y in 14 hours, or less, with surface areas and porosity comparable to conventional zeolites supplied by a common manufacturer of zeolites. All catalysts were characterised by XRD, nitrogen adsorption-

desorption, ICP-OES, TPD-NH_3, ^{27}Al MAS-NMR and ^{29}Si MAS-NMR. Additionally, FTIR-pyridine was used to quantify the acid sites and SEM was used to determine the morphological changes of H-ZSM-5. We then tested the hierarchical zeolites, modified by alkaline treatment on the Friedel-Crafts alkylation of benzyl alcohol with benzene as a probe reaction to evaluate the effect of enhanced porosity on catalytic activity.

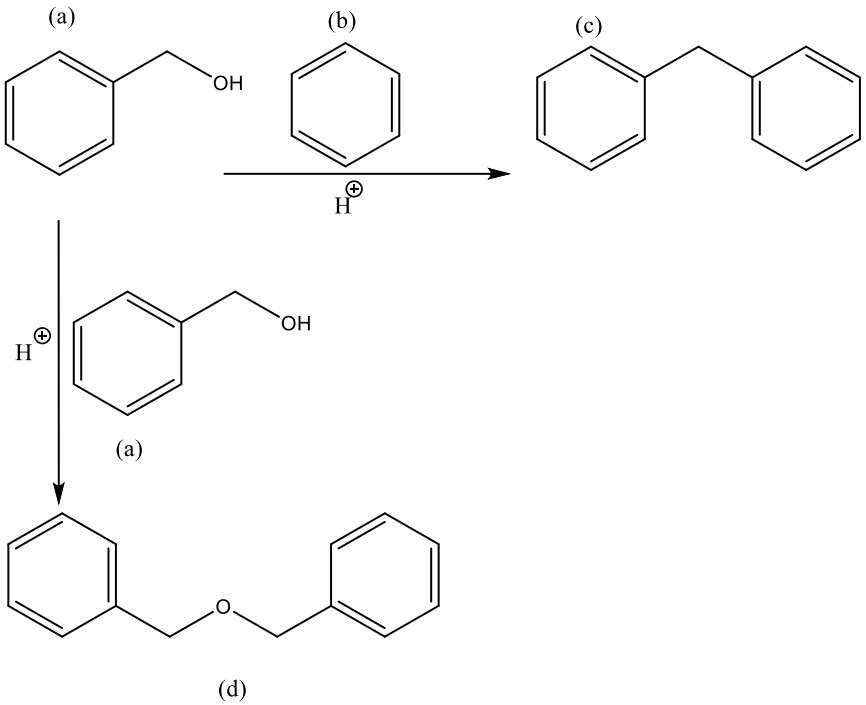

Scheme 3.1 Reaction pathway of the Friedel-Crafts alkylation of benzyl alcohol with benzene. (a) benzyl alcohol, (b) benzene, (c) diphenylmethane, (d) dibenzyl ether.

3.2 Experimental

In this section, the preparation of H-ZSM-5, H-Beta and H-Y using microwave assisted heating is described. Then, the modification of these zeolites using alkaline treatment using sodium hydroxide is presented. Finally, experimental details on the Friedel-Crafts alkylation of benzyl alcohol is detailed.

3.2.1 Preparation of H-form zeolites from commercial zeolites

The ammonium form of ZSM-5 was treated at 550 °C for 6 hours in static air with a heating ramp of 1 °C min^{-1} to produce the proton form of the same material. This was

repeated for subsequent calcinations. The parent samples are denoted as zeolite-silica-alumina ratio. For example, the parent H-ZSM-5 with a SiO_2/Al_2O_3 ratio equal to 30 is denoted as H-ZSM-5 (30).

3.2.2 Synthesis of H-ZSM-5, H-Beta and H-Y by microwave assisted heating

In this section, the synthesis of H-ZSM-5, H-Beta and H-Y by microwave assisted heating is discussed. The chemical composition, particularly SiO_2/Al_2O_3 molar ratios and synthesis parameters are presented.

3.2.2.1 H-ZSM-5

Conventional zeolite ZSM-5 was synthesised using microwave assisted heating based on the method from Jin et al.[108] from a precursor solution which contained tetraethoxysilane (TEOS) as the silicon source, 25% in water t-propylammonium hydroxide (TPAOH) as the structure directing agent, aluminium isoproxide (AIP) as the aluminium source and water as the solvent. Our method was based in the following molar ratio composition: 100 SiO_2:Al_2O_3:11.5 TPAOH:1000 H_2O. In typical synthesis aluminium isopropoxide was dissolved in water and TPAOH. Upon complete dissolution of aluminium isopropoxide, TEOS was added and stirred overnight for complete hydrolysis of TEOS. 23 mL of the precursor solution was placed into a 35 mL vial and heated by microwave assisted heating at 165 ^oC for 6 hrs. The solution was filtered and dried overnight at 100 ^oC. The powder was brought into its ammonium form by ion exchange with 1 M ammonium nitrate at 80 ^oC for 2 hours. A ratio of 50 mL g^{-1} was used. The zeolite was brought into its H-form by calcination as described in section 3.2.1.

3.2.2.2 H-Beta

The synthesis of H-Beta zeolite was a modification of the based on the method devised by Kim et al.[159] using microwave assisted heating. Our study did not involve optimisation sysnthesis studies. H-Beta was synthesised from a precursor gel which contained colloidal silica (40 wt%) as the silicon source, 25% in water t-ethylammonium hydroxide (TEAOH) as the structure directing agent, sodium

aluminate (45-50 wt% Al_2O_3) as the aluminium source and water as the solvent. The solutions were prepared based on the following molar ratio composition: SiO_2:0.1 Al_2O_3 :0.35 TPAOH : 11.6 H_2O. Colloidal silica, TEAOH and water were stirred at ambient conditions in a conical flask until a transparent solution appeared. In a separate flask, sodium aluminate was dissolved in water and then added to the first mixture. 23 mL of the precursor solution was placed into a 35 mL vial and heated by microwave irradiation at 140 ^oC for 14 hrs. The solution was filtered and dried overnight. The powder was brought into its ammonium form and then its proton by ion exchange with 1 M ammonium nitrate at 80 ^oC for 2 hours. A ratio of 50 mL g^{-1} was used. The zeolite was brought into its H-form by calcination as described in section 3.2.1.

3.2.2.3 H-Y

The synthesis of FAU was a modification of the work based on the seeding gel and feedstock gel two step synthesis method by Karge et al.[160] Our method was carried out using microwave assisted heating instead of conventional heating. Our method was based on using the synthesised time based on the synthesis of H-ZSM-5 using microwave assisted heating. Optimisation synthesised studies were not carried out. Sodium hydroxide and sodium aluminate were stirred in deionised water until complete dissolution. Colloidal silica was then added to the mixture and stirred for one hour. The solution was aged at room temperature for 24 hours without stirring. The molar composition of the seeding gel was: 10 SiO_2 : Al_2O_3 : 10.7 Na_2O : 180 H_2O. The following method describes the synthesis of the feedstock gel. Sodium hydroxide, sodium aluminate was added to water and stirred until complete dissolution of the solids. Colloidal silica was then added to the mixture and left until the gel became homogenous. The molar composition of the feedstock gel was: 10 SiO_2: Al_2O_3 : 4.3 Na_2O : 180 H_2O. The feedstock gel was then added to the seeding gel using a 95:5 feedstock/ seeding gel solution (w/w). The mixture was stirred for 30 minutes and, 23 g of the mixture was transferred to a 35 mL microwave vial and at 100 ^oC for 6 hours under microwave irradiation.

3.2.3 Preparation of hierarchical zeolite by alkaline treatment

The synthesis of hierarchical zeolite was based on the work by Groen et al.[156] The desilication procedure was performed by treating the ammonium form of the zeolite with

0.2 M sodium hydroxide (30 mL g^{-1}). The mixture was stirred for 30 minutes at 65 °C and then quenched in an ice bath to prevent further desilication. The slurry was filtered using Whatman grade 1 filter paper. The sample was washed with an abundant amount of water and dried overnight in an oven at 110 °C. The desilicated catalyst was converted to the ammonium form by treating the sample with 1 M ammonium nitrate for 120 minutes at 80 °C (20 mL g^{-1}). The suspension was cooled, and then filtered under vacuum and dried overnight at 110 °C. Finally, the zeolite was converted from the ammonium form into the proton form by calcination as described in section 3.2.1. Identical conditions were used for H-Beta and H-Y zeolites. Alkaline treated zeolites are denoted as zeolite-silica to alumina ratio-concentration of alkaline treatment. For example, H-ZSM-5 with a SiO_2/Al_2O_3 molar ratio of 30 treated with 0.2 M solution of NaOH is denoted as H-ZSM-5 (30.2).

3.2.4 Friedel-Crafts alkylation of benzyl alcohol with benzene using microwave assisted heating

Friedel-Crafts alkylation of benzyl alcohol with benzene was carried out as follows; Benzyl alcohol (3.18 mmol), benzene (253 mmol) and tridecane (0.67 mmol) in the presence of a catalyst (70 mg) were placed in a 35 mL microwave vessel (standard vessel). All reactions were carried out at 100 °C for 6 hours with stirring under microwave assisted heating. After the reaction, the liquid was allowed to cool to room temperature. The liquid phase was separated from the spent catalyst by centrifugation at 14,000 rpm for 5 minutes. Due to the excessive amount of benzene, conversion was calculated based on the concentration of benzyl alcohol. The conversion, yield and mass balance was calculated as shown in Equation 3.1

$$\text{Conversion}_{BA}\ (\%) = \frac{[BA]_{initial} - [BA]_{end}}{[BA]_{initial}} \text{ x } 100$$

$$\text{Yield}_{product}\ (\%) = \frac{[product]}{[BA]_{initial}} \text{ x } 100$$

$$\text{Mass balance}\ (\%) = \frac{\sum[\text{known products} + BA_{end}]}{[BA]_{initial}} \text{ x } 100$$

Equation 3.1 Equations used to determine conversion, yield and mass balance.

3.3 Results and discussion

In this section, the physical and chemical properties of zeolites are presented and discussed in detail. H-ZSM-5 (30 and 80) were subjected to alkaline treatment of 0.2 and 0.4 M NaOH, whereas H-ZSM-5 (100) was treated with 0.2 M NaOH only. H-Beta and H-Y were treated with 0.2 M NaOH only.

The results of the characterisation techniques are presented in the following order; XRD and elemental analysis, nitrogen adsorption-desorption, TPD-NH_3, FT-IR-pyridine adsorption, solid state NMR and microscopy studies. The physical and chemical properties of alkaline treated zeolites with its untreated parent. Catalyst characterisation analyses will be shown in the order: H-ZSM-5, H-Beta and H-Y. The results of the Friedel-Crafts alkylation of benzyl alcohol with benzene as a probe reaction are discussed, investigating the effect of porosity and acidity on catalytic activity.

3.3.1 XRD and Elemental analysis

Powder X-ray diffraction (XRD) was recorded in the 2θ angle range of 5-50^o for all zeolites and their alkaline treated counterparts. Crystallinities of all alkaline treated zeolites were measured semi-quantitatively, using the most intense peak of the parent. Unless stated otherwise, the same scale was used for the y axis for the parent and alkaline modified zeolites.

ICP-OES was used to determine the effect of alkaline treatment on SiO_2/Al_2O_3 molar ratios. The SiO_2/Al_2O_3 molar ratio was calculated using the concentrations of Si and Al in ppm and using the molecular weight of SiO_2 and Al_2O_3. Thermogravimetric analysis

(TGA) was used to determine the stability of all zeolites and observing the weight loss at temperatures ~550 ºC under air flow, simulating calcination conditions.

3.3.1.1 H-ZSM-5

The parent H-ZSM-5 zeolite was compared to the alkaline treated zeolite and the intensity of the [101] peak in the 2θ angle 7.9º was used for the crystallinity calculation; assuming 100% crystallinity for the commercially untreated H-ZSM-5 zeolite. A similar method calculating crystallinity using the parent as a standard was used by Xing et al.[161] The physical and chemical properties of H-ZSM-5 zeolites are displayed in Table 3.1 (below)

Table 3.1 Physical and chemical properties of untreated and alkaline treated H-ZSM-5 zeolites.

Catalyst	NaOH treatment (M)	Theoretical SiO_2/Al_2O_3 ratio[a]	Experimental SiO_2/Al_2O_3 ratio[b]	Crystallinity (%)[c]	Weight loss at 550 ºC (%)[d]	Yield (%)[e]
H-ZSM-5 (30)	0	30	28	100	7.1	100
H-ZSM-5 (30)	0.2	-	23	92	7.5	75
H-ZSM-5 (30)	0.4	-	20	87	7.5	69
H-ZSM-5 (80)	0	80	71	100	5.5	100
H-ZSM-5 (80)	0.2	-	49	84	7.4	41
H-ZSM-5 (80)	0.4	-	31	31	6.5	32
H-ZSM-5 (100)	0	100	115	100	3.3	n/a
H-ZSM-5 (100)	0.2	-	131	43	3.6	n/a

(a) displayed by manufacturer, (b) determined by ICP-OES (c) determined by XRD
(d) determined by TGA and (e) final mass (g) / initial mass before desilication (g)

Table 3.1 provides information regarding the desilication procedure. Treatment of H-ZSM-5 (30) with 0.2 and 0.4 M NaOH showed a yield of 75% and 69% for H-ZSM-5 (30.2) and H-ZSM-5 (30.4) respectively. This shows the loss of the structure after the desilication process. In comparison, treatment of H-ZSM-5 (80) with 0.2 and 0.4 M NaOH with 0.2 and 0.4 M NaOH substantially reduced the yield to 41% and 31% for H-ZSM-5 (80) and H-ZSM-5 (80.4). This confirms that alkaline treatment extracted and removed a significant amount of the zeolite structure, and was lost during the washing stage.

All H-ZSM-5 samples showed reflections based on the diffractograms of the reference H-ZSM-5 from the International Zeolite Association (IZA), showing reflections for 2θ angles; 7.9, 8.8, 23.1º for the peaks associated with the [hkl]

planes [101], [020] and [501] respectively. It was found that unmodified and alkaline treated H-ZSM-5 catalysts, calcined at 550 ^{o}C under oxidising conditions generally matched the XRD patterns as shown in the literature.[162] The XRD diffractograms of the commercially untreated and alkaline treated H-ZSM-5 (30, 80 and 100) zeolites are shown in Figures 3.1-3.3 respectively.

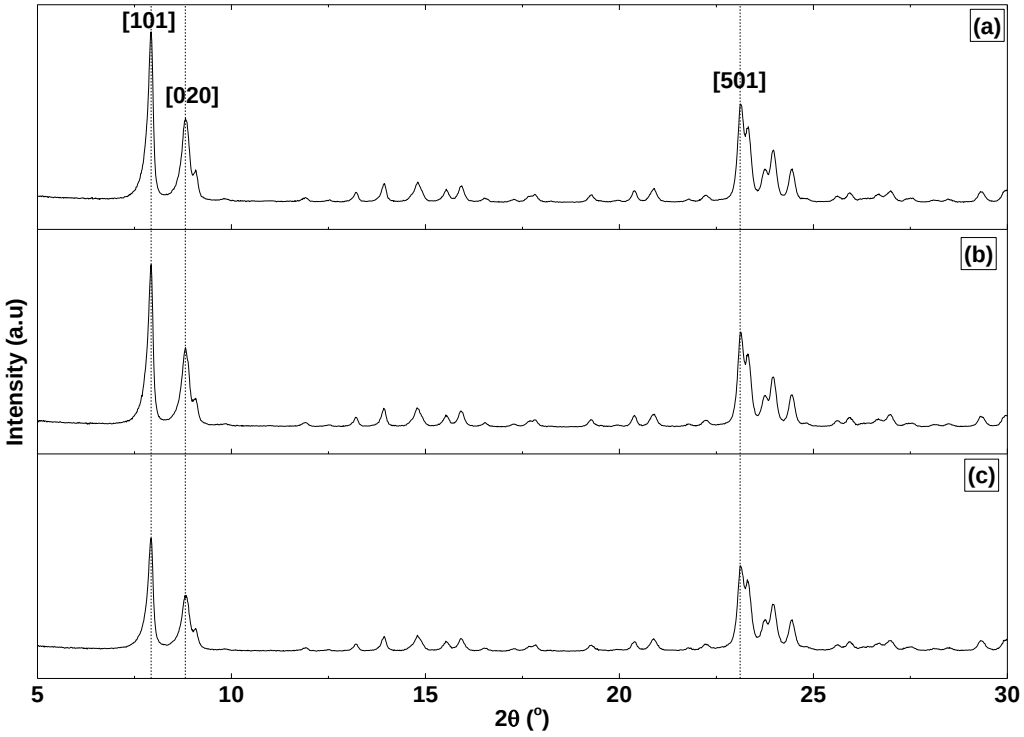

Figure 3.1 XRD diffractograms of untreated and alkaline treated H-ZSM-5 (30) zeolites; (a)H-ZSM-5 (30), (b) H-ZSM-5 (30.2) and (c) H-ZSM-5 (30.4).

The XRD diffractograms of H-ZSM-5 (30, 30.2 and 30.4) are shown in Figure 3.1 It was found that treatment of H-ZSM-5 (30) with 0.2 M NaOH reduces crystallinity to 92% as evidenced by the presence of diffraction lines [101], [020] and [501], typical of H-ZSM-5 diffraction patterns. This suggests that the overwhelming majority of aluminium atoms in the parent are located in the framework position. Treatment of H-ZSM-5 (30) up to 0.4 M NaOH decreased crystallinity to 87 % of the original zeolite. This shows that H-ZSM-5 (30) is largely resistant to treatment of sodium hydroxide up to 0.4 M. Under the treatments utilised, a progressive reduction in crystallinity is observed when the concentration of sodium hydroxide increases.

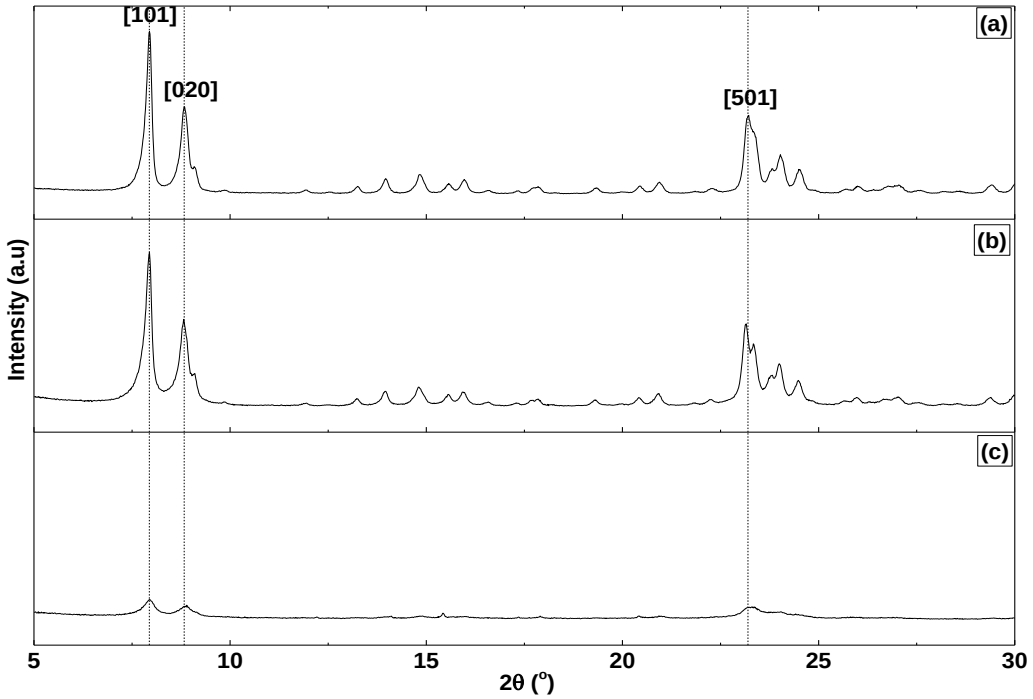

Figure 3.2 XRD diffractograms of untreated and alkaline treated H-ZSM-5 (80) zeolites; (a)H-ZSM-5 (80), (b) H-ZSM-5 (80.2) and (c) H-ZSM-5 (80.4).

Figure 3.2 showed the XRD diffractograms of H-ZSM-5 (80, 80.2 and 80.4). Treatment of H-ZSM-5 (80) with 0.2 M NaOH led to a small loss of crystallinity of 16%. However, treatment of H-ZSM-5 (80) with 0.4 M of sodium hydroxide led to a significant loss in crystallinity with H-ZSM-5 (80.4) showing only 31% crystallinity compared to the untreated parent. This demonstrates that treatment of H-ZSM-5 (80) with 0.4 M was too harsh a treatment.

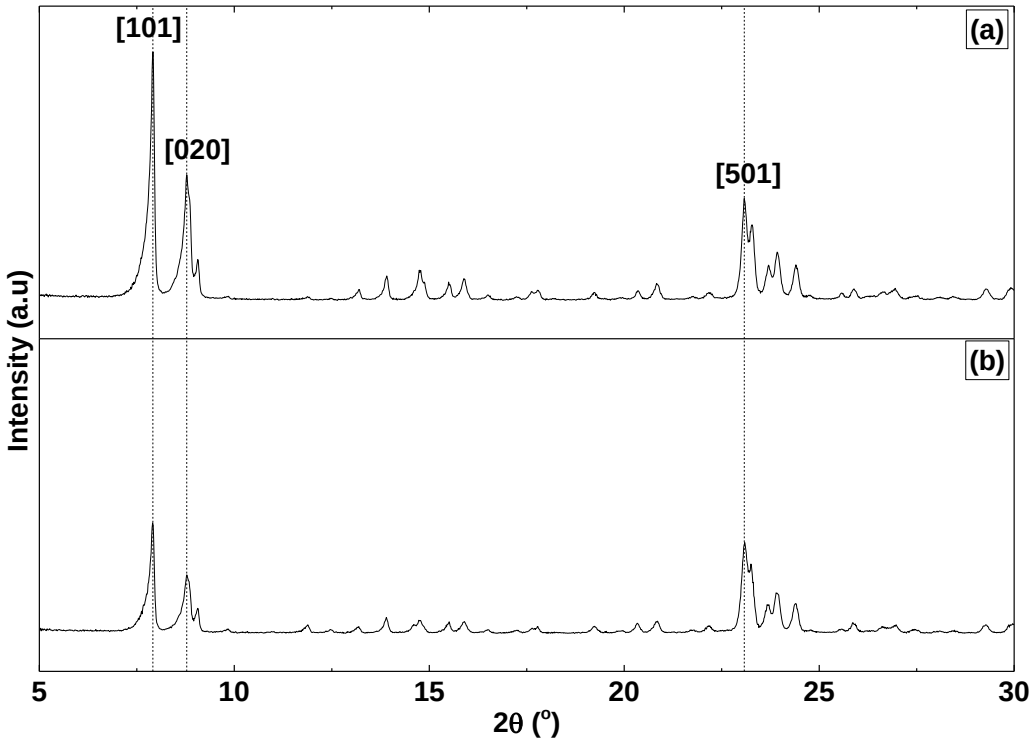

Figure 3.3 XRD diffractograms of (a) H-ZSM-5 (100) and (b) H-ZSM-5 (100.2).

Treatment of H-ZSM-5 (100) zeolite (Figure 3.3) decreased crystallinity to 43% of the parent sample. Despite having a lower SiO_2/Al_2O_3 molar ratio than H-ZSM-5 (80), the crystallinity for H-ZSM-5 (100.2) was higher after alkaline treatment than H-ZSM-5 (80.2). This suggests that aluminium was largely positioned in the framework for H-ZSM-5 (100).

Elemental analyses showed that the SiO_2/Al_2O_3 molar ratios determined experimentally closely matched the theoretical SiO_2/Al_2O_3 molar ratios supplied by the manufacturer (shown in Table 3.1). Alkaline treatment of H-ZSM-5 (30), even under extreme conditions had an effect on the final SiO_2/Al_2O_3 molar ratios. However, alkaline treatment of H-ZSM-5 (80) had a profound effect on the final SiO_2/Al_2O_3 molar ratios, decreasing from the initial value of 71 for the parent to 49 using 0.2 M NaOH. When 0.4 M NaOH was used, the final SiO_2/Al_2O_3 molar ratio decreased to 31. The SiO_2/Al_2O_3 molar ratio for H-ZSM-5 (100) increased after treatment with sodium hydroxide from 115 to 131. It is possible that this was due to removal of extra-framework aluminium. This strongly correlates with the XRD patterns, confirming that alkaline treatment on H-ZSM-5 with lower SiO_2/Al_2O_3 molar ratios inhibit silicon extraction. Next, the thermal stability of H-ZSM-5 (30,

30.2 and 30.4) were analysed using TGA and are shown below in Figure 3.4. To save space, the remaining TGA profiles of all zeolites will only be described.

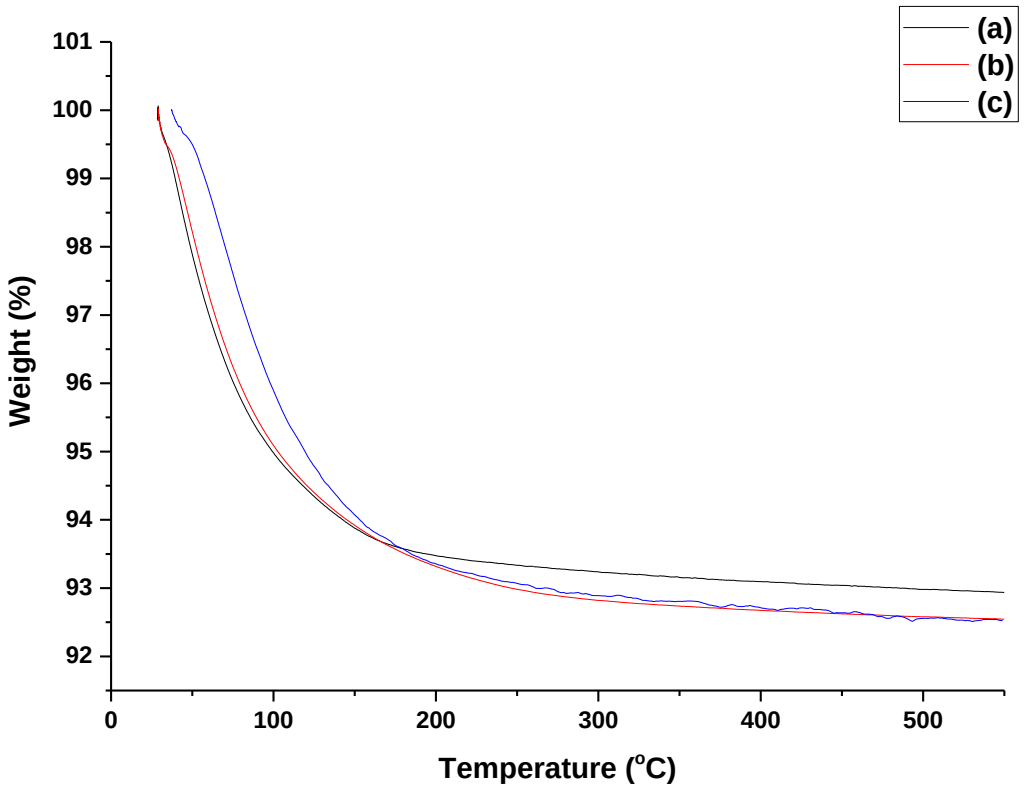

Figure 3.4 TGA profile of (a) H-ZSM-5 (30), (b) H-ZSM-5 (30.2) and (c) H-ZSM-5 (30.4).

Figure 3.4 showed that all H-ZSM-5 zeolites were stable at temperatures up to 550 °C under oxidising conditions. The weight loss from all H-ZSM-5 catalysts appeared to be a continuous step up to 550 °C. From the derivative weight loss as a function of temperature, it can be seen that the overwhelming weight loss occurred at temperatures less than 200 °C, due to water desorption from the external surface. The remaining weight loss above 200°C was due to the removal of water from the micropores.[163]

3.3.1.2 H-Beta

Crystallinity measurements for untreated and alkaline treated H-Beta samples summarised in Table 3.2 and shown in Figure 3.5. The parent zeolite was compared to the alkaline treated zeolite and the intensity of the [101] peak in the 2θ angle of

7.7º was used for the crystallinity calculation. A similar method was used to determine crystallinity of desilicated H-Beta samples compared to their parent by Wang et al.[164] The 2θ angle range 5-30º is shown to save space.

Table 3.2 Physical and chemical properties of untreated and alkaline treated H-Beta zeolites.

Catalyst	NaOH treatment (M)	Theoretical SiO_2/Al_2O_3 ratio[a]	Experimental SiO_2/Al_2O_3 ratio[b]	Crystallinity (%)[c]	Weight loss at 550 ºC (%)[d]
H-Beta (10)	0	10	11	100	7.0
H-Beta (10)	0.2	-	11	129	7.6
H-Beta (25)	0	25	20	100	14.7
H-Beta (25)	0.2	-	15	147	15.0
H-Beta (38)	0	38	31	100	11.2
H-Beta (38)	0.2	-	20	30	8.5
H-Beta (360)	0	360	154	100	5.2
H-Beta (360)	0.2	-	62	11	6.4

(a) displayed by manufacturer, (b) determined by ICP-OES (c) determined by XRD and (d) determined by TGA.

All H-Beta parents showed diffractions based on the reference H-Beta zeolite from the International Zeolite Association (IZA), showing diffractions for 2θ angles; 7.7, 14.5, 22.5 and 29.2º for the peaks associated with the [hkl] planes [101], [201], [116] and [411] respectively. The XRD diffractograms of the parent and alkaline modified H-Beta zeolites with 0.2 M NaOH are shown in Figure 3.5.

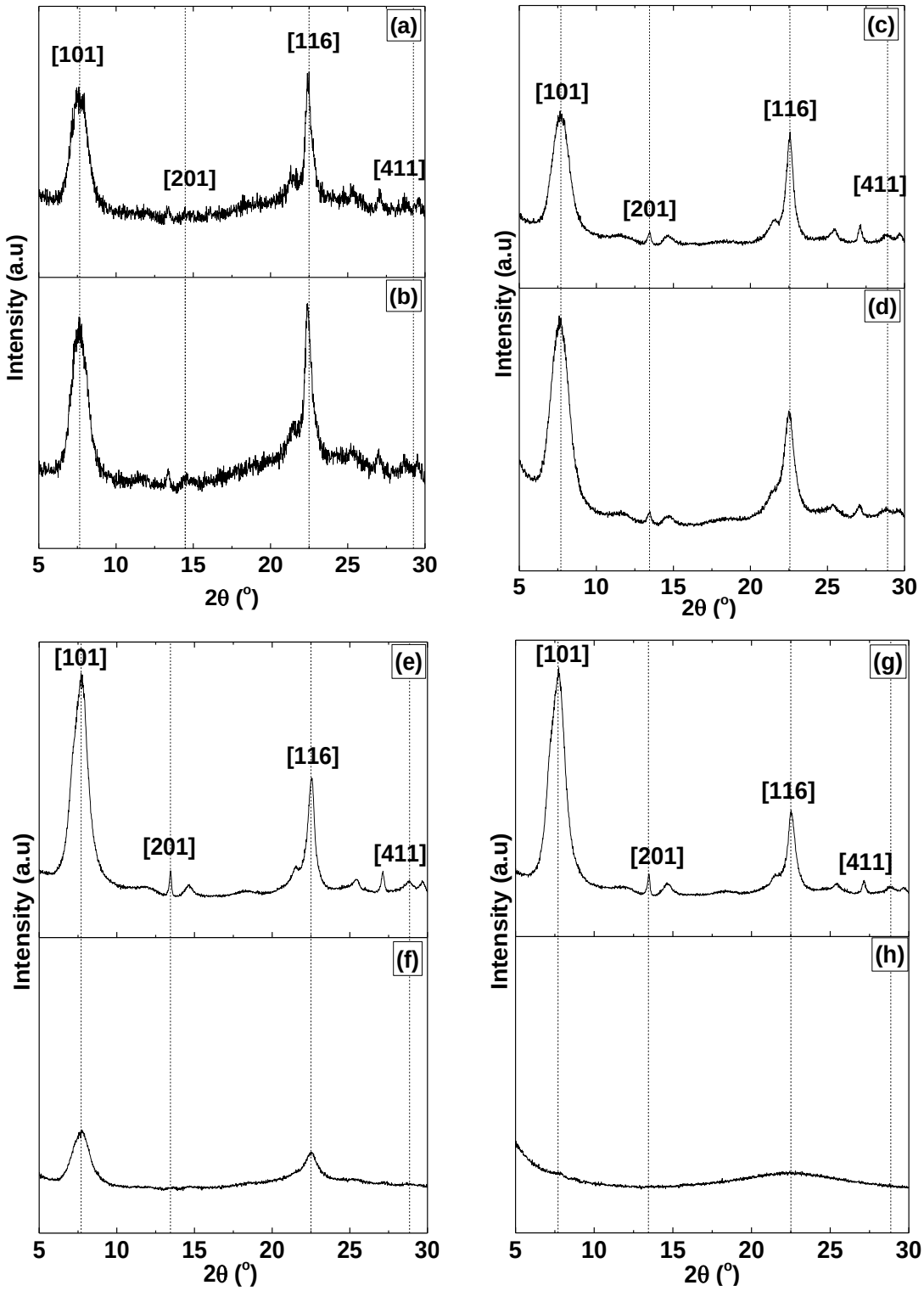

Figure 3.5 XRD diffractograms of untreated and alkaline treated H-Beta zeolites with varying SiO_2/Al_2O_3 molar ratios; (a) H-Beta (10), (b) H-Beta (10.2), (c) H-Beta (25), (d) H-Beta (25.2), (e) H-Beta (38), (f) H-Beta (38.2), (g) H-Beta (360) and (h) H-Beta (360.2).

The effect of alkaline treatment had a more pronounced effect on the crystallinity of H-Beta than H-ZSM-5. Alkaline treatment of H-Beta zeolites with low SiO_2/Al_2O_3 ratios shows that the untreated parent was less crystalline. Similar findings were found by Rac et al.[165] which showed that extraction of amorphous silica can lead to enhanced crystallinity after alkaline treatment. This strongly indicates that extra-framework amorphous silica had been removed during alkaline treatment.[166] Treatment on H-Beta (38) resulted in only a 30% crystalline material compared to its parent is obtained in XRD. In the case of H-Beta (360), alkaline treatment resulted in a phase transformation from a crystalline phase to an amorphous phase. This was hardly surprising due to the low aluminium content. The results are in excellent agreement with the study carried out by Groen et al.[157] which demonstrated the optimal conditions applied to H-ZSM-5 (i.e 0.2 M NaOH, 65 ^oC, 30 mins) is too severe for H-Beta. It was concluded that a further optimisation study is required on H-Beta zeolites to preserve the crystallinity.

Elemental analysis by ICP-OES showed discrepancy between the theoretical SiO_2/Al_2O_3 molar ratio supplied by the manufacturer and the SiO_2/Al_2O_3 molar determined experimentally for H-Beta (360). ICP-OES analysis of our own H-Beta zeolite, the SiO_2/A_2O_3 molar ratio closely matched the theoretical SiO_2/A_2O_3 molar ratio (Table 3.1). Similar to H-ZSM-5, alkaline treatment of H-Beta zeolites with low SiO_2/Al_2O_3 molar ratios had a lesser effect. Unsurprisingly, the SiO_2/Al_2O_3 molar ratio decreased from 154 for H-Beta (360) to 54 for H-Beta (360.2).

TGA demonstrated that H-Beta zeolites were stable up to temperatures up to 550 ^oC. The ~10% weight loss at 100 ^oC was due to physisorbed water on the external surface of the zeolite and the remaining weight loss up to 550 ^oC can be assigned as the removal of water from the micro-/mesopores.

3.3.1.3 H-Y

The parent H-Y zeolites were compared to H-Y zeolites after treatment with 0.2 M NaOH by XRD. The intensity of the [111] peak in the 2θ angle 6.3^o was used to determine the change in crystallinity of the alkaline treated zeolite relative to its parent, with the assumption that the parent was 100% crystalline. Crystallinity,

elemental and thermal stability results are shown in Table 3.3. With the exception of H-Y (80) zeolites, the XRD diffractograms are shown with identical scales for the y axis.

Table 3.3 Physical and chemical properties of untreated and alkaline treated H-Y zeolites.

Catalyst	NaOH treatment (M)	Theoretical SiO_2/Al_2O_3 ratio[a]	Experimental SiO_2/Al_2O_3 ratio[b]	Crystallinity (%)[c]	Weight loss at 550 ^oC (%)[d]
H-Y (10)	0	10	4	100	20.1
H-Y (10)	0.2	-	4	77	6.5
H-Y (12)	0	12	14	100	12.8
H-Y (12)	0.2	-	11	27	16.6
H-Y (80)	0	80	111	100	6.8
H-Y (80)	0.2	-	50	3	5.0

(a) Determined by manufacturer, (b) Determined by ICP-OES and (c) determined by XRD and (d) determined by TGA.

All H-Y samples show diffractions based on the diffractograms from the reference H-Y zeolite from the International Zeolite Association (IZA), showing diffractions in the 2θ angles of; 6.15, 10.07, 11.79, 15.53, 18.55 and 20.22^o for the peaks associated with the [hkl] planes; [111], [220], [311], [331], [422] and [440] respectively. The XRD diffractograms of untreated and H-Y zeolites treated with 0.2 M of sodium hydroxide solution are shown in Figure 3.6 with the intensity axis of the alkaline treatment zeolite shown to be the same scale as the unmodified zeolite.

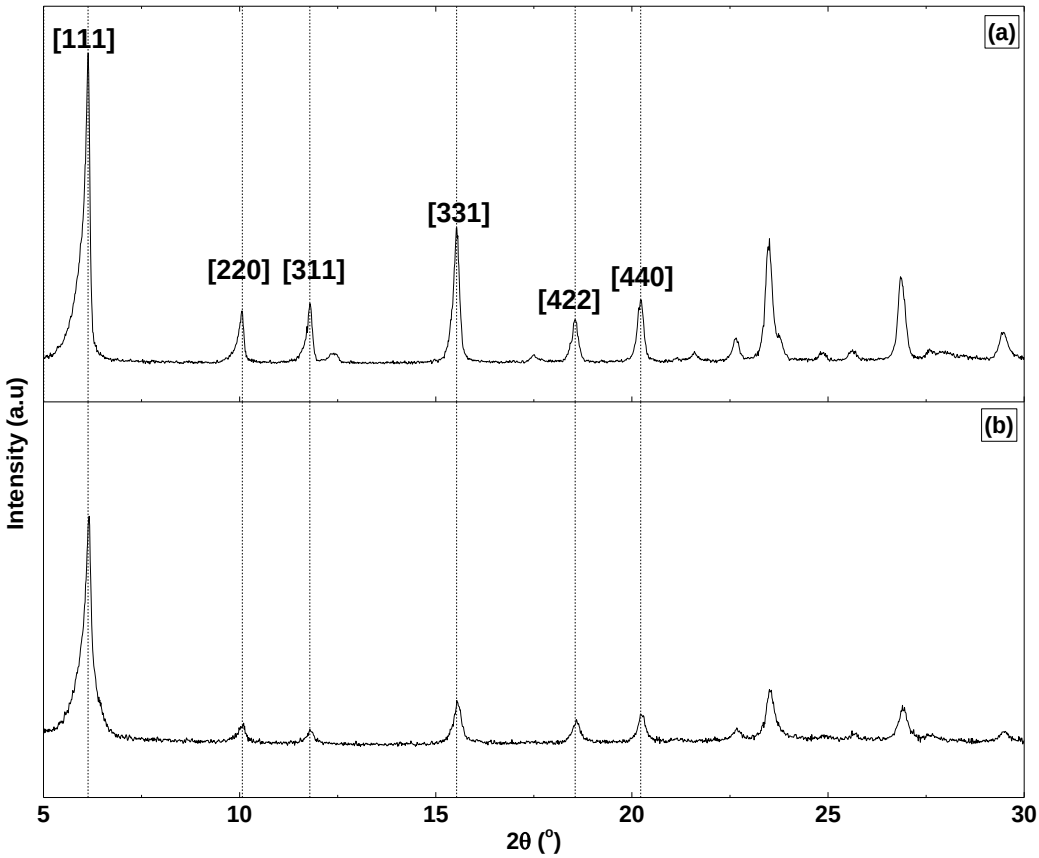

Figure 3.6 XRD diffractograms of (a) H-Y (10) and (b) H-Y (10.2).

XRD diffractograms of H-Y (10 and 10.2) showed that the synthesis of H-Y by microwave assisted heating was highly crystalline without any purity and matched the diffraction patterns based on the reference sample. Based on the intensity of the [111] reflection at 2θ angle 6.15°, it can be seen that treatment of H-Y (10) with 0.2 M of sodium hydroxide solution led to 77% of the crystalline structure remaining after alkaline treatment This suggests that there is a significant amount of aluminium located in the framework position. The results are largely in agreement with Huang et al. [167] which showed that alkaline treatment on H-Y zeolites with SiO_2/Al_2O_3 molar ratios equal to 10 largely preserved long range crystallinity. Overall, it can be seen that alkaline treatment of the laboratory synthesised H-Y (10) zeolite was successfully treated with 0.2 M sodium hydroxide solution with limited crystallinity loss.

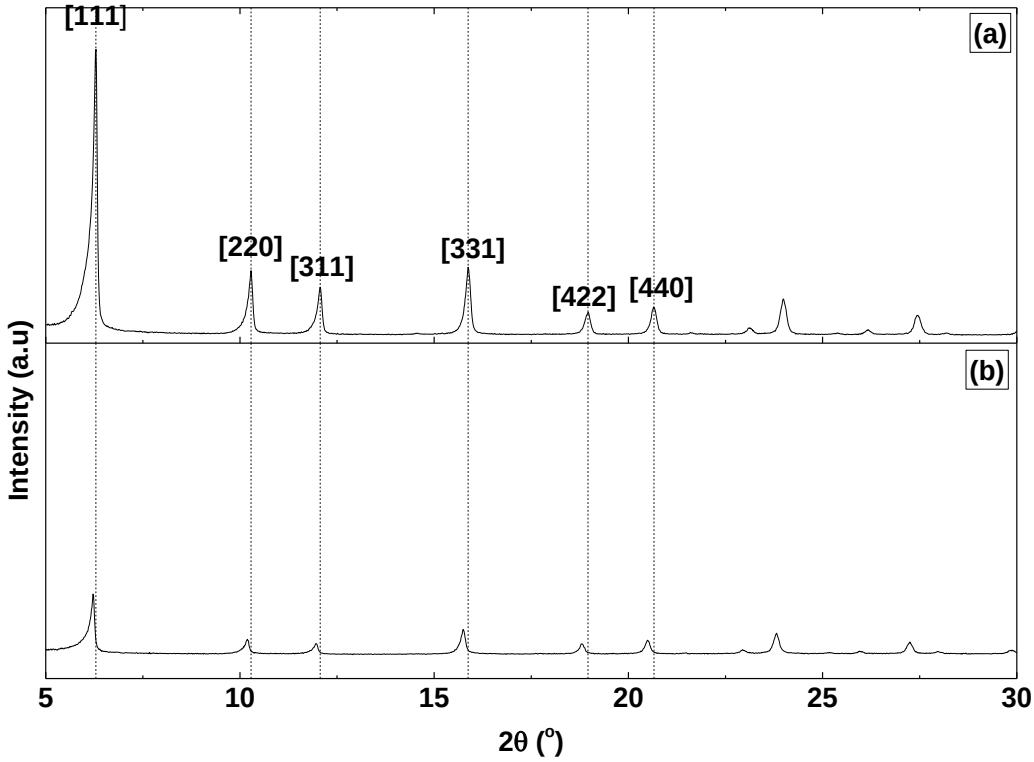

Figure 3.7 XRD diffractograms of (a) H-Y (12) and (b) H-Y (12.2).

H-Y (12 and 12.2) diffractograms shown in Figure 3.7 confirmed that H-Y (12) was highly crystalline without any impurity and matched the diffraction patterns based on the reference sample. Based on the [111] reflection plane, there was 23% of the crystalline phase remaining after alkaline desilication. Despite having a similar SiO_2/Al_2O_3 molar ratio as our laboratory synthesised H-Y zeolite, alkaline treatment of H-Y (12) zeolite had a different effect on the overall crystallinity. Therefore, it could be argued that a concentration of 0.2 M of sodium hydroxide solution was too harsh a treatment, and therefore, milder conditions are required.

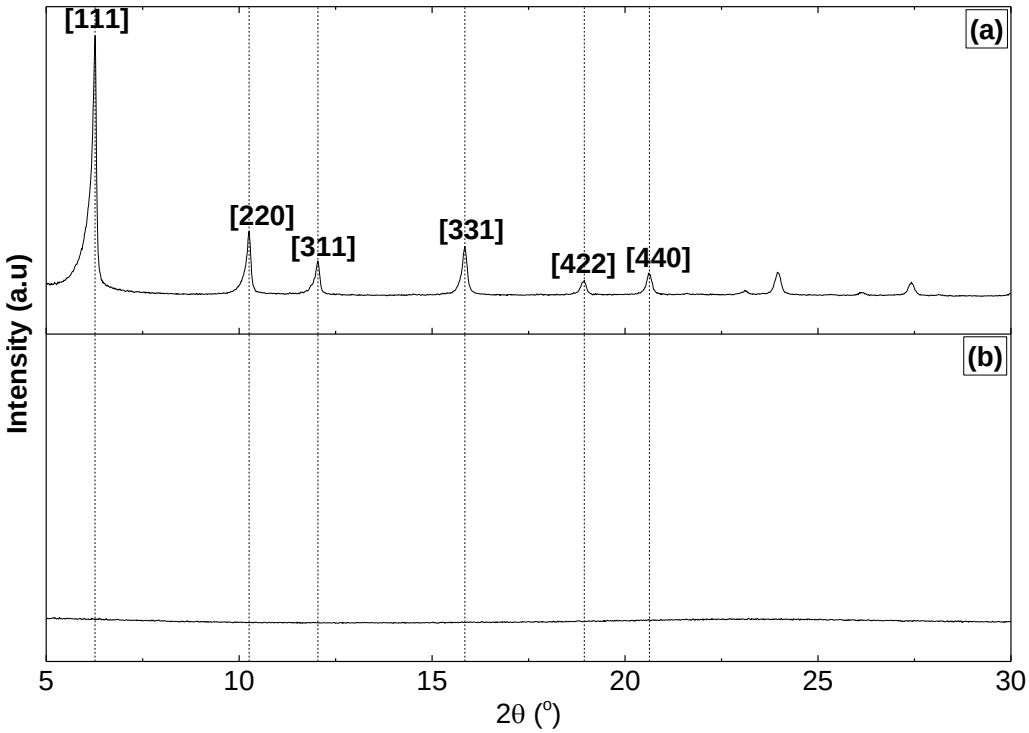

Figure 3.8 XRD diffractograms of (a) H-Y (80) and (b) H-Y (80.2).

The XRD patterns of H-Y (80 and 80.2) shown in Figure 3.8 (not to the same scale) showed that alkaline treatment of H-Y (80) with 0.2 M of sodium hydroxide solution had a significant effect on crystallinity. It can be seen that alkaline treatment resulted in the transformation of a crystalline phase to an amorphous phase, with the complete disappearance of the [111] reflection plane. Studies have shown that in the case of H-Y zeolites with higher SiO_2/Al_2O_3 molar ratios, milder reaction conditions (15 minutes at room temperature) are required to prevent complete amorphisation of the zeolite structure.[168, 169]

Elemental analyses of commercial H-Y zeolites with theoretical SiO_2/Al_2O_3 molar ratios of 12 and 80 showed 14 and 111 when determined experimentally. After alkaline treatment with 0.2 M NaOH, the SiO_2/Al_2O_3 molar ratios decreased to 11 and 50 respectively. ICP-OES analysis of our laboratory H-Y zeolite with a theoretical SiO_2/Al_2O_3 molar ratios of 10 showed a SiO_2/Al_2O_3 molar ratio of 4 when measured experimentally. This strongly suggested that silicon was not being incorporated into the zeolite structure. After crystallisation using microwave assisted heating, the quartz vessel showed two phases; a solid phase and an aqueous phase. We assumed that silicon may have been extracted during the crystallisation

process due to the presence of sodium hydroxide in the aqueous phase. The aqueous phase was analysed and measured for silicon and aluminium. It must be noted that elemental analysis of the precursor gel prior to crystallisation showed a Si/Al molar ratio of 5, therefore eliminating the possibility of experimental error of the precursor gel. Elemental analysis showed the aqueous phase contained trace amounts of aluminium. However, it was revealed that the aqueous phase contained significant amounts of silicon which explains the discrepancy between the theoretical SiO_2/Al_2O_3 molar ratio and experimental SiO_2/Al_2O_3 molar ratio of H-Y (10).

The TGA profiles showed H-Y was stable at temperatures up to 550 ^oC under oxidising conditions. Generally, the majority of the weight loss occurred ca. 100 ^oC due to desorption of water on the external surface of the zeolite, with the remaining weight loss up to 550 ^oC attributable to water loss from the microporous network.

3.3.2 Surface area and porosity measurements

Specific surface area measurements was carried out at -196 ^oC by nitrogen adsorption-desorption isotherms using a 5 point adsorption measurement in the P/P_o range 0.05-0.30. The total pore volume was measured using a single point adsorption measurement (P/Po = 0.99). For H-ZSM-5 zeolites, the micropore volume was calculated using Hovarth-Kawazoe (HK) model with the assumption that the pores were cylindrical (Saito-Foley model). For H-Beta and H-Y zeolites, microporosity was calculated based on the assumption that the pores possessed spherical geometry.[170] Pore size distributions were carried out using the BJH method (Barrett-Joyner-Halenda) derived from the adsorption branch of the isotherm for pore sizes greater than 2 nm and using the Harkins and Jura equation for pores with cylindrical geometry.[171] The external volume was calculated by the difference between the total pore volume and the micropore volume. Nitrogen adsorption-desorption isotherms of all zeolites are shown in the Appendix and will only be described here.

3.3.2.1 H-ZSM-5

Nitrogen isotherms confirm that the structure of H-ZSM-5 (30) and H-ZSM-5 (80) are predominately microporous with a classic type I isotherm. There was a small hysteresis in the isotherms for H-ZSM-5 (30) and H-ZSM-5 (80), suggesting limited mesoporosity. Nitrogen isotherms of H-ZSM-5 (30.2) and H-ZSM-5 (80.2) showed a combination of type I and type IV isotherms with increased uptake of nitrogen and pronounced hysteresis. Figure 3.9 summarises the main findings and how the external surface area is generated during the desilication process.

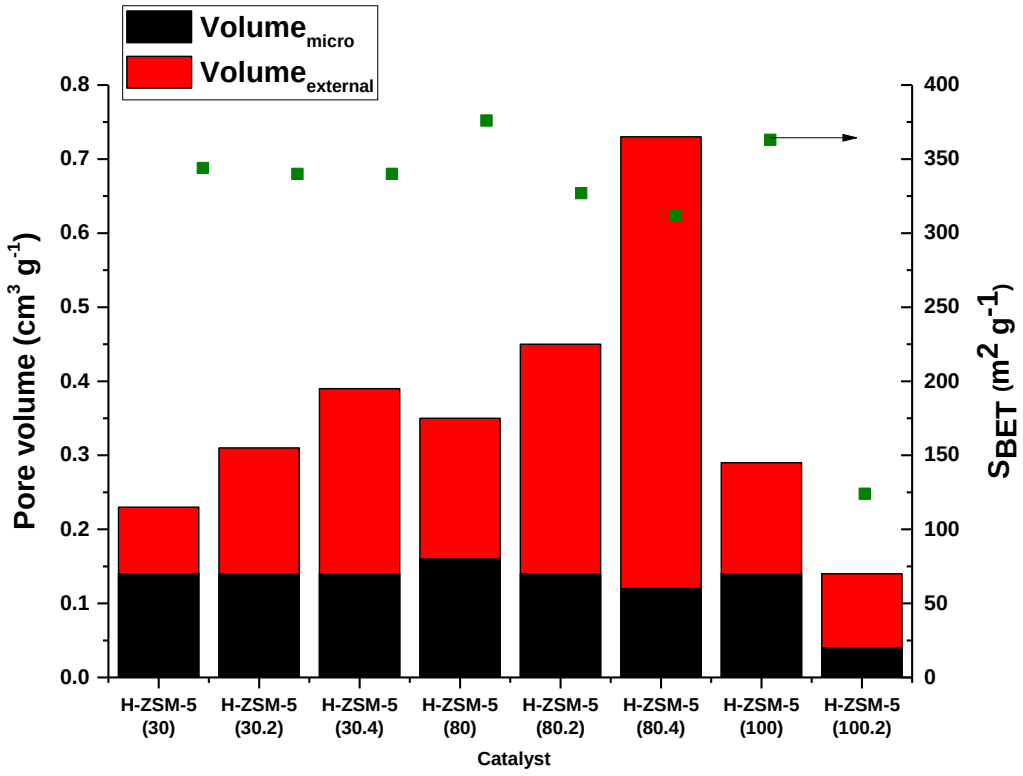

Figure 3.9 Surface area and porosity measurements for untreated and alkaline treated H-ZSM-5 zeolites.

Specific surface area measurements showed that alkaline treatment had minimal effect on the specific surface area of H-ZSM-5 (30). Upon treatment of H-ZSM-5 (30) with 0.2 M and 0.4 M of NaOH, the external volume increased from 0.09 cm^3 g^{-1} for H-ZSM-5 (30) to 0.17 cm^3 g^{-1} and 0.25 cm^3 g^{-1} for H-ZSM-5 (30.2) and H-ZSM-5 (30.4) respectively. The micropore volume was largely preserved.

For H-ZSM-5 (80), the specific surface area and microporosity decreased after NaOH treatment. The specific surface area decreased from 376 m^2 g^{-1} for H-ZSM-5 (80) to 312 m^2 g^{-1} and the micropore volume from 0.16 cm^3 g^{-1} to 0.12 cm^3 g^{-1} for H-ZSM-5 (80.4). Alkaline treatment also had a profound effect on external volume, which increased from 0.09 cm^3 g^{-1} for H-ZSM-5 (80) to 0.61 cm^3 g^{-1} for H-ZSM-5 (80.4). All alkaline treated H-ZSM-5 catalysts showed a H3 hysteresis loop closing at P/P_o equal ca. 0.4 due to the tensile strength effect.[126]

The porosity changes in both H-ZSM-5 (30) and H-ZSM-5 (80) further corroborate the restrictions of desilication of zeolites with lower SiO_2/Al_2O_3 ratios. Therefore, further studies are required to enhance porosity of H-ZSM-5 (30). Treatment of H-ZSM-5 (80) up to 0.4 M NaOH enhanced porosity without significantly compromising microporosity or the specific surface area.

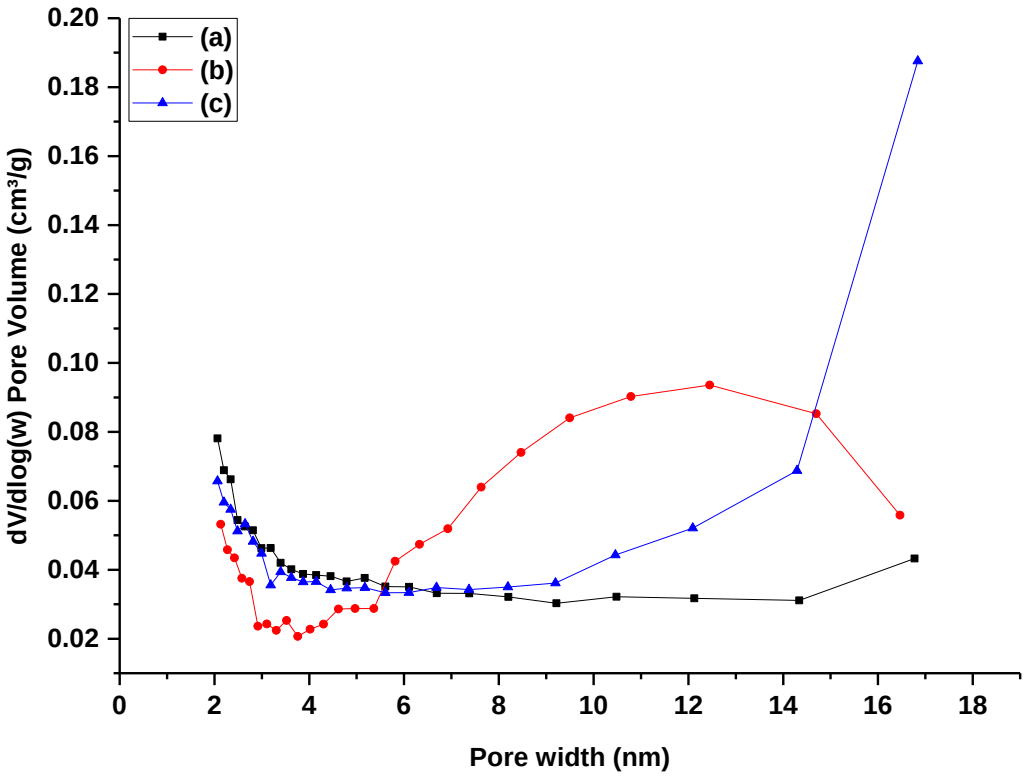

Figure 3.10 Pore size distribution of (a) H-ZSM-5 (30), (b) H-ZSM-5 (30.2) and (c) H-ZSM-5 (30.4).

BJH measurements (Figure 3.10) taken at the adsorption branch confirmed the presence of mesopores in H-ZSM-5 (30) with an evenly distributed array of pores

of width 2-17 nm. The majority of the mesopores are approximately 2 nm in diameter. Due to the fact that microporosity was largely unaffected after treatment with 0.2 M NaOH, larger mesopores were generated at the expense of smaller mesopores. When H-ZSM-5 (30) was treated with 0.4 M NaOH, microporosity was largely unaffected. Clearly, the increased external pore volume for H-ZSM-5 (30.4) can be accounted for by the generation of mesoporosity in the region of ca. 17 nm. Therefore, it could be concluded that treatment of H-ZSM-5 (30) with 0.2 M of sodium hydroxide led the broad distribution of mesoporosity, whereas under more extreme conditions led to a narrow distribution range of mesopores formed.

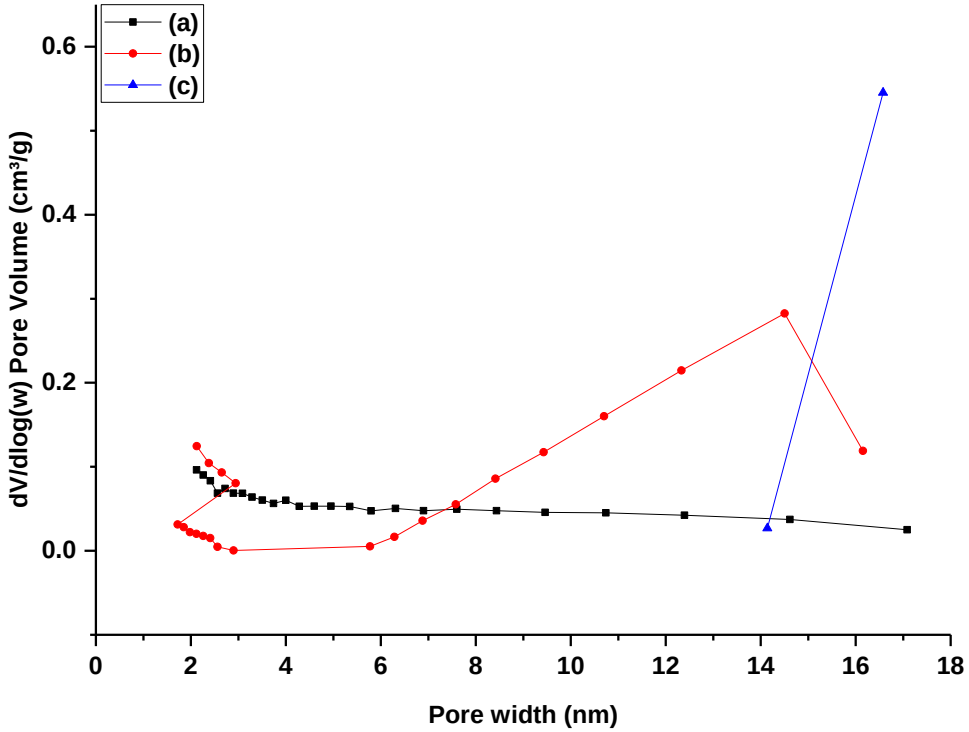

Figure 3.11 Pore size distribution of (a) H-ZSM-5 (80), (b) H-ZSM-5 (80.2) and (c) H-ZSM-5 (80.4).

The pore size distribution profile of H-ZSM-5 (80) zeolites and its alkaline treated counterparts shown in Figure 3.11 showed that the profile of H-ZSM-5 (80) is extremely similar to H-ZSM-5 (30). Mesoporosity is largely 2-10 nm, with a smaller distribution of mesopores between 11-14 nm. Unlike H-ZSM-5 (30), microporosity was reduced after alkaline treatment. When H-ZSM-5 (30) was treated with 0.2 M of sodium hydroxide solution, this resulted in the formation of mesopores between 8-17 nm. It could be possible that these larger mesopores are

formed at the expense of mesopores between 3-8 nm, with the generation of smaller mesopores formed at the expense of microporosity. However, treatment of H-ZSM-5 (80) with 0.4 M NaOH resulted in the external pore volume increasing from 0.19 cm^3 g^{-1} for H-ZSM-5 (80) to 0.61 cm^3 g^{-1} for H-ZSM-5 (80.4) forming larger mesopores between 14-17 nm. We believe that it is likely that the generation of larger mesopores between 14-17 nm region is likely formed at the expense of microporosity and smaller mesopores. Next, we measured the effect of alkaline treatment on our laboratory H-ZSM-5 (100) zeolites with 0.2 M NaOH. The BJH adsorption profiles are shown in (Figure 3.12).

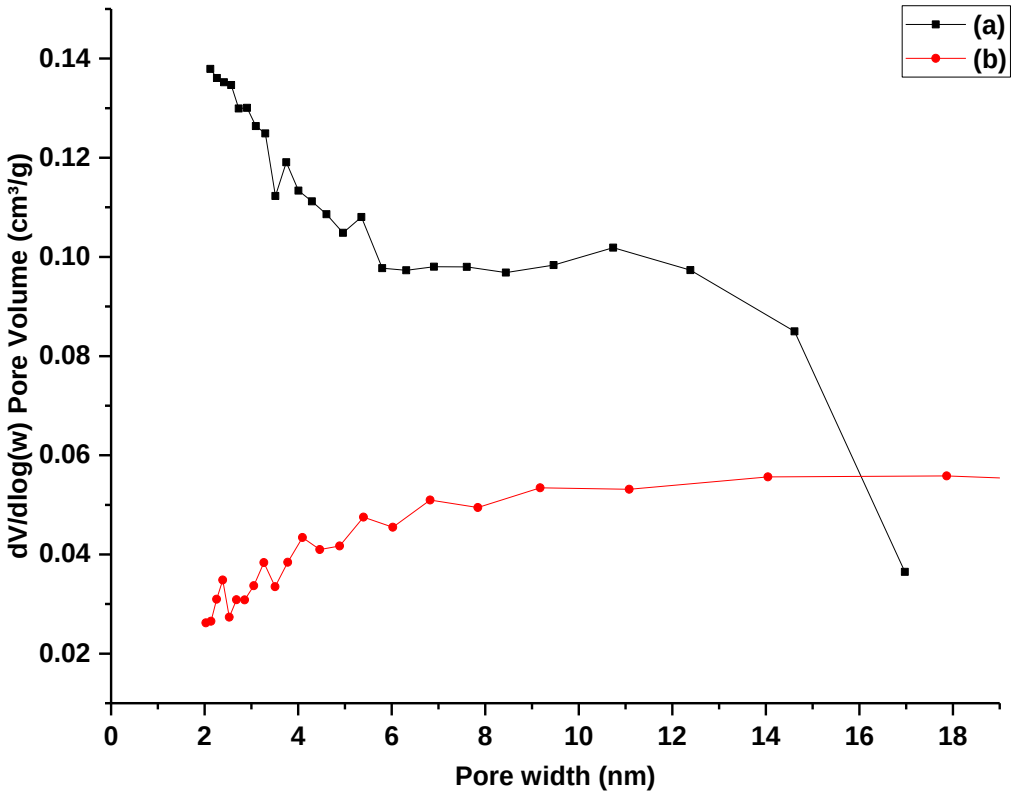

Figure 3.12 Pore size distribution of (a) H-ZSM-5 (100) and (b) H-ZSM-5 (100.2).

Characterisation of H-ZSM-5 (100 and 100.2) seemed not to follow the same pattern as desilicated H-ZSM-5 (30 and 80) zeolites. BJH measurements taken for H-ZSM-5 (100 and 100.2) are shown in Figure 3.12. The untreated laboratory synthesised parent zeolite showed an external volume of 0.15 cm^3 g^{-1} with a broad distribution of mesopores ranging from 2-17 nm. Surprisingly, when the laboratory

synthesised H-ZSM-5 zeolite was subjected to alkaline treatment, the external volume decreased from 0.15 to 0.10 cm^3 g^{-1}. Additionally, micropore volume decreased from 0.14 to 0.04 cm^3 g^{-1}. This strongly indicates that alkaline treatment of the laboratory synthesised H-ZSM-5 zeolite was largely unsuccessful without generating mesoporosity. It is clear that further studies are required to optimise mesoporosity whilst preserving surface area for desilication studies on H-ZSM-5 (100).

3.3.2.2 H-Beta

Next, the effect of alkaline treatment on surface area and porosity was studied on H-Beta zeolites with SiO_2/Al_2O_3 molar ratios; 10, 25, 38 and 360. Nitrogen isotherms of alkaline treated H-Beta zeolites with lower SiO_2/Al_2O_3 molar ratios were largely unchanged, implying that alkaline treatment had a limited effect. H-Beta (25) and H-Beta (25.2) isotherms showed a combination type I and type IV with increased uptake of nitrogen and pronounced hysteresis. The specific surface area and porosity measurements are shown in Figure 3.13.

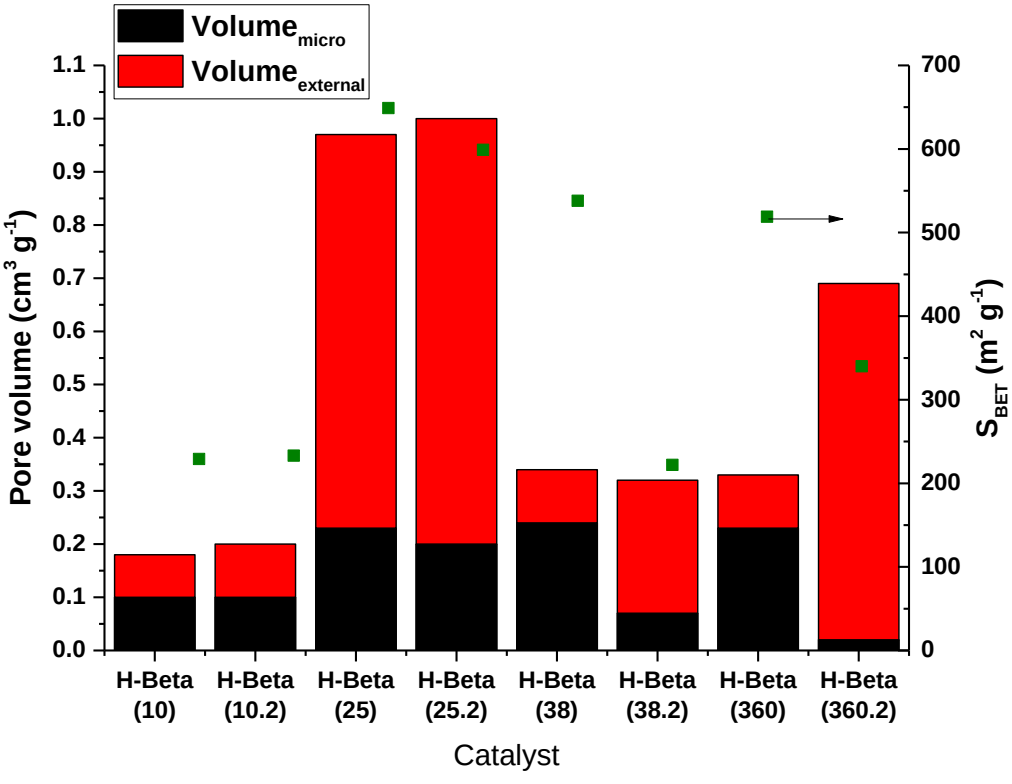

Figure 3.13 Surface area and porosity measurements for untreated and alkaline treated H-Beta zeolites.

After desilication of H-Beta (25), the specific surface area decreased from 649 to 599 m^2g^{-1}. H-Beta (25.2) showed a lower uptake at lower relative pressure than H-Beta (25). The nitrogen isotherm of H-Beta (38) showed a large uptake at lower relative pressure. This is a strong indication that H-Beta (38) is predominantly microporous. Desillication of H-Beta (38) showed a dramatic change in the isotherm with H-Beta (38.2), showing a profound increased uptake at higher relative pressure than H-Beta (38). Comparison of the isotherms H-Beta (38) and H-Beta (38.2), it is likely that H-Beta (38) has a greater proportion of microporosity than H-Beta (38.2). The specific surface area of H-Beta (38) decreased from 538 to 222 m^2g^{-1} for H-Beta (38.2). Likewise, H-Beta (360) showed an isotherm with a higher uptake at lower relative pressure, therefore confirming the largely dominant microporous network. However, H-Beta (360.2) showed a much lower uptake at lower relative pressure, confirming the generation of mesopores at the expense of microporosity. The pore size distributions of H-Beta zeolites are shown in Figures 3.14-3.16.

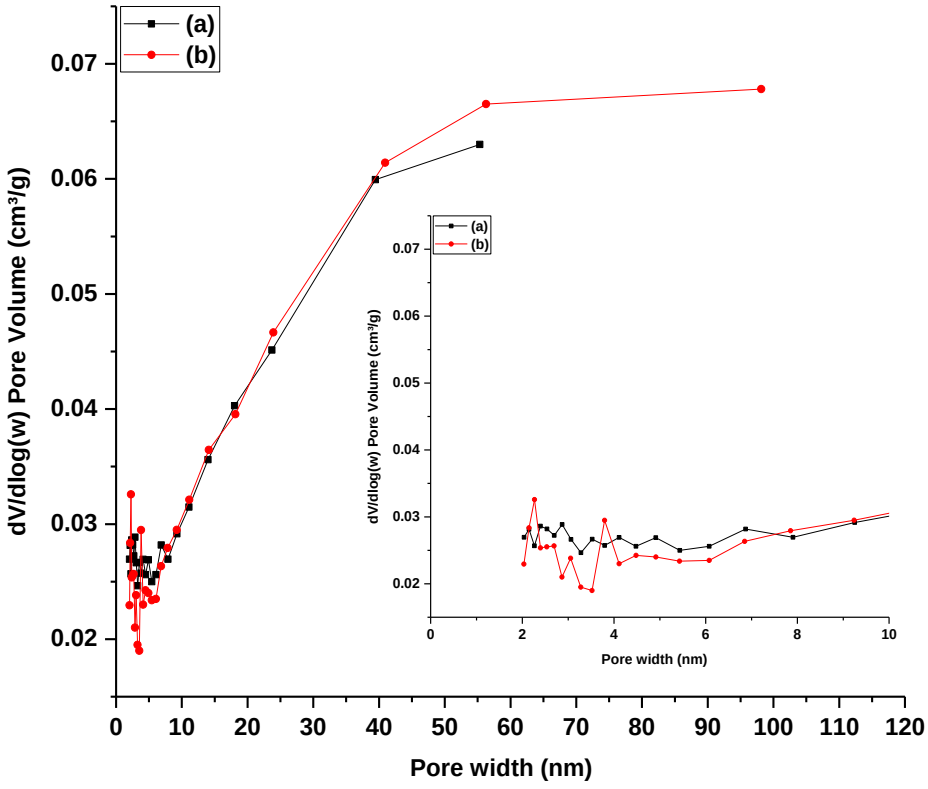

Figure 3.14 Pore size distribution of (a) H-Beta (10) and (b) H-Beta (10.2).

Pore size distribution measurements of the laboratory synthesised H-Beta zeolite (10) and H-Beta (10.2) are shown in Figure 3.14. It can be can be seen from the surface area and porosity measurements (Figure 3.13) that alkaline treatment of H-Beta (10) resulted did not have an impact on microporosity. Alkaline treatment resulted in the generation of mesoporosity in the region of approximately 2.5 and 3 nm. In addition, it can be seen that alkaline treatment did not result in the generation of larger mesopores in the region >10 nm. Since alkaline treatment had an insignificant impact on surface area and porosity, this strongly suggests the presence of aluminium located within the framework. With the assumption that the overwhelming majority of the aluminium is located within the framework, it could be concluded that more extreme alkaline conditions are required to generate larger mesopores without compromising the overall zeolite structure.

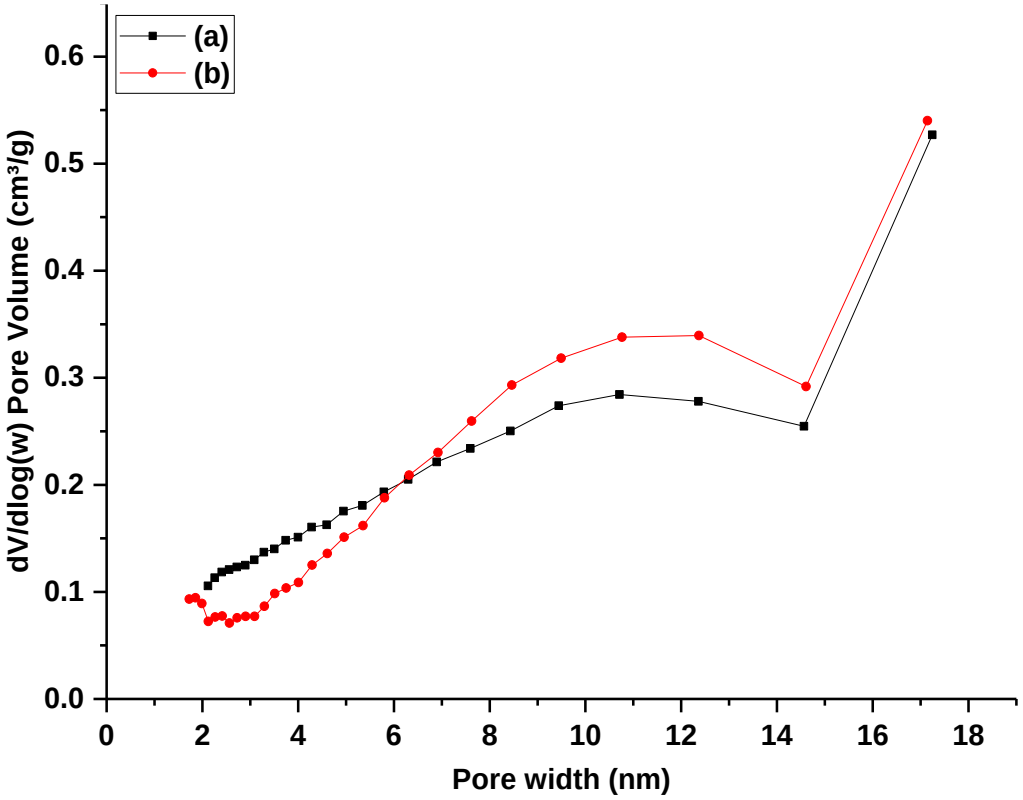

Figure 3.15 Pore size distribution of (a) H-Beta (25) and (b) H-Beta (25.2).

As can be seen from Figure 3.15, the parent H-Beta (25) zeolite possessed mesopores in the region between 2-17 nm. Unlike in the case of H-Beta (10), desilication of H-Beta (25) with 0.2 M of sodium hydroxide solution led to a

reduction of the micropore volume, with microporosity decreasing from 0.23 to 0.20 cm^3 g^{-1}. BJH measurements clearly show that H-Beta (25) possessed a greater proportion of microporosity located in the region ca. 2-5 nm. However, H-Beta (25.2) possessed enhanced mesoporosity located in the region ca. 7-17 nm. This strongly implies that mesoporosity in H-Beta (25.2) was generated at the expense of microporosity and small mesopores in the region between 2-5 nm. It is worth noting that despite H-Beta (25) having a similar SiO_2/Al_2O_3 molar ratio as H-ZSM-5 (30), alkaline treatment had a greater effect on the physical properties on H-Beta (25) than H-ZSM-5 (30).

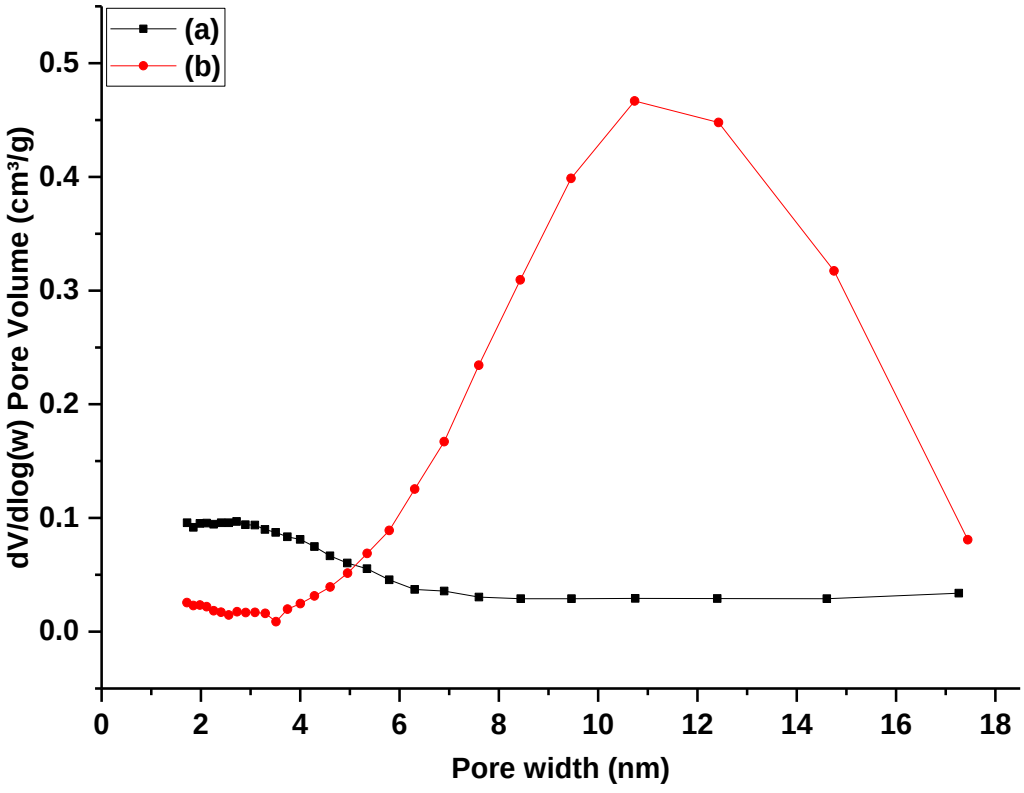

Figure 3.16 Pore size distribution of (a) H-Beta (38) and (b) H-Beta (38.2).

Desilication of H-Beta (38) with 0.2 M of sodium hydroxide solution had a marked effect on the resulting surface area and porosity. Figure 3.13 showed microporosity decreased for the untreated parent from 0.34 to 0.32 cm^{-3} g^{-1} for H-Beta (38.2), with mesoporosity increasing from 0.10 cm^{-3} g^{-1} for H-Beta (38) to 0.25 cm^{-3} g^{-1} for H-Beta (38.2). From the pore size distribution measurements (Figure 3.16) it can be

seen H-Beta (38) possessed a broad distribution of mesopores with a significant proportion of mesopores ca. 2-5 nm. Alkaline treatment showed generate a broad distribution mesopores with the structure having mesopores > 8 nm. Alkaline treatment had a detrimental effect on the specific surface area of the zeolitic structure of H-Beta (38.2), with H-Beta (10.2 and 25.2) largely preserving its microporous network.

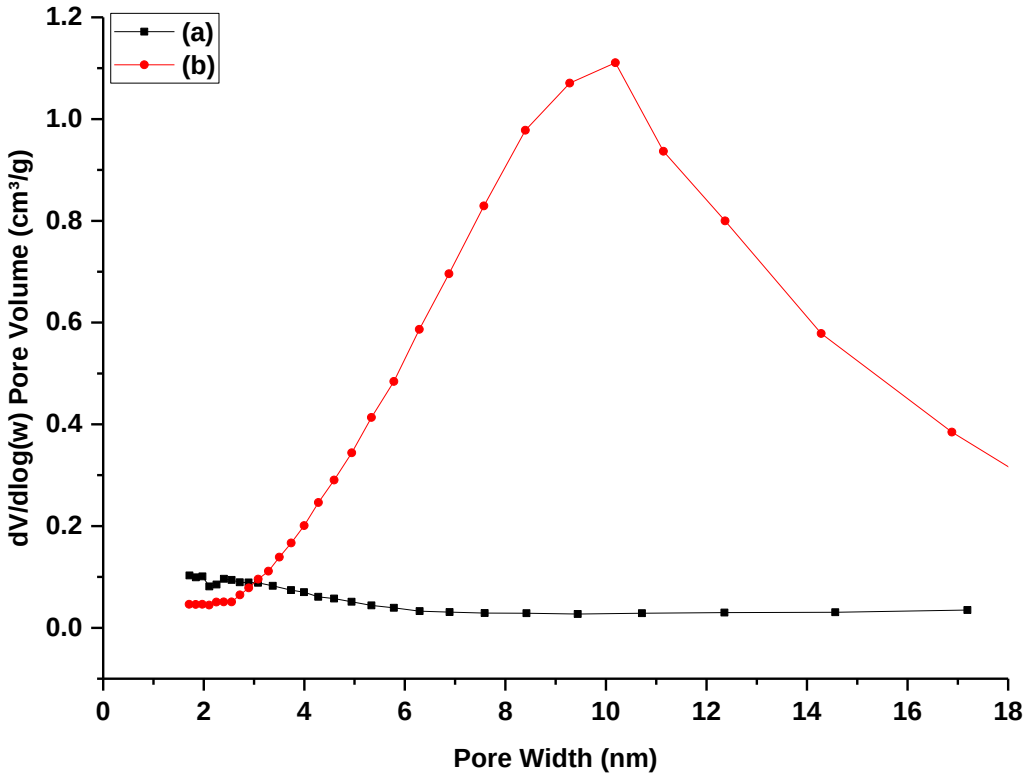

Figure 3.17 Pore size distribution of (a) H-Beta (360) and (b) H-Beta (360.2).

Alkaline treatment of H-Beta (360) resulted in almost the complete elimination of microporosity with the micropore volume decreasing from 0.23 cm^{-3} g^{-1} for H-Beta (360) to 0.02 cm^{-3} g^{-1} for H-Beta (360.2). BJH measurements confirmed the parent zeolite possessed an evenly broad distribution of mesopores. However, alkaline treatment of H-Beta (360) resulted in an unevenly distribution of mesopores, with the largest contribution having a pore radius of ca. 10 nm. Clearly, mesoporosity in H-Beta (360.2) was largely generated at the expense of microporosity and mesoporosity in the region <3 nm. It could be concluded that alkaline treatment of H-Beta zeolites with lower SiO_2/Al_2O_3 molar ratios resulted in the generation of

mesopores at the expense of microporosity and small mesopores without having a significant impact on overall microporosity However, alkaline treatment on H-Beta zeolites with higher SiO_2/Al_2O_3 molar ratios resulted in the generation of mesopores with almost the complete elimination of the microporous network, forming predominantly a mesoporous network.

After alkaline treatment on H-ZSM-5 and H-Beta zeolites resulted in marked differences in the surface area and porosity, the effect of mild alkaline treatment on the surface area and porosity for H-Y zeolites. It is worth noting that since H-Y (10) was synthesised in the laboratory, it was not assumed that mild alkaline treatment would have the same effect on the surface area and porosity as on the commercially obtained H-Y zeolites.

3.3.2.3 H-Y

The nitrogen isotherms of all H-Y zeolites can be found in the Appendix. Nitrogen isotherms showed that H-Y (12) consisted of a combination of type I and IV isotherm which implies that the parent zeolite possessed both micro- and mesoporosity. This was confirmed by HK and BJH measurements. Upon alkaline treatment of H-Y (12) with 0.2 M NaOH the nitrogen isotherm showed that H-Y (12.2) had a larger uptake at higher relative pressure than its parent with a more defined hysteresis loop closing at P/P_o equal to 0.4, indicating mesoporosity. However, nitrogen sorption isotherms of H-Y (80 and 80.2) had a type I isotherm with H3 hysteresis loop, which were obtained from slit-shaped pores. The overlaid isotherm profiles showed that H-Y (80) had a much larger uptake at lower and higher relative pressure than H-Y (80.2), indicating that H-Y possessed significantly more porosity than its alkaline treated counterpart. Pore size distribution measurements of all H-Y zeolites used in this study are shown in Figure 3.18.

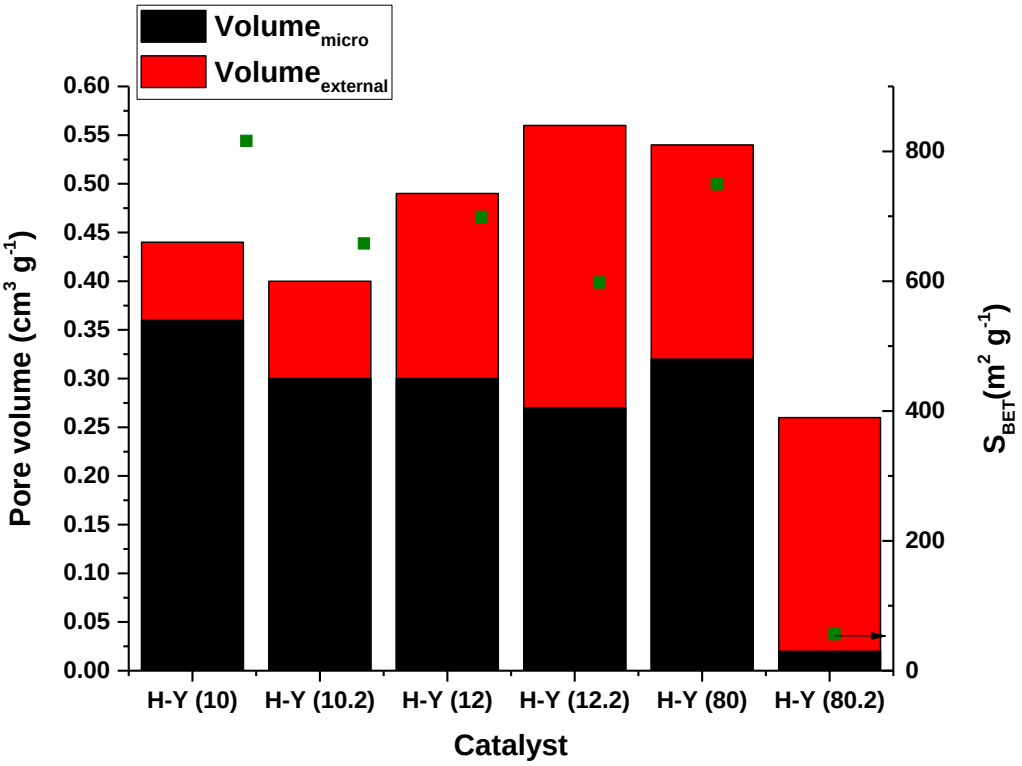

Figure 3.18 Surface area and porosity measurements for untreated and alkaline treated H-Y zeolites.

H-Y (10) zeolite had a specific surface area of 816 m^2 g^{-1} with a predominately microporous channel network. After alkaline treatment, the specific surface area decreased to 658 m^2 g^{-1}, possibly due to the removal of tetrahedral atoms from the zeolitic framework. For the commercial H-Y (12) zeolite, the specific surface area decreased from 699 m^2 g^{-1} to 598 m^2 g^{-1} for H-Y (12.2). As a result, total porosity increased by approximately 14% at the expense of microporosity. The external volume increased from 0.19 cm^{-3} g^{-1} for H-Y (12) to 0.29 cm^{-3} g^{-1} for H-Y (12.2). It is apparent that alkaline treatment of H-Y zeolites with particularly low SiO_2/Al_2O_3 molar ratios had a measurable effect on the surface area. In contrast, alkaline treatment on H-Y (80) showed a complete collapse of the structure with the specific surface area decreasing dramatically from 749 m^2 g^{-1} to 56 m^2 g^{-1}. Clearly, treatment of H-Y (80) with 0.2 M of sodium hydroxide was too severe a treatment, and therefore, milder conditions are required to prevent a detrimental effect on the final specific surface area. Therefore, future work is required to optimise the desilication process of H-Y (80) without compromising the crystallinity or surface area.

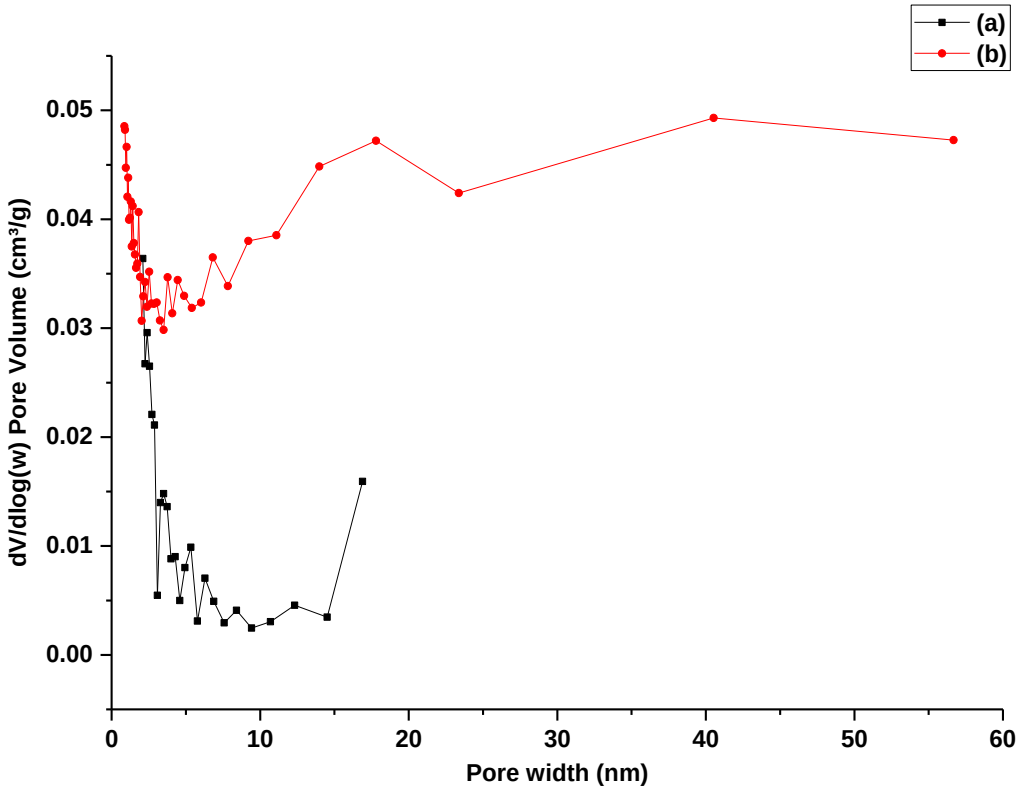

Figure 3.19 Pore size distribution of (a) H-Y (10) and (b) H-Y (10.2).

Our unmodified H-Y zeolite contained only a small distribution of mesopores, with a pore width in the region of 2-16 nm. Alkaline treatment of the laboratory synthesised H-Y zeolite resulted in the partial elimination of microporosity with a broader distribution of mesopores. It is likely that the formation of mesopores with a pore radii <5 nm were generated at the expense of microporosity. It is possible that pores with a diameter >10 nm were generated due to extraction of silicon in close proximity to mesoporous walls with a pore diameter 6-10 nm.

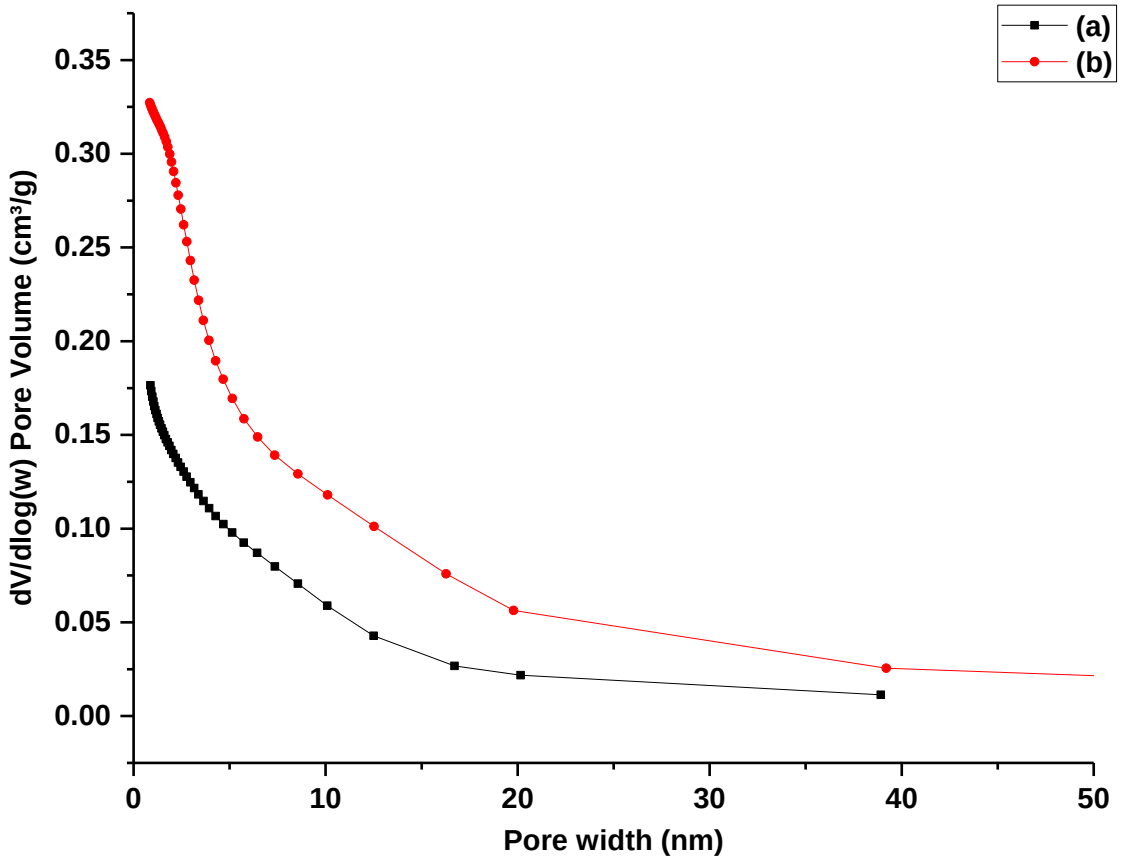

Figure 3.20 Pore size distribution of (a) H-Y (12) and (b) H-Y (12.2).

Figure 3.20 shows that the parent zeolite had a broad distribution of mesopores, with the overwhelming majority having a pore diameter >20 nm. However, it can be seen that treatment of the parent sample under mild basic conditions showed a similar pore size distribution. However, it can be seen that alkaline treatment resulted in a greater contribution of mespores in the region 2-40 nm. It is possible that alkaline treatment resulted in the unblocking of some of the unaccessible mesopores by removal of amorphous material from the structure. The BJH measurement is in agreement the specific surface area values obtained which showed a minimal effect of alkaline treatment.

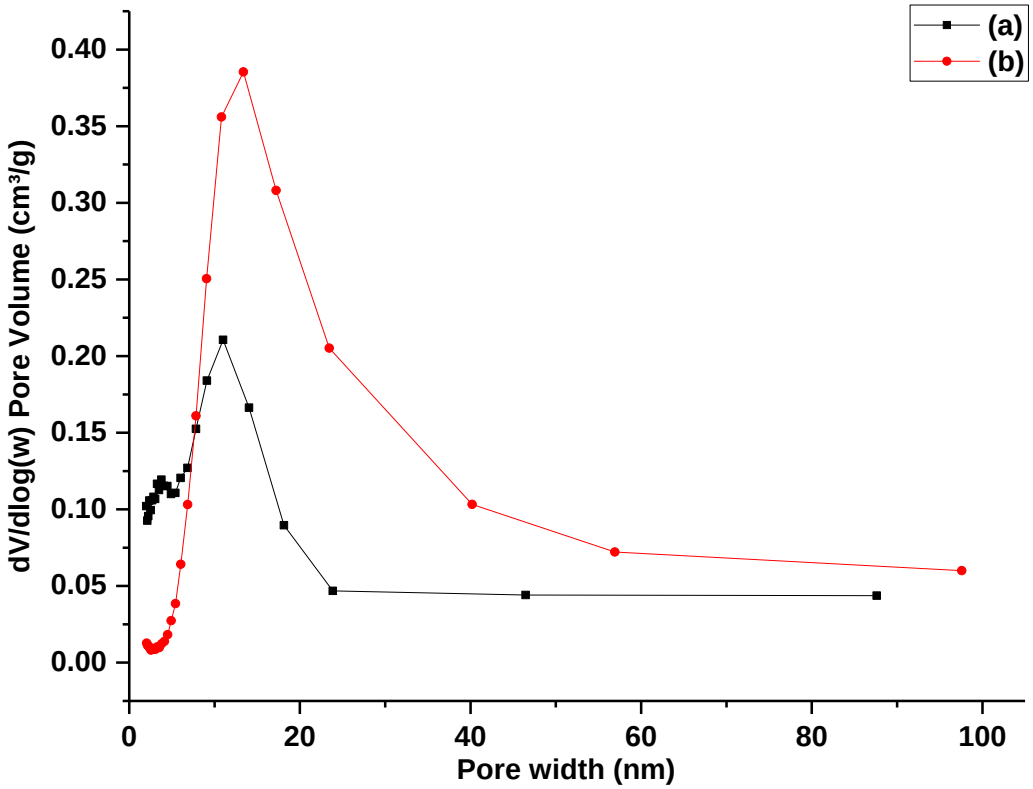

Figure 3.21 Pore size distribution of (a) H-Y (80) and (b) H-Y (80.2).

Figure 3.21 shows the effect of alkaline treatment on commercial H-Y (80) on the pore size distribution measurement. Porosity measurements confirmed that alkaline treatment led to a zeolitic material almost completely mesoporous in nature. BJH measurements show the reduction of mesopores in the region between 2-10 nm. This probably resulted in the enhancement of mesopore contribution with a pore diameter ca. 20 nm.

3.3.3 Temperature programmed desorption measurements of zeolites

Temperature programmed desorption of ammonia (NH_3-TPD) experiments can be used to determine the number and strength of acid sites. In this study, the sample was calcined in helium up to 550 ^oC to remove physisorbed water and cooled to 150 ^oC, at which point ammonia was adsorbed onto the catalyst. The sample was heated to 700 ^oC with a ramp of 10 ^oC min^{-1}, with ammonia desorption was measured as a function of temperature. Ammonia desorption was measured and normalised taking into account the mass of the catalyst loaded and plotted as a function of temperature to directly compare the profiles of the parent zeolite and its alkaline treated counterpart. The acid site density can be calculated by the addition of the weak acid site and strong acid concentrations. The first

desorption peak at ~225 °C was assumed to be desorption from the weak acid sites whereas the second desorption peak at ~ 385 °C was assigned to strong acid sites. Similar assumptions were made by Zhao et al.[172]

3.3.3.1 H-ZSM-5

Temperature programmed desorption profiles of H-ZSM-5 (30, 30.2 and 30.4) and H-ZSM-5 (80, 80.2 and 80.4) are shown in Figures 3.22-3.23.

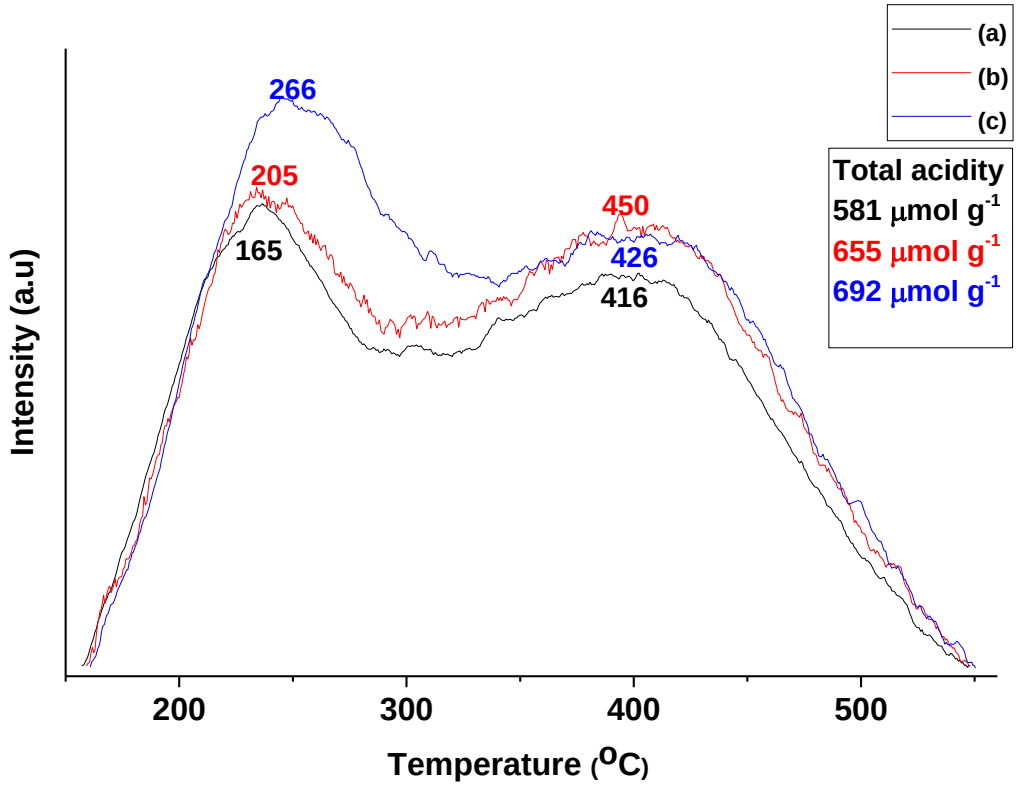

Figure 3.22 Temperature programmed desorption profiles of (a) H-ZSM-5 (30), (b) H-ZSM-5 (30.2) and (c) H-ZSM-5 (30.4).

There were two desorption peaks in NH_3-TPD profiles in H-ZSM-5 (30, 30.2 and 30.4). The acid site density value of both the parent H-ZSM-5 (30) and H-ZSM-5 (80) are in general agreement with the data present in the literature. [173] In the case of the parent H-ZSM-5 (30) the rigid zeolite structure and close proximity of the framework Si and Al (Lowenstein's rule) prevents facile desilication to some

extent. As shown in Figure 3.22, the acid site density increased from 581 µmol g^{-1} for H-ZSM-5 (30) to 655 and 692 µmol g^{-1} for H-ZSM-5 (30.2) and H-ZSM-5 respectively. The most pronounced change in the acidity profile was found to come from the weak acid sites. It was suggested by Rodriguez-Gonzalez et al.[174] that weakly bound ammonia can physisorb onto itself within the pores. The amount of strong acid sites increased slightly for treated samples by a maximum of 8 % of the parent value. This is in good agreement with the literature.[175] Next, TPD-NH_3 studies of H-ZSM-5 (80, 80.2 and 80.4) were carried out using. The profiles are shown in Figure 3.23.

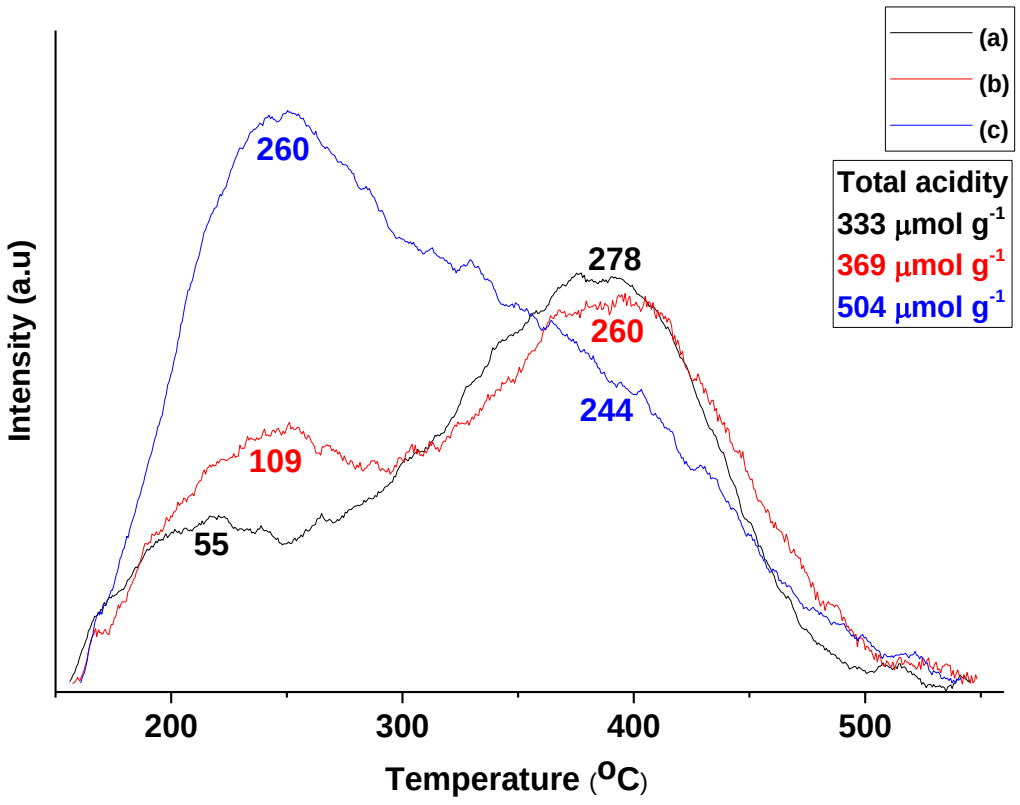

Figure 3.23 Temperature programmed desorption profiles of (a) H-ZSM-5 (80), (b) H-ZSM-5 (80.2) and (c) H-ZSM-5 (80.4).

The acidity changed more evidently in the case of H-ZSM-5 (80) as shown in Figure 3.23. The acid site density increased from 333 µmol g^{-1} for H-ZSM-5 (80) to 369 and 504 µmol g^{-1} for H-ZSM-5 (80.2) and H-ZSM-5 (80.4) respectively. This was mainly due to the increase in concentration of the weak acid sites. This was accompanied by the steep decrease in SiO_2/Al_2O_3 ratio from 72 for H-ZSM-5

(80) to 50 and 31 for H-ZSM-5 (80.2) and H-ZSM-5 (80.4). The amount of strong acid sites in this case decreased slightly for treated samples by 13 % of the parent value. This implies the extraction of framework aluminium from the tetrahedral sites. The temperature programme desorption profile of the laboratory synthesised H-ZSM-5 zeolite (Figure 3.24).

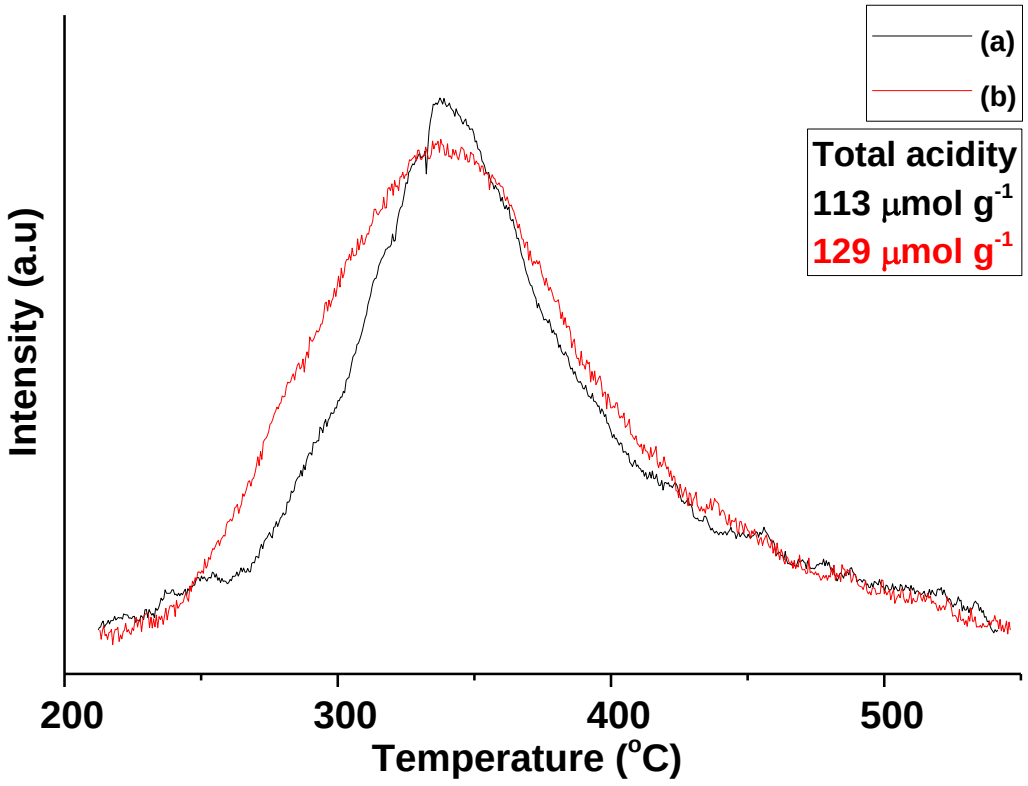

Figure 3.24 Temperature programmed desorption profiles of (a) H-ZSM-5 (100) and (b) H-ZSM-5 (100.2).

Figure 3.24 showed one desorption peak with T_{max} at ca. 350 °C, indicative of strong acid sites. The small shoulder at ca. 225-275 °C suggests the presence of weak acid sites. Our untreated laboratory H-ZSM-5 (100) zeolite had lower acid site density than commercial H-ZSM-5 (30 and 80), likely due to its higher SiO_2/Al_2O_3 molar ratio. Treatment of H-ZSM-5 (100) with 0.2 M of sodium hydroxide solution resulted in an increase in the total number of acid sites from 113 µmol g^{-1} to 129 µmol g^{-1} for H-ZSM-5 (100.2). After the TPD-NH_3 profile had been normalised by taking into account the mass of the samples, the desorption peak at ca. 350 °C for H-ZSM-5 (100.2) decreased slightly. The intensity of the peak attributed to strong acid sites increased. This can be ascribed to the re-insertion

of aluminium into the framework. The intensity of the peak increased in the region ca. 250-300 ^{o}C, confirming the formation of Lewis acid sites. This is in excellent agreement to the results obtained for H-ZSM-5 (80) zeolite after alkaline treatment.

3.3.3.2 H-Beta

TPD-NH_3 profiles of all H-Beta catalysts can be found in the appendix. To save space, they are simply described in this section. The results were plotted as a function of total of acid sites for each catalyst. The plots are summarised in Figure 3.25 (below).

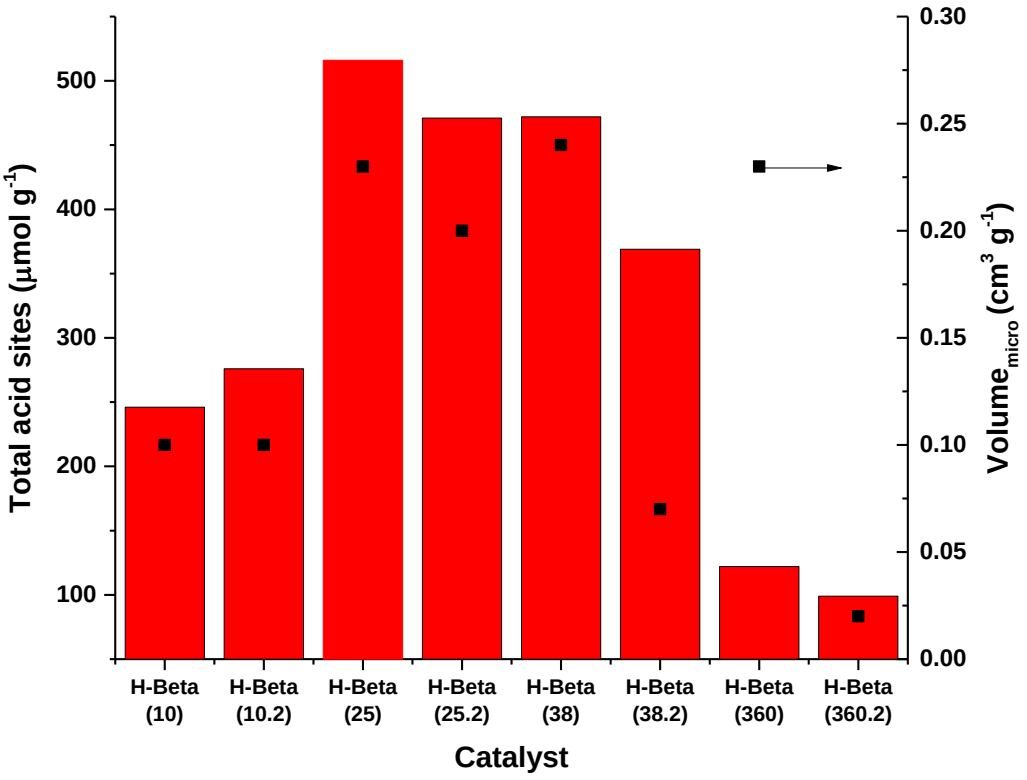

Figure 3.25 Acid site density versus micropore volume for H-Beta zeolites.

There was a broad desorption peak in NH_3-TPD profiles of H-Beta zeolites with desorption reaching T_{max} at around 300 ^{o}C. This was higher than H-ZSM-5 zeolites, which occurred at <250 ^{o}C. This shows that H-Beta zeolites acid sites of greater strength. The total acid strength of the untreated commercial H-Beta zeolites increased in the order H-Beta (360) > H-Beta (38) > H-Beta (25), likely due to the increased aluminium content in the framework. The NH_3-TPD profile of H-Beta (10) showed that alkaline treatment using 0.2 M NaOH had an insignificant effect

on acid site density. There was a slight shoulder ca. 400 ºC indicating that H-Beta (10.2) had more acid sites of stronger strength than its parent. However, alkaline treatment of commercial H-Beta did not follow the same trend, which showed a decrease in acid site density. Alkaline treatment of H-Beta (25) showed T_{max} decreased from 260 ºC to 230 ºC after alkaline treatment with the number of total acid sites decreasing 516 from parent to 471 μmol g^{-1} to H-Beta (25.2). Treatment of H-Beta (38) with 0.2 M NaOH resulted in a decrease in acid site density from 472 to 369 μmol g^{-1}. The results are in agreement with reported results in the literature.[176,177, 178] Wang et al. [164] found that a decrease in the acid site density was due to the decrease of Brønsted acid sites, confirmed by FTIR-pyridine adsorption measurements. It can be seen that desilication of H-Beta zeolites resulted in decreased microporosity. Since microporosity is correlated to Brønsted acidity,[179] this further supports the hypothesis that a reduction of acid site density was due to the loss of Brønsted acidity.

3.3.3.3 H-Y

Similar to H-Beta zeolites and their desilicated counterparts, the TPD-NH_3 profiles of all H-Y zeolites are shown in the Appendix and are only described here. As in the case of H-Beta, the acid site density for each H-Y zeolite and its alkaline treated counterpart were plotted and shown in Figure 3.26.

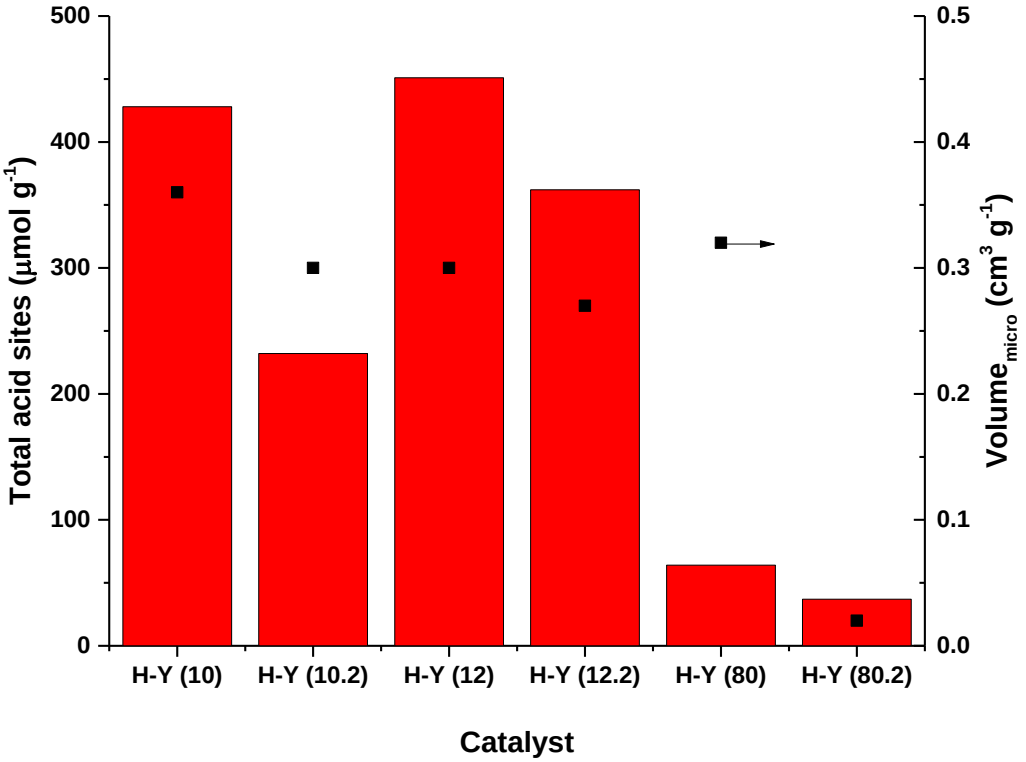

Figure 3.26 Acid site density versus micropore volume for H-Y zeolites.

Similar to H-Beta, the temperature programmed desorption profiles of the parent H-Y zeolites exhibited one peak with T_{max} shifting to a higher desorption temperature with increasing SiO_2/Al_2O_3 ratios, demonstrating that aluminium is predominately positioned in the framework position for zeolites with a higher SiO_2/Al_2O_3 molar ratio. H-Y zeolites with lower SiO_2/Al_2O_3 molar ratios had a significant proportion of aluminium present in the extra-framework position. Generally, alkaline treatment of H-Y zeolites with 0.2 M NaOH decreased the total number of acid sites, due to the removal of framework aluminium.

3.3.4 FT-IR pyridine adsorption measurements of H-ZSM-5 zeolites

The nature of acidity plays an important role in heterogonous catalysis and is crucial to understanding the role of the catalyst. One of the major limitations of temperature programmed desorption using ammonia (NH_3-TPD) as a probe molecule is the inability to distinguish between Brønsted and Lewis acid sites. This can be overcome by using pyridine as a probe molecule. In this study the nature of the acid sites of H-ZSM-5 zeolites were determined using Diffuse Reflectance Infrared Fourier Transform (DRIFT). FT-IR

with pyridine adsorption was conducted on H-ZSM-5 zeolites with SiO_2/Al_2O_3 ratios of 30 and 80 and alkaline treated counterparts to determine the nature of acidity, more specifically the nature of Brønsted and Lewis acid sites. The Brønsted (B) and Lewis (L) acid site ratios were determined using the peak intensities at 1540 cm^{-1} and 1450 cm^{-1} respectively. The peak at 1490 cm^{-1} is a band resulting from pyridine bonding to both Brønsted and Lewis acid sites.[180] The concentrations of Brønsted and Lewis acidity were determined using the B/L ratio and used in conjunction with the acid site density value determined by TPD-NH_3. FT-IR pyridine adsorption profiles and measurements for H-ZSM-5 (30) and H-ZSM-5 (80) zeolites are shown in Figures 3.27-3.28.

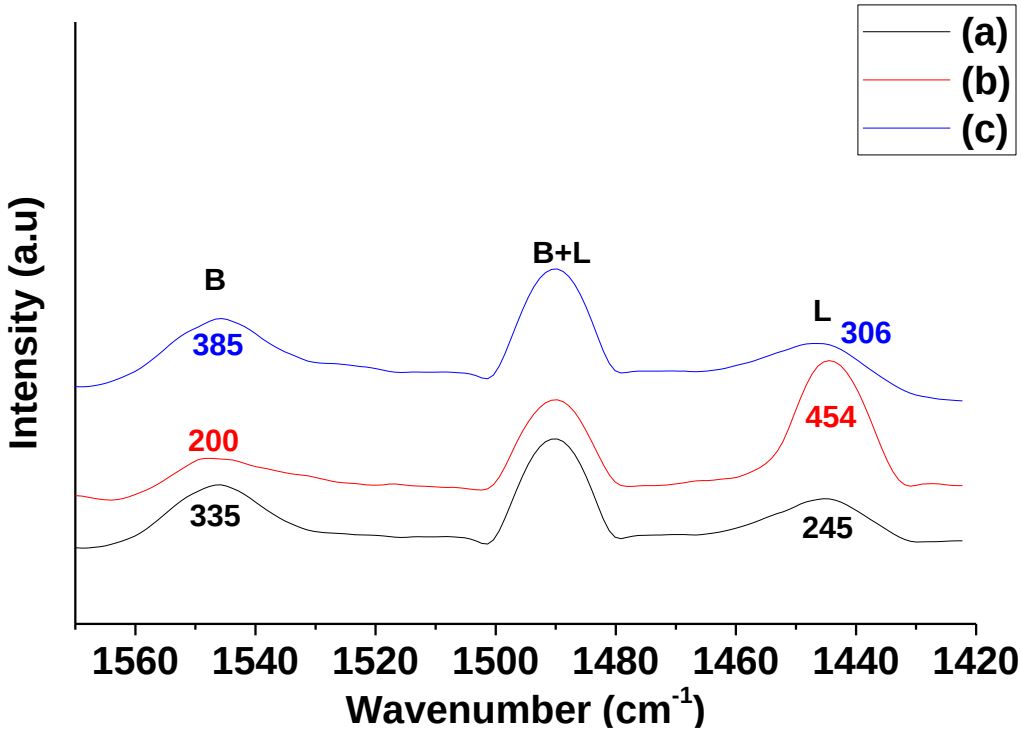

Figure 3.27 FTIR-pyridine adsorption plots of (a) H-ZSM-5 (30), (b) H-ZSM-5 (30.2) and (c) H-ZSM-5 (30.4).

H-ZSM-5 (30) had both Brønsted and Lewis acid sites as determined by the peaks shown at 1540 cm^{-1} and 1450 cm^{-1} respectively with a B/L ratio of 1.4. Alkaline treatment of H-ZSM-5 with 0.2 M NaOH led to a decrease in the concentration of Brønsted acid sites from 335 to 200 μmol g^{-1}. This can be ascribed to the removal of the tetrahedral aluminium species. The increase of Lewis acid sites from 143 to 338 μmol g^{-1} was due to the formation of extra-framework aluminium. These results were largely in agreement with the work carried out by Gou et al.[181] which

showed that due to extraction of framework aluminium, the Lewis acid site density increased after alkaline treatment. It was suggested that aluminium and silicon could re-insert back into the framework position during longer reaction times, increasing the strong acid site density at the expense of weaker acid sites. This is largely in accordance with the results obtained for H-ZSM-5 (30) when treated with 0.4 M NaOH. XPS studies carried out by Fernandez et al[182] confirmed that during the desilication process, aluminium species is re-precipitated back onto the external surface. Since the re-insertion of aluminium into the framework does not occur, this resulted in the formation of Lewis acid sites. Next, studies were carried out to distinguish the Brønsted and Lewis acid sites in H-ZSM-5 (80, 80.2 and 80.4), with the results shown in Figure 3.28.

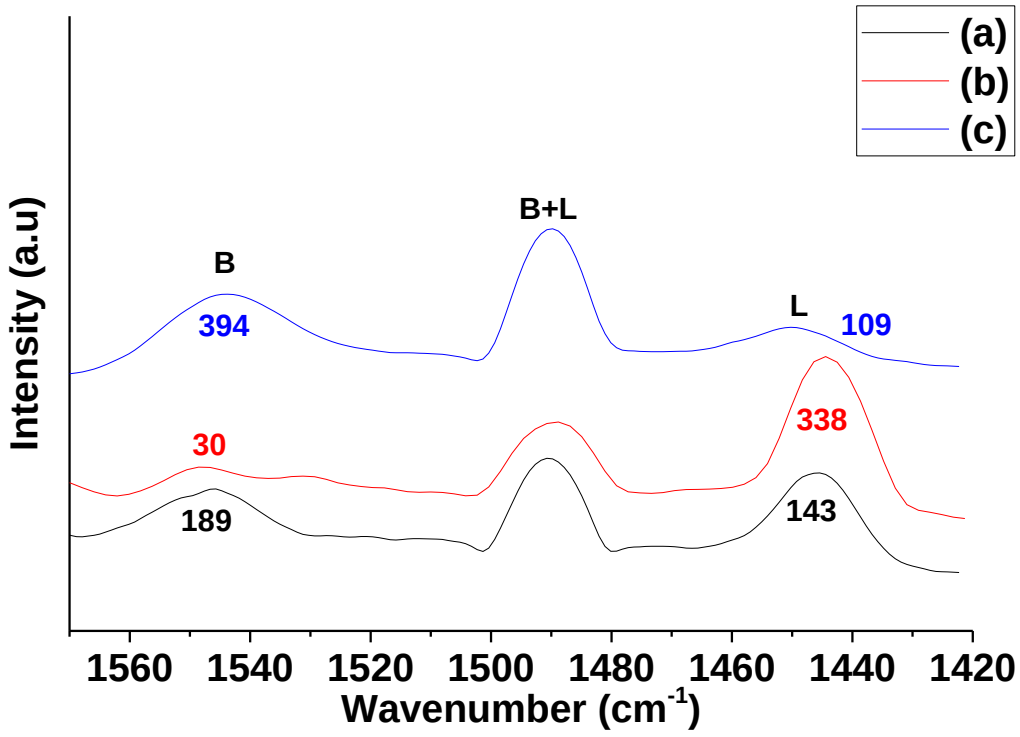

Figure 3.28 FTIR-pyridine adsorption plots of (a) H-ZSM-5 (80), (b) H-ZSM-5 (80.2) and (c) H-ZSM-5 (80.4).

FT-IR-pyridine studies of H-ZSM-5 (80) and its alkaline treated counterparts showed an identical trend as H-ZSM-5 (30). Unsurprisingly, H-ZSM-5 (30) had a larger concentration of Brønsted acid sites than H-ZSM-5 (80), owing to the increased amount of aluminium within the tetrahedral framework. Figure 3.28 showed that H-ZSM-5 (80) contained very similar levels of Brønsted and Lewis

acid sites. Mild alkaline treatment of H-ZSM-5 (80) led to a significant decrease in the number of Brønsted acid sites, leading to a catalyst with predominately Lewis acidity. Treatment of H-ZSM-5 (80) under more extreme alkaline conditions led to a decrease in Lewis acidity and the formation of a catalyst with nearly four times more Brønsted than Lewis acid sites.

3.3.5 Solid state NMR studies

In this subsection, ^{27}Al and ^{29}Si MAS-NMR spectra are presented for the first time showing the effect of alkaline treatment of zeolites with sodium hydroxide on the coordination of aluminium and silicon species.

3.3.5.1 ^{27}Al NMR

^{27}Al MAS-NMR measurements were performed to determine the coordination of aluminium in the zeolite samples before and after alkaline treatment. Solid state NMR spectra show peaks centred at ca. 54 and 0 ppm correspond to framework aluminium in tetrahedral coordination (Al_F) and extra-framework (Al_{Ext}) respectively.[183] Al_F/Al_{EXT} ratios were calculated based on intensities after baseline correction using OriginPro (2015) software using Guassian fitting of the peaks centred at ~50 ppm and 0 ppm.

3.3.5.1.1 H-ZSM-5

The ^{27}Al MAS-NMR spectra for H-ZSM-5 zeolites are shown in Figures 3.29-3.31, with the subsequent plots showing the Al_F/Al_{Ext} ratio.

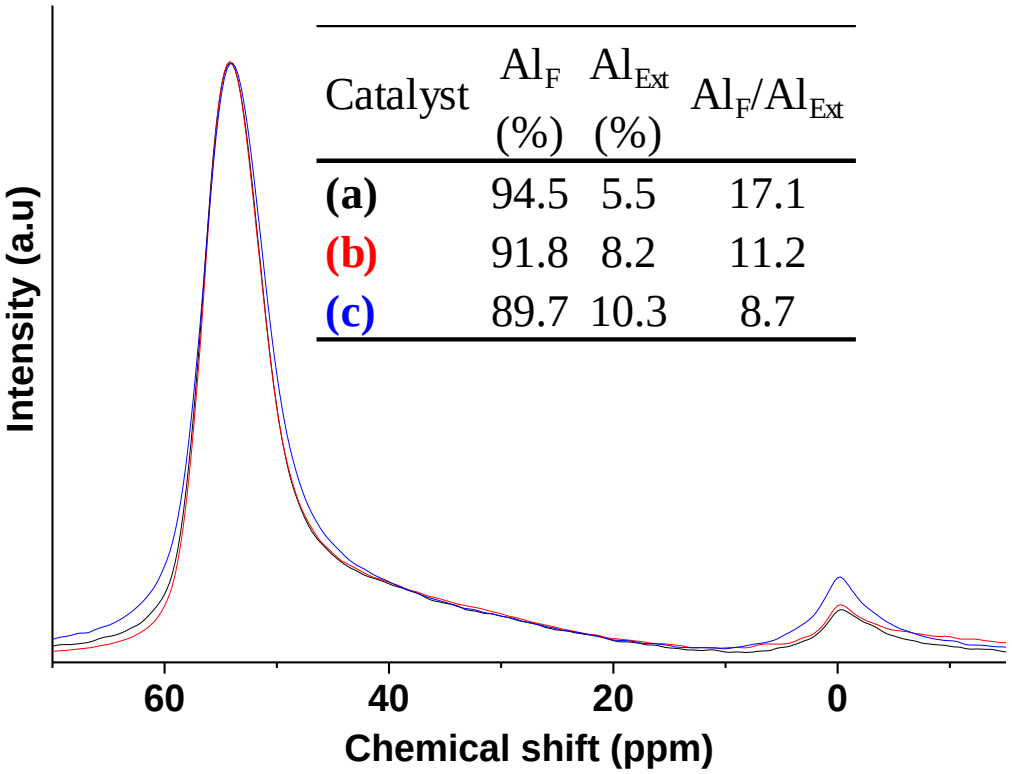

Catalyst	Al_F (%)	Al_{Ext} (%)	Al_F/Al_{Ext}
(a)	94.5	5.5	17.1
(b)	91.8	8.2	11.2
(c)	89.7	10.3	8.7

Figure 3.29 ^{27}Al MAS-NMR spectra of (a) H-ZSM-5 (30), (b) H-ZSM-5 (30.2) and (c) H-ZSM-5 (30.4).

^{27}Al MAS-NMR measurements confirmed the parent zeolite possessed aluminium species largely located in the tetrahedral framework, which gives rise to the large number of Brønsted acid sites. This is in good agreement with TPD-NH_3 and FTIR-pyridine studies. The area of the peak assigned to extra-framework aluminium increased with increasing concentration of NaOH which confirms that aluminium was not re-inserted back into the framework. It is worth nothing that extra-framework aluminium species act as Lewis acid centres.[184] Based on FTIR-pyridine studies, the decrease in intensity of the Lewis acid sites for H-ZSM-5 (30.4) compared to H-ZSM-5 (30.2) could be attributed to the removal of trigonally coordinated silicon species, possibly formed by dehydroxylation during the calcination step during the manufacturing stage. Next, studies were carried out on H-ZSM-5 (80, 80.2 and 80.4) with the ^{27}Al MAS-NMR shown in Figure 3.30.

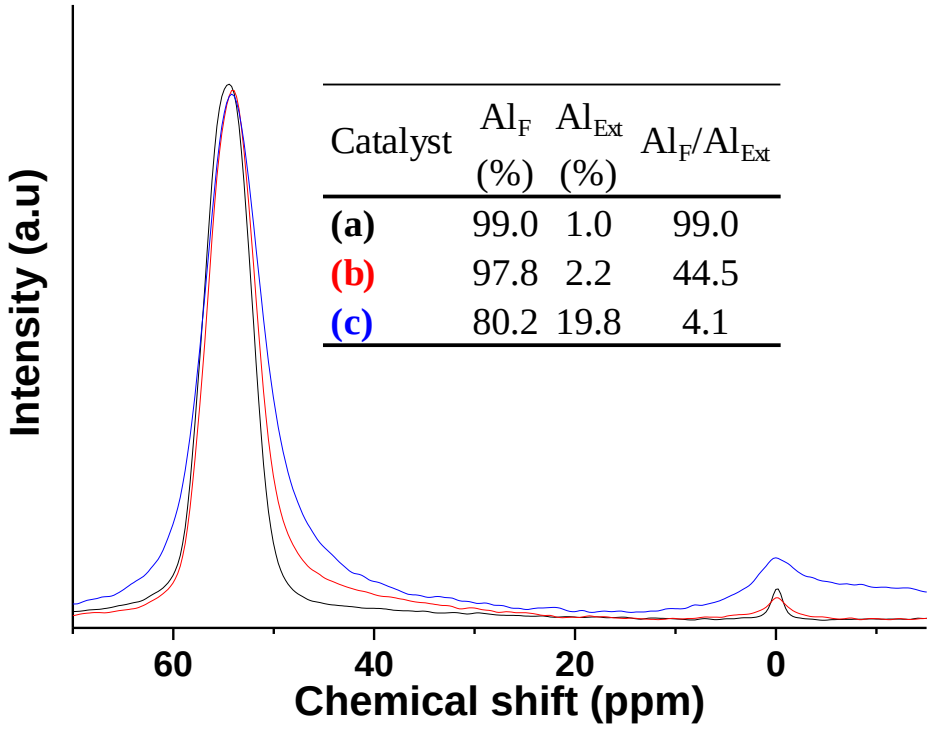

Catalyst	Al_F (%)	Al_{Ext} (%)	Al_F/Al_{Ext}
(a)	99.0	1.0	99.0
(b)	97.8	2.2	44.5
(c)	80.2	19.8	4.1

Figure 3.30 ^{27}Al MAS-NMR spectra of (a) H-ZSM-5 (80), (b) H-ZSM-5 (80.2) and (c) H-ZSM-5 (80.4).

A similar effect was observed in Figure 3.30 for H-ZSM-5 (80) with alkaline treatment than for H-ZSM-5 (30, 30.2 and 30.4). ^{27}Al MAS-NMR measurements showed that 99% of aluminium was located in the framework position for H-ZSM-5 (30), acting as Brønsted acid site centres. Treatment of H-ZSM-5 (80) with 0.2 M of NaOH resulted in a small extraction of aluminium from the framework into the extra-framework positon. This combined with FTIR-pyridine studies confirm that enhancement of Lewis acid sites was due to the formation of extra-framework aluminium.[185] Treatment of H-ZSM-5 (80) with 0.4 M NaOH led to extraction of aluminium from the framework with the ratio decreasing from 99% to 80.2%. FTIR-pyridine studies confirmed the Lewis acid concentration significantly decreased after treatment with 0.4 M of NaOH, likely due to the removal of the Lewis acidic silicon. Next, studies showing the ^{27}Al MAS-NMR spectra for our H-ZSM-5 (100 and 100.2) zeolites can be found in Figure 3.31.

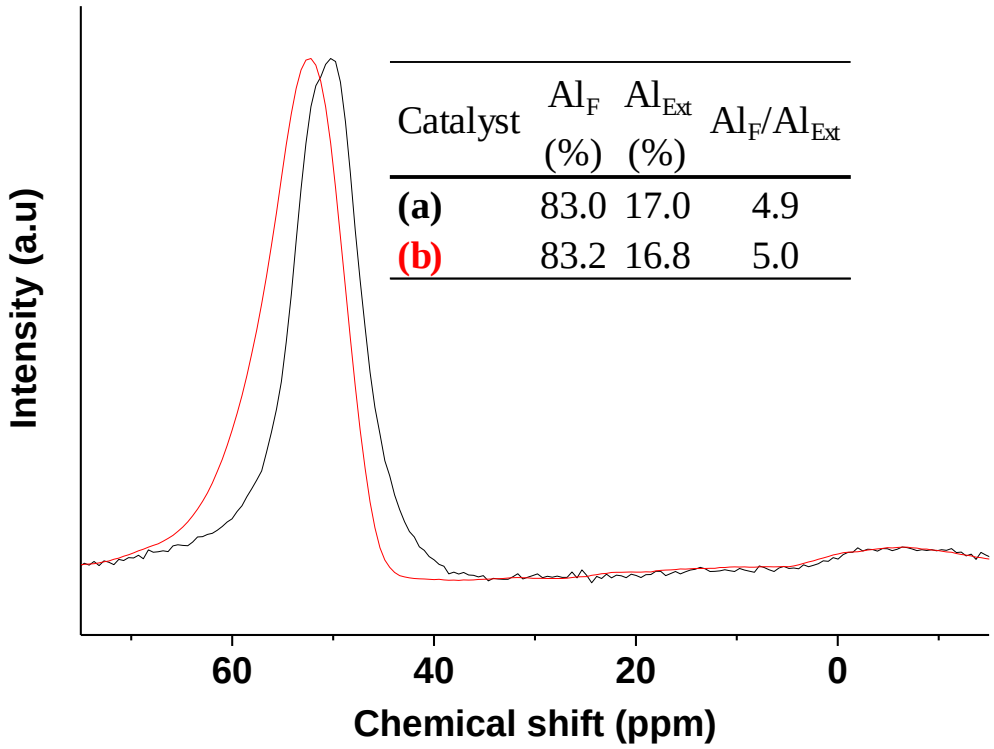

Catalyst	Al_F (%)	Al_{Ext} (%)	Al_F/Al_{Ext}
(a)	83.0	17.0	4.9
(b)	83.2	16.8	5.0

Figure 3.31 ^{27}Al MAS-NMR spectra of H-ZSM-5 (100) and H-ZSM-5 (100.2).

Our H-ZSM-5 (100) showed that 83% of aluminium was located in the tetrahedral position, considerably lower than for H-ZSM5 (30 and 80). Therefore, it was hardly surprising that treatment of H-ZSM-5 (100) with 0.2 M NaOH resulted in a significant decrease in surface area. Unlike in the case of H-ZSM-5 (30 and 80), alkaline treatment resulted in a slight increase in intensity of the peak at ca. 60 nm, due to the re-insertion of aluminium into the framework of mesoporous walls forming acidic hydroxyls.[186] This result is in general agreement with the study carried out by Yoo et al.[187] which demonstrated the re-insertion of extra-framework aluminium into the framework position for ZSM-5 with a Si/Al ratio close to 50.

3.3.5.1.2 H-Beta

After analysing the effect of alkaline treatment on the coordination of aluminium in H-ZSM-5 zeolites, studies were carried out investigating the effect of mild alkaline treatment on the coordination of aluminium in H-Beta zeolites with initial SiO_2/Al_2O_3 molar ratios; 25, 38 and 360. The ^{27}Al MAS-NMR measurements for H-Beta zeolites are shown in Figures 3.32-3.34.

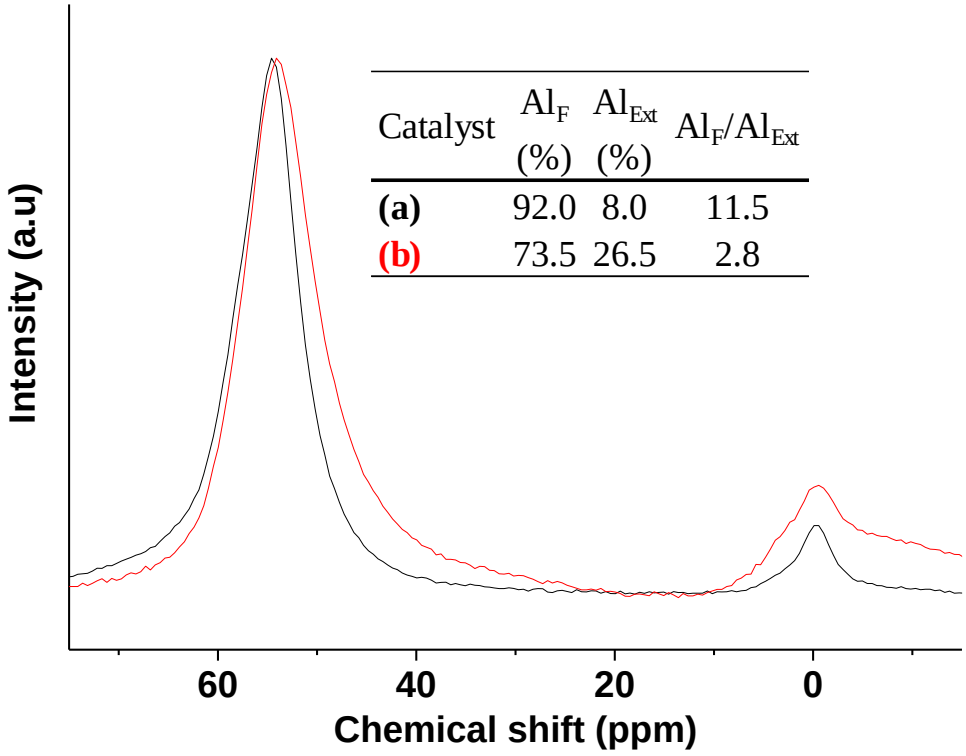

Catalyst	Al_F (%)	Al_{Ext} (%)	Al_F/Al_{Ext}
(a)	92.0	8.0	11.5
(b)	73.5	26.5	2.8

Figure 3.32 ^{27}Al MAS-NMR spectra of untreated (a) H-Beta (25) and H-Beta (25.2).

Figure 3.32 showed that for H-Beta (25), 92% of aluminium was located in the tetrahedral framework, similar to H-ZSM-5 (30). Despite H-Beta (25) and H-ZSM-5 (30) having a similar SiO_2/Al_2O_3 molar ratio and percentage of aluminium in the framework, there were marked differences on the effect of mild alkaline treatment. Mild alkaline treatment resulted in a significant decrease in the intensity of Al_F for H-Beta (25.2), decreasing from 92 to 73.5%. Clearly, this resulted in the formation of extra-framework aluminium. For H-ZSM-5 (30), Al_F decreased slightly from 94.5% for the parent to 91.8% for H-ZSM-5 (30.2). We believe that this difference was due to H-Beta (25) possessing larger porosity than H-ZSM-5 (30), facilitating extraction of tetrahedral atoms from the framework. This result is clearly in accordance with TPD-NH_3, which confirmed that the decrease in acid site density was due to the reduction of Brønsted acid sites.

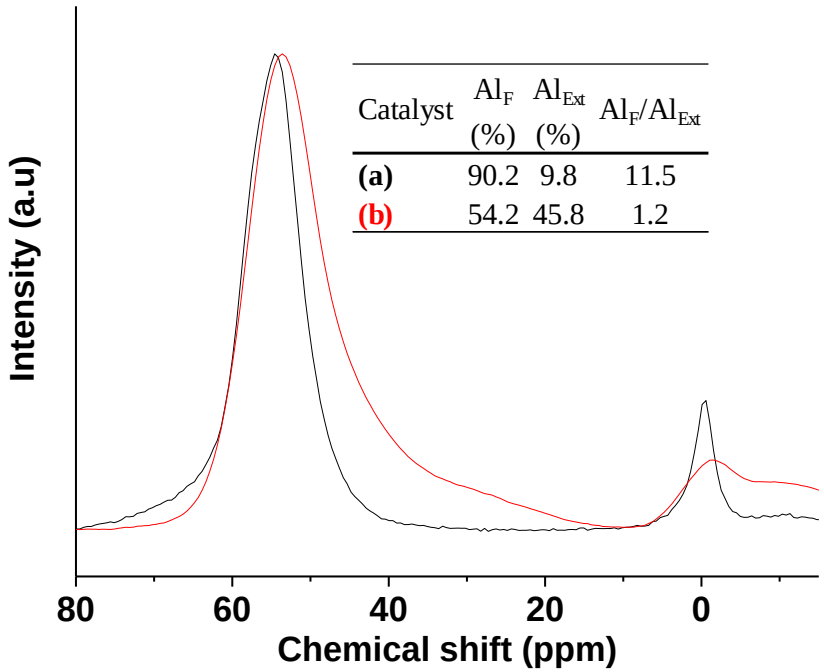

Catalyst	Al_F (%)	Al_{Ext} (%)	Al_F/Al_{Ext}
(a)	90.2	9.8	11.5
(b)	54.2	45.8	1.2

Figure 3.33 ^{27}Al MAS-NMR spectra of H-Beta (38) and H-Beta (38.2).

The proportion of tetrahedral aluminium (Al^{IV}) of H-Beta (38) was >90%. Mild alkaline treatment resulted in a dramatic decrease in Al^{IV} from 90.2% to 54.2%. The proportion of Al_{Ext} increased from 9.8% for H-Beta (38) to 45.8% for H-Beta (38.2). The slight shoulder observed at ca. 40 ppm is attributable to the formation of penta-coordinated aluminium (Al^{V}) for H-Beta (38.2). The obtained values are in general agreement with those obtained for H-Beta (25) and H-Beta (25.2). It is now apparent that mild alkaline treatment has a different effect on both the physical and chemical properties of H-ZSM-5 and H-Beta with similar SiO_2/Al_2O_3 molar ratios. For H-Beta zeolites with low SiO_2/Al_2O_3 molar ratios, it is clear that further experimental studies are required to restore the proportion of Brønsted acid sites after mild alkaline treatment. Wang et al.[164] demonstrated that the total number of acid sites can be restored by a mild acid washing of the desilicated H-Beta zeolite.

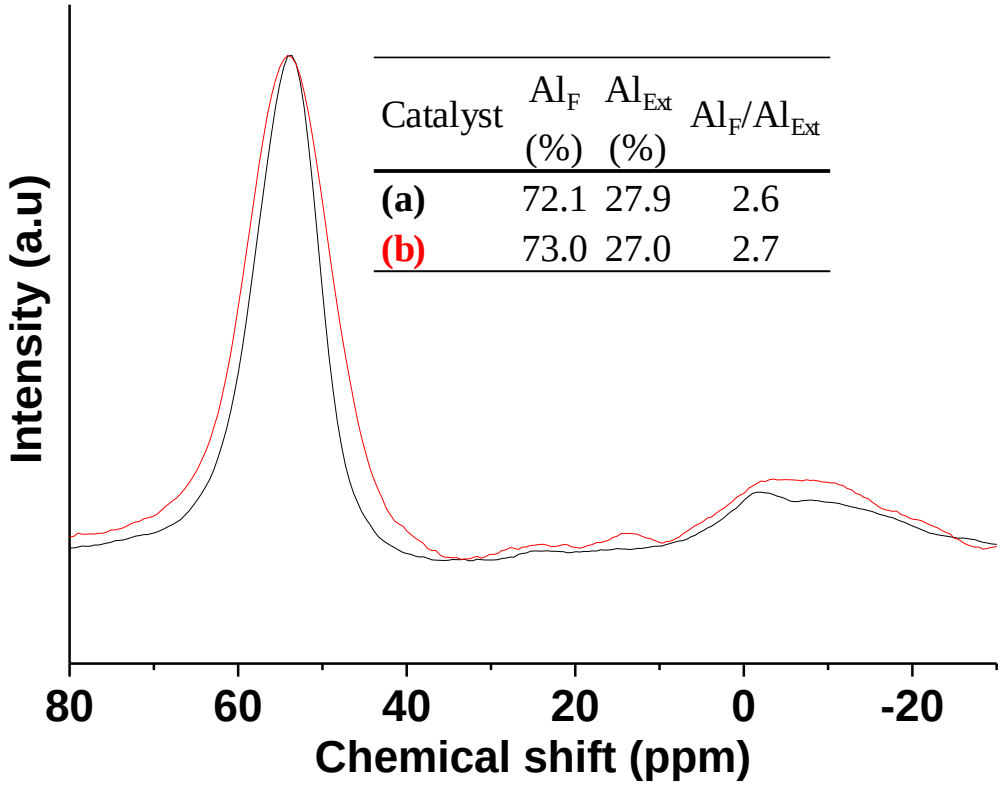

Figure 3.34 ^{27}Al MAS-NMR spectra of H-Beta (360) and H-Beta (360.2).

^{27}Al MAS-NMR for H-Beta (360) showed that 72.1% of aluminium was present as Al^{IV}. Due to the near symmetric shape of the peak at 60 nm, it was assumed that Al^{V} was not present and that extra-framework aluminium was attributed to Al^{VI}. Due to the lower ratio of Al^{IV} and large SiO_2/Al_2O_3 molar ratio of H-Beta (360), it was hardly surprising that even mild alkaline treatment resulted in an almost complete amorphisation of the zeolite. The ratio of Al^{IV} increased slightly from 72.1% for the parent to 73% for the modified zeolite. This would normally imply the re-insertion of Al^{VI} into the tetrahedral sites forming Al^{IV}. However, TPD-NH_3 studies confirmed acid site density decreased after alkaline treatment as opposed to increasing. Therefore, it is likely that the increase in ratio for Al^{IV} was due to the removal of Al^{VI}. The slight shoulder at ca. 40 ppm was due to the formation of extra-framework Al^{V} species which are not highly acidic species.[173] Together with TPD-NH_3 studies, the decrease in acid site density was largely due to the removal of Al^{VI} and formation of Al^{V} species. Despite XRD studies showing the complete amorphization of H-Beta (360.2), the structure was able to retain Al^{IV} species. This is in excellent agreement with the work carried out by Sadowska et al.[188] However, the broader signal of the peak at ca 60 ppm confirms loss of homogeneity of the framework environment.

3.3.5.1.3 H-Y

Next, our studies focused on the effect on mild alkaline treatment of the co-ordination of aluminium species in H-Y zeolites. Given the fact that H-Beta and H-Y contain 12 rings[189, 190] with similar pore sizes, [191,192] it was anticipated that mild alkaline treatment would have a similar effect on the coordination of aluminium species for H-Y as for H-Beta. ^{27}Al MAS-NMR spectra for H-Y zeolites are shown in Figures 3.35-3.37.

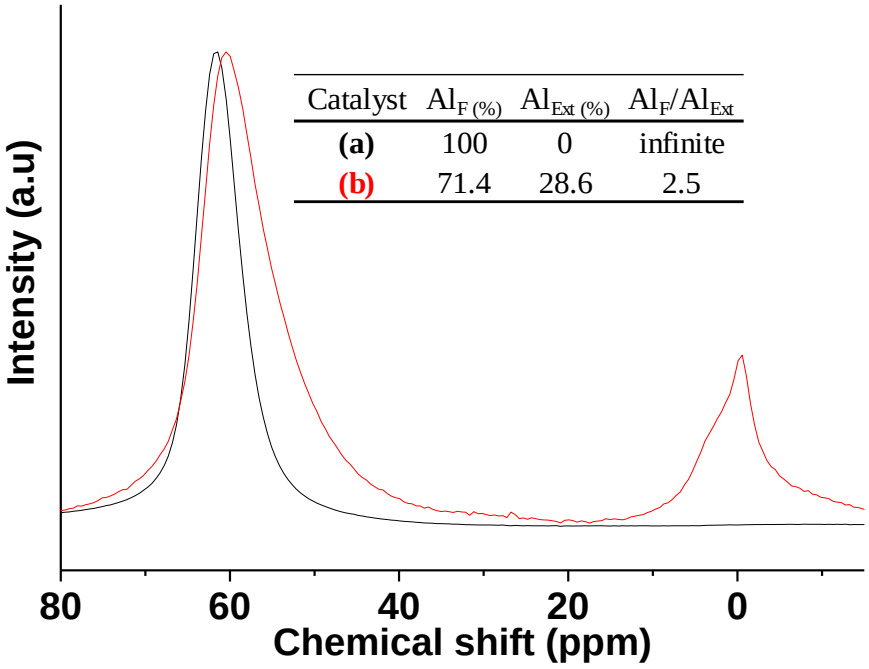

Figure 3.35 ^{27}Al MAS-NMR spectra of H-Y (10) and H-Y (10.2).

H-Y (10) exhibited an intense peak centred at around 54 ppm, due to Al^{IV}. No peak was detected at ca. 40 or 0 ppm indicating Al^{V} or Al^{VI} was not present. Despite this, mild alkaline treatment resulted in the partial collapse of the structure. The ratio of Al^{IV} decreased from 100% for the parent to 71.4% for the alkaline treated zeolite. It was unsurprising significant loss of Al^{IV} resulted in significant loss of acid site density shown in TPD-NH_3 studies due to the reduction of Al^{IV}; i.e. Brønsted acid sites. Alkaline treatment of H-Y (10) gave an Al_F/Al_{EXT} ratio of 2.5, indicating that aluminium was extracted from the framework. ^{27}Al MAS-NMR spectrum of H-Y (10.2) showed a slight shoulder at ca. 30 ppm due to the formation of extra-framework penta-coordinated aluminium. It could be concluded that despite H-Y (10) having 100% of aluminium

species located in the framework position, alkaline treatment under mild conditions resulted in extraction of Al^{IV}.

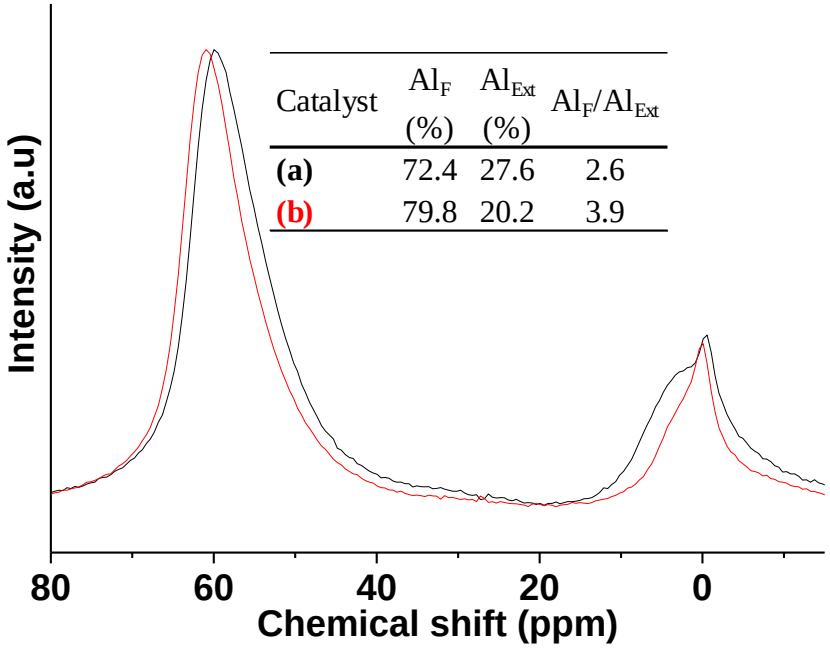

Figure 3.36 ^{27}Al MAS-NMR spectra of H-Y (12) and H-Y (12.2).

Despite the laboratory H-Y (10) and commercial H-Y (12) zeolite having similar SiO_2/Al_2O_3 molar ratios, there were clear differences of alkaline treatment on Al coordination on the ^{27}Al MAS-NMR spectra. When H-Y (12) was treated with 0.2 M NaOH the intensity of Al^{IV} increased from 72.4% to 79.8%, whereas the intensity for Al^{IV} decreased significantly. Since TPD-NH_3 studies showed that the acid site density was compromised after alkaline treatment, this can be ascribed to the removal of Al^{VI} during the desilication process. This is supported by the fact there does not appear to be Al^{V} due to the largely absent peak at ca. 40 ppm. Therefore, alkaline treatment led to the reduction the loss of trigonally coordinated silicon and Al^{VI} (Lewis acid centres). Future studies are required to quantify the number of Brønsted and Lewis acid sites before and after alkaline treatment.

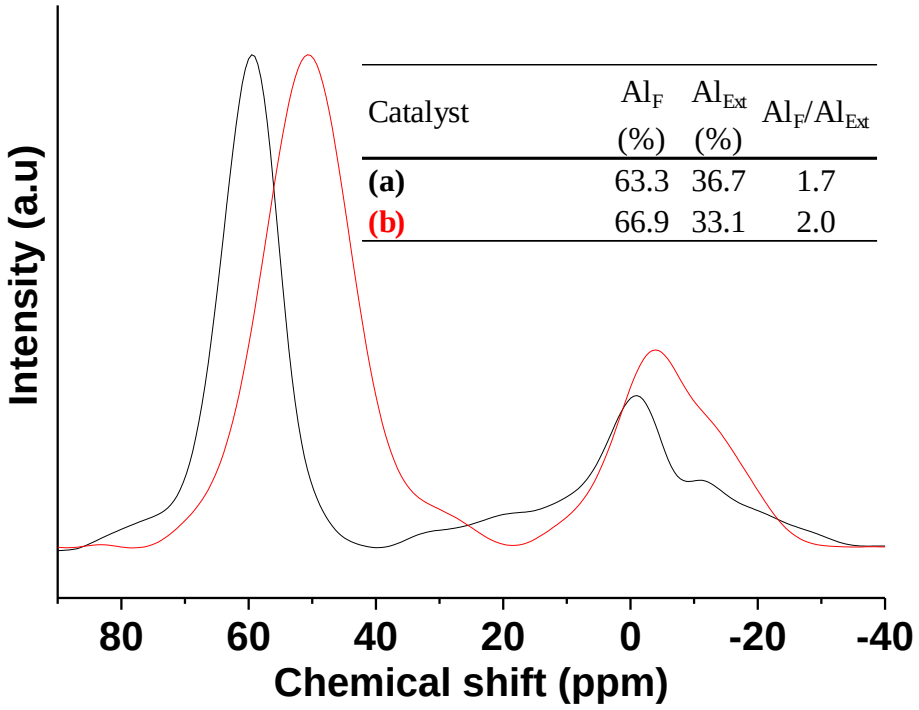

Catalyst	Al_F (%)	Al_{Ext} (%)	Al_F/Al_{Ext}
(a)	63.3	36.7	1.7
(b)	66.9	33.1	2.0

Figure 3.37 ^{27}Al MAS-NMR spectra of H-Y (80) and H-Y (80.2).

^{27}Al MAS-NMR spectra for H-Y (80) showed that the parent had 63.3% of the aluminium atoms located in the tetrahedral framework, considerably lower than H-Y (10 and 12). Due to the low Al^{IV} content and large SiO_2/Al_2O_3 ratio, it was hardly surprising that mild treatment of H-Y (80) resulted in the complete amorphization of the structure as confirmed by XRD. Treatment of H-Y (80) with 0.2 M NaOH led to an increase in intensity of Al^{IV} at the expense of Al^{VI} species. The Al_F/Al_{EXT} increased from 1.7 to 2.0, demonstrating extraction of Al^{VI} species from the structure. It can be seen that after alkaline treatment the isotropic shift of the peak at 54 ppm is widened as after treatment with sodium hydroxide. Quantum studies by Sklenak et al.[193] attributed this to a change of T-O-T angles in the framework (T is either Al or Si).

3.3.5.2 ^{29}Si NMR

^{29}Si MAS-NMR was performed to determine the coordination of the silicon atoms before and after alkaline treatment with sodium hydroxide. ^{29}Si MAS-NMR spectra exhibit main resonances between -112 ppm corresponding to $Si(OSi)_4$ and a resonance at ca. 106 ppm corresponding to $Si(OSi)_3(OAl)$. The relative peak areas were calculated from baseline corrected spectra and manually fitted using Gaussian functions to match the spectra using

OriginPro (2015) software. The framework Si/Al ratio is denoted as $(Si/Al)_F$ and was calculated using Equation 3.2 (below), where Al_F and Al_{Ext} are the peak percentages of the framework and extra-framework aluminium atoms, respectively.

$$\left(\frac{\mathrm{Si}}{\mathrm{Al}}\right)_{\mathrm{framework}} = \frac{\left(\frac{\mathrm{Si}}{\mathrm{Al}}\right)_{\mathrm{bulk}}}{\mathrm{Al_F}/(\mathrm{Al_F} + \mathrm{Al_{Ext}})}$$

Equation 3.2 Calculation used to determine Si/Al framework ratio[194]

3.3.5.2.1 H-ZSM-5

The ^{29}Si MAS-NMR spectra are only described save space and are summarised in Table 3.4. ^{29}Si MAS-NMR spectra of our H-ZSM-5 (100) and H-ZSM-5 (100.2) are shown in Figure 3.38 to represent a typical ^{29}Si MAS-NMR spectra before and after desilication. The framework aluminium per unit cell was calculated based on the assumption that a unit cell contains 96 (Si + Al atoms).[195]

Table 3.4 Relative intensities of peaks in untreated and alkaline treated H-ZSM-5 zeolites observed by ^{29}Si MAS-NMR.

Catalyst	%		$(Si/Al)_{bulk}$	$(Si/Al)_F$	Al unit cell^{-1}
	$Si(OAl)_{1-4}$	$Si(OSi)_4$			
H-ZSM-5 (30)	11.4	88.6	13.9	14.7	6.5
H-ZSM-5 (30.2)	9.5	90.5	11.8	12.8	7.5
H-ZSM-5 (30.4)	9.2	90.8	10.2	11.3	8.5
H-ZSM-5 (80)	10.6	89.4	35.4	35.8	2.7
H-ZSM-5 (80.2)	9.4	90.6	24.5	25.0	3.8
H-ZSM-5 (80.4)	8.5	91.5	15.4	19.2	5.0
H-ZSM-5 (100)	36.2	63.8	57.7	69.5	1.4
H-ZSM-5 (100.2)	25.5	74.5	65.7	79.0	1.2

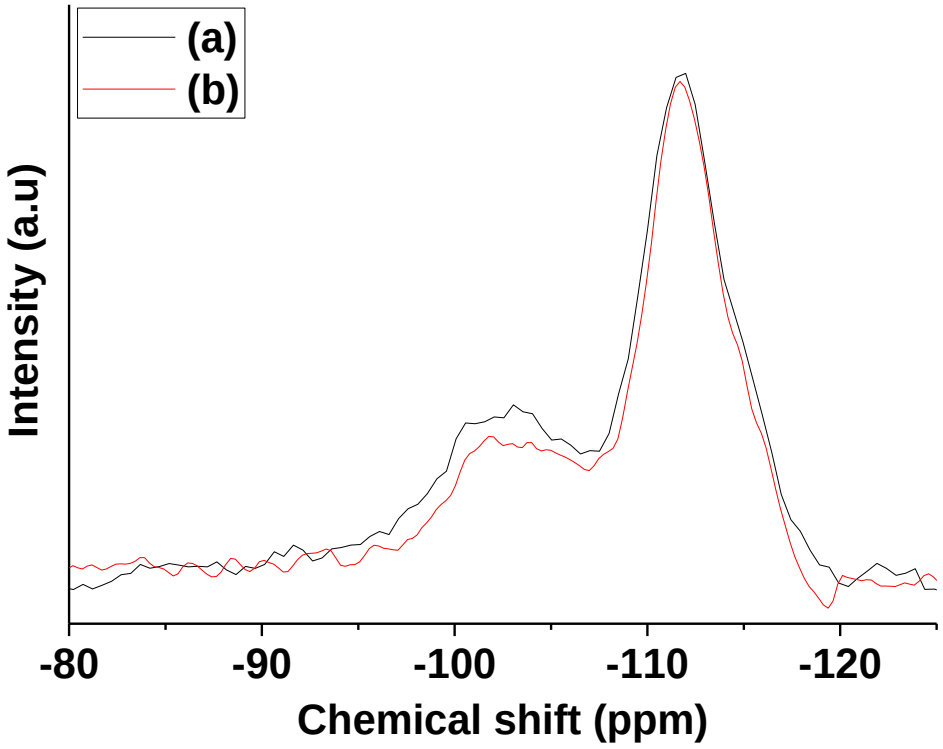

Figure 3.38 ^{29}Si MAS-NMR spectra for H-ZSM-5 (100) and H-ZSM-5 (100.2).

The ^{29}Si MAS-NMR spectra showed the commercially untreated H-ZSM-5 (30 and 80) and alkaline treated zeolites are highly siliceous with predominately $Si(OSi)_4$ environments, confirmed by the peak at chemical shift at ca.110 ppm. After treatment of H-ZSM-5 (30) with 0.2 M NaOH, the intensity of the $Si(OSi)_4$ peak increased from 88.6% to 90.5% for H-ZSM-5 (30.2). When the concentration of NaOH was increased to 0.4 M, the intensity of the $Si(OSi)_4$ increased to 90.77%. The signal at -105 ppm can result in the overlap between Si(OAl) and silanol groups.[195] It is likely that the increase of the $Si(OSi)_4$ peak is due to the removal of SiOH groups; i.e. silanol nests. This is supported by FTIR, which showed that after alkaline treatment the silanol nest band (3460 cm^{-1}) disappeared.[196] Treatment of H-ZSM-5 (80) with 0.2 M NaOH showed the proportion of $Si(OSi)_4$ increased from 89.4% to 90.6%. ^{29}Si MAS-NMR revealed H-ZSM-5 (100) has a much lower $Si(OSi)_4$ content than commercial H-ZSM-5 (30) and H-ZSM-5 (80). This strongly indicates that aluminium is largely located in the framework position for our laboratory H-ZSM-5 (100) zeolite. Alkaline treatment of H-ZSM-5 (100) with 0.2 M NaOH showed an increase of the $Si(OSi)_4$ peak from 63.8% to 74.5% for H-ZSM-5 (100.2). The $(Si/Al)_F$ ratio increased after alkaline treatment of laboratory synthesised H-ZSM-5 from 69.5 to 79. Since the ^{27}Al MAS-NMR spectra showed

the extra-framework peak was largely unchanged after alkaline treatment, it is likely that the $(Si/Al)_F$ ratio was larger for H-ZSM-5 (100.2) than its parent due to extraction of Al^{IV}.

3.3.5.2.2 H-Beta

The ^{29}Si MAS-NMR spectra of H-Beta zeolites were similar than those obtained for H-ZSM-5 zeolites. They contain predominately $Si(OSi)_4$ environments, with the spectrum showing 2 peaks. It was assumed that the peak corresponding to -110 ppm represented $Si(OSi)_4$ environment, and the peak at -102 ppm corresponded to Si(OAl). ^{29}Si MAS-NMR measurements were carried out on all H-Beta zeolites with the exception of our laboratory synthesised H-Beta zeolite. The results are summarised in Table 3.5 (below).

Table 3.5 Relative intensities of peaks in untreated and alkaline treated H-Beta zeolites observed by ^{29}Si MAS-NMR.

Catalyst	%		$(Si/Al)_{bulk}$	$(Si/Al)_F$	Al unit $cell^{-1}$
	$Si(OAl)_{1-4}$	$Si(OSi)_4$			
H-Beta (25)	21.8	78.3	9.9	13.5	8.9
H-Beta (25.2)	22.9	77.1	7.7	13.3	7.2
H-Beta (38)	18.8	81.2	15.6	17.2	5.6
H-Beta (38.2)	38.8	61.3	10.0	18.4	5.2
H-Beta (360)	15.8	84.2	77.4	107.3	0.9
H-Beta (360.2)	42.9	57.2	31.2	42.8	2.2

H-Beta zeolites with larger SiO_2/Al_2O_3 molar ratios showed enhanced $Si(OSi)_4$ environments. After alkaline treatment the peak at -110 ppm decreased in all H-Beta zeolites, attributable to a reduction of $Si(OSi)_4$. For H-Beta (25), this decrease was minuscule, likely due to the large quantity of Al^{IV}. The peak corresponding to $Si(OSi)_4$ decreased more significantly for H-Beta (38) and (360) after alkaline treatment. Worth noting is that $(Si/Al)_F$ was generally larger than the $(Si/Al)_{bulk}$. This confirms the presence of amorphous aluminium. This was in good agreement with ^{27}Al MAS-NMR studies. The

$(Si/Al)_F$ ratio decreased after alkaline treatment of H-Beta (360) from 107.3 to 42.8 due to extraction of tetrahedral silicon atoms. This is supported by ^{27}Al MAS-NMR studies which confirmed that the proportion of Al^{IV} species was largely unchanged after alkaline treatment.

3.3.5.2.3 H-Y

^{29}Si MAS-NMR spectra of the laboratory synthesised H-Y zeolite, H-Y (10) showed 5 distinct peaks. The results are summarised in Table 3.6.

Table 3.6 Relative intensities of peaks in untreated and alkaline treated H-Y zeolites observed by ^{29}Si MAS-NMR.

Catalyst	%		Si/Al_{bulk}	$(Si/Al)_F$	Al unit $cell^{-1}$
	$Si(OAl)_{1-4}$	$Si(OSi)_4$			
H-Y (10)	93.1	6.9	2.2	2.2	43.3
H-Y (10.2)	86.5	14.6	2.2	3.1	31.1
H-Y (12)	24.5	75.5	6.9	9.6	10.0
H-Y (12.2)	55.4	45.6	5.7	7.1	13.5
H-Y (80)	95.0	5.0	55.9	88.3	1.1
H-Y (80.2)	20.2	79.8	24.9	37.2	2.6

The peak corresponding to $Si(OSi)_4$ for the laboratory H-Y (10) zeolite was 6.9%. After desilication, the peak increased to 14.6%. The amount of aluminium per unit cell decreased from 43.3 to 31.1 after treatment. The peak owing to $Si(OAl)_{1-4}$ decreased to 86.5% for H-Y (10.2), confirming extraction of Al^{IV}. The $(Si/Al)_F$ ratio increased from 2.2 to 3.1, confirming the presence of amorphous Al_{Ext}. Alkaline treatment of H-Y (12) with 0.2 M NaOH significantly reduced the peak for $Si(OSi)_4$ from 75.5% to 45.6%, ascribed to the removal of Si-O-Si. In conjunction with XRD, this confirms that a significant proportion of silicon extracted was highly crystalline. It is possible that alkaline treatment of H-Y (12) led to the removal of amorphous silica and Al_{Ext}. This is supported by XRD and $(Si/Al)_F$ calculations with both decreasing after alkaline treatment.

Despite H-Y (80) being predominately siliceous, the ^{29}Si MAS-NMR spectra showed the peak intensity for $Si(OSi)_4$ was only 5%. This sharply increased after alkaline treatment to ca. 80%, indicating that the remaining proportion of H-Y (80) after alkaline treatment consisted of amorphous Si-O-Si species. Clearly, alkaline treatment had a more profound effect on the commercial zeolites than the laboratory synthesised zeolite owing to the significant proportion of Al_{Ext} present in commercial zeolites.

3.3.6 Microscopy of parent and alkaline treated H-ZSM-5 zeolites

The morphology of H-ZSM-5 (30, 30.2, 80 and 80.4) was investigated using scanning electron microscopy (SEM) as shown in Figure 3.39.

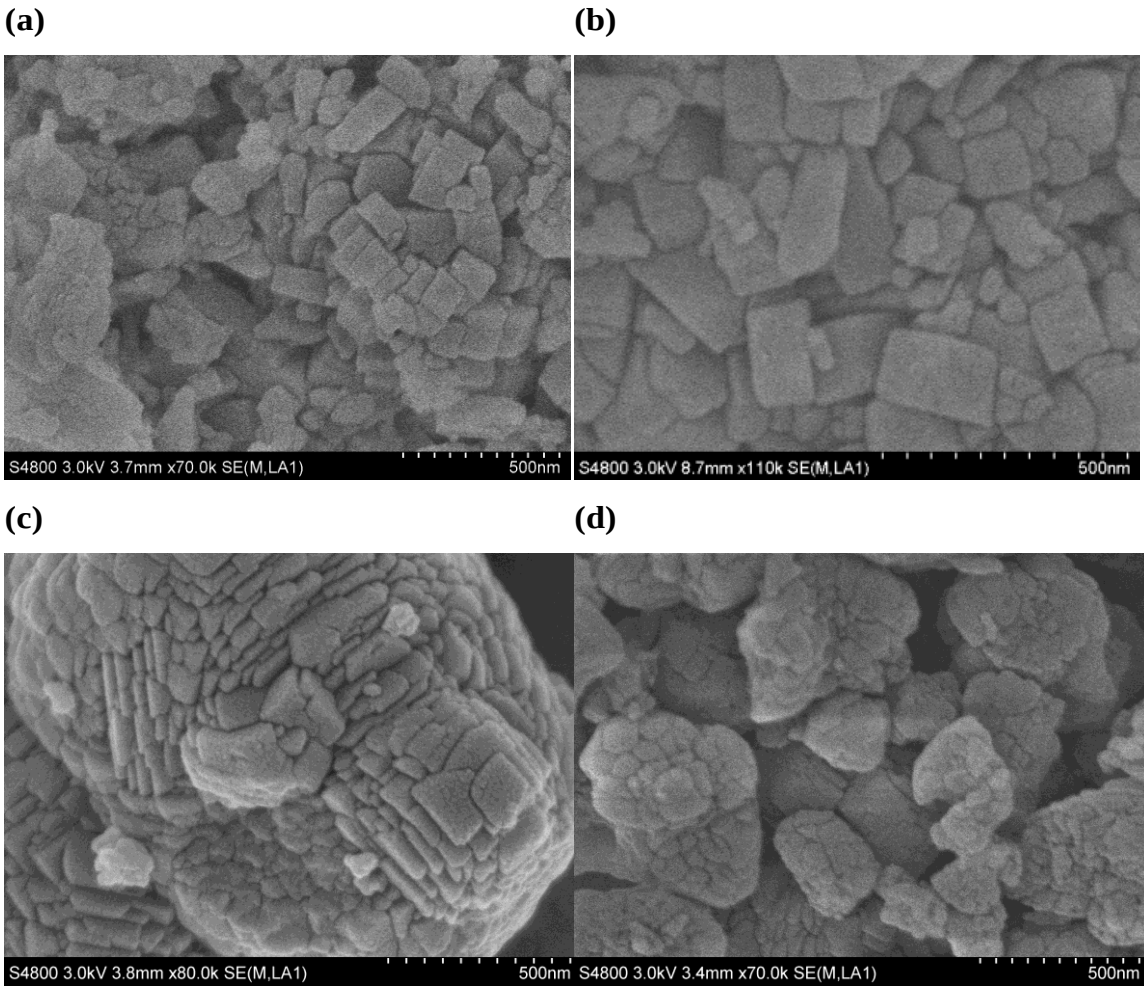

Figure 3.39 Scanning Electron microscopy of untreated and alkaline treated H-ZSM-5 zeolites (a) H-ZSM-5 (30), (b) H-ZSM-5 (30.2), (c) H-ZSM-5 (80), (d) H-ZSM-5 (80.2).

SEM measurements showed H-ZSM-5 displayed well defined morphologies of compact particle sizes ca. 250 nm. Alkaline treatment with sodium hydroxide had contrasting effects on the morphologies of H-ZSM-5 (30) and H-ZSM-5 (80). The external surfaces remained largely intact upon mild treatment with sodium hydroxide. This suggests that silicon extraction did not largely take place on the external surface of the zeolite crystals. Similar conclusions were reported by Sadowaska et al.[188] Alkaline treatment had minimal effect on the morphology of H-ZSM-5 (30) whereas for H-ZSM-5 (80) there was a clear change in morphology of the crystal structure after alkaline treatment, as can be seen from the formation of a less compact structure.

3.3.7 Friedel-Crafts alkylation of benzyl alcohol in the presence of zeolites

The Friedel-Crafts alkylation reaction between benzyl alcohol and benzene is commonly used as a probe reaction to study the porosity of hierarchical zeolites. The main observation of alkylation reactions using hierarchical zeolites is the activity due to increased accessibility of the active sites. The modification of zeolites by alkaline treatment provides an excellent opportunity to demonstrate increased intracrystalline diffusion. There have been numerous studies investigating the effect of increased mesoporosity on the catalytic activity in the Friedel-Crafts alkylation of benzyl alcohol with benzene.[147-149] Here, we investigated the effect of alkaline treatment of H-ZSM-5, H-Beta and H-Y and then tested them in the Friedel-Crafts alkylation reaction. The results were then compared to zeolites that had not been desilicated.

3.3.7.1 Blank reaction

Blank experiments were performed without a catalyst at 100 ^{o}C under stirring for 6 hours. Blank experiments showed less than 1% conversion, demonstrating the presence of an acid catalyst is required for the Friedel-Crafts alkylation reaction between benzene and benzyl alcohol.

3.3.7.2 The effect of time on the alkylation of benzyl alcohol

Preliminary experiments were performed to determine the reaction time that would be used for subsequent experiments. H-ZSM-5 (30) was chosen as the catalyst. Reactions were carried out at reaction times; 1, 3 and 6 hours at 100 °C with the results shown in Figure 3.40.

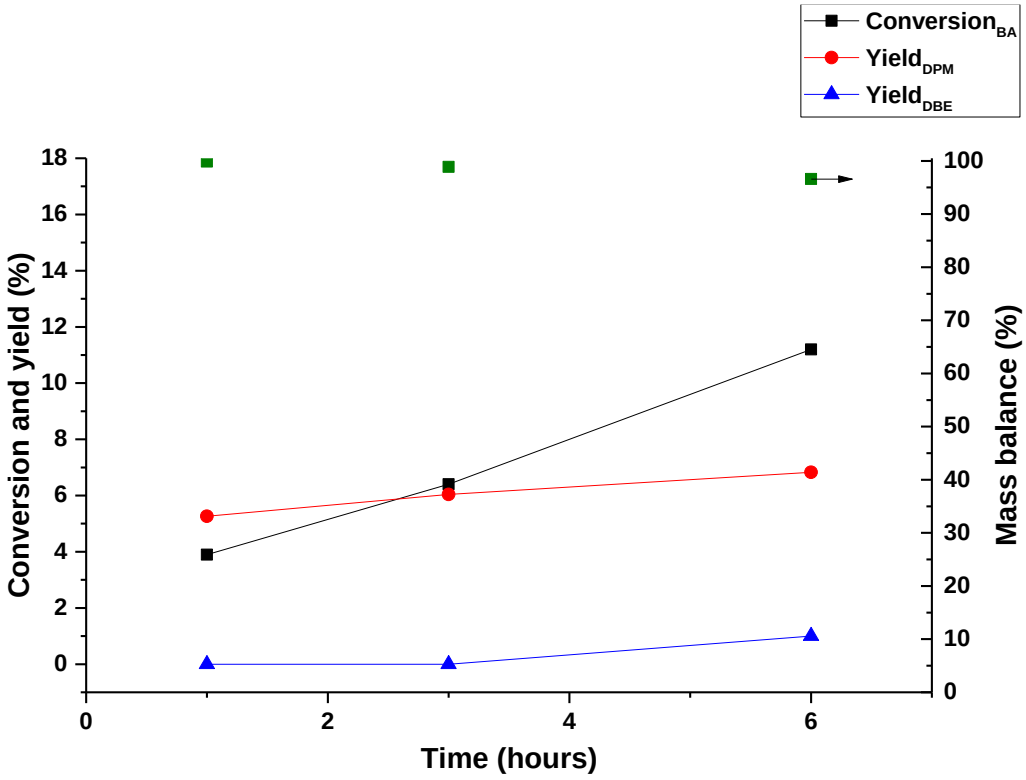

Figure 3.40 Conversion, product yield and mass balances for the BA alkylation of benzyl alcohol with benzene at various times for H-ZSM-5 (30) zeolite. Reaction conditions; 70 mg catalyst, 0.14 M BA in benzene, 100 °C.

Figure 3.40 shows the reaction time had an effect on the conversion and DPM yield. After 1 hour, conversion of BA was <4% with a DPM yield of 5.3%. DBE was not produced. The mass balance was 100%, confirming DPM was the only product. After 6 hours, a yield of 6.8% was obtained for DPM, with a total conversion of 11.2%. Candu et al.[197] found that a decrease in selectivity towards DPM was due to the formation of DBE and polyalkylated benzene. The formation of DBE in our study was due to acid catalysed etherification of BA. A 1% yield of DBE was obtained with a total mass balance 96.6% after 6 hours. We obtained similar levels of conversion as Sun et al.[147] They asserted that H-ZSM-5 had low catalytic activity after 10 hours at 80 °C due to mass transport phenomenon. Recycling tests performed by the same group showed excellent

reproducibility. In our study, recycling tests were not carried out. Reproducibility experiments were carried out, with the results shown in Chapter 4.

3.3.7.3 The effect of hierarchical zeolites on the Friedel-Crafts alkylation of benzyl alcohol with benzene

3.3.7.3.1 H-ZSM-5

The catalytic performance of six different H-ZSM-5 zeolites was investigated to examine the role of mesoporosity and acidity on the production of DPM in the benzyl alkylation of benzyl alcohol. H-ZSM-5 zeolites with initial SiO_2/Al_2O_3 molar ratios of 30, 80 and 100 were treated with 0.2 M NaOH and compared. The reaction was carried out using 0.14 M benzyl alcohol, for 6 hours at 100 ^oC. 70 mg of catalyst was used. The results of benzylation of BA with benzene with untreated and alkaline modified H-ZSM-5 (30, 30.2 and 30.4), H-ZSM-5 (80, 80.2 and 80.4) and H-ZSM-5 (100 and 100.2) are displayed in Figure 3.41-3.43. H-ZSM-5 (30.4) and H-ZSM-5 (80.4) were not tested and are merely demonstrated in this chapter for characterisation purposes.

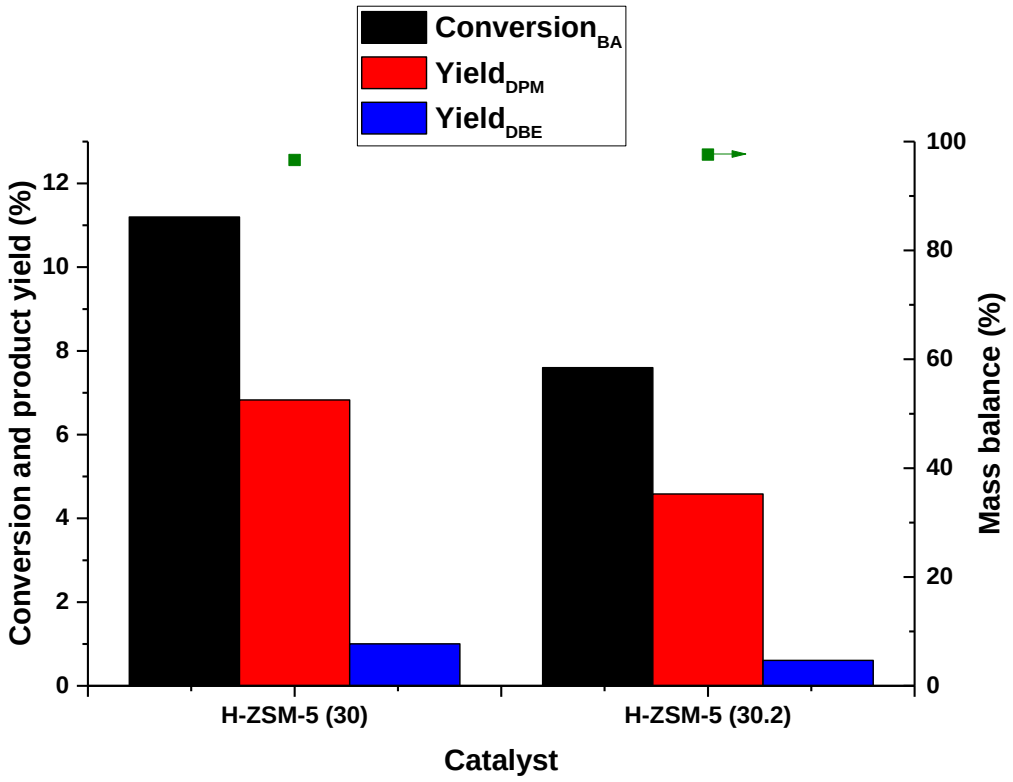

Figure 3.41 Conversion, product yield and mass balances for the BA alkylation of benzyl alcohol with benzene for H-ZSM-5 (30) and H-ZSM-5 (30.2) Reaction conditions; 70 mg catalyst, 0.14 M BA in benzene, 100 ^{o}C. 6 hours.

Conversion of BA over H-ZSM-5 (30) was 11.2% after 6 hours, whereas H-ZSM-5 (30.2) showed conversion of 7.6% after the same reaction time. Based on the findings in the literature, it is highly unlikely that alkaline treatment inhibited accessibility of the acid sites.[198-200] Therefore, decreased activity was assumed not to be related to the accessibility of the active sites. Since alkaline treatment had a limited effect on the total porosity, the decrease in catalytic activity could possibly due to enhanced acidity which facilitates hydrolysis of DBE, resulting in the re-formation of the starting material, BA. Unpublished work from our group found a similar trend with a laboratory synthesised H-Y zeolite with enhanced acidity to its predominantly microporous parent. H-ZSM-5 (30) produced a larger yield of DPM (6.8%) compared to 4.6% for H-ZSM-5 (30.2).

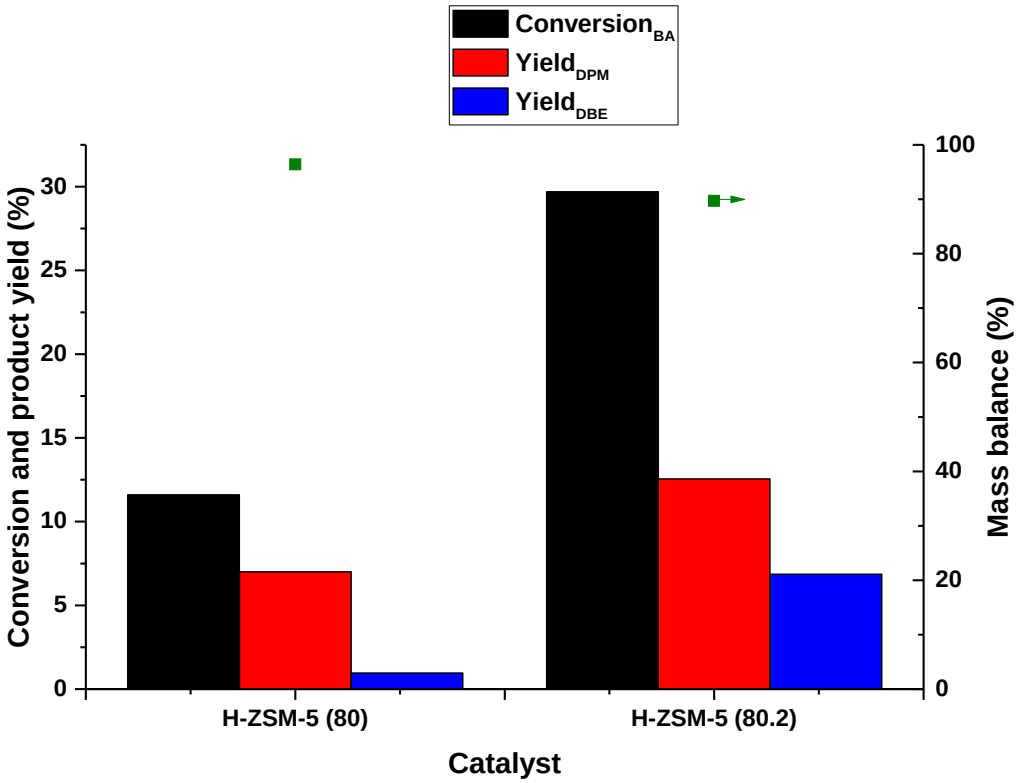

Figure 3.42 Conversion, product yield and mass balances for the BA alkylation of benzyl alcohol with benzene for H-ZSM-5 (80) and H-ZSM-5 (80.2) Reaction conditions; 70 mg catalyst, 0.14 M BA in benzene, 100 ^{o}C. 6 hours.

Conversion for H-ZSM-5 (80) was similar to H-ZSM-5 (30). This suggests that Brønsted acidity is largely absent on the external surface. This hypothesis is in good agreement with the work carried out by Jin et al.[149] Conversion for H-ZSM-5 (80.2) was 29.7%, nearly 3 times greater than H-ZSM-5 (80). The yield of DPM increased from 7% for H-ZSM-5 (80) to 12.6% for H-ZSM-5 (80.2). Interestingly, the yield of DBE increased from <1% for H-ZSM-5 (80) to ca. 7% for H-ZSM-5 (80.2). The mass balance decreased 96.4% to 89.7% due to the formation of polyaromatics, which were not calibrated in our study. The decrease in strong acid sites from 278 µmol g^{-1} for H-ZSM-5 (80) to 260 µmol g^{-1} for H-ZSM-5 (80.2) as shown from TPD-NH_3 studies strongly indicates that catalytic activity is enhanced by mesoporosity. Previous studies have shown that desilication of H-ZSM-5 zeolites increases accessibility of the acid sites.[186, 198, 199] Therefore, enhanced catalytic activity in H-ZSM-5 (80.2) can be attributed to enhanced accessibility of the active sites.

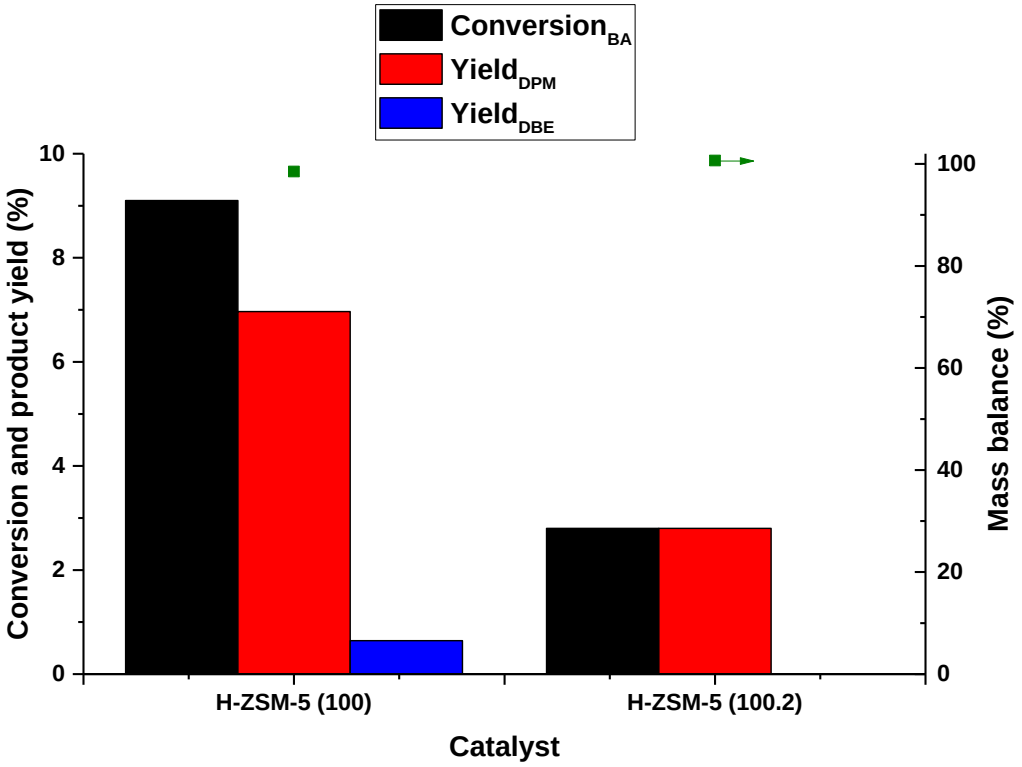

Figure 3.43 Conversion, product yield and mass balances for the BA alkylation of benzyl alcohol with benzene for H-ZSM-5 (100) and H-ZSM-5 (100.2) Reaction conditions; 70 mg catalyst, 0.14 M BA in benzene, 100 ^{o}C. 6 hours.

Conversion of BA was ca. 9% when H-ZSM-5 (100) was tested, with a DPM yield of 5.7%. A yield of only 1% was produced for DBE. A mass balance of 97% was obtained, suggesting polyaromatics were formed. Comparison of this result with H-ZSM-5 (100.2) showed that the alkaline treated zeolite was far less active in the Friedel-Crafts alkylation than its parent. Conversion of BA for H-ZSM-5 (100.2) was <3% with a DPM yield of 2.8%. No traces of DBE or polyaromatics were found. The decrease in catalytic activity in the alkaline treated zeolite was likely due to a combined effect of reduced surface area and porosity.

3.3.7.3.2 H-Beta

Next, the Friedel-Crafts alkylation of benzyl alcohol was tested over laboratory synthesised and commercial H-Beta zeolites, and then compared to their alkaline treated counterparts. H-Beta (38) and (38.2) were not tested in this reaction. They were included in this section primarily for characterisation purposes and were used for reactions carried

out in Chapter 5. Conversion, product yield and mass balance measurements for H-Beta (10 and 10.2) are shown in Figure 3.44.

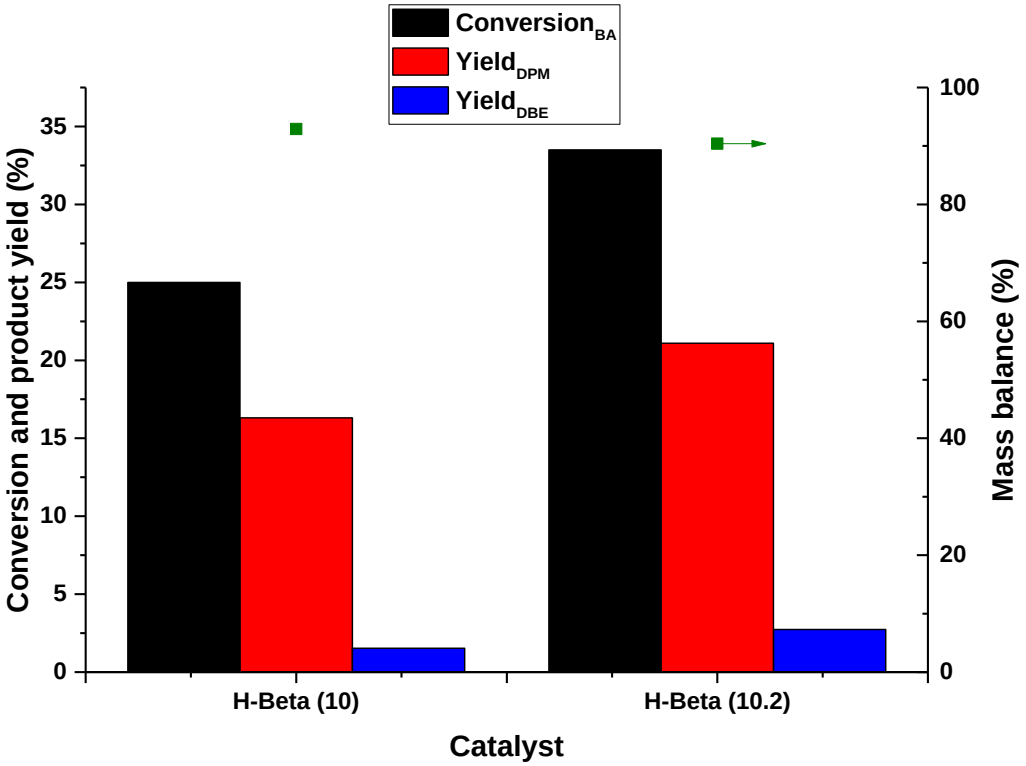

Figure 3.44 Conversion, product yield and mass balances for the BA alkylation of benzyl alcohol with benzene for H-Beta (10) and H-Beta (10.2). Reaction conditions; 70 mg catalyst, 0.14 M BA in benzene, 100 ^{o}C. 6 hours.

Our H-Beta zeolite showed 25% conversion of BA. Yields of 15.2% and 2.3% were obtained for DPM and DBE respectively. An overall mass balance of 92% was measured for H-Beta (10), suggesting the formation of polyaromatics. Unlike in the case of H-ZSM-5(30 and 100), alkaline treatment of H-Beta (10) with 0.2 M NaOH resulted in enhanced catalytic activity, with conversion of BA increasing to 33.6%. Furthermore, yields of DPM and DBE increased to 20.0 and 3.5% respectively. The mass balance obtained for H-Beta (10.2) was slightly lower than for H-Beta (10). The overall catalytic activity for our H-Beta zeolite was generally more active than all the H-ZSM-5 zeolites. It's difficult to ascertain whether increased catalytic activity in our alkaline treated H-Beta zeolite was primarily due to enhanced acidity, mesoporosity or both.

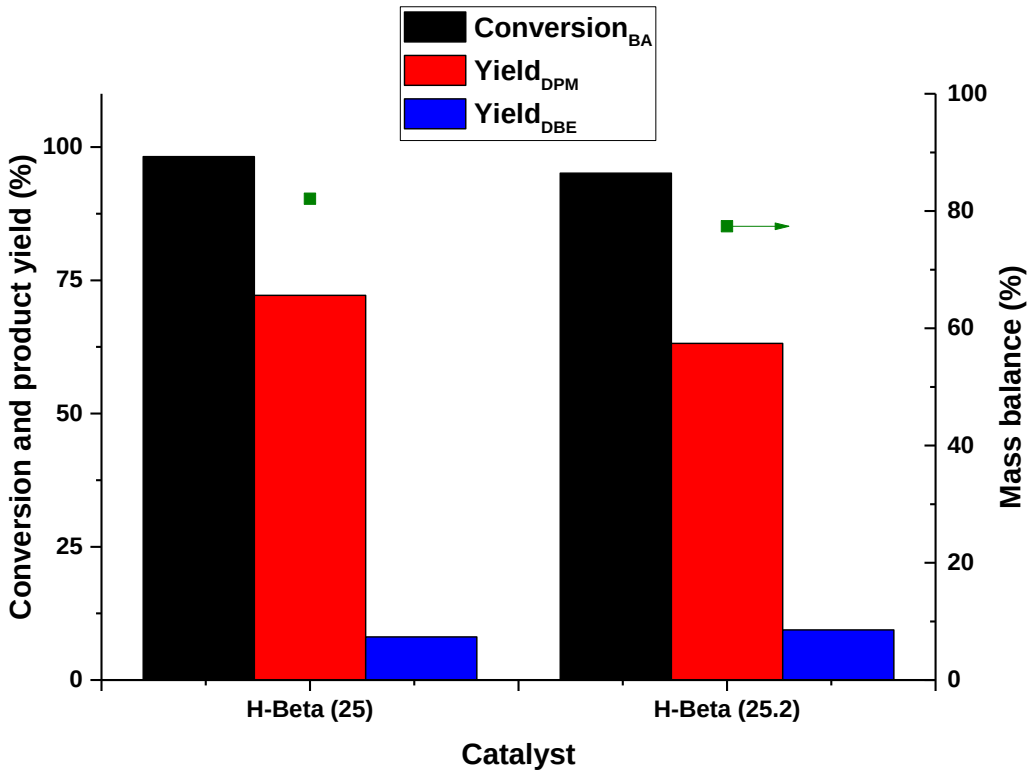

Figure 3.45 Conversion, product yield and mass balances for the BA alkylation of benzyl alcohol with benzene for H-Beta (25) and H-Beta (25.2). Reaction conditions; 70 mg catalyst, 0.14 M BA in benzene, 100 ^{o}C. 6 hours.

Despite lower SiO_2/Al_2O_3 molar ratios, H-Beta (10 and 10.2) showed lower catalytic activity compared to commercial H-Beta zeolites. Untreated H-Beta (25) showed 98% conversion, with DPM being the dominant product. A yield of <10% was obtained for DBE. This strongly suggests that H-Beta (25) favoured alkylation over etherification. Mass balance measurements showed 82%. Alkaline treatment of H-Beta (25) with 0.2 M NaOH resulted in a catalyst with slightly inferior catalytic activity than its parent, with conversion decreasing to 95.4%. Despite only slightly lower conversion compared to its parent, H-Beta (25.2) showed a DPM yield of 62.9%. Interestingly, higher yields of DBE were obtained for H-Beta (25.2) than its untreated parent. Our findings were in general agreement with the study carried out by Wang et al.[164] who found treatment H-Beta (SiO_2/Al_2O_3 = 33) with 0.2 M NaOH displayed worse catalytic activity than its unmodified parent. They attributed worse catalytic activity of the alkaline treated H-Beta zeolite to a reduction of Brønsted acid sites. Our TPD-NH_3 and ^{27}Al MAS-NMR studies seemed to agree with this hypothesis which confirmed the reduction of acid site density and reduction of tetrahedral framework aluminium species.

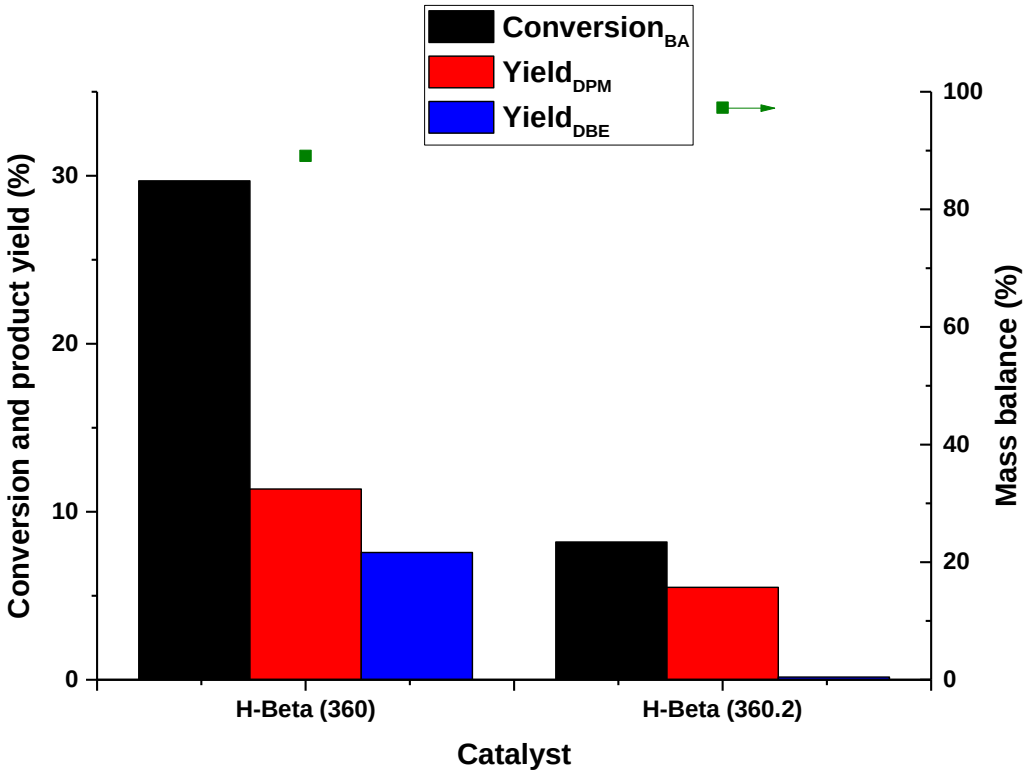

Figure 3.46 Conversion, product yield and mass balances for the BA alkylation of benzyl alcohol with benzene for H-Beta (360) and H-Beta (360.2). Reaction conditions; 70 mg catalyst, 0.14 M BA in benzene, 100 ^{o}C. 6 hours.

Despite limited microporosity for H-Beta (360.2), Figure 3.46 showed conversion decreased from 29.7% for H-Beta (360) to 8.2% for H-Beta (360.2). Since H-Beta (25 and 360) have different total pore volumes and acidities, it is difficult to determine with certainty whether catalytic activity was greater for H-Beta (25) than H-Beta (360) due to enhanced pore size or increased acid site density of H-Beta (25), or both. Mild alkaline treatment of H-Beta (25 and 360) showed lower levels of conversion than their parent. Since H-Beta (25.2) had similar porosity as its parent but lower acid site density, it is likely that reduced catalytic activity for H-Beta (25.2) can be attributed to the reduction of acid sites.

3.3.7.3.3 H-Y

After the catalytic testing of H-ZSM-5 and H-Beta zeolites in the Friedel-Crafts alkylation reaction, four different H-Y zeolites were tested. In this section, H-Y zeolites were tested

to determine whether alkaline treatment would enhanced catalytic activity in the Friedel-Crafts reaction. The results are shown in Figures 3.47-3.48.

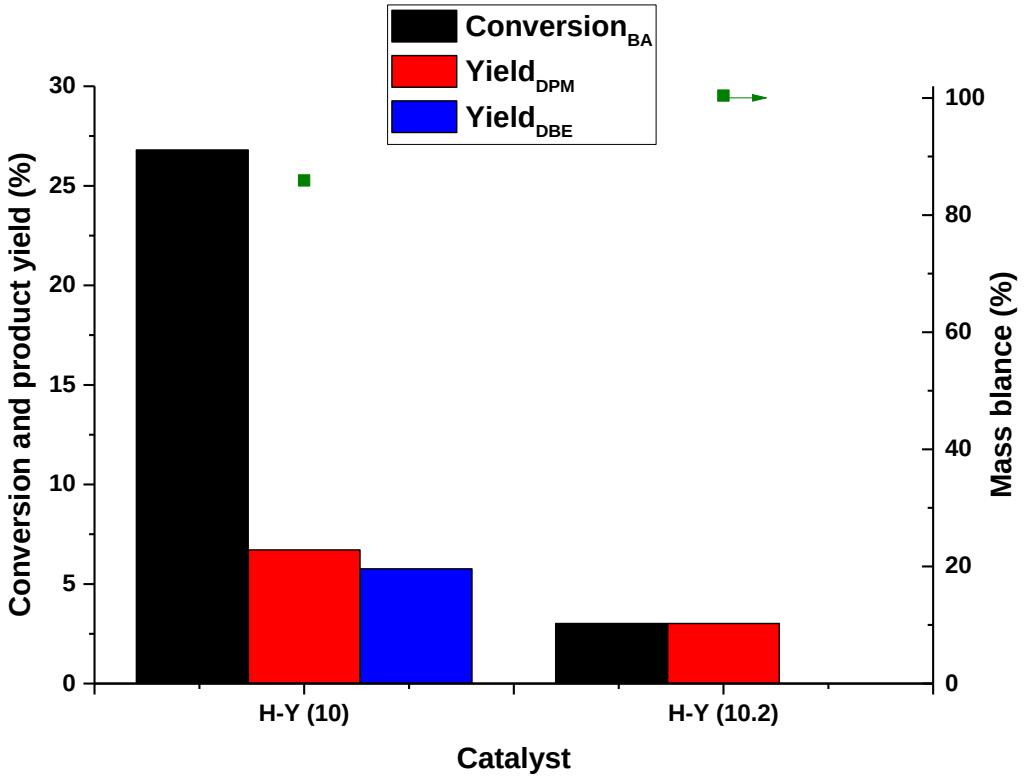

Figure 3.47 Conversion, product yield and mass balances for the BA alkylation of benzyl alcohol with benzene for H-Y (10) and H-Beta (10.2). Reaction conditions; 70 mg catalyst, 0.14 M BA in benzene, 100 ^{o}C. 6 hours.

H-Y (10) showed similar levels of conversion as H-Beta (10). Despite this, there was an obvious difference between the products distributions, with H-Beta (10) showing higher yields of DPM compared to H-Y (10). Despite having similar SiO_2/Al_2O_3 molar ratios, they had different catalytic properties in the Friedel-Crafts reaction. Firstly, H-Beta (10) had a much lower surface area and total acid density than H-Y (10). The enhanced acid site density of H-Y (10) promoted unwanted side reactions producing polyaromatics, therefore reducing the yield DPM. This is confirmed by the lower mass balance of H-Y (10) compared to H-Beta (10). Treatment of H-Y (10) with 0.2 M NaOH resulted in lower conversion than its parent, producing only DPM. Since the amount of acid sites decreased after desilication of H-Y (10), lower catalytic activity for H-Y (10.2) can be attributed to a reduction in acid site density.

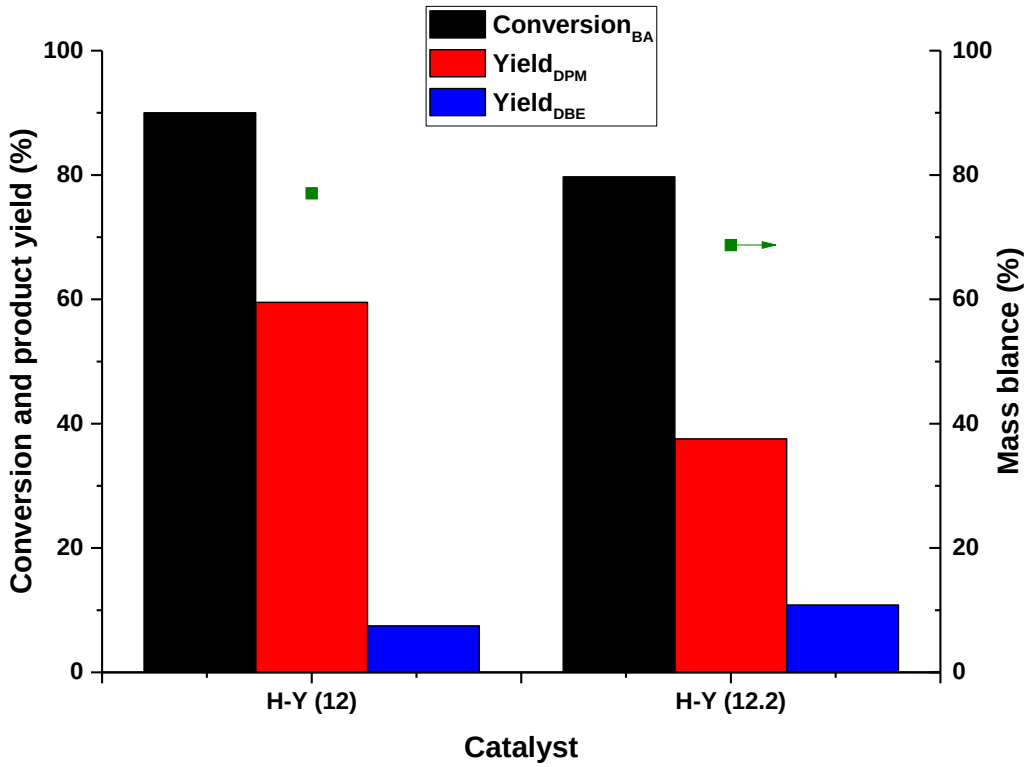

Figure 3.48 Conversion, product yield and mass balances for the BA alkylation of benzyl alcohol with benzene for H-Y (12) and H-Beta (12.2). Reaction conditions; 70 mg catalyst, 0.14 M BA in benzene, 100 ^{o}C. 6 hours.

The effect was less pronounced for H-Y (12 and 12.2). Clearly H-Y (12) showed remarkably high catalytic activity due to its acidity and surface area. Despite increasing mesoporosity upon alkaline treatment, catalytic performance was worse. This was probably due to the reduction of acid site density from 451 μmol g^{-1} for H-Y (12) to 362 μmol g^{-1} for H-Y (12.2). Additionally, we believe that this effect was also due to the lower concentration of benzyl alcohol, which increased the diffusion rate out of the pores.

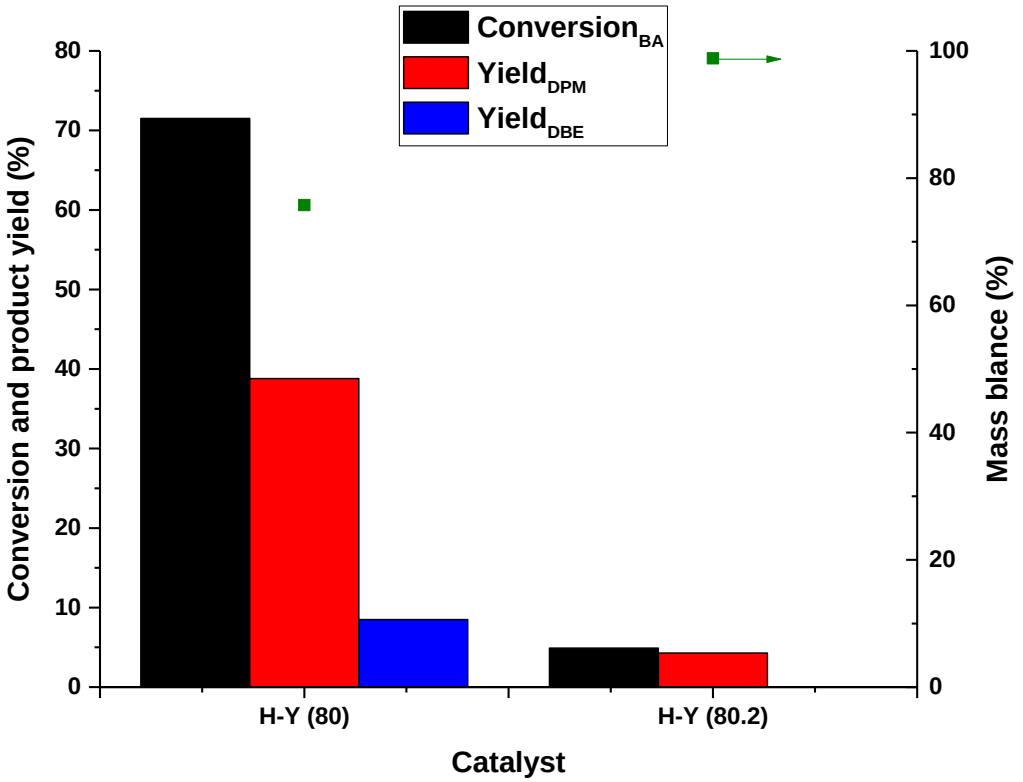

Figure 3.49 Conversion, product yield and mass balances for the BA alkylation of benzyl alcohol with benzene for H-Y (80) and H-Beta (80.2). Reaction conditions; 70 mg catalyst, 0.14 M BA in benzene, 100 ^{o}C. 6 hours.

Unsurprisingly, H-Y (80) displayed worse catalytic activity than H-Y (12). Despite H-Y (12) and H-Y (80) having similar levels of porosity, H-Y (80) had significantly lower acid site density than H-Y (12). This demonstrates that both acidity and porosity is required for high catalytic activity. For H-Y (80.2), a yield of 4.3% obtained for DPM at ca. 4.9% conversion. Trace amounts of DBE were produced. This was unsurprising since the specific surface area decreased to 56 m^2 g^{-1}. This is in good agreement with XRD analysis, which showed the complete amorphization of H-Y (80) after alkaline treatment.

3.3.7.4 The effect of concentration of benzyl alcohol on conversion

H-Y (12) and H-Y (12.2) were chosen to study the effect of the concentration of benzyl alcohol on conversion due to the fact that its external volume increased from 0.19 cm^3 g^{-1} for H-Y (12) to 0.29 cm^3 g^{-1} for H-Y (12.2) whilst largely preserving microporosity. The reactions were carried out at 100 ^{o}C using 70 mg of catalyst for 6 hours. The concentration of benzyl alcohol was varied 0.14-0.42 M.

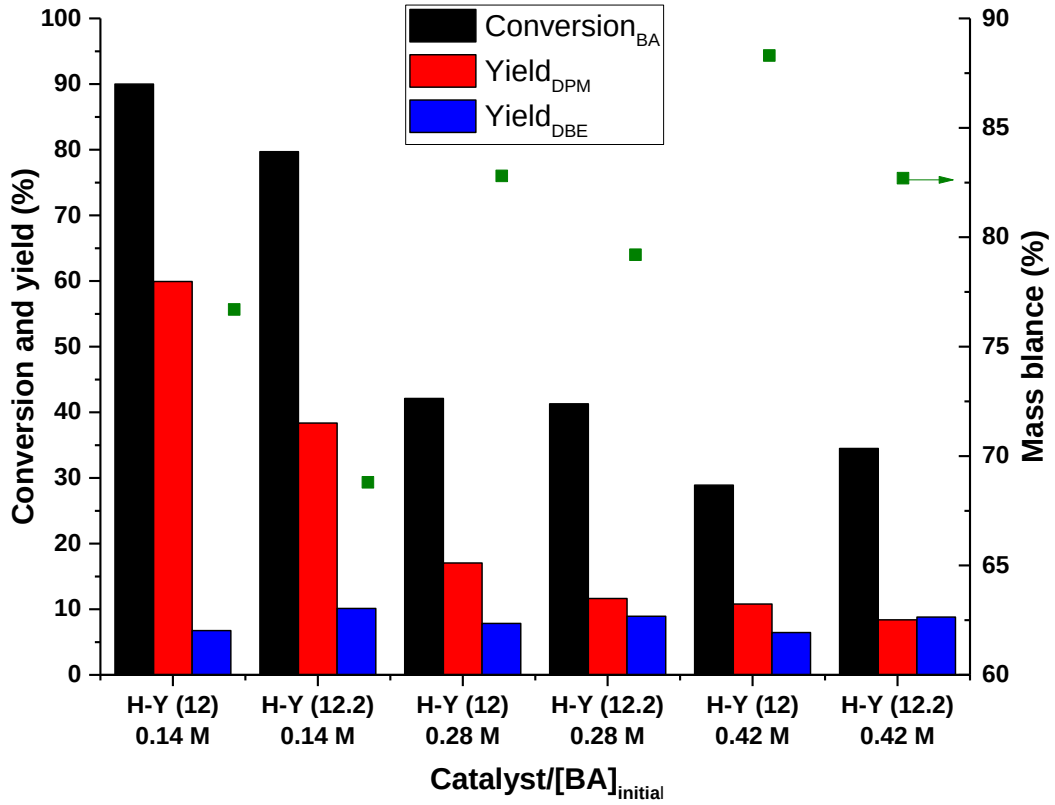

Figure 3.50 Conversion, product yield and mass balances for the BA alkylation of benzyl alcohol with benzene for H-Y (12) and H-Y (12.2) with varying BA concentration. Reaction conditions; 70 mg catalyst, 100 ^{o}C. 6 hours.

Figure 3.50 depicts the catalytic data for H-Y (12 and 12.2) showing the effect of BA concentration. Generally, the results show that increasing the initial concentration of BA led to a decrease in conversion for H-Y (12) zeolites, with lower yields obtained for DPM. Mass balance calculations confirmed the presence of unidentified polyaromatics.[149] The optimum concentration that displayed the highest conversion was 0.12 M for H-Y (12). After alkaline treatment of H-Y (12) with 0.2 M NaOH, catalytic activity was inferior to the parent at concentrations 0.12-0.28 M. This was possibly be due to faster diffusion in the micropores, resulting in shorter contact time and worse catalytic activity. When the concentration of benzyl alcohol was increased to 0.42 M it was found that H-Y (12.2) had higher catalytic activity than its parent. Clearly, enhanced catalytic activity was due to enhanced porosity.

3.4 Conclusions

In this study, commercially obtained H-ZSM-5, H-Beta and H-Y were treated with sodium hydroxide solution, increasing the mesoporosity in almost all cases. H-ZSM-5 and H-Y zeolites were synthesised using microwave assisted heating in 14 hours or less, with H-ZSM-5 and H-Y displaying similar physical and chemical properties similar to those prepared using conventional heating. It was found that zeolites with low SiO_2/Al_2O_3 molar ratios were particularly resilient to alkaline treatment such as H-ZSM-5 (30), H-Beta (10 and 25) and H-Y (10 and 12). XRD studies confirmed that alkaline treatment generally reduced the crystallinity of the parent zeolites. Surprisingly, in the case of H-Beta (10 and 25) it was found that alkaline treatment actually enhanced crystallinity. This is likely due to the removal of an amorphous phase. Alkaline treatment on zeolites with high SiO_2/Al_2O_3 molar ratios such as H-Beta (360) and H-Y (80) showed an amorphous phase. Surface area measurements showed that alkaline treatment on the parent increased the total porosity. After desilication, the total number of acid sites in H-ZSM-5 zeolites increased, which can be attributed to the formation of Lewis acid sites. Acidity measurements using pyridine and ammonia on the commercially obtained H-ZSM-5 and their alkaline treated counterparts suggests the increase in acid site density is likely due to the formation of Lewis acid sites. Harsher alkaline treatment of H-ZSM-5 retained the Brønsted/Lewis acid ratio. In contrast, alkaline treatment of H-Beta and H-Y reduced the acid site density as measured by temperature programmed desorption. Solid state NMR results confirmed that under milder alkaline treatment, H-ZSM-5 is largely unaffected regardless of the SiO_2/Al_2O_3 molar ratio, unlike H-Beta and H-Y which were largely affected.

Friedel-Crafts alkylation of BA was used a probe reaction under microwave assisted heating using unmodified and alkaline treated zeolites. Our study showed that 6 hours reaction time gave acceptable levels of conversion and was used for subsequent reactions. Alkaline treated H-ZSM-5 (30) and H-Beta (10) showed higher levels of catalytic activity than their untreated parent when 0.14 M of BA was initially used. When the concentration of benzyl alcohol was increased from 0.14 M to 0.42 M, H-Y (12.2) zeolite displayed better catalytic activity than its unmodified parent. This effect demonstrates that enhanced porosity and greater accessibility to the acid sites can increase catalytic activity when mass transport phenomenon are taken into consideration. It could be concluded that desilication is a cheap, effective process for the generation of mesoporosity in zeolite catalysts.

However, factors such as mass transport phenomenon must be considered to achieve optimum catalytic activity and that desilication is a post-synthesis treatment that requires multi-step procedures to produce the active zeolite.

3.5 Future work

Despite promising results obtained showing the effect of alkaline treatment of H-ZSM-5, H-Beta and H-Y, optimisation studies are required. Our results showed the optimum desilication conditions of H-ZSM-5 could not directly be applied to H-Beta and H-Y zeolites, especially with high SiO_2/Al_2O_3. Therefore future studies are required to increase mesoporosity in both H-Beta and H-Y whilst retaining the overall structure. Desilication also resulted in drastic changes in acidity of all zeolite samples. Reactions that are sensitive to both porosity and acidity, it is difficult to determine whether catalytic activity is affected primarily by an increase in porosity, variation in acidity or both. Therefore, future studies are required which demonstrates enhanced mesoporosity whilst retaining the acid site density. We were able to quantify the Brønsted and Lewis acid sites of parent and desilicated H-ZSM-5 zeolites. However, further work is required to quantify Brønsted and Lewis acid sites of our H-Beta and H-Y zeolites. Despite quantification of Brønsted and Lewis acid sites in our H-ZSM-5 zeolites, further studies are required to quantify the accessibility of the active sites. Previous studies have shown that the accessibility of the active sites can be determined by using collidine as a probe molecule.[199] A study carried out by Groen et al.[201] directly demonstrated enhanced diffusion in hierarchical H-ZSM-5. However, to the best of our knowledge, studies showing the effect of increased mesoporosity has not been applied to hierarchical H-Beta or H-Y. Finally, solid state NMR studies were not performed on our home-made synthesised H-Beta zeolite or its alkaline treated counterpart and, therefore could not confirm whether the negligible effect of alkaline treatment was primarily due to the location of the aluminium species.

Chapter 4

Templated Microwave Synthesis of H-ZSM-5 for Friedel-Crafts Alkylation

4 Templated microwave synthesis of H-ZSM-5 for Friedel-Crafts alkylation

4.1 Introduction

Microwave assisted heating is proving to be a reliable alternative route for synthesis of zeolites compared to conventional heating methods. The main advantage is the reduction of synthesis time from days to hours. Also, homogenous heating throughout the mixture resulting in rapid crystal growth and a smaller particle size distribution.[202] Due to its dielectric constant, water is an ideal solvent for the synthesis of zeolites with microwave assisted heating. The first synthesis of H-ZSM-5 using microwave assisted heating was patented by Mobil in 1988,[203] with the first study in the open literature reported by Jansen et al.[99] five years later, showing a crystalline material consistent with the XRD pattern of ZSM-5 could be synthesised in just 30 minutes at 140 ^{o}C. However, these conventional zeolite materials are largely microporous materials and still possess mass transport limitations. Several strategies have been adopted to synthesis hierarchical zeolites and remove mass transport limitations. The first is the top down approach, which involves the post-synthesis extraction of aluminium[204, 205] or silicon[129, 206, 207]. However, these approaches generate hierarchical zeolites with a partial collapse in the zeolite structure. In addition, chemical parameters such as acidity are altered during the post-synthesis treatment. Other strategies include the addition of hard templating agents. The process usually involves three steps: the addition of the hard templating agent to the precursor solution or gel, following by zeolite crystallisation around and/ or inside the template. The template is usually removed by combustion under oxidising conditions. The main drawback of using this method is the non-recyclability of the hard templating agent. Carbonaceous species have been applied as hard templating agents, generating mesoporosity. Koo et al[208] generated comparable mesoporosity for H-ZSM-5 in just 1 hour using microwave assisted heating compared to 6 days using conventional hydrothermal conditions. However, studies have shown that carbonaceous species are of non-uniform shape which is likely to show unreproducible results.[209] Polystyrene has shown to be an effective hard templating agent for the generation of mesoporosity. One of the major advantages of using polystyrene as a templating agent is the particles showing uniform shape with a narrow particle size distribution. However, low crystallisation temperatures must be used due to the glass transition temperature of the polymer. Studies involving the use of polystyrene as a hard templating agent for the synthesis of H-ZSM-5

is limited.[115, 139, 210, 211] In addition, studies comparing conventional H-ZSM-5 and hierarchical H-ZSM-5 using polystyrene as a hard templating agent were carried out with varying crystallisation temperatures. To the best of our knowledge, there has been no reported study showing the synthesis of synthesis of conventional H-ZSM-5 and hierarchical H-ZSM-5 using polystyrene as a hard templating agent with identical crystallisation parameters with microwave assisted heating.

In this study, we report the synthesis of conventional H-ZSM-5 crystals in 6 hours using microwave assisted heating, with physical and chemical properties comparable to H-ZSM-5 synthesised by conventional heating methods. For comparison, we report the synthesis of hierarchical H-ZSM-5 by addition of polystyrene nano-spheres to the precursor solution. The influence of varying the crystallisation temperature and calcination ramp rate on mesoporosity of hierarchical H-ZSM-5 was studied. In addition, conventional and hierarchical H-ZSM-5 was synthesised using identical crystallisation parameters to determine the direct effect of the hard template on the physical and chemical properties of H-ZSM-5. The catalysts were characterised using XRD to determine crystallinity, nitrogen sorption to determine surface area and porosity and temperature programmed desorption of ammonia to determine the acid density. The catalytic behaviour of the hierarchical zeolites were studied in a Friedel-Crafts alkylation reaction between benzyl alcohol and benzene. The catalytic activity was compared to our untemplated laboratory synthesised H-ZSM-5 catalyst.

4.2 Experimental

4.2.1 Hard templating agent and catalyst preparation

In this section, the synthesis parameters and chemical compositions that were used to synthesised the hard templating agent, conventional and hierarchical H-ZSM-5 zeolites by microwave assisted heating are presented.

4.2.2 Synthesis of polystyrene (PS) nanospheres

Polystyrene (PS) nanospheres were synthesised using the method carried out by He et al.[212] Ammonium persulfate (APS) was used as the initiator. Sodium dodecyl

sulphate (SDS) was used as the surfactant. Water was used as the solvent. Prior to the synthesis, styrene was washed with 4 x 25 mL aqueous sodium hydroxide (0.1 M) and 4 x 25 mL deionised water to remove the inhibitor. APS (0.08 g) and SDS (0.5 for 60 nm nanospheres or 4 g for 30 nm nanospheres) was added to water (84 mL) and stirred until a homogenous solution appeared. The solution was then heated to 80 ^{o}C. A styrene/1-pentanol mixture (14 mL styrene/0.2 mL) was added dropwise using a syringe pump at a rate of 157 μL min^{-1} for 1.5 hours under stirring. The solution was stirred for an additional hour at 80 ^{o}C before being cooled to ambient temperature. An aliquot was taken for particle size analysis using dynamic light scattering. Polystyrene was precipitated using cold ethanol and then filtered under gravity overnight. The powder was dried in an oven at 50 ^{o}C for 48 hours. A sample was taken for FTIR and SEM measurements.

4.2.3 Synthesis of conventional H-ZSM-5 using microwave assisted heating

H-ZSM-5 with a SiO_2/Al_2O_3 ratio of 100 as described in section 3.2.2.1. 23 mL of the mother solution was placed into a 30 mL quartz pressure vial and heated under microwave assisted heating (CEM, Discover® SP™, maximum power of 300 W) at 165 ^{o}C for 6 hours. The mixture was cooled to room temperature before being filtered under gravity (Whatman grade 1 filter paper) and washed with an abundant amount of distilled water. The solid was dried in an oven overnight at 110 ^{o}C before being calcined as described in section 3.2.1. At this point a sample was taken for XRD analysis to confirm the MFI structure. The sample was then brought into the proton form by ion exchange with ammonium nitrate (1M) at 80 ^{o}C for 2 hours under reflux conditions and calcined again. Additionally, another conventional H-ZSM-5 (molar SiO_2/Al_2O = 100) zeolite was synthesised with a crystallisation time of 12 hours at 120 ^{o}C. This sample is discussed in more detail in section 4.3.2.4.

4.2.4 Synthesis of hierarchical H-ZSM-5 using microwave assisted heating

Typically, 23 mL of the precursor solution was mixed with 3g of PS in a 35 mL microwave vial and stirred at room temperature using a spatula to ensure complete mixing. The vial was heated with microwave assisted heating at 100^{o}C (unless stated otherwise) for 1,2,3,6 and 12 hours to determine the optimisation crystallisation time. The solution was filtered under gravity and air dried. The sample was calcined in an ash furnace with a heating rate

of 1^{o}C min^{-1} (unless stated otherwise) to remove PS and structure directing agent. As this point a portion of the sample was analysed for XRD analysis. The zeolite was brought into its ammonium form by ion exchange with ammonium nitrate (1M) at 80 ^{o}C for 2 hours under reflux conditions and calcined as described in section 3.2.1.

4.2.5 Friedel-Crafts alkylation of benzyl alcohol with benzene

Friedel-Crafts alkylation of benzyl alcohol with benzene was carried out as described in section 3.2.4. The reaction method was not modified throughout this chapter. Conversion, yield and mass balances were calculated as shown in Equation 3.1.

4.3 Results and discussion

In this section, the physical and chemical properties of our laboratory synthesised H-ZSM-5 zeolite is presented and discussed in detail. The physical and chemical properties of the hard templating agent, polystyrene, is also presented. The results of the physical and chemical properties of PS were analysed by FT-IR, SEM and DLS. Characterisation techniques of conventional and hierarchical H-ZSM-5 are generally shown in the following order; XRD, ICP-OES, nitrogen adsorption-desorption, TPD-NH_3, solid state NMR and SEM. Following characterisation studies, H-ZSM-5 catalysts synthesised in this chapter were tested in the Friedel-Crafts alkylation of benzyl alcohol with benzene as a probe reaction to determine the effect of porosity and acidity on catalytic activity.

4.3.1 Characterisation of hard templating agent and H-ZSM-5 zeolites synthesised by microwave assisted heating

In this section, the physical and chemical properties of the hard templating agent is discussed. The hard templating agent was analysed using FT-IR to determine functional groups, SEM to determine the particle shape and to give an indication of the dispersity. Dynamic light scattering measurements were carried out to provide information on the average particle size of the nanospheres.

4.3.1.1 Analysis of polystyrene

FT-IR was used as a qualitative measurement to determine the functional groups of styrene and polystyrene. The FT-IR spectra of styrene and polystyrene are shown in Figure 4.1. The mean average particle diameters were measured using dynamic light scattering (DLS). This was compared to manual measurements of the particles, which was carried out using ImageJ software 1.48V by counting 100 particles. For DLS measurements, an aliquot of the latex mixture was taken after cooling and mixed with de-ionised water in 10:1 volume to volume ratio (v/v) of water/latex mixture. The composition of polystyrene was determined using SEM. Particle size distributions determined by DLS are inserted into SEM images (Figures 4.2-4.4).

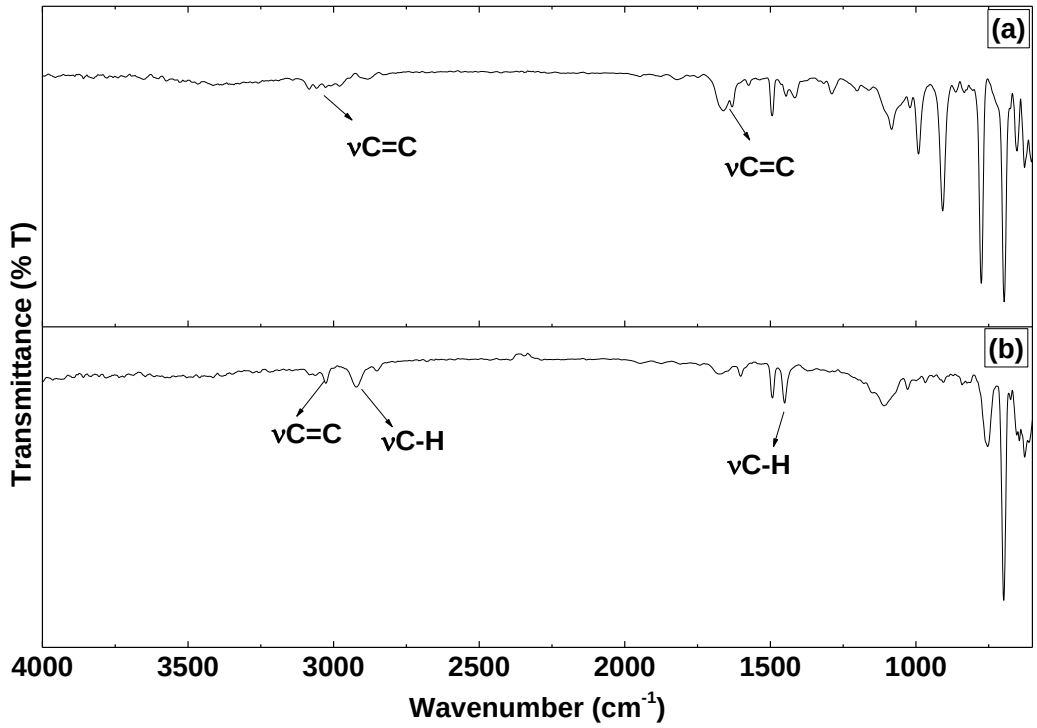

Figure 4.1 FT-IR spectra of (a) styrene and (b) polystyrene (60 nm).

The FT-IR spectrum for styrene shows the *ν*C=C at >3000 cm^{-1} associated with $HC=CH_2$ attached to the aromatic ring in the ortho position.[213] *ν*C=C of the aromatic ring appears between 1490 cm^{-1}. The band around 1750 cm^{-1} can be attributed to the aromatic ring mono-substituted aromatic ring. The bands described are typical for styrene. Therefore, the liquid was assumed to pure styrene and not subjected for further analysis. After

microemulsion polymerisation, the FT-IR spectrum of the white solid showed a similar FT-IR spectrum as styrene, with the band between 1490 cm^{-1} remaining intact, which can be ascribed to *v*C=C of the benzene ring. However, there appears to be a new band formed slightly above 3000 cm^{-1}. This band can be ascribed to the *v*C-H substituted onto the aromatic ring. The infrared spectrum is in excellent agreement with the literature, confirmation of polystyrene.[214] The spectra showed no evidence of water due to the absence of peaks associated for water such as the O-H stretching and vibrations at 3280 and 1630 cm^{-1} respectively.[215]

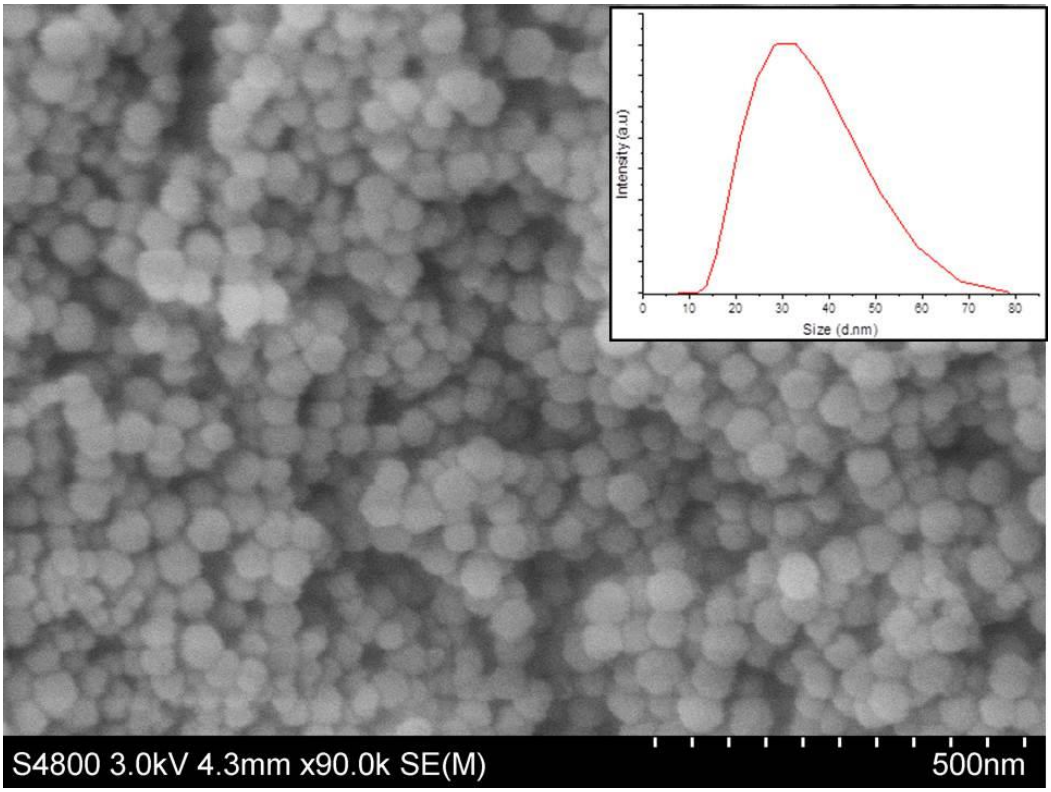

Figure 4.2 SEM image of polystyrene nanospheres synthesised using 4 g SDS with particle size distribution attached.

Figure 4.2 revealed an ordered array of polystyrene particles with sizes ranging from 10-80 nm were obtained by microemulsion polymerisation at 80 ^{o}C. The average diameter was 25 nm over 3 measurements by dynamic light scattering.

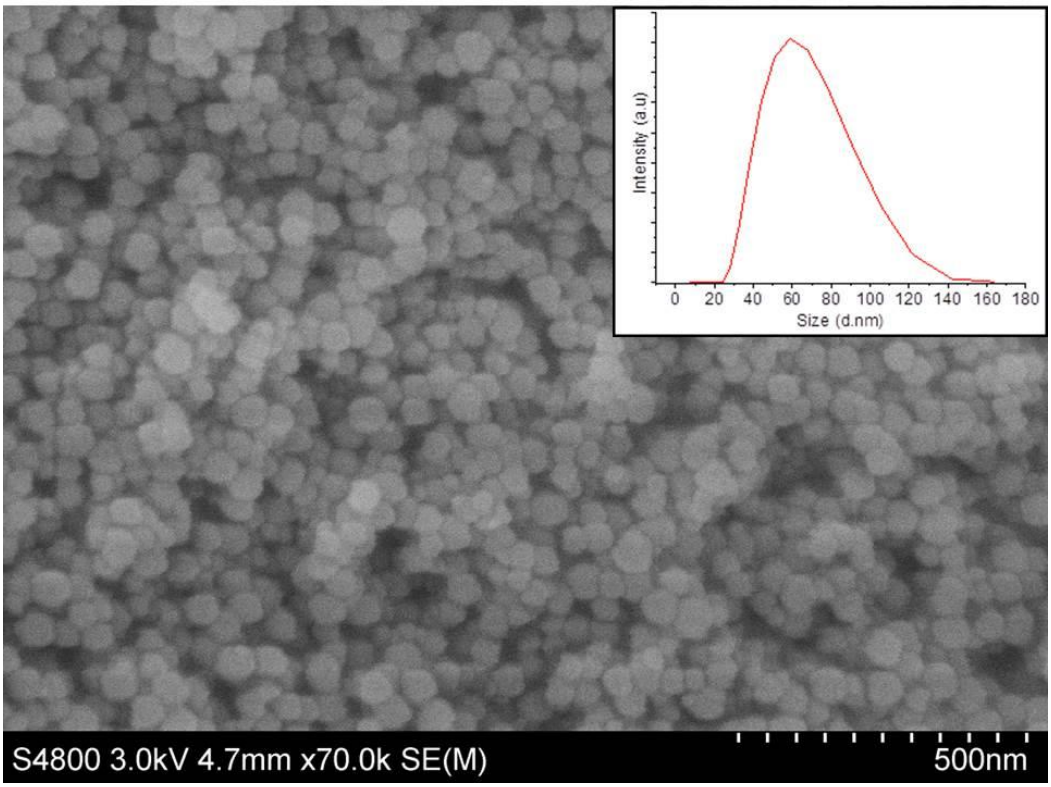

Figure 4.3 SEM image of polystyrene nanospheres synthesised using 0.5 g SDS with particle size distribution attached.

Likewise, Figure 4.3 also showed an ordered array of polystyrene particles. Dynamic light scattering measurements revealed particles sizes ranging from ca. 20-160 nm, with a mean particle size of 58 nm.

4.3.1.2 Effect of crystallisation time on the crystallinity of hierarchical H-ZSM-5

PS with an average diameter size of 30 nm was chosen as the hard template for ZSM-5 zeolites for preliminary studies to determine the crystallisation time for subsequent syntheses. PS (30 nm) was chosen for preliminary studies since higher surface area and porosity values were obtained than PS (60 nm) under hydrothermal conditions using conventional heating. Crystallisation times were: 1, 3, 6 and 12 hours at 100 ^{o}C under static conditions with microwave assisted heating. Samples were analysed by XRD prior to and after calcination to determine the optimum crystallisation time using the relative intensity. The zeolite which showed optimum crystallinity was characterised and the remaining samples were not characterised beyond XRD. The XRD diffractograms are displayed in Figure 4.4.

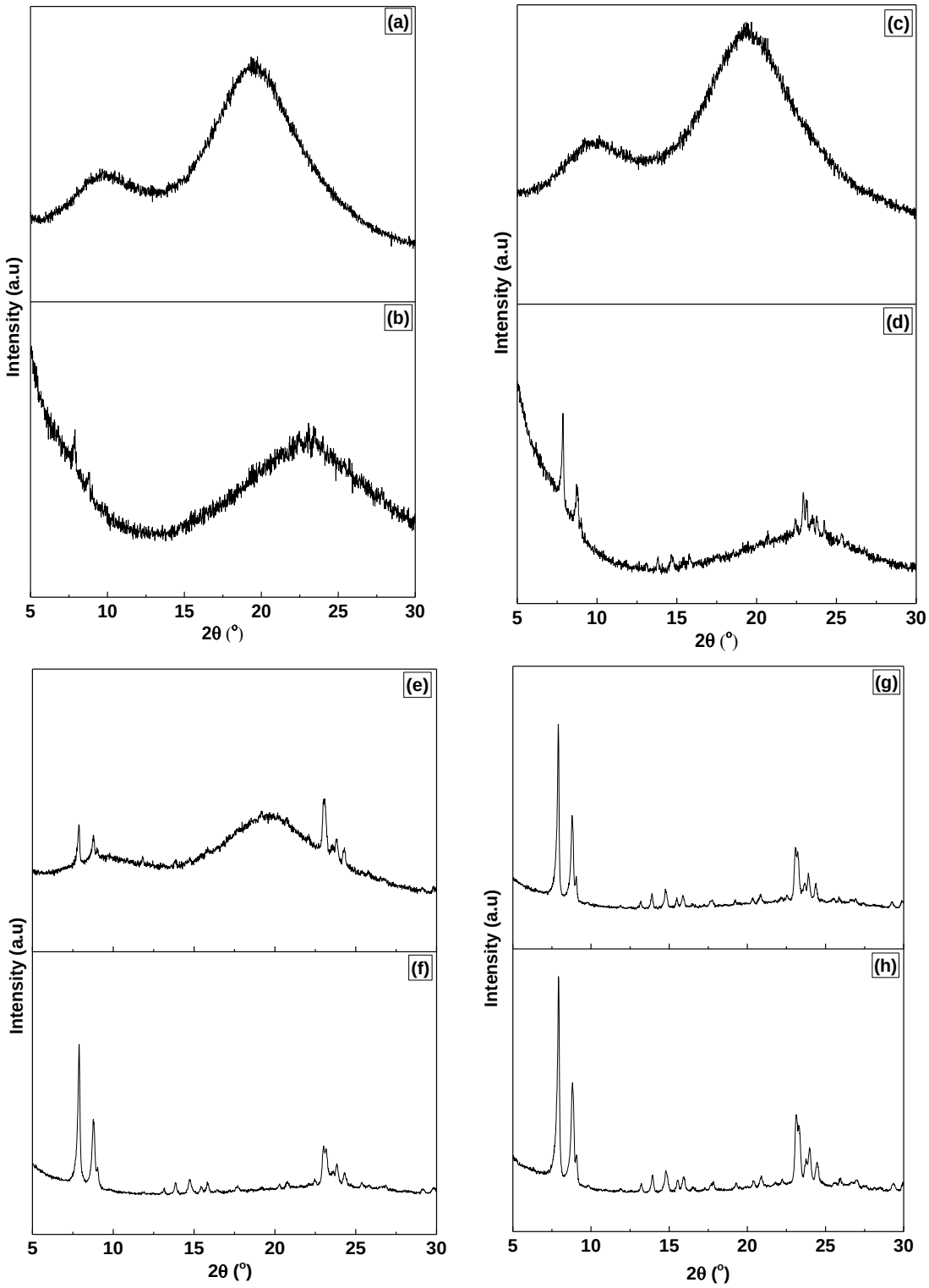

Figure 4.4 XRD studies showing the effect of crystallisation time on crystallinity of templated H- ZSM-5; (a) H-ZSM-5 (100)-PS30 pre 1 hour, (b) H-ZSM-5 (100)-PS30 post 1 hour, (c) H-ZSM-5 (100)-PS30 pre 3 hours, (d) H-ZSM-5 (100)-PS30 post 3 hours, (e) H-ZSM-5 (100)-PS30 pre 6 hours, (f) H-ZSM-5 (100)-PS30 post 6 hours, (g) H-ZSM-5 (100)-PS30 post 12 hours, (h) H-ZSM-5 (100)-PS60 post 12 hours.

Figure 4.4 indicates that varying the crystallisation time had a profound effect on the XRD patterns of templated ZSM-5. A crystallisation time of only 1 hour showed weak

intensities of the peaks at 2θ angles 7.9 and 8.8º and is almost completely amorphous. XRD diffractograms revealed that calcination led to the removal of the hard template. The first evidence of ZSM-5 with a crystalline phase representative to that from previous studies was detected after 6 hours. The peak at 2θ angle 7.9º became slightly more intense after 12 hours. Since a purely crystalline phase of H-ZSM-5 was successfully synthesised after 6 hours, this was used for subsequent studies as the untemplated zeolite (unless states otherwise).

4.3.1.3 Preliminary studies.

Preliminary studies were carried out investigating the effect of PS spheres with varying diameters (30 and 60 nm) on the physical and chemical properties on H-ZSM-5. In this study, untemplated H-ZSM-5 was synthesised for 6 hours at 165 ºC and compared to hierarchical H-ZSM-5 synthesised at 100 ºC for 12 hours by XRD, ICP, nitrogen sorption and porosity measurements, TPD-NH_3 and solid NMR studies. After determining which PS template showed the H-ZSM-5 catalyst with the highest surface area and porosity, this would be used for subsequent optimisation studies. In this study, the untemplated zeolite is denoted as H-ZSM-5 (100)-MW and the templated zeolites are denoted as H-ZSM-5 (100)-MW-PSx, where x is the average diameter of the polystyrene nanosphere.

4.3.1.3.1 XRD and elemental studies

XRD studies were measured in the 2θ range of 5-50º. The crystallinity of the zeolites was not calculated and only identified to determine H-ZSM-5 using the [101], [020] and [501] reflections in the 2θ regions of; 7.9, 8.8, 23.1º respectively. For comparison, the same scale has been used for the intensity axis.

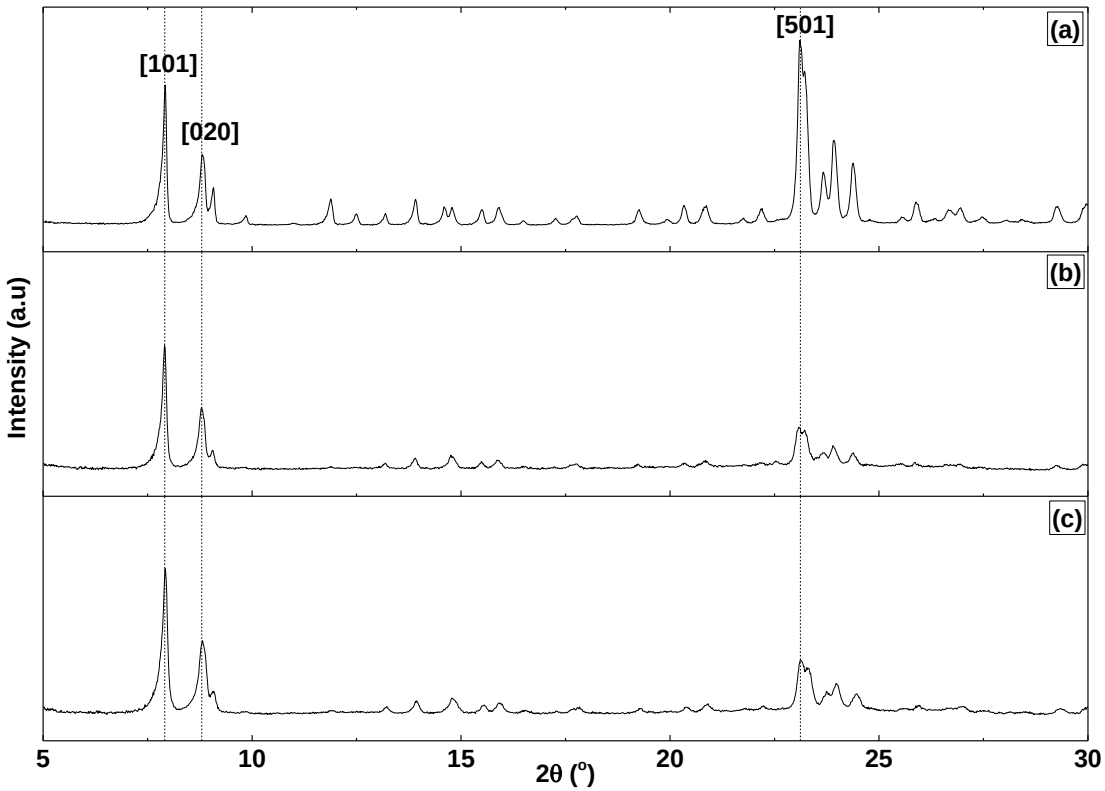

Figure 4.5 XRD studies showing untemplated and hierarchical H-ZSM-5 synthesised using polystyrene of various particle size. (a) H-ZSM-5 (100)-MW, (b) H-ZSM-5 (100)-MW-PS30 and (c) H-ZSM-5 (100)-MW-PS60.

XRD diffractograms (Figure 4.5) show the well resolved peaks in the 2θ region at 5-30° marked by the most intense peaks for the untemplated zeolite, indicative of the MFI structure. Due to the absence of sodium from the precursor solution, it was assumed that the formation of analcime was highly unlikely therefore, a pure phase of the MFI was present. The reflections for the templated zeolites appear to be less sharp which strongly suggests the templated zeolites are not wholly crystalline. Clearly, polystyrene was removed after calcination, due to the removal of an amorphous polystyrene phase.[216] The [101] reflection plane for the untemplated zeolite appears at a slightly lower 2θ region than the templated zeolites, suggesting the untemplated zeolite contains a lower content of crystalline aluminium species.[217] Elemental analysis studies which showed SiO_2/Al_2O_3 molar ratios of 93 and 76 for H-ZSM-5-MW and H-ZSM-5-MW-PS60 respectively. Elemental analysis was not performed on H-ZSM-5-MW-PS30. It was suggested by Pushparaj et al.[218] that ethanol produced by hydrolysis of TEOS lowers the dielectric constant of the medium and enhances crystallinity of the zeolitic material. The relative intensity of the peak corresponding to the [101] reflection plane increased slightly with

increasing PS particle size for the templated zeolites, indicating the larger size of the crystal domain.[219] Koo et al.[208] hypothesised carbon plays a vital role as a microwave absorber and results in a stronger interaction with the silicon source, resulting in an enhanced rate of crystallisation.

4.3.1.3.2 Surface area and porosity measurements

All nitrogen adsorption/desorption isotherms generally exhibited a sharp uptake at P/P_o <0.01, indicating similar levels of microporosity. The untemplated zeolite displayed a I and IV type with a small hysteresis loop, indicative of the creation of mesopores.[220] The templated zeolites showed a combination of type I and IV isotherm with H3 hysteresis loop, suggesting slit shaped pores of nonuniform size.[221] The templated zeolites showed increasing nitrogen uptake at higher relative pressures than the untemplated zeolite, with H-ZSM-5-MW-PS60 showing the highest uptake at P/P_o = 1. This suggests that the size of the polystyrene nanosphere played a vital role in the formation of mesoporosity.

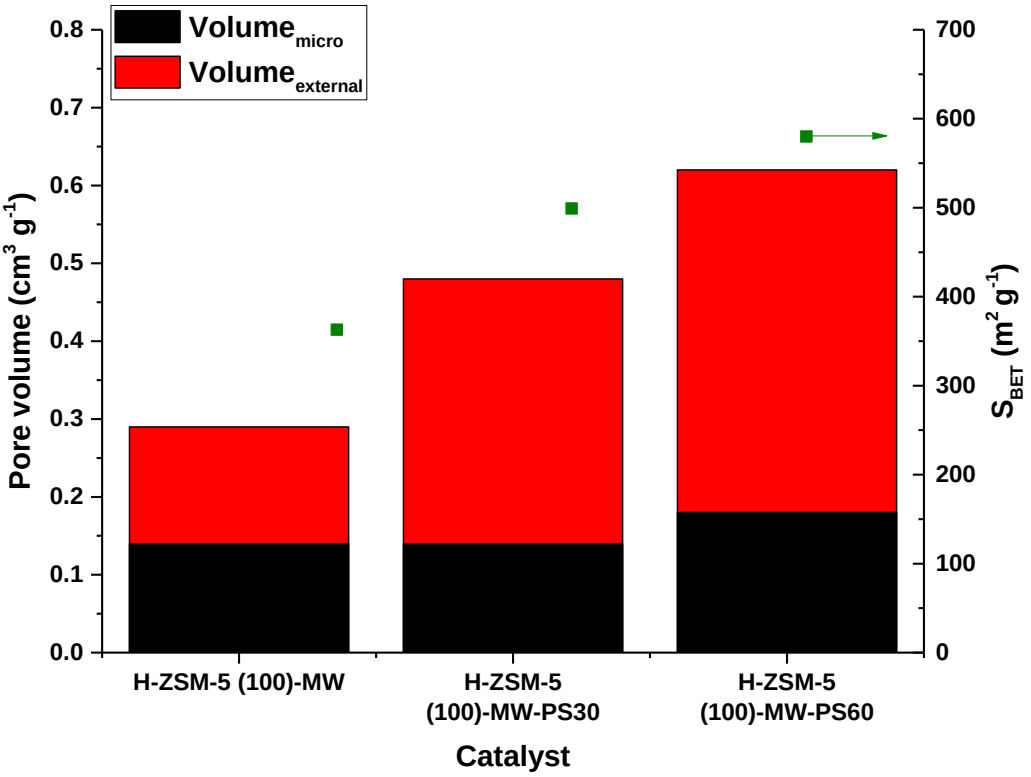

Figure 4.6 Surface area and porosity measurements for H-ZSM-5 (100), H-ZSM-5 (100)-MW-PS30 and H-ZSM-5 (100)-MW-PS60.

Figure 4.6 shows the surface area and porosity measurements for untemplated and templated ZSM-5. The specific surface area of the microwave untemplated was 363 $m^2 g^{-1}$ with a total pore volume of 0.29 $cm^3 g^{-1}$. This is in excellent agreement with surface area measurements of H-ZSM-5 synthesised by conventional heating.[222] The templated zeolites showed much higher surface areas than the untemplated zeolite. However, it is likely that this effect was simply due to the smaller particle sizes of the templated zeolites due to the lower crystallisation temperature.[223] Despite this, the more pronounced surface area of the templated zeolites compared to the untemplated zeolite is caused by the extraordinary increase in mesoporosity.[224] Saito-Foley measurements up to 2 nm confirmed that H-ZSM-5 (100)-MW and H-ZSM-5-MW-PS30 possessed identical micropore volumes (0.14 $cm^3 g^{-1}$). The addition of polystyrene with an average particle diameter of 60 nm to the precursor solution increased the micropore volume of the final zeolite slightly to 0.18 $cm^3 g^{-1}$. The proportion of microporosity for both templated zeolites was 29%, much lower than the proportion of microporosity for the untemplated zeolite (48%). It was suggested by Sashkina et al[210] that the greater proportion of microporosity leads to enhanced crystallinity. Saito-Foley measurements support XRD studies showing that the untemplated zeolite was more crystalline due to the increased proportion of microporosity. However, our XRD study showed that H-ZSM-5 (100)-MW-PS60 displayed more crystallinity than H-ZSM-5-MW-PS30 despite having identical proportions of microporosity. This is good agreement with the work carried out by Meng et al[225] who showed that secondary porosity was generated by aggregation of the particles, with similar levels of microporosity. The external pore volume was 0.34 $cm^3 g^{-1}$ and 0.44 $cm^3 g^{-1}$ for H-ZSM-5 (100)-MW-PS30 for H-ZSM-5 (100)-MWPS60, much larger than for H-ZSM-5 (100)-MW, which was only 0.15 $cm^3 g^{-1}$. This shows that the average size of the polystyrene played an important role in the generation of mesoporosity.

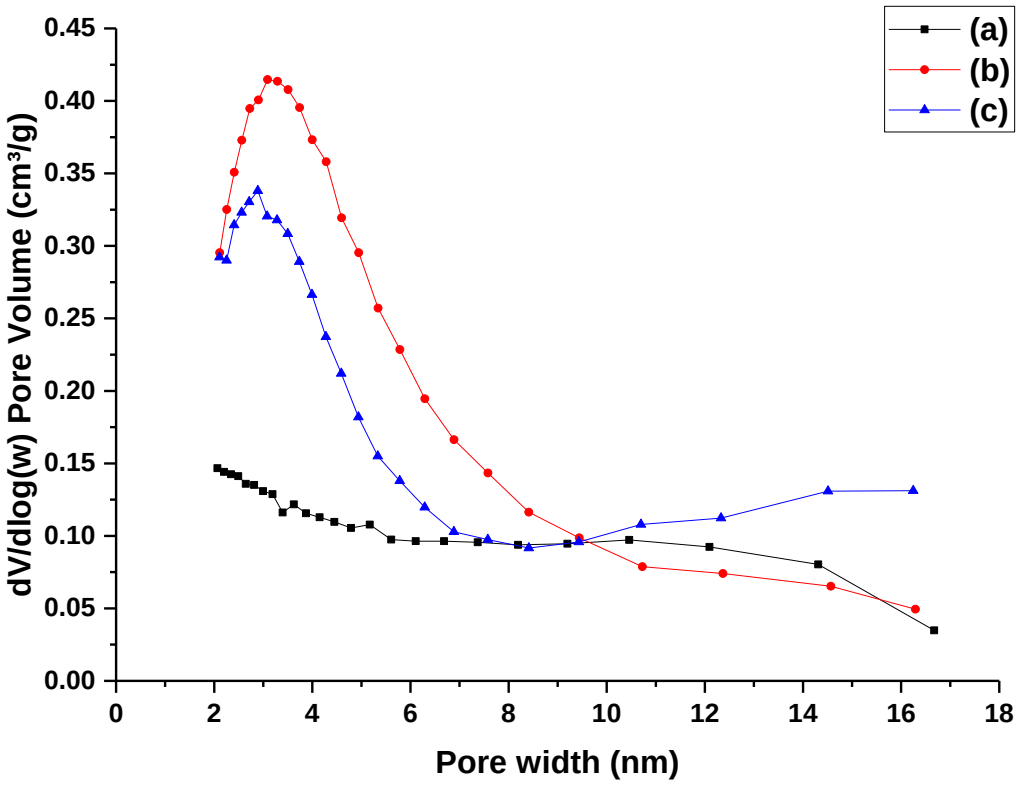

Figure 4.7 Pore size distribution measurements for untemplated and hierarchical H-ZSM-5 synthesised using polystyrene of various particle size; (a) H-ZSM-5 (100)-MW, (b) H-ZSM-5 (100)-MW-PS30 and (c) H-ZSM-5 (100)-MW-PS60.

The results of pore size distribution measurements taken at the adsorption branch are presented in Figure 4.7. The laboratory synthesised zeolite, H-ZSM-5 (100)-MW, showed a broad distribution of mesopores up to 17 nm with a significant proportion pore radii ca. 2 nm. The increase of the external volume for the templated zeolites was due to an increase in proportion of mesopores with pore widths 2- 9 nm. Clearly, the larger external pore volume for H-ZSM-5 (100)-MW-PS60 compared to H-ZSM-5 (100)-MW and H-ZSM-5 (100)-MW-PS30 can be attributed to the formation of mesopores with pore width >10 nm. Since H-ZSM-5 (100)-MW-PS60 showed a larger surface area and external volume, H-ZSM-5 (100)-MW-PS30 was not characterised further. Therefore, subsequent studies involving templated zeolites, the catalyst H-ZSM-5 (100)-MW-PS60 was used.

4.3.2 Temperature programmed desorption studies

The temperature programmed desorption of H-ZSM-5 (100)-MW and (b) H-ZSM-5 (100)-MW-PS60 are shown in Figure 4.8.

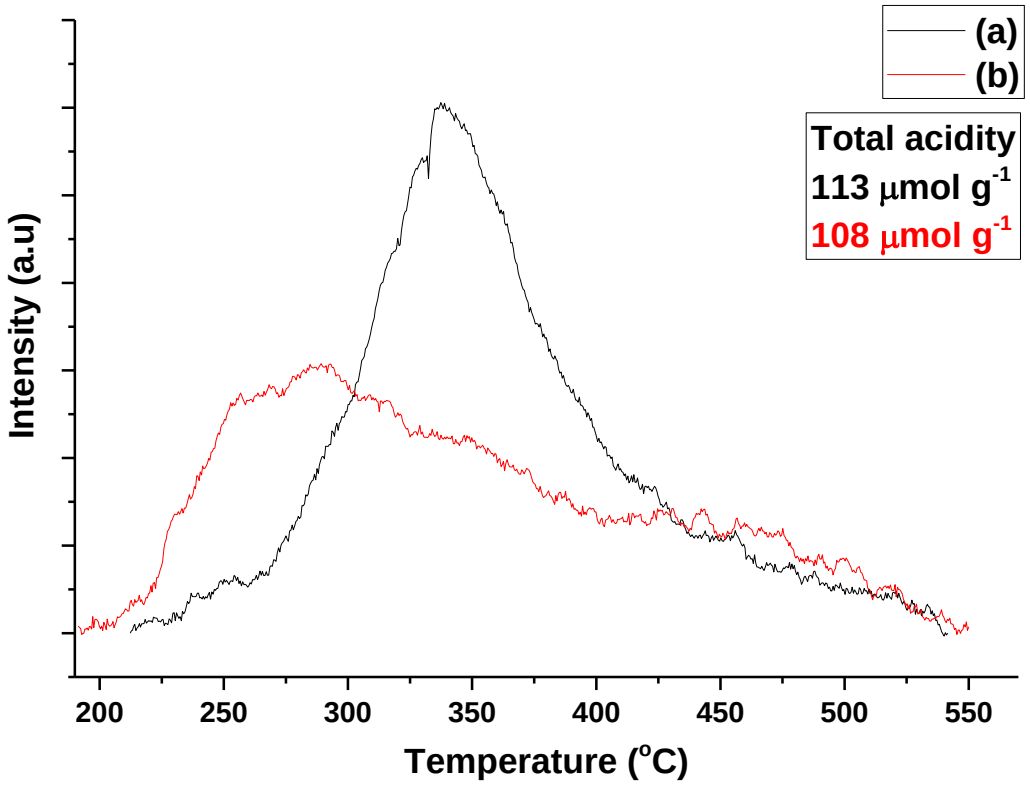

Figure 4.8 Temperature programmed desorption measurements of (a) H-ZSM-5 (100)-MW and (b) H-ZSM-5 (100)-MW-PS60.

Acidity measurements of the laboratory synthesised zeolites showed the untemplated zeolite had one desorption peak with T_{max} at 337 °C and acid site density of 113 μmol g^{-1}. This largely implies our untemplated zeolite consisted of strong acid sites with aluminium largely located in the tetrahedral framework position. Templation of H-ZSM-5 using polystyrene with an average particle diameter size of 60 nm resulted in a desorption peak with T_{max} at 289 °C with an acid site density value of 108 μmol g^{-1}, suggesting our templated zeolite contains extra-framework aluminium due to the lower crystallisation temperature. This result was in general agreement with the study carried out by Xu et al.[115] who hypothesised the lower acidity of their hierarchical zeolite using polystyrene nanospheres of ca. 580 nm was due to the amorphous nature of the macroporous walls. Since only TPD-NH_3 studies were carried out to determine the acid site density for catalysts in this and subsequent studies in this chapter, it was impossible to accurately determine the exact contribution of Lewis and Brønsted acid sites. Other methods such as FT-IR with pyridine adsorption are required to separately measure the Brønsted and Lewis acid sites.

4.3.2.1.1 Solid state NMR studies

In this subsection, ^{27}Al and ^{29}Si MAS-NMR spectra are presented showing the effect of hard templating using polystyrene on the coordination of aluminium and silicon species. The ^{27}Al and ^{29}Si MAS-NMR spectra are shown in Figure 4.9 and Figure 4.10 respectively.

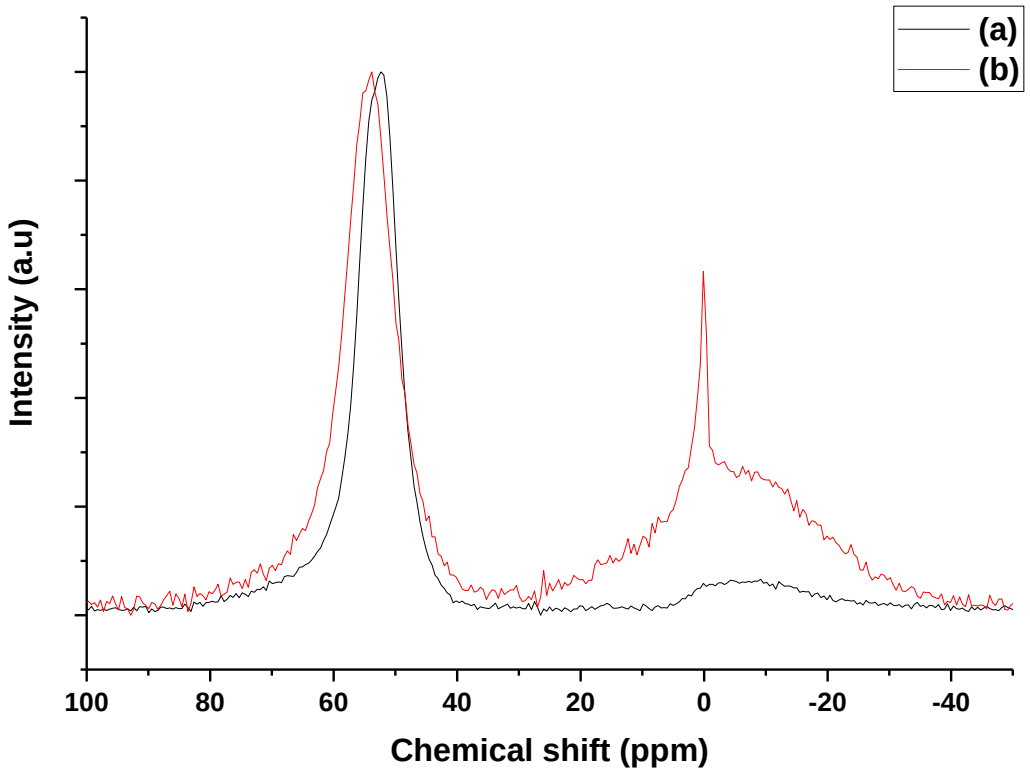

Figure 4.9 ^{27}Al MAS-NMR spectra of (a) H-ZSM-5 (100)-MW and (b) H-ZSM-5 (100)-MW-PS60.

Figure 4.9 shows the ^{27}Al MAS-NMR spectra of H-ZSM-5 (100)-MW and H-ZSM-5 (100)-MW-PS60. The spectrum for H-ZSM-5 (100)-MW is dominated by a signal at ca. 55 nm, corresponding to tetrahedrally coordinated framework aluminium (Al^{IV}), with a smaller signal at ca. 0 ppm corresponding to extra-framework octahedrally coordinated aluminium (Al^{VI}). The symmetric peak between 40-80 ppm suggests extra-framework aluminium (Al^{V}) was not formed during crystallisation. Integration of the peaks using Gaussian fittings revealed 89% of the aluminium atoms were located within the tetrahedral framework as Al^{IV}. This result is in excellent agreement with TPD-NH_3 studies. Templation of H-ZSM-5 using polystyrene (60 nm) resulted in two sharp peaks at 55 and 0 ppm, indicating the presence of Al^{IV} and Al^{VI}. Similar to the untemplated

zeolite, it appears that templation did not result in the formation of Al^V species. Our results showed that only 55% of the aluminium species were located in the framework position. Therefore, this confirms that the lower acid site density value determined by TPD-NH_3 for H-ZSM-5 (100)-MW-PS60 was due to the formation of extra-framework aluminium species.

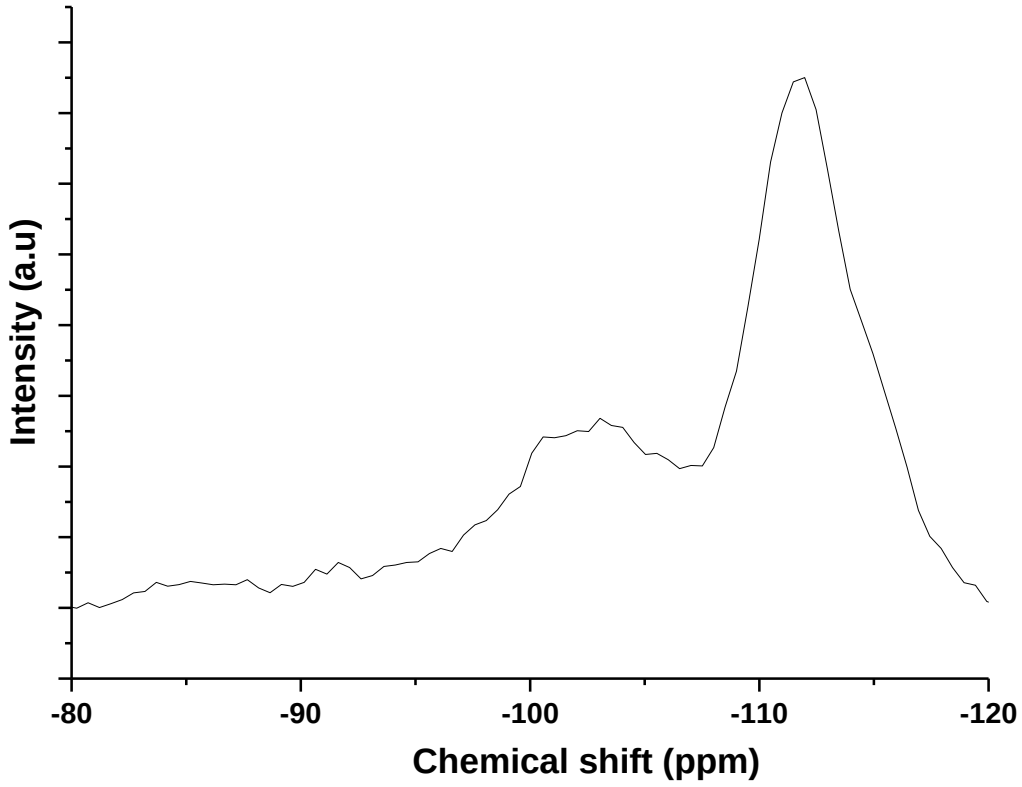

Figure 4.10 ^{29}Si-MAS-NMR spectrum of H-ZSM-5 (100)-MW.

As expected, Figure 4.10 illustrates that the ^{29}Si-MAS-NMR spectrum of H-ZSM-5 (100)-MW showed a highly siliceous material with approximately 61% of the material consisting of Si-O-Si located in the extra-framework position,[226] as evidenced by the sharp peak at ca. -110 ppm with another band at ca -103 ppm which correspond to a mixture of silanol groups and Si(OAl).[227] Wang et al.[228] hypothesised the formation of silanol groups can arise from the mesoporous surface. The $(Si/Al)_F$ was determined as 52.2, higher than 46.5 determined for the $(Si/Al)_{bulk}$ which can be attributed to extra-framework aluminium species.

4.3.2.2 Effect of crystallisation temperature on catalytic properties of hierarchical H-ZSM-5

After promising results were obtained for the templated zeolite synthesised at 100 ^{o}C for 12 hours, optimisation studies were carried out. Synthesis of H-ZSM-5 using polystyrene with an average particle size of 60 nm gave poor yields of only 6% compared to 31% for the untemplated zeolite. Therefore, the effect of crystallisation temperature on the physical and chemical properties of hierarchical H-ZSM-5 was studied. For this study, polystyrene with an average particle diameter of 60 nm was used as the hard template. A precursor solution was synthesised as described in section 4.2.3. In a typical synthesis, the precursor solution/hard template mixture was subjected to hydrothermal treated with microwave assisted heating at temperatures 100, 120, 140 and 165 ^{o}C for 12 hours. The catalysts were brought into the active form as described in section 4.2.4. The catalysts were characterised by XRD, nitrogen sorption, TPD-NH_3 and SEM. In this study, the templated zeolites are denoted as H-ZSM-5 (100)-MW-PS60-x, where x is the crystallisation temperature. The counts of the XRD diffractograms are shown only in this study to demonstrate the relative intensity and to give an indication of the relative crystallinity of each sample.

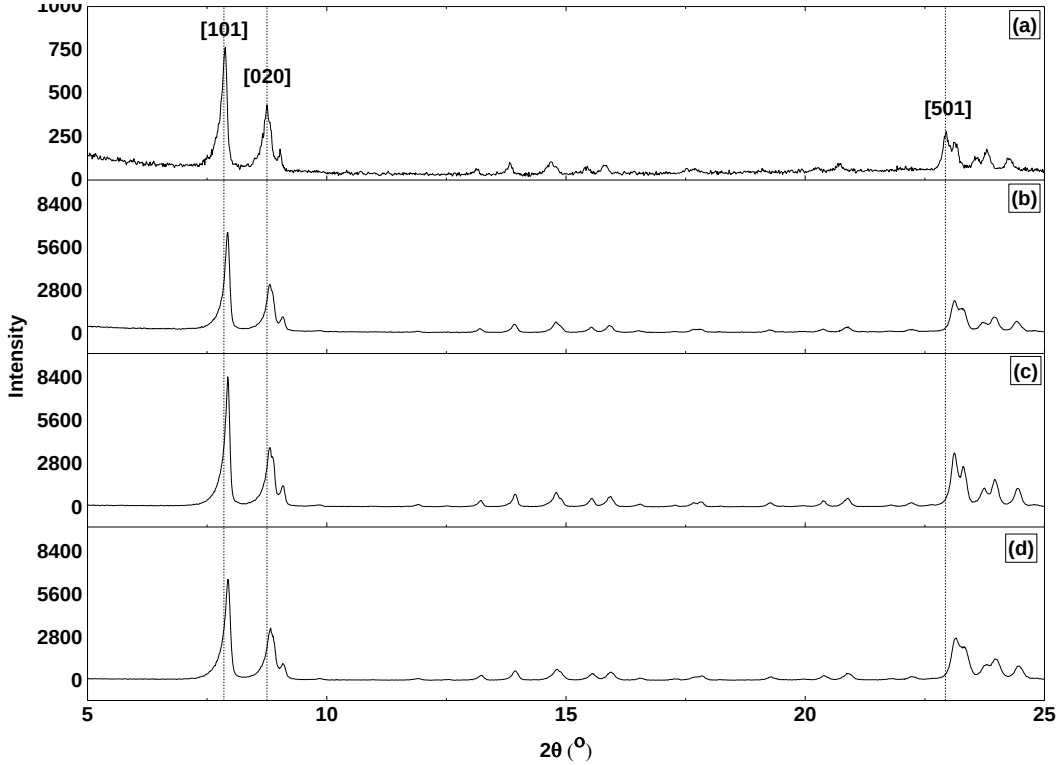

Figure 4.11 XRD diffractograms of various hierarchical H-ZSM-5 zeolites synthesised with varying crystallisation temperatures; (a) H-ZSM-5 (100)-MW-PS60-100, (b) H-ZSM-5 (100)-MW-PS60-120, (c) H-ZSM-5 (100)-MW-PS60-140 and (d) H-ZSM-5 (100)-MW-PS60-165.

All the materials of H-ZSM-5 zeolites synthesised with various crystallisation temperatures showed crystalline structures, as confirmed by the XRD diffractograms in Figure 4.11, depicting the typical H-ZSM-5 structure. The relative intensity of the [101] reflection plane generally increased with increasing crystallisation temperature. This can be accounted for due to the increasing particle size with increasing temperature.[229]

The nitrogen isotherm of H-ZSM-5 (100)-MW-PS100-100 is described in greater detail in section 4.3.1.3. H-ZSM-5 (100)-MW-PS60-120 showed a combination of a type I and IV isotherm with a pronounced H3 hysteresis loop from 0.40 to 1.0, confirming aggregates with slit pores of nonuniform size.[230] However, H-ZSM-5 (100)-MW-P60-140 and H-ZSM-5 (100)-MW-PS60-165 showed an almost type I isotherm with a sharp uptake at relative P/P_o <0.05 and minuscule hysteresis, implying the structures are dominated by microporosity.

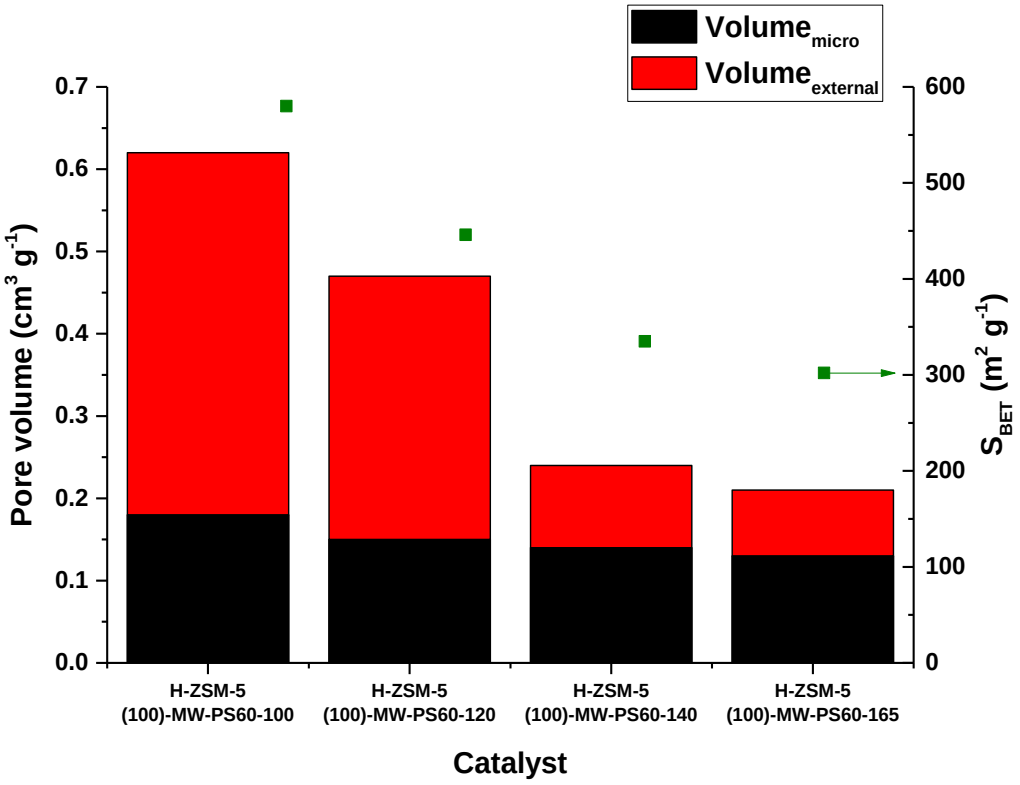

Figure 4.12 Surface area and porosity measurements for templated H-ZSM-5 synthesised with varying temperatures.

Nitrogen sorption measurements of the templated zeolites shown in Figure 4.12 showed a direct correlation between the specific surface area and crystallisation temperature. Generally, the zeolites synthesised at lower crystallisation temperatures showed the highest specific surface area with increased mesoporosity, with specific surface areas of 580 $m^2 g^{-1}$ and 302 $m^2 g^{-1}$ for the zeolite synthesised at 100 and 165 ^oC respectively. This was due to the formation smaller crystallites at lower crystallisation temperatures. Similar results were obtained by Petushkov et al.[231] who also showed that reduction of the precursor volume by partial evaporation prior to hydrothermal treatment led to smaller crystallites, confirming ethanol promotes crystallinity.[179] Comparison of surface area porosity measurements of H-ZSM-5 (100)-MW-PS60-165 with H-ZSM-5 (100)-MW in section 4.3.1.3 clearly showed the hard template inhibited the formation of mesoporosity when crystallised at 165 ^oC.

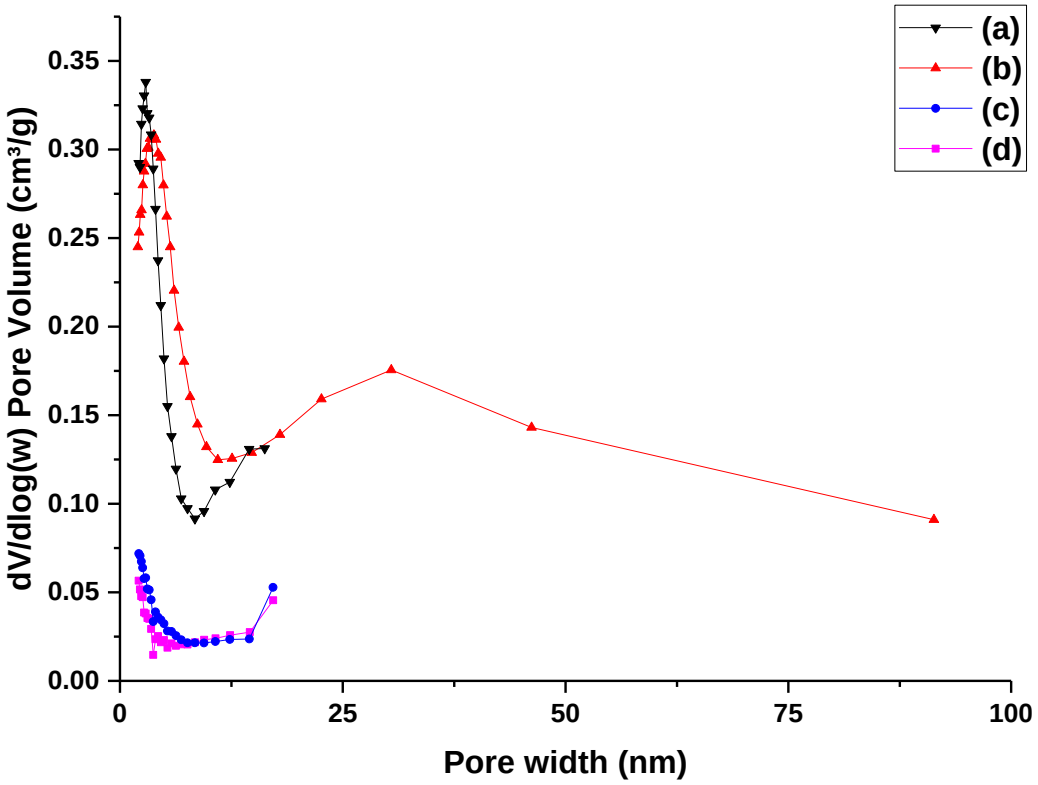

Figure 4.13 Pore size distribution measurements of various hierarchical H-ZSM-5 zeolites synthesised with varying crystallisation temperatures; ; (a) H-ZSM-5 (100)-MW-PS60-100, (b) H-ZSM-5 (100)-MW-PS60-120, (c) H-ZSM-5 (100)-MW-PS60-140 and (d) H-ZSM-5 (100)-MW-PS60-165.

Pore size distribution measurements of the laboratory synthesised H-ZSM-5 zeolites, synthesised at various temperatures showed a wide distribution of mesopores formed. The adsorption isotherms for H-ZSM-5 (100)-MW-PS60-165 and H-ZSM-5 (100)-MW-PS60-140 showed mesopores <13 nm. When lower crystallisation temperatures were used, mesoporosity became more pronounced. It can clearly be seen that a wider distribution of mesopores were formed for zeolites synthesised at lower temperature. The majority of the formed mesopores for H-ZSM-5 (100)-MW-PS60-120 and H-ZSM-5 (100)-MW-PS60-100 had pore radii < 12.5 nm. Unlike H-ZSM-5 (100)-MW-PS60-165 and H-ZSM-5 (100)-MW-PS60-140, the zeolites synthesised at lower temperatures had a proportion of mesopores of pore width > 12.5 nm.

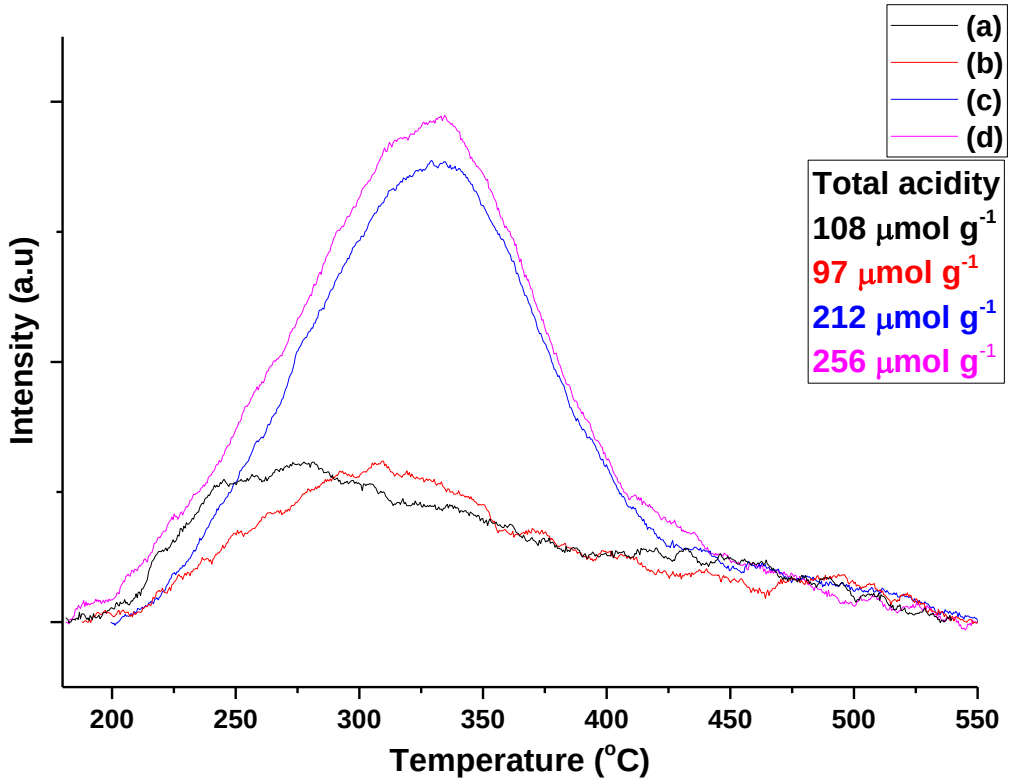

Figure 4.14 Temperature programmed desorption profile of various hierarchical H-ZSM-5 zeolites synthesised with varying crystallisation temperatures; ; (a) H-ZSM-5 (100)-MW-PS60-100, (b) H-ZSM-5 (100)-MW-PS60-120, (c) H-ZSM-5 (100)-MW-PS60-140 and (d) H-ZSM-5 (100)-MW-PS60-165.

In the TPD-NH_3 profiles of laboratory H-ZSM-5, synthesised at different crystallisation temperatures shown in Figure 4.14, a well resolved symmetrical peak is dominant with T_{max} at 334 ^oC for H-ZSM-5 (100)-MW-PS60-165 is observed, suggesting it is dominated by strong acid sites likely due to aluminium atoms located in the tetrahedral framework. As the crystallinity of the laboratory synthesised H-ZSM-5 decreases, the main peak decreases and shifts to lower temperature, suggesting weaker acid sites becomes more dominant. The zeolites H-ZSM-5 (100)-MW-PS60-120 and H-ZSM-5 (100)-MW-PS60-100 showed total acidities of 97 and 108 μmol g^{-1} with T_{max} at 309 and 289 ^oC respectively, evidence of sites corresponding of low/medium strength.[232] Therefore, it is highly likely that for zeolites synthesised at lower temperature, extra-framework aluminium species becomes more significant.

SEM was used to determine the morphology and compactness of H-ZSM-5 zeolites after the removal of the hard templating agent by calcination. Particle sizes were counted using ImageJ software 1.48V. Typically, 100 measurements were made and plotted to obtain a

general representation of the average particle size. The SEM images and particle size distributions are shown in Figures 4.15-4.18.

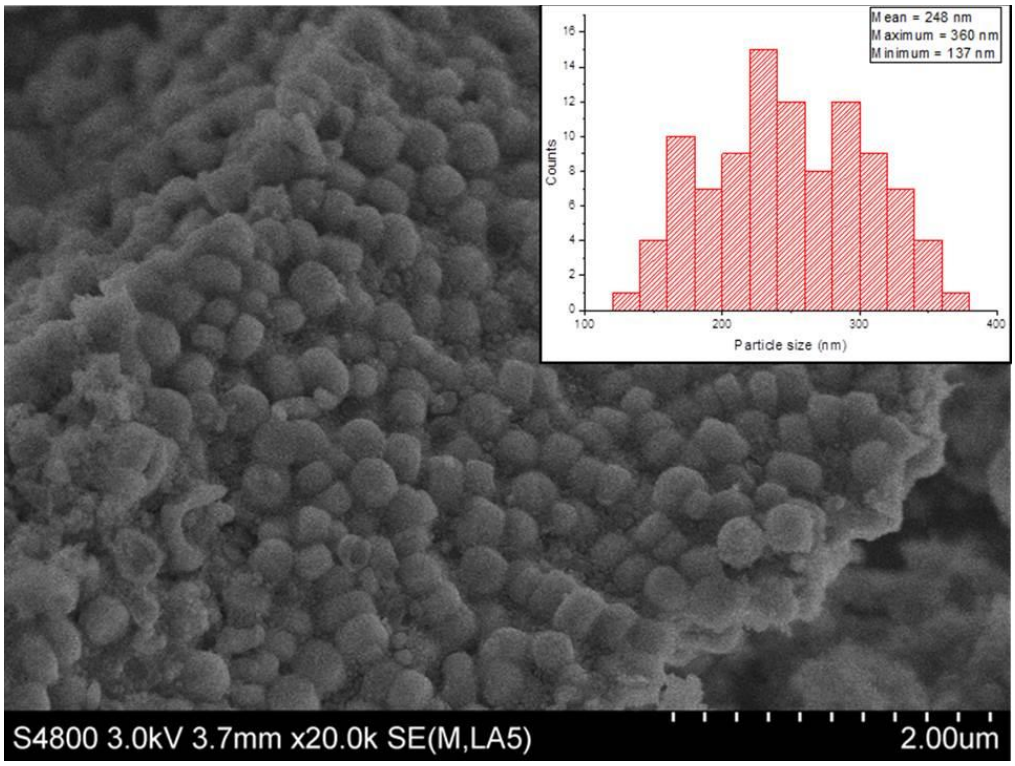

Figure 4.15 SEM of H-ZSM-5 (100)-MW-PS60-100.

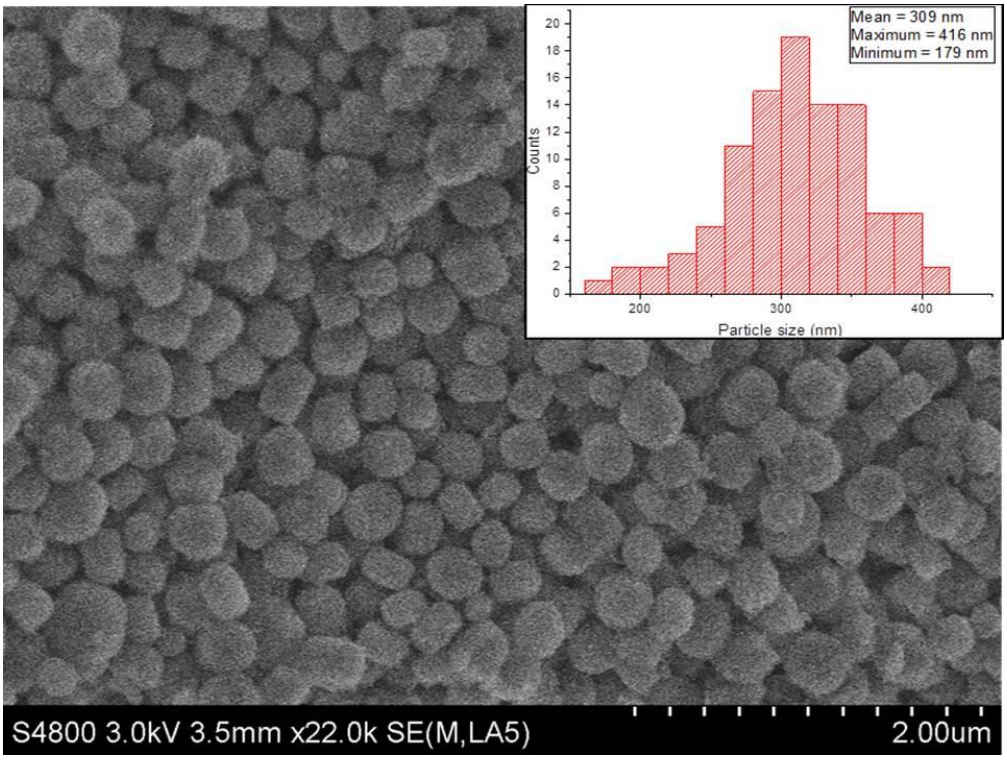

Figure 4.16 SEM image of H-ZSM-5 (100)-MW-PS60-120.

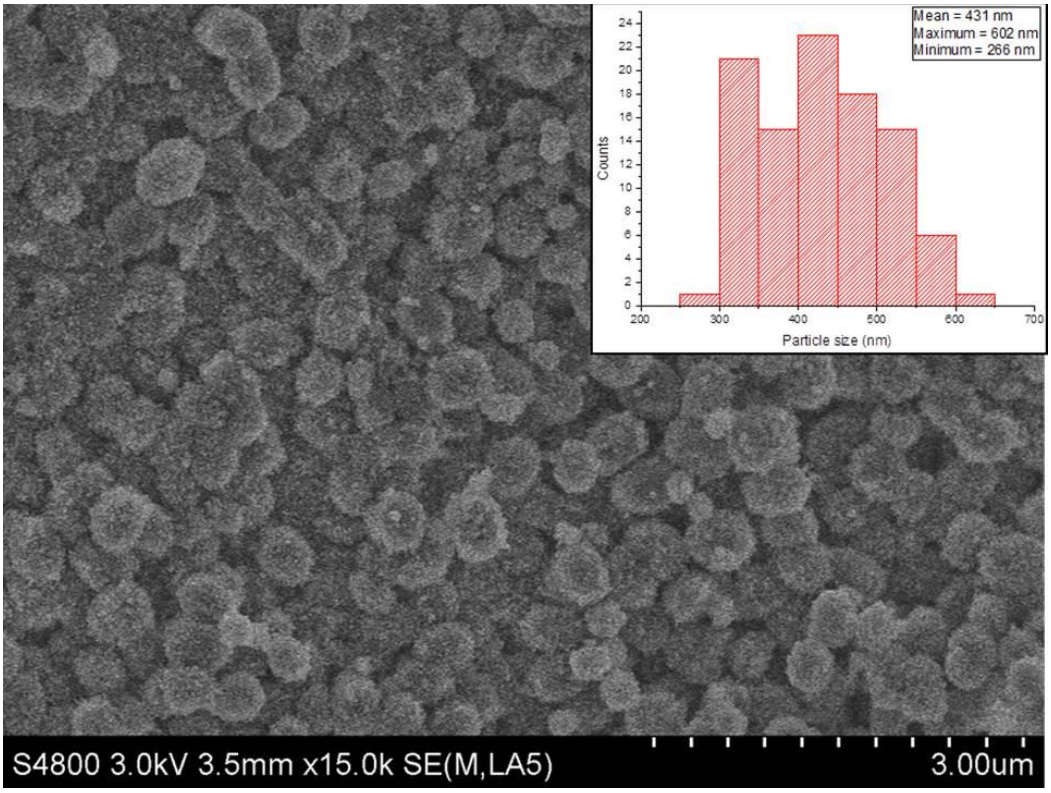

Figure 4.17 SEM image of H-ZSM-5 (100)-MW-PS60-140.

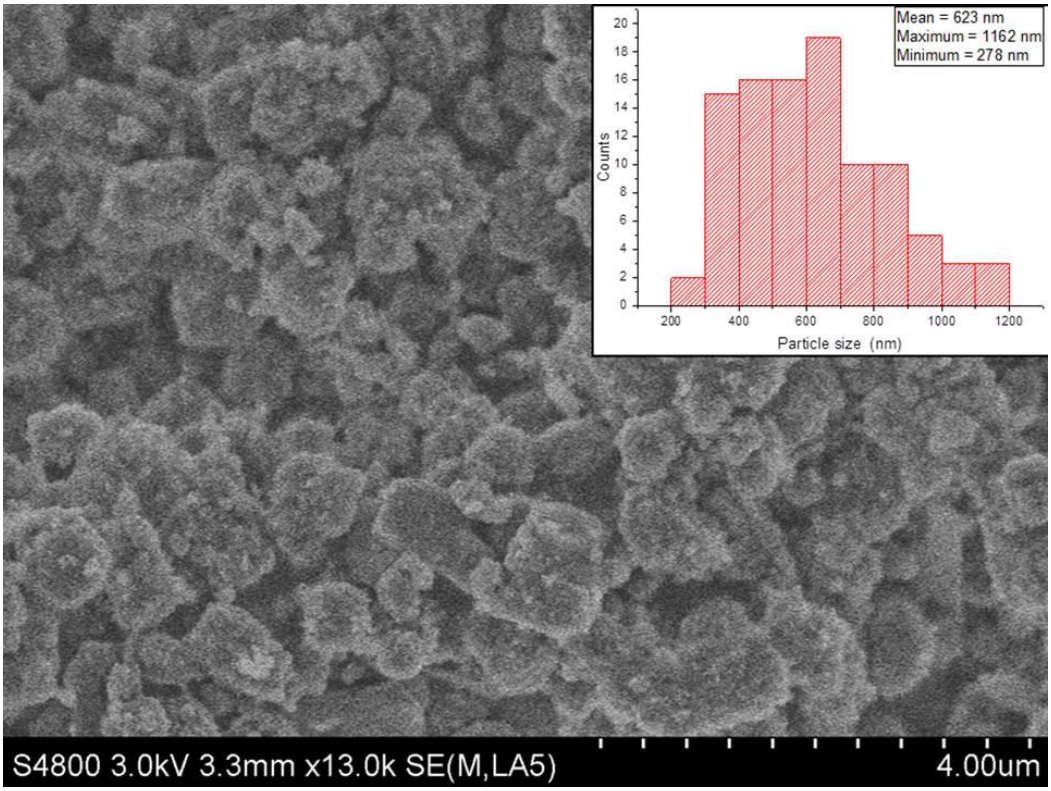

Figure 4.18 SEM image of H-ZSM-5 (100)-MW-PS60-165.

H-ZSM-5 synthesised using various crystallisation temperature had a varying effect on the shape and size of the particles, as shown in Figures 4.15-4.18 H-ZSM-5 (100) synthesised at 100 ^{o}C resulted in the formation of spherical particles with an average mean particle size of 248 nm with cavities due to the removal of the polystyrene (60 nm) from the structure. It must be noted that despite its relatively small crystal size, the XRD diffrractograms produced confirm a highly pure MFI structure. The spherical geometry of the particles is consistent with carried out by Aguado et al [233] for low temperature synthesis of H-ZSM-5, who hypothesised that synthesis of H-ZSM-5 at <100 ^{o}C favours the nucleation step over crystal growth resulting in the formation of aggregated nanoparticles. Increasing the crystallisation temperature generally increased the particle sizes with crystallisation at 165 ^{o}C producing H-ZSM-5 particles of non-uniform shape, with a mean size of 623 nm.

4.3.2.3 Effect of calcination ramp rate on catalytic properties of hierarchical H-ZSM-5

There have been studies which have shown the effect of the calcination temperature[73, 234] and environment[229] on the physical and chemical properties of H-ZSM-5. However, to the best of our knowledge, the number of studies studying the effect of the calcination ramp rate on the physical and chemical properties of H-ZSM-5 is limited. Therefore, we aimed to remove the hard templating using various ramp rates to study the effect on crystal structure, surface area, porosity and acidity. For this study, the following ramp rates were used; 0.5, 1 and 7 ^{o}C min^{-1} and held at 550 ^{o}C for 6 hours. The catalysts in this study are denoted as H-ZSM-5 (100)-MW-PS-x, where x is the calcination ramp rate in ^{o}C min^{-1}. After calcination, the catalysts were analysed using XRD, nitrogen sorption and TPD-NH_3. For XRD studies, the intensity axis is not shown on the same scale for each catalyst. For this purpose, we were only interested in whether the calcination ramp rate would disrupt the crystalline structure. The change in peak positions are shown relative to H-ZSM-5 (100)-MW-PS60-1.

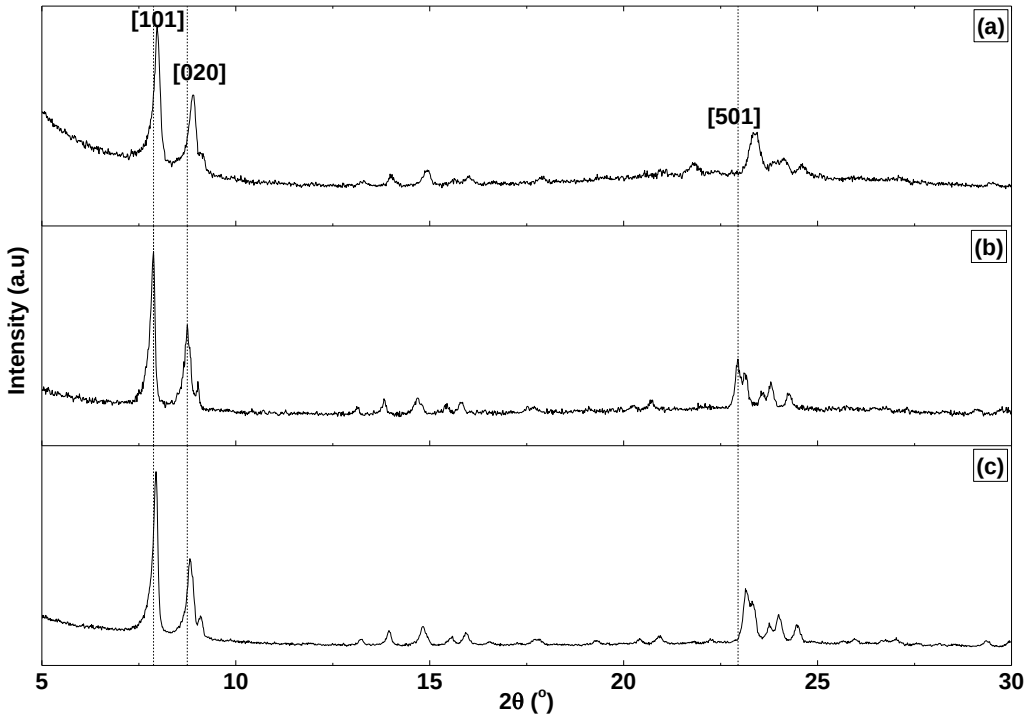

Figure 4.19 XRD diffractograms of hierarchical H-ZSM-5 zeolites calcined with various ramp rates; (a) H-ZSM-5 (100)-MW-PS60-0.5, (b) H-ZSM-5 (100)-MW-PS60-1 and (c) H-ZSM-5 (100)-MW-PS60-7.

XRD diffractograms (Figure 4.19) show that the removal of the hard templating agent, polystyrene (60 nm) using various calcination ramp rates retained the long range crystal order of the MFI structure, as shown by the [101], [020] and [501] reflection planes. Additionally, it can be seen that no other impure phase was produced. Analyses of the peak positions show a shift to higher 2θ for H-ZSM-5 (100)-MW-PS60-0.5 and H-ZSM-5 (100)-MW-PS60-7 relative to the peak positions for H-ZSM-5 (100)-MW-PS60-1. This corresponds to a smaller d-space due to the larger Si-O bond lengths, suggesting partial dealumination of the zeolite sample. It is possible that calcination with a slow ramp rate such as 0.5 ^{o}C min^{-1} resulted in partial extraction of framework aluminium due to physisorbed water located within the pores.[235] The presence of water within the pores is supported by thermogravimetric studies. Unfortunately, ICP-AES measurements were not carried out on H-ZSM-5 (100)-MW-PS60-0.5 and H-ZSM-5 (100)-MW-PS60-7. Since this effect appeared to occur with ramp rates of 0.5 and 0.7 ^{o}C min^{-1} and not with 1 ^{o}C min^{-1}, the effect on calcination ramp rate for the removal of the hard templating agent on the chemical properties appears not to show a direct trend and therefore, remains unclear.

Next, nitrogen sorption measurements were carried out to study the effect of the removal of the hard templating agent on the surface area and porosity of the hierarchical zeolite. Analysis of the nitrogen isotherm for H-ZSM-5 (100)-MW-PS60-0.5 revealed a combination of type I and IV isotherm with a type 3 hysteresis loop, closing at P/P_o = 0.4-1.0 for the desorption branch. The closure of the loop at P/P_o = 0.4 is not an indication of the amount of mesoporosity, but is due to the tensile strength effect of the condensate. Thielemann et al.[236] attributed the closure at P/P_o at 0.4 to the emptying of mesopores of approximately 5 nm in width, with pores less than 5 nm showing no hysteresis loop. H-ZSM-5 (100)-MW-PS60-1 and H-ZSM-5 (100)-MW-PS60-7 showed isotherms almost identical to H-ZSM-5 (100)-MW-PS60-0.5, revealing the presence of non-ordered slit shaped pores.

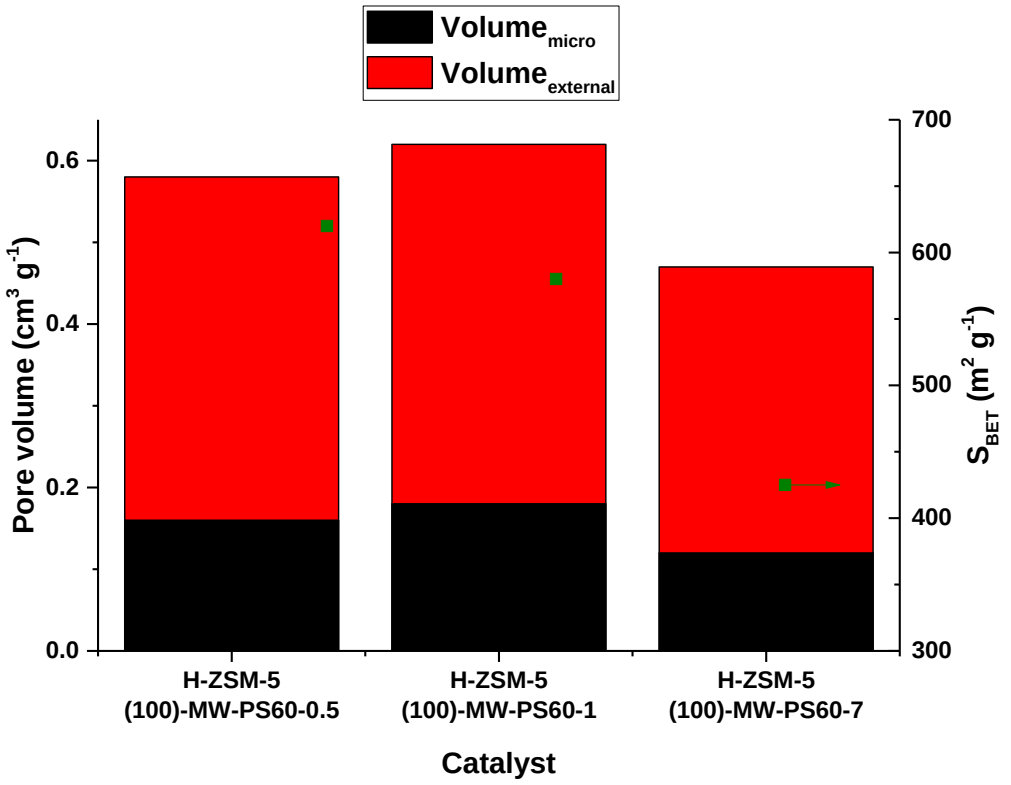

Figure 4.20 Surface area and porosity measurements for templated H-ZSM-5 zeolites calcined with varying ramp rates.

Surface area and porosity measurements revealed a clear trend in the calcination ramp rate on the specific surface area and porosity on H-ZSM-5. Figure 4.20 shows there is an inverse proportional relationship between the specific surface area and calcination ramp rate, with the specific surface area decreasing from 620 to 425 m^2g^{-1} for samples calcined at 0.5 and 7 $^oC\ min^{-1}$ respectively. This suggests the particle size increases with faster calcination ramp rates. We believe that faster ramp rates resulting in an increase in particle size highly unlikely and must be attributed to other factors. It can be seen that the total porosity for H-ZSM-5 calcined at 0.5 and 1 $^oC\ min^{-1}$ showed a total pore volume of 0.58 and 0.62 $cm^3\ g^{-1}$, whereas H-ZSM-5 calcined at 7 $^oC\ min^{-1}$ showed a dramatic decrease in total pore volume to 0.47 $cm^3\ g^{-1}$. At this stage, it was unclear as to whether the specific surface area variation was due to a particle size effect or simply due to variation in total porosity.

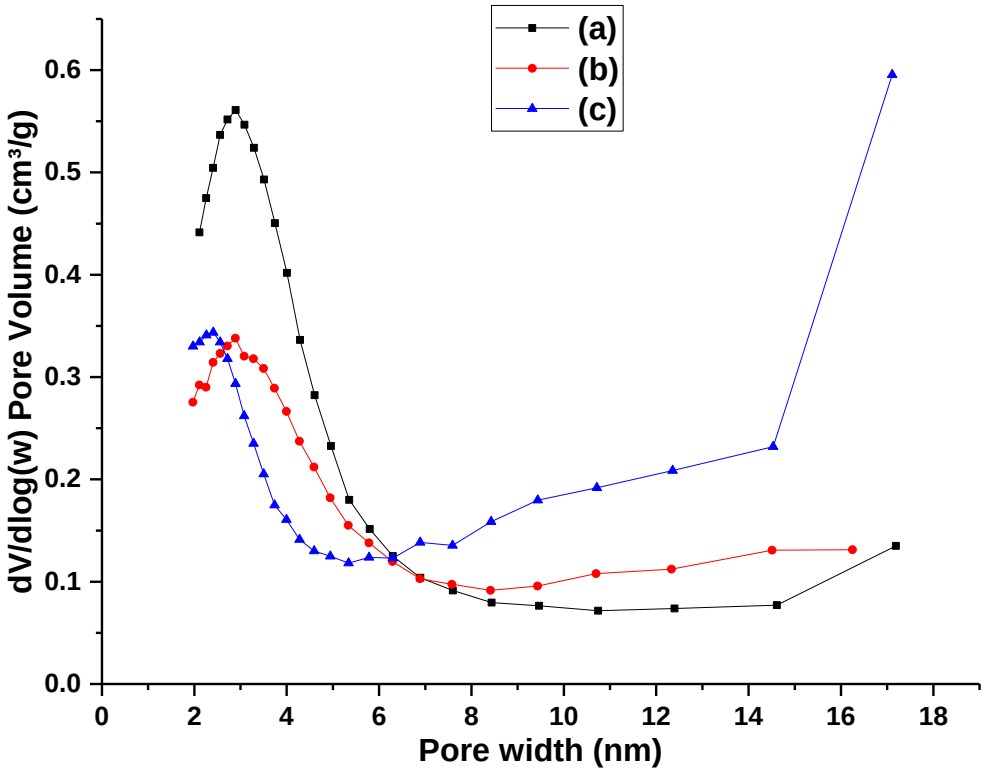

Figure 4.21 Pore size distribution measurements of hierarchical H-ZSM-5 zeolites calcined with various ramp rates; (a) H-ZSM-5 (100)-MW-PS60-0.5, (b) H-ZSM-5 (100)-MW-PS60-1 and (c) H-ZSM-5 (100)-MW-PS60-7.

Pore size distributions of H-ZSM-5 calcined with varying calcination ramp rates, shown in Figure 4.21 reveal that hard templated H-ZSM-5 calcined with a ramp rate of 0.5 ^{o}C min^{-1} showed a contribution of mesopores 2-17 nm with the majority of mesopores <6 nm. An increase of the ramp rate from 0.5 ^{o}C min^{-1} to 1 and 7 ^{o}C min^{-1} resulted in a similar contribution of mesopores ranging from 2-17 nm. However, the BJH profile clearly shows a lower contribution of mesopores ca. 2 nm for H-ZSM-5 (100)-MW-PS60-1 and H-ZSM-5 (100)-MW-PS60-7 compared to H-ZSM-5 (100)-MW-PS60-0.5. Generally, BJH plots measurements showed a proportional relationship with calcination ramp rate and the generation of mesopores with pore width > 6 nm. It could be possible that the highly oxidising nature of the calcination treatment resulted in a thermal shock which generated cracks and voids.[237] This hypothesis strongly supports the shape of the hysteresis loop found in the nitrogen adsorption-desorption isotherms, which indicated slit shape pores on non-uniform size.

Temperature programmed desorption of H-ZSM-5 calcined with varying ramp rates was carried out to determine whether the calcination ramp rate would affect the total number

of acid sites and more importantly, the strength of acid sites. It was anticipated that calcination using a ramp rate of 0.5 and 7 ^{o}C min^{-1}would have a detrimental effect on the total number of acid sites relative to the number of acid sites for H-ZSM-5 calcined at 1 ^{o}C min^{-1}, largely due to partial dealumination from the framework position, as suggested by XRD studies.

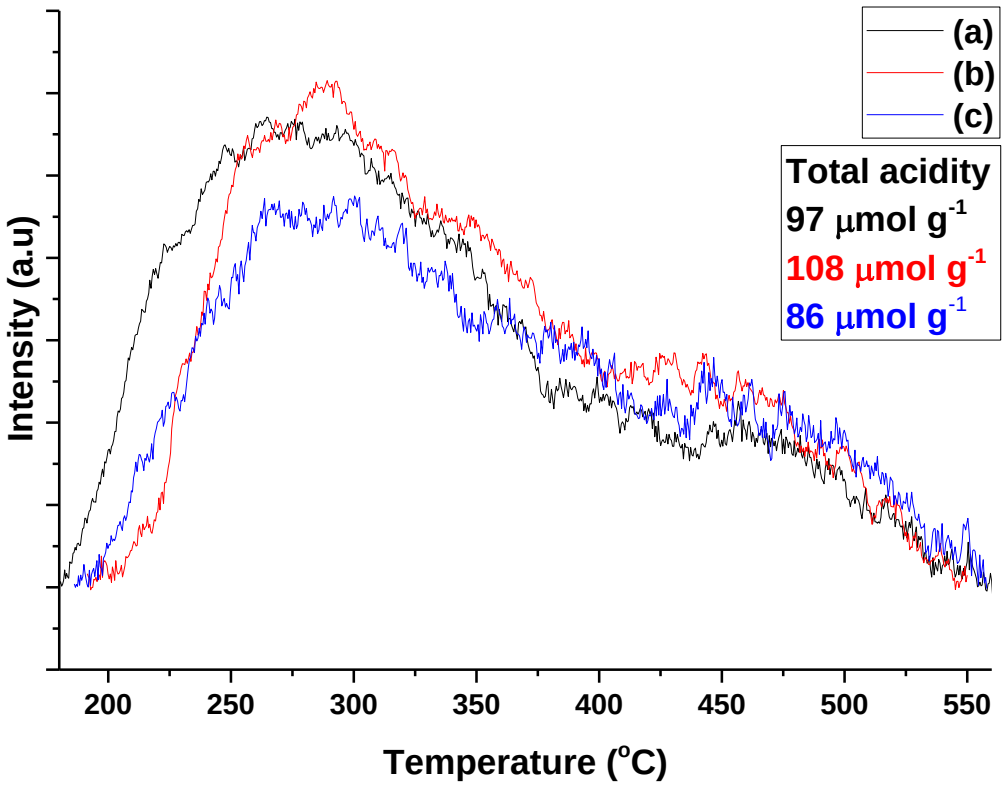

Figure 4.22 Temperature programmed desorption measurements of hierarchical H-ZSM-5 zeolites calcined with various ramp rates; (a) H-ZSM-5 (100)-MW-PS60-0.5, (b) H-ZSM-5 (100)-MW-PS60-1 and (c) H-ZSM-5 (100)-MW-PS60-7.

Temperature programmed desorption profiles of hard templated H-ZSM-5 calcined with ramp rates of 0.5, 1 and 7 ^{o}C min-^{1} showed the total number of acid sites was independent of the calcination ramp rate, and therefore no clear trend was observed. H-ZSM-5 calcined at a ramp rate of 0.5 ^{o}C min^{-1} showed a TPD-NH_3 profile with an acid site density value of 97 µmol g^{-1} with T_{max} at 264 ^{o}C. This largely suggests H-ZSM-5 (100)-MW-PS-0.5 mainly consists of acid sites of weak-medium strength, which can be ascribed to aluminium located in the extra-framework position. The H-ZSM-5 catalyst which demonstrated optimum acidity and T_{max} value in this study was H-ZSM-5 calcined at a ramp rate of 1 ^{o}C min^{-1}, with a total acid site density of 108 µmol g^{-1} and T_{max} of 289 ^{o}C,

confirming H-ZSM-5 (100)-MW-PS60-1 possesses stronger acidity than H-ZSM-5 (100)-MW-PS-0.5, due to the larger proportion of aluminium located in the framework. Clearly, the faster calcination ramp rate of 7 ^{o}C min^{-1} resulted in a decreased quantity of acid sites and strength with the total number of acid sites equal to 86 µmol g^{-1} and T_{max} at 266 ^{o}C. This was largely due to the destructive nature of the zeolitic material caused by the highly oxidising nature caused by the ramp rate.

Since nitrogen sorption measurements showed a clear trend between calcination ramp rate and specific surface are and total porosity of the zeolitic materials, particle sizes were determined using SEM to establish whether the effects of specific surface were due to varying particle sizes, or simply an effect of total porosity. In this study, 100 particles were measured manually using ImageJ software 1.48V to determine a general representation of the particle sizes, and plotted to determine a particle size distribution. The mean value was taken as the size of the particle for the zeolitic material after a particular calcination ramp rate. The SEM images and the particle size distributions are shown in Figures 4.23-4.25.

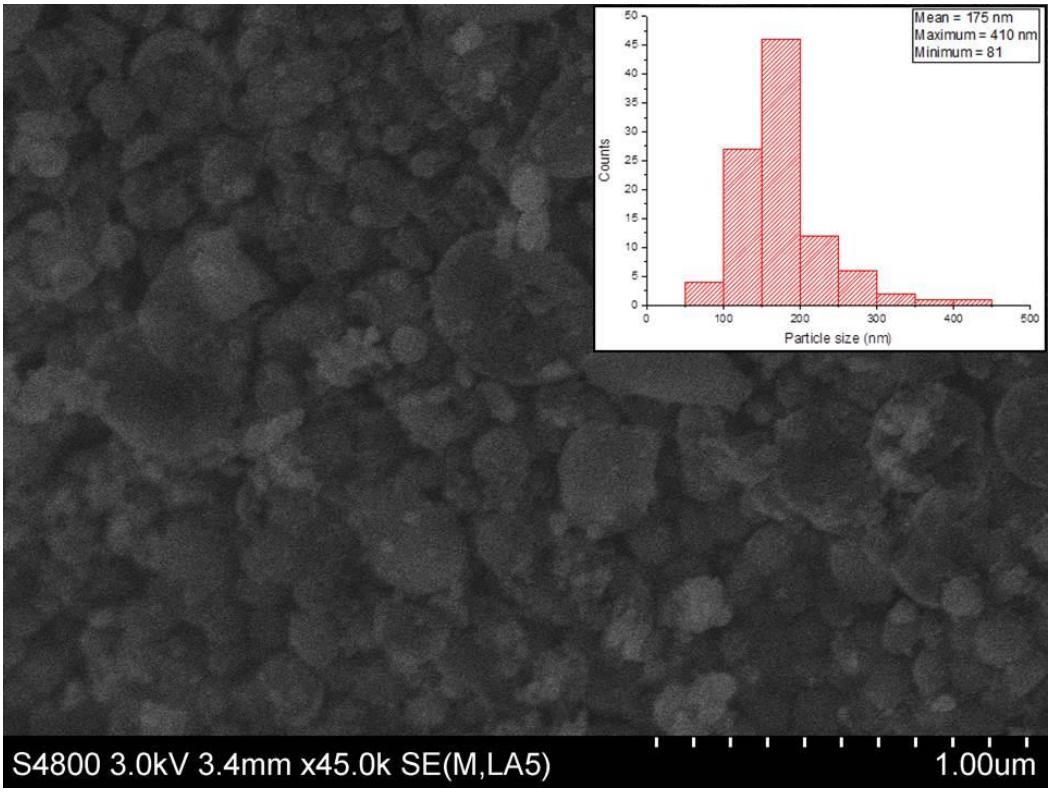

Figure 4.23 SEM image of H-ZSM-5 (100)-MW-PS60-0.5.

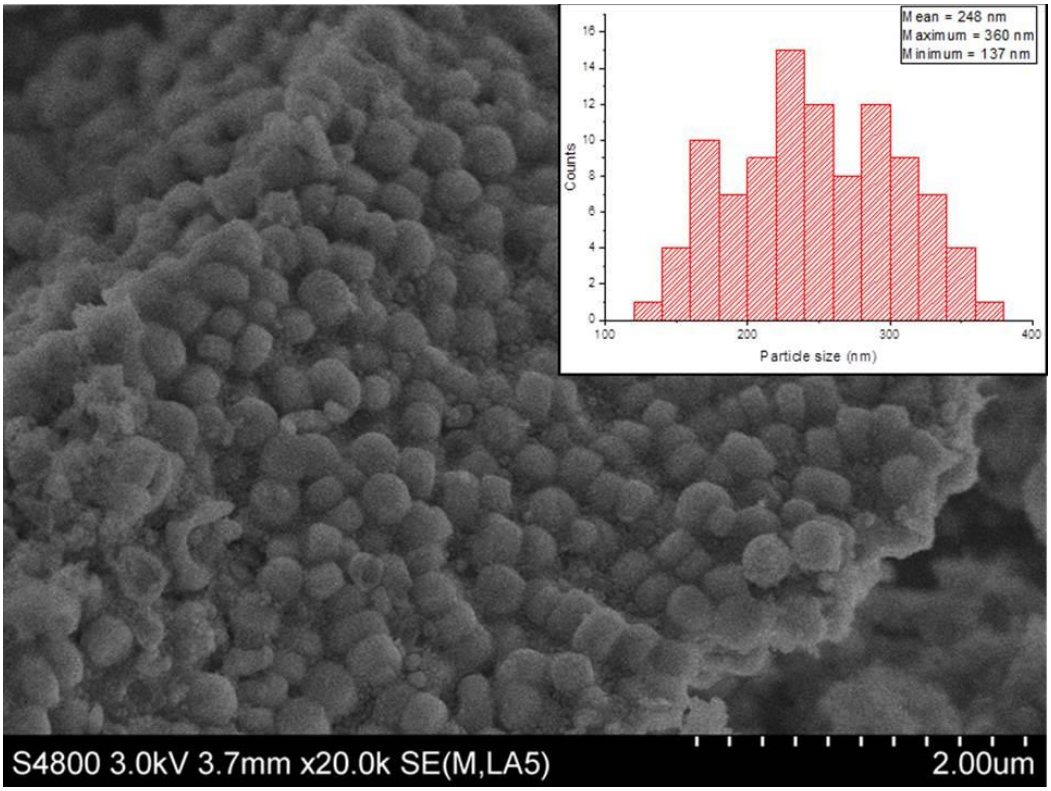

Figure 4.24 SEM image of H-ZSM-5 (100)-MW-PS60-1.

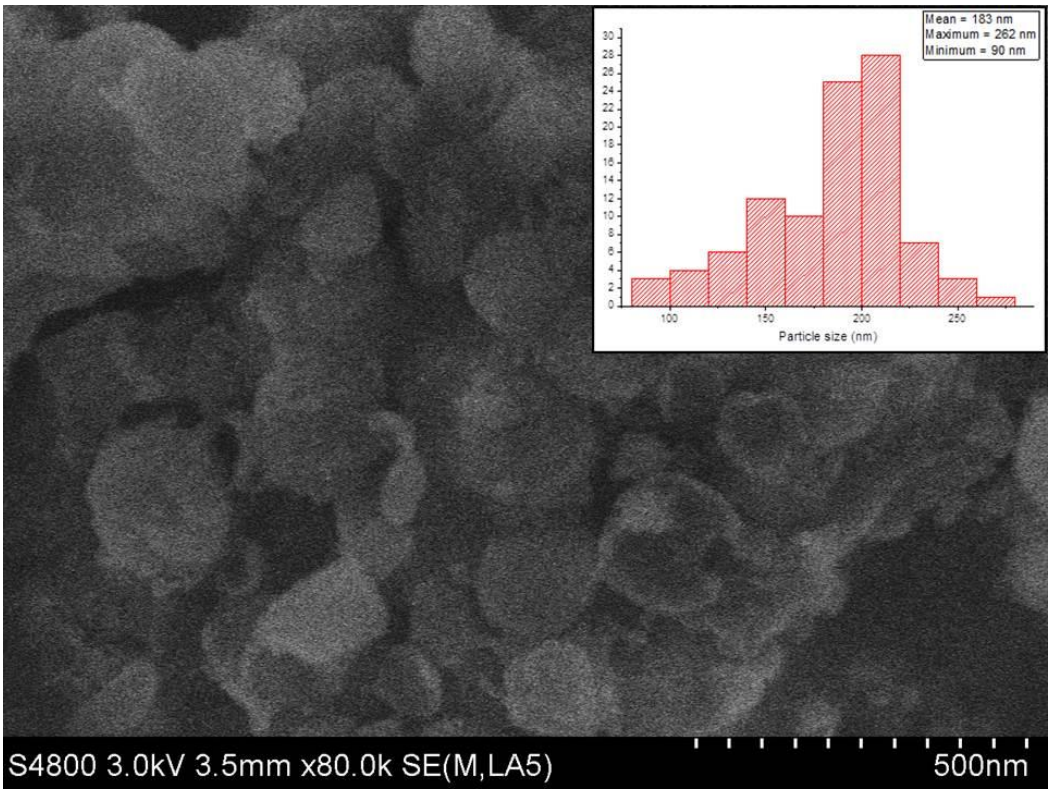

Figure 4.25 SEM image of H-ZSM-5 (100)-MW-PS60-7.

Templated H-ZSM-5 calcined at a ramp rate of 0.5 ^{o}C min^{-1} resulted in the formation of particles with non-uniform shape or size, with some particles displaying spherical geometry and others displaying clusters of particles with no defined shape. Manual measurement of 100 particles showed that a calcination ramp rate of 0.5 ^{o}C min^{-1} resulted in a mean particle size of 175 nm. It can be seen that the particles are aggregated with no defined interparticle porosity. Therefore, the porosity for H-ZSM-5 (100)-MW-PS60-0.5 can be solely attributed to intraparticle mesoporosity. Calcination of H-ZSM-5 with a ramp rate of 1 ^{o}C min^{-1} resulted in the formation of highly compact particles with spherical geometry, with an average particle size of 248 nm with a smaller distribution of particle sizes than H-ZSM-5 (100)-MW-PS60-0.5. Particle size measurements are consistent with surface area and porosity measurements for H-ZSM-5 (100)-MW-PS60-0.5 and H-ZSM-5 (100)-MW-PS60-1, confirming that the variation in surface area is due to a particle size effect. This is also supported by the fact that H-ZSM-5 (100)-MW-PS60-1 has a larger total pore volume than H-ZSM-5 (100)-MW-PS60-0.5 and confirms that the variation in surface area in this case is independent of the total pore volume. The reason for this is unclear at the present time. The formation of cavities within the particles was due to the removal of the hard templating agent. This is largely in agreement with nitrogen sorption studies which showed a type H3 hysteresis loop. Surprisingly, a calcination ramp rate of 7 ^{o}C min^{-1} resulted in a dramatic decrease in the specific surface area to 425 m^{2} g^{-1} with a total pore volume of 0.47 cm^{3} g^{-1}, much lower than H-ZSM-5 calcined at 0.5 and 1 ^{o}C min^{-1}. We hypothesised that a faster calcination ramp would unlikely result in the formation of larger particle sizes, especially compared to (100)-MW-PS60-0.5 and H-ZSM-5 (100)-MW-PS60-1. On the contrary, it was anticipated that the particle size of ZSM-5 (100)-MW-PS60-7 would at least be equal to, if not smaller than H-ZSM-5 particles calcined at 0.5 and 7 ^{o}C min^{-1}. SEM confirmed the average particle size of hard templated H-ZSM-5 calcined at 7 ^{o}C min^{-1} resulted in a mean particle size of 183 nm, with a much smaller particle size distribution than ZSM-5 (100)-MW-PS60-0.5 and ZSM-5 (100)-MW-PS60-1. This confirmed that the discrepancy between the specific surface area measurements was not primarily due to a particle size effect. Also, it can be see there

appears to be limited interparticle porosity. This confirms that the total porosity for all samples calcined with various ramp rates can be attributed to intraparticle porosity.

4.3.2.4 Effect of templation versus non-templation under identical crystallisation conditions

Despite promising results obtained in sections 4.3.1.3-4.3.2.3, it was still unclear what the direct implications of the addition of a hard templating agent on the physical and chemical properties of the zeolite, H-ZSM-5. We had shown the synthesis of H-ZSM-5 using polystyrene with an average particle diameter of 30 and 60 nm at 100 ^{o}C could promote mesoporosity. However, at lower temperatures and different crystallisation times, it was unclear as to whether this was a direct consequence of the addition of the hard template, with lower crystallisation temperature resulting in smaller particles agglomerating or a combination of both effects. Therefore, in this study, we attempted to demonstrate that the addition of polystyrene could promote mesoporosity. Since subjecting the initial precursor solution to 100 ^{o}C did not generate any solid material regardless of the crystallisation time, it was clear that a higher crystallisation temperature was required. Our first attempt focused on crystallisation at 120 ^{o}C since the templated zeolite synthesised at 120 ^{o}C showed a relatively higher specific surface area and total porosity than commercial H-ZSM-5 zeolites as shown in the literature.[198] Crystallisation of the initial precursor solution produced a white solid. This was characterised using XRD, nitrogen sorption, TPD-NH_3 and SEM. XRD diffractograms are shown in Figure 4.26 (below). It must be noted that the intensity axis for each sample are not to the same scale. The primary purpose of XRD in this study was to determine whether the material possessed crystallinity. Particle sizes were measured and compared using SEM.

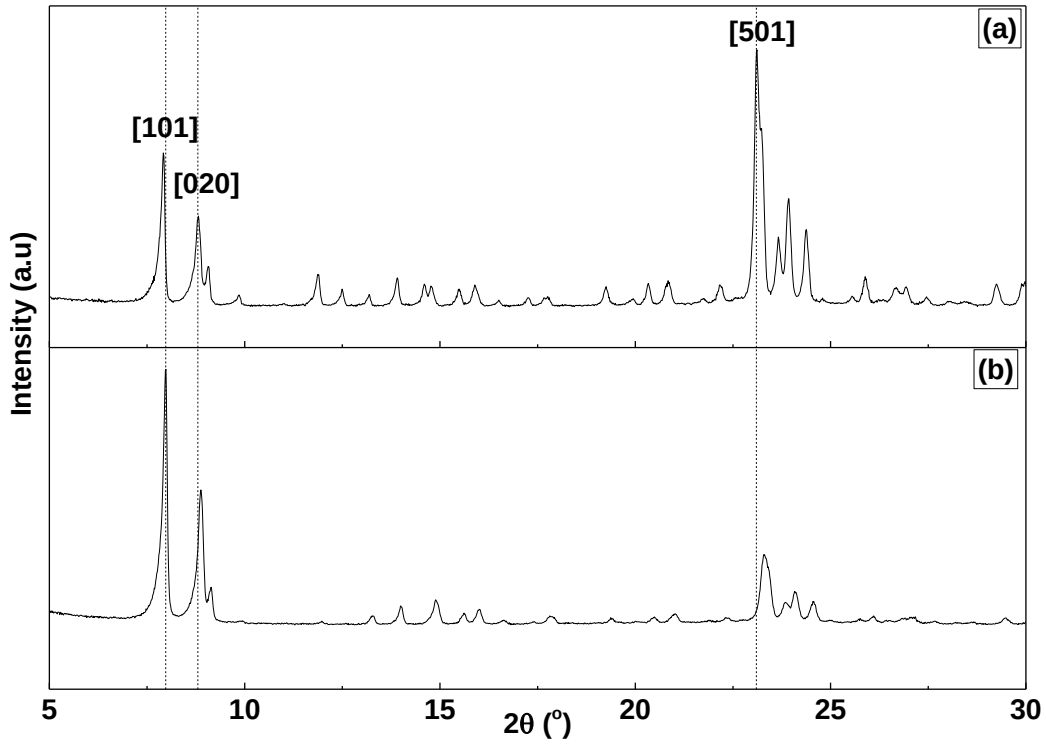

Figure 4.26 XRD diffractograms of (a) H-ZSM-5 (100)-MW-120 and (b) H-ZSM-5 (100)-MW-PS60-120.

XRD patterns of untemplated and templated H-ZSM-5 zeolites synthesised under identical crystallisation conditions showed that both zeolites displayed the typical MFI structure, as shown by the diffraction planes [101], [020] and [501] in in the 2θ regions of 7.9, 8.8, 23.1° respectively. However, there are noticeable differences between the untemplated and templated zeolite. Firstly the broader diffraction patterns for the templated zeolite in the 2θ region 22-25° suggests smaller particles than the untemplated zeolite. Secondly, the addition of polystyrene inhibited growth along the [501] plane when the crystallisation temperature was 120 °C. When compared to the XRD patterns in Figure 4.5 it can clearly be seen growth along the [501] plane when crystallisation was carried out at 165 °C with the absence of polystyrene in the precursor solution. Similar results were obtained by Sashkina et al.[210] In their study however, conventional and the hierarchical zeolite was crystallised under different crystallisation conditions. Therefore, our study confirms that polystyrene inhibits growth along the [501] direction.

After XRD studies had been carried out, the untemplated and templated zeolites were characterised using nitrogen sorption to determine the effect of hard templating using polystyrene nanospheres under identical crystallisation conditions. It was this

measurement that would finally determine whether polystyrene promotes mesoporosity, and not because of the lower crystallisation temperatures as described in the literature. The results of the nitrogen adsorption-desorption isotherm showed a type I isotherm with a flat curve at lower relative pressures, due to the adsorbent filling of the micropores.[139] The sharp increase at higher relative pressure with a small hysteresis at P/P = 0.9-1.0 strongly indicates the formation of mesoporosity in coexistence with well-developed microporosity in the sample.[238, 239] However, a hysteresis loop in this region could also be an indication of interparticle mesoporosity.[240] SEM measurements were carried out to determine the extent of interparticle mesoporosity. The isotherm of H-ZSM-5 (100)-MW-PS60-120 showed a combination of type I and IV isotherm with a much more pronounced hysteresis closing at P/P_o at 0.4, strongly indicating the templated zeolite possessing a significant amount of mesoporosity. Comparison of the nitrogen adsorption-desorption isotherms of both zeolites showed that the templated zeolite displayed a much higher nitrogen uptake at higher relative pressure, indicating the templated zeolite possessed greater porosity than the untemplated zeolite. The specific surface area and porosity measurements are shown in Figure 4.27.

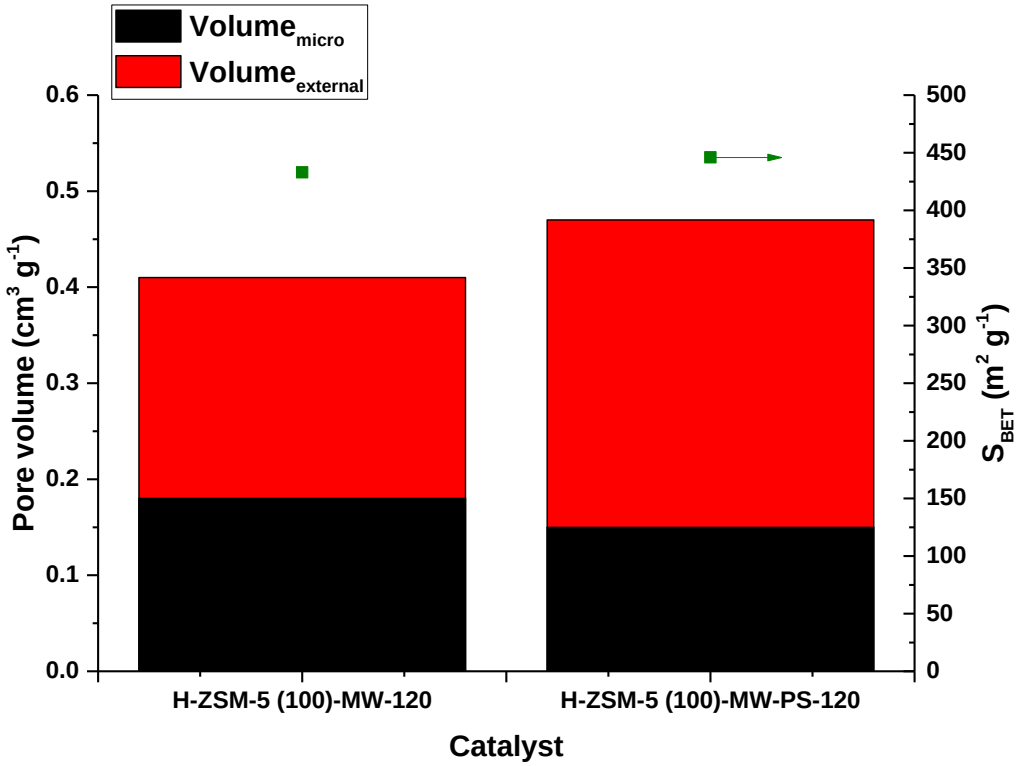

Figure 4.27 Surface area and porosity measurements for H-ZSM-5 (100)-MW-120 and H-ZSM-5 (100)-MW-PS-120.

The specific surface area of the untemplated zeolite was 433 m^2 g^{-1} with a total pore volume of 0.41 cm^3 g^{-1}. Saito-Foley measurements up to 2 nm showed the micropore volume was 0.18 cm^3 g^{-1}. The addition of polystyrene (60 nm) to the precursor solution prior to hydrothermal treaterment resulted in the specific surface area of 446 m^2 g^{-1} for the templated zeolite with a total pore volume of 0.47 cm^3 g^{-1}. The micropore volume decreased slightly from 0.18 cm^3 g^{-1} to 0.15 cm^3 g^{-1} for the untemplated and templated zeolites respectively. The higher specific surface area of the untemplated zeolite implies that templation resulted in smaller particle sizes with more agglomeration compared to the untemplated zeolite.

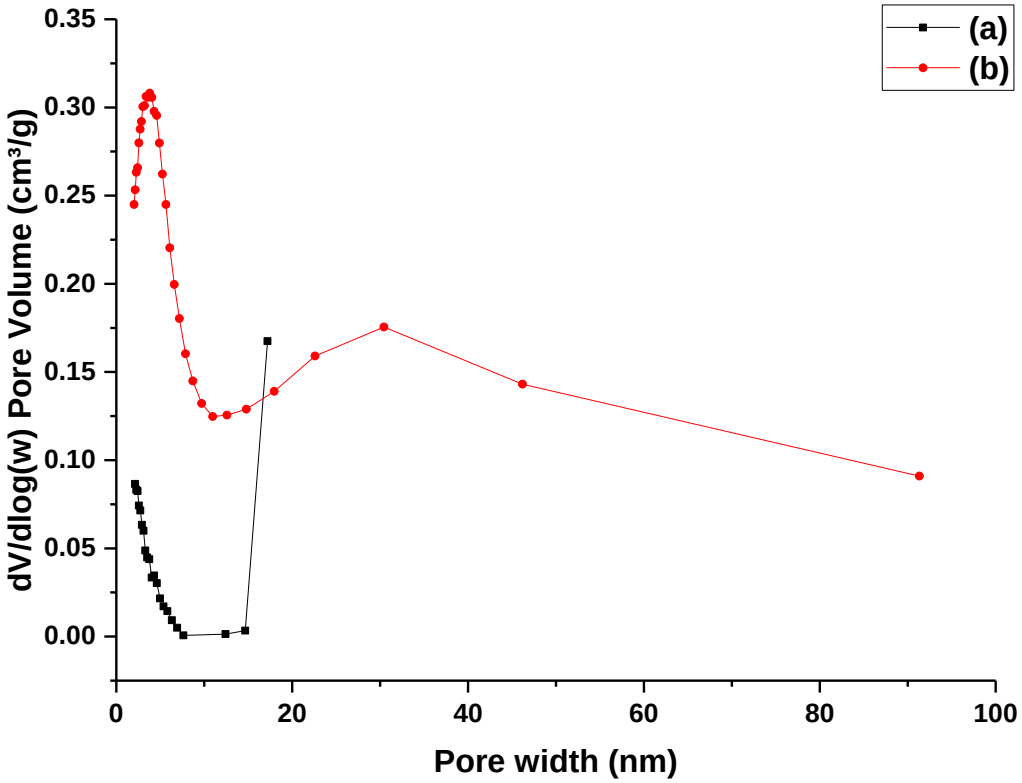

Figure 4.28 Pore size distribution measurements of (a) H-ZSM-5 (100)-MW-120 and (b) H-ZSM-5 (100)-MW-PS60-120.

Based on BJH adsorption measurements shown in Figure 4.28, the zeolite H-ZSM-5 (100)-MW-120 exhibited mesoporosity in the range of 2-17 nm with the majority of the mesopores with pore widths ca. 17 nm, confirming the presence of mesoporosity even without the addition of the hard template. When the BJH adsorption isotherm of the untemplated zeolite is compared to H-ZSM-5 (100)-MW-PS60-120, it is apparent that an increase in mesoporosity for the templated ZSM-5 catalysts was due to the addition of polystyrene (60 nm) to the precursor solution, as evidence by the generation of mesoporosity > 17 nm. However, the majority of the mesopores formed in the templated zeolite possessed pore widths <10 nm.

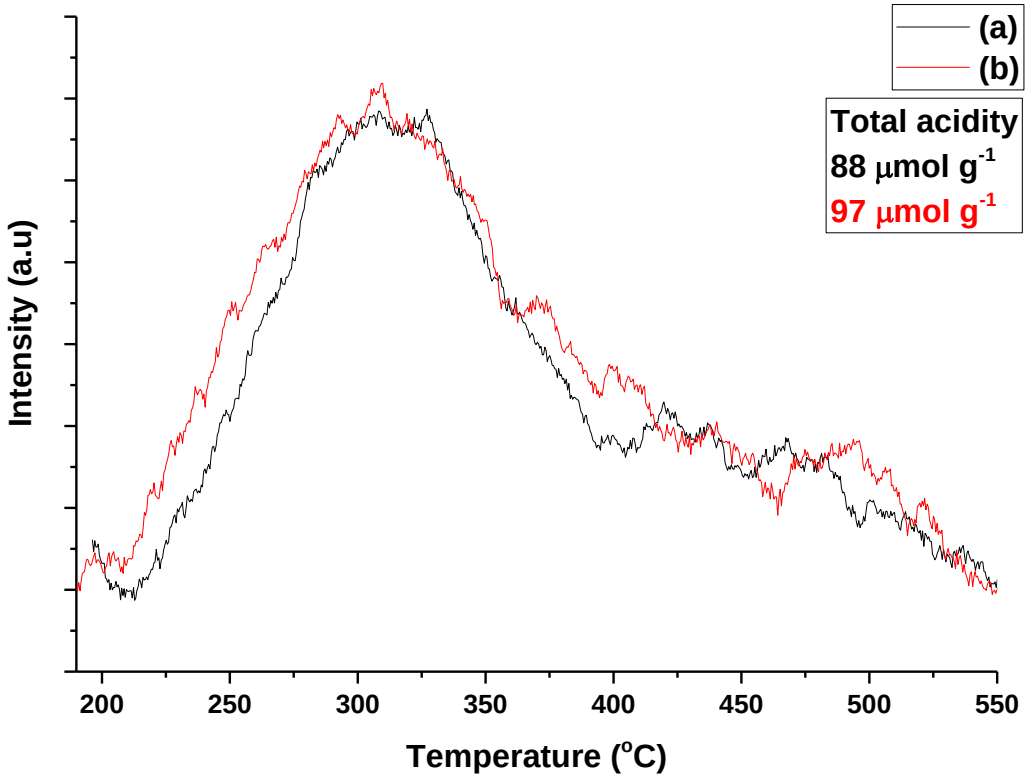

Figure 4.29 Temperature programmed desorption measurements of (a) H-ZSM-5 (100)-MW-120 and (b) H-ZSM-5 (100)-MW-PS60-120.

There was one desorption peak in both laboratory synthesised zeolites. The total number of acid sites for H-ZSM-5 (100)-MW-120 was calculated as 88 μmol g^{-1} with T_{max} at 327 ^{o}C and a narrow distribution of ammonium desorption, indicative that strong acid sites were dominant even when synthesised at 120 ^{o}C. This suggests that for H-ZSM-5 (100)-MW-120, aluminium was largely located in the framework position. Analysis of H-ZSM-5 (100)-MW-PS60-120 confirmed that the acid site density was 97 μmol g^{-1} with T_{max} at 309 ^{o}C. This is in good agreement with XRD and surface area and porosity measurements which show a correlation between crystallinity and microporosity.

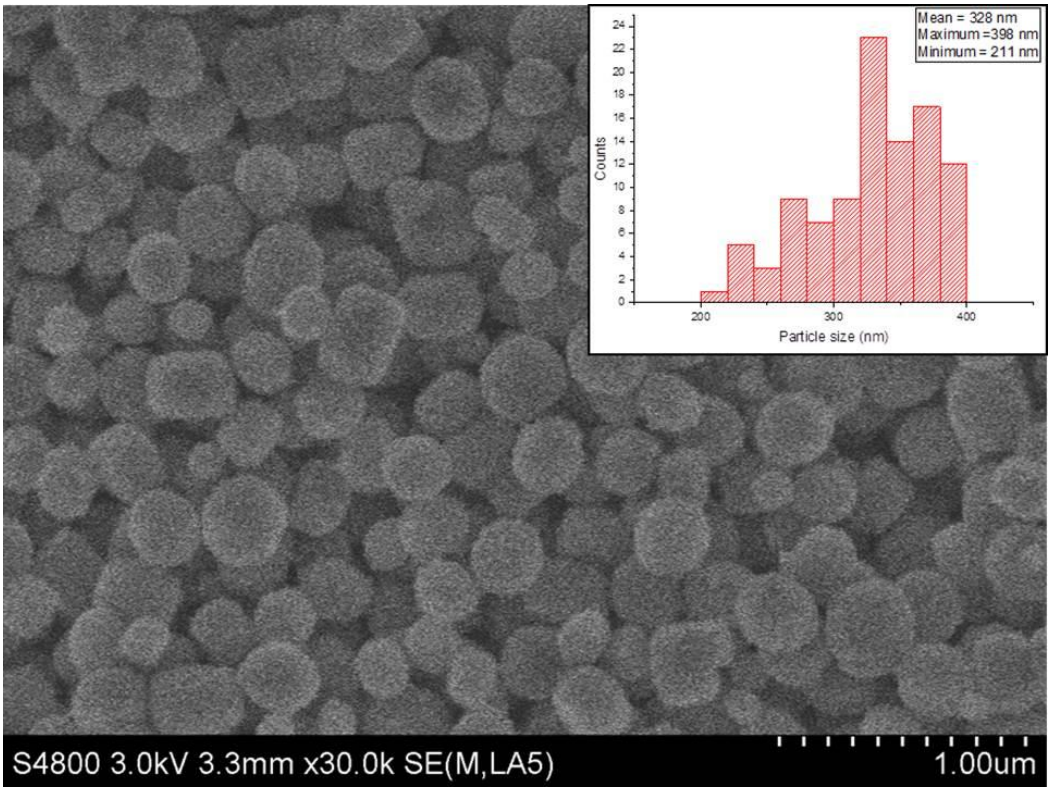

Figure 4.30 SEM image of H-ZSM-5 (100)-MW-120.

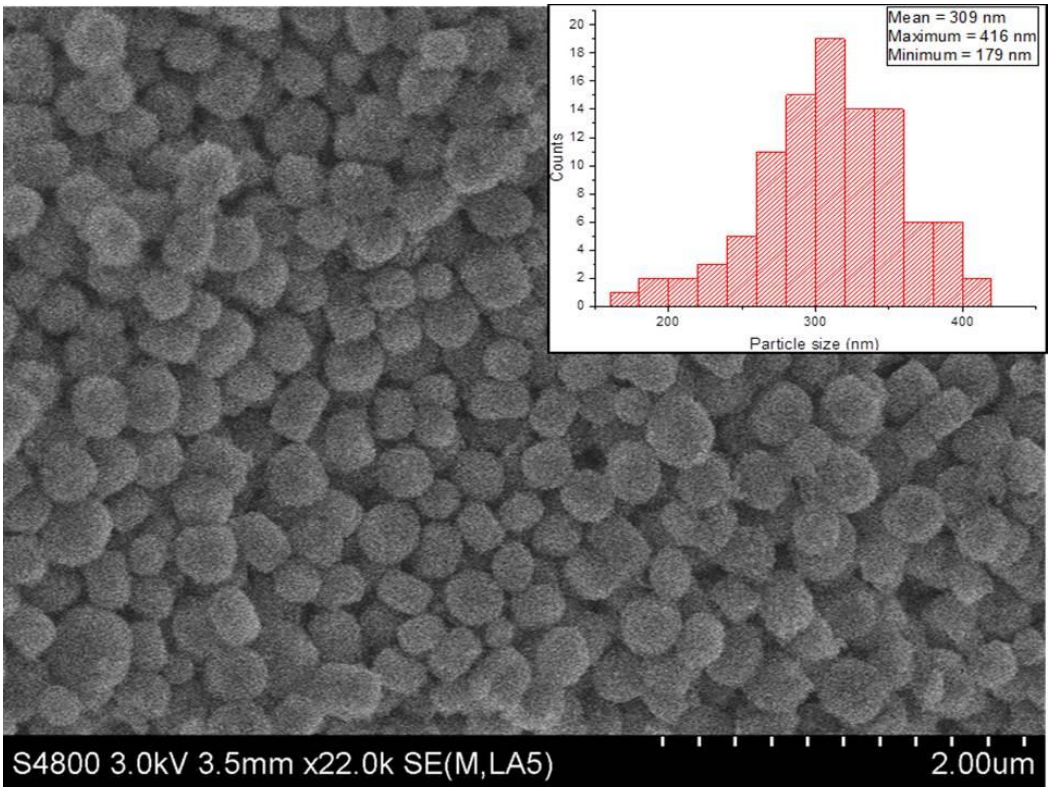

Figure 4.31 SEM image of H-ZSM-5 (100)-MW-PS60-120.

SEM micrographs of H-ZSM-5 (100)-MW-120 and H-ZSM-5 (100)-MW-PS60-120 illustrated in Figure 4.30 and Figure 4.31 showed no distinct differences between the external surface morphology of untemplated and templated zeolites. However, H-ZSM-5 (100)-MW-120 showed particles of almost uniform spherical shape with a size from 211 to 398 nm with a maximum distribution at 328 nm, whereas H-ZSM-5 (100)-MW-PS60-120 exhibited a smaller mean particle diameter of 309 nm, with particle sizes ranging from 179 to 416 nm. Additionally, the intercrystalline voids between the particles for H-ZSM-5 (100)-MW-120 appeared to be longer than between the individual particles for H-ZSM-5 (100)-MW-PS60-120. This confirms that the larger external pore volume for H-ZSM-5 (100)-MW-PS60-120 was primarily due to intracrystalline mesoporosity and not intercrystalline voids between the particles.

4.3.3 Friedel-Crafts alkylation of benzyl alcohol with benzene over hierarchical H-ZSM-5 synthesised using microwave assisted heating

In Chapter 3, we used the Friedel-Crafts alkylation reaction of benzyl alcohol with benzene as a probe reaction to examine the effect of increased on catalytic activity. However, studies in Chapter 3 showed that although alkaline treatment resulted in increased mesoporosity, the acidic properties were affected. Alkaline treatment of H-ZSM-5 resulted in an increase in acid site density due to the creation of Lewis acid sites. In the case of H-Y zeolites, alkaline treatment generally resulted in a decrease in acid site density due to the removal of framework aluminium species. Therefore, catalytic studies presented in this chapter sought to investigate the effect of H-ZSM-5 zeolites on the Friedel-Crafts alkylation with varying pore sizes, but with similar acid site density values.

Since blank experiments were studied in great detail in Chapter 3, they will not be discussed further here. The catalysts synthesised in this chapter were tested in the catalytic conversion of benzyl alcohol with benzene in the Friedel-Crafts alkylation reaction using microwave assisted heating.

4.3.3.1 Reproducibility studies

In this study, we examined whether the catalytic conversion of benzyl alcohol with benzene using microwave assisted heating would generate reproducible results. The untemplated zeolite, synthesised at 165 ^{o}C for 6 hours was chosen for reproducibility studies. The catalysts were pre-treated at 150 ^{o}C prior to the reaction to remove physisorbed water. The results are shown in Figure 4.32.

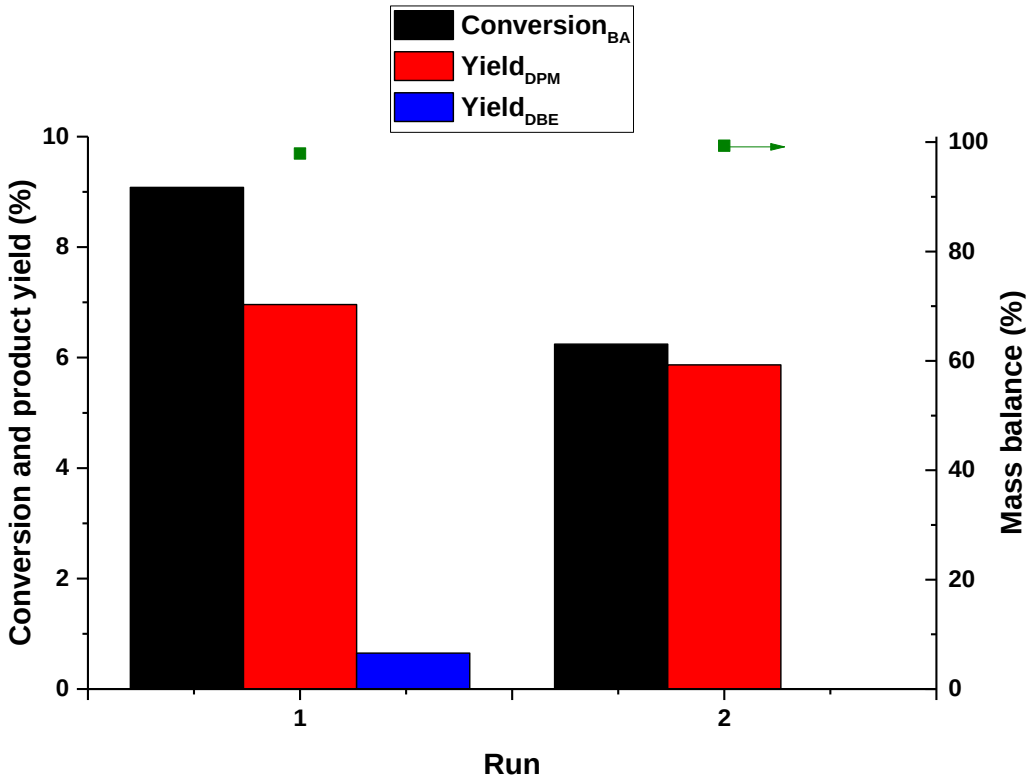

Figure 4.32 Conversion, product yield and mass balances obtained for the alkylation of benzene with benzyl alcohol over H-ZSM-5 (100)-MW to determine reproducbility.

Our untemplated H-ZSM-5 showed conversions of 9 and 6% after run 1 and 2 respectively, obtaining yields of 6.9 and 5.8% for DPM. Trace amounts of DBE were produced in both cases. The carbon mass balance obtained was >98%. The results confirm benzyl alcohol alkylation with benzene carried out using microwave assisted heating showed appreciable levels of reproducibility after experimental error had been taken into consideration.

4.3.3.2 Preliminary studies

In this study, the effect of catalytic conversion of benzyl alcohol with benzene was examined, comparing an untemplated H-ZSM-5 zeolite synthesised at 165 ^{o}C for 6 hours and a hierarchical H-ZSM-5 zeolite, synthesised using polystyrene as a hard templating agent. This zeolite was synthesised at 100 ^{o}C for 12 hours. Since hierarchical H-ZSM-5 synthesised using polystyrene (30 nm) generated inferior catalytic properties such as lower specific surface area and porosity than hierarchical H-ZSM-5 synthesised using polystyrene (60 nm), H-ZSM-5 (100)-MW-PS60 was the hierarchical zeolite chosen for this study. The catalysts chosen for this study are denoted as; H-ZSM-5 (100)-MW for the untemplated zeolite and H-ZSM-5 (100)-MW-PS60 for the hierarchical zeolite. The results are shown in Figure 4.33 (below).

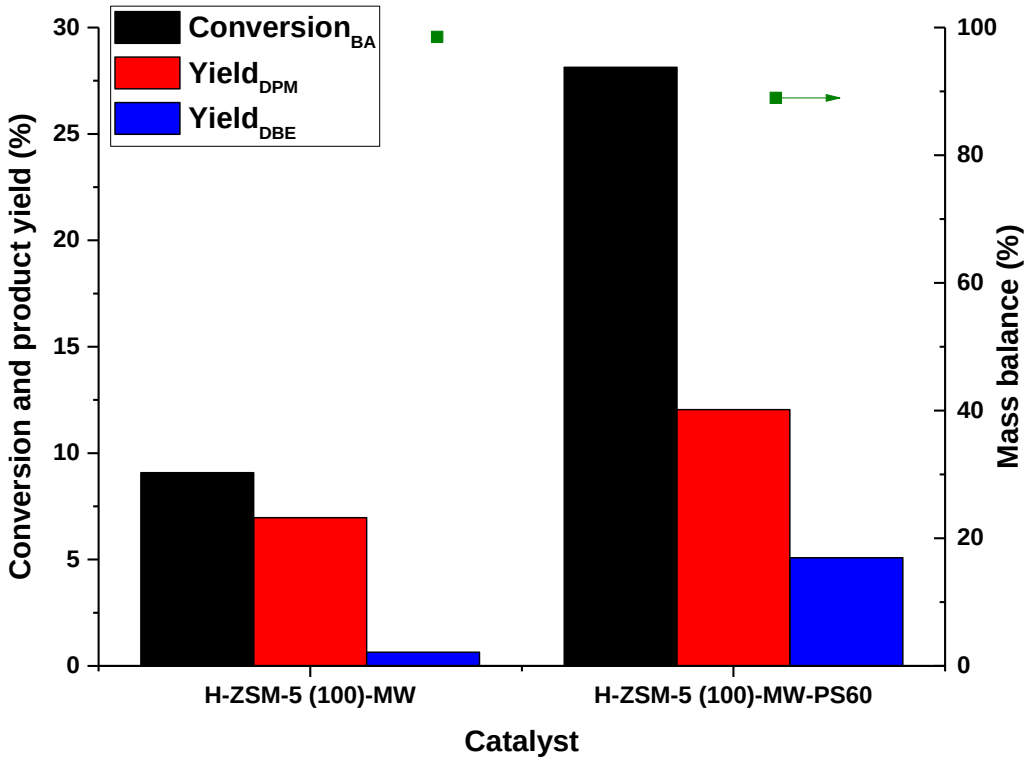

Figure 4.33 Conversion, product yield and mass balances obtained for preliminary experiments for the alkylation of benzene with benzyl alcohol over untemplated and hierarchical H-ZSM-5.

Hierarchical H-ZSM-5, synthesised using polystyrene (60 nm) as a hard templating agent showed superior catalytic activity in the Friedel-Crafts alkylation of benzyl alcohol with benzene than the untemplated H-ZSM-5 catalyst, with conversion increasing from 9.1%

for H-ZSM-5 (100)-MW to 28.1% for H-ZSM-5 (100)-MW-PS60, nearly a 3 fold increase in catalytic activity. At the same time, the yield of DPM increased from ca. 7% for the untemplated zeolite to 12% for the hierarchical H-ZSM-5 zeolite. The carbon mass balance decreased with increasing conversion due to the formation of unidentified polyaromatics.[149] This result confirms that our untemplated laboratory synthesised H-ZSM-5 showed comparable levels of conversion as commercial H-ZSM-5 (30) in Chapter 3, with similar yields of DPM obtained despite having a lower SiO_2/Al_2O_3 molar ratio. This could be due to the accessibility of the active sites, possibly due to deactivation caused by pore blocking. Since reactions were not carried longer than 6 hours, this remains unclear. The superior catalytic performance of H-ZSM-5 (100)-MW-PS60 cannot primarily be due to the number of acid sites, since both zeolites showed similar acid site density values. Therefore, it is likely that the enhanced catalytic activity of H-ZSM-5 (100)-MW-PS60 relative to H-ZSM-5 (100)-MW was due to improved accessibility of the active sites due to enhanced porosity. Since the untemplated and templated zeolites were synthesised with varying crystallisation temperatures, it remains unclear whether the location of acid sites are comparable. Zhang et al[241] showed the superior adsorption properties of nano H-ZSM-5 with probe molecules compared to micro H-ZSM-5 particles. However, it was not clear whether the active sites for the nano-particles were located in close proximity to the external surface area.

4.3.3.3 Effect of crystallisation temperature

After promising results were obtained in section 4.3.3.2, the effect of catalytic activity of H-ZSM-5 zeolites synthesised with varying crystallisation temperatures was studied. In this study, the catalysts are denoted as H-ZSM-5 (100)-MW-PS60-x, where x is the crystallisation temperature. For example, H-ZSM-5, templated with polystyrene (60 nm) synthesised at 100 ^oC is denoted as H-ZSM-5 (100)-MW-PS60-100. The results are shown in Figure 4.34 (below).

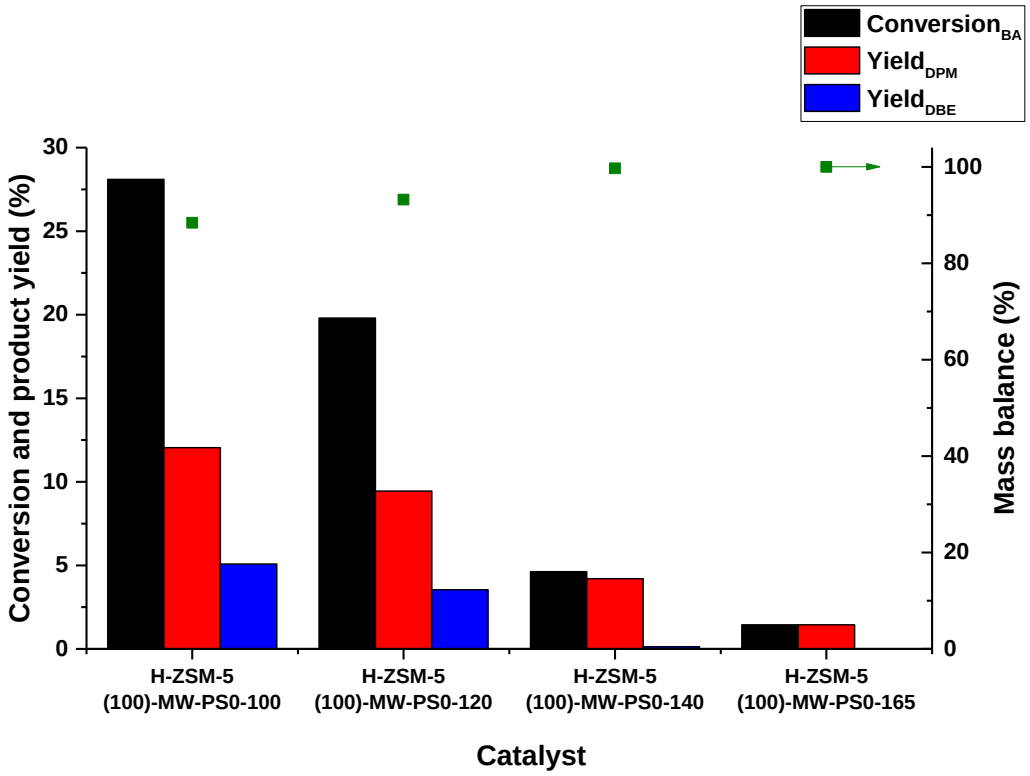

Figure 4.34 Conversion, product yield and mass balances obtained for the alkylation of benzene with benzyl alcohol over hierarchical H-ZSM-5 synthesised with varying crystallisation temperatures.

Catalytic activity varied for hierarchical H-ZSM-5 zeolites synthesised at different crystallisation temperatures, as shown in Figure 4.34. The conversion of benzyl alcohol over the reference hierarchical H-ZSM-5 (100)-MW-PS60-100 zeolite was 28.1% with a yield of ca. 12% obtained for DPM. A yield of 5.1% of DBE was produced due to etherification of BA.[164] The carbon mass balance of 89% confirms the presence of polyaromatics. Catalytic activity became less pronounced with H-ZSM-5 zeolites synthesised at higher crystallisation temperature, with conversion decreasing to 19.8% for H-ZSM-5 (100)-MW-PS60-120 with yields of 9.5 and 3.5% for DPM and DBE respectively. It can also be seen that the carbon mass balance increased to 93%, confirming that selectivity to polyaromatics was lower at low conversion. H-ZSM-5 (100)-MW-PS60-140 and H-ZSM-5 (100)-MW-PS60-165 showed worse catalytic activity than H-ZSM-5-MW-PS60-x synthesised at lower temperature. However, H-ZSM-5 (100)-MW-PS-165 showed a carbon mass balance of approximately 100%, confirming that this zeolite was completely selective to DPM. The clear trend in activity of the zeolitic materials synthesised with varying crystallisation temperatures can be attributed to varying porosity, with H-ZSM-5 (100)-MW-PS60-165 displaying an external

pore volume of only 0.08 cm^3 g^{-1} compared to 0.44 cm^3 g^{-1} for H-ZSM-5 (100)-MW-PS60-100. This is supported by TPD-NH_3 studies which showed zeolites synthesised at higher crystallisation temperatures had a greater amount of total acid sites. Therefore, the effect of acidity on catalytic activity in this study was assumed was to be insignificant.

4.3.3.4 Effect of calcination ramp

To further investigate the performance of hierarchical H-ZSM-5 on the Friedel-Crafts alkylation reaction of benzyl alcohol with benzene, the effect of hierarchical H-ZSM-5 synthesised by the removal of polystyrene (60 nm) using various calcination ramp rates was tested. Since varying calcination ramp rates produced H-ZSM-5 zeolites with different physical and chemical properties, we studied the impact of catalytic activity using hierarchical H-ZSM-5 catalysts possessing varying surface area and porosity, with the total number of acid sites remaining relatively constant. In this study, the catalysts are denoted as H-ZSM-5 (100)-MW-PS60-x, where x is the calcination ramp rate in ^oC min^{-1}. The results are shown in Figure 4.35 (below).

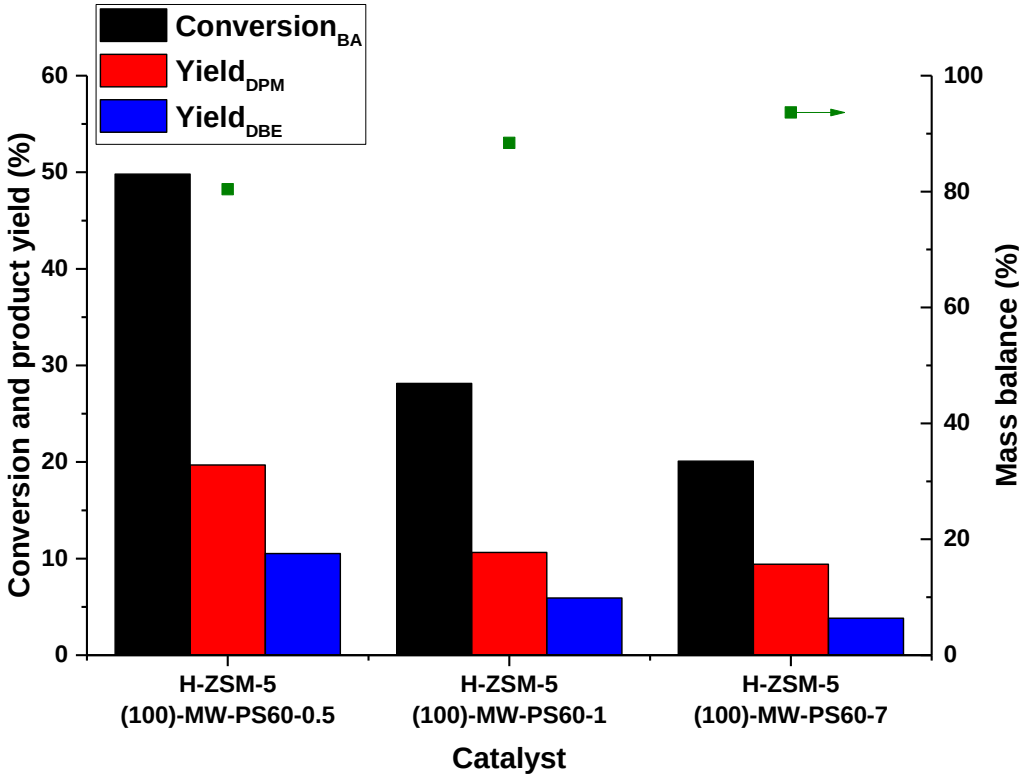

Figure 4.35 Conversion, yield and mass balances obtained for the alkylation of benzene with benzyl alcohol over hierarchical H-ZSM-5 calcined with varying ramp rates.

Reactions between benzyl alcohol with benzene showed a clear correlation between hard templated H-ZSM-5 calcined with different ramp rates and catalytic activity. H-ZSM-5 (100)-MW-PS60-0.5 showed remarkably superior catalytic activity compared to the reference hierarchical zeolite, H-ZSM-5 (100)-MW-PS60-1, with conversion ca. 50%. Yields of 19.7 and 10.5% were obtained for DPM and DBE respectively. Carbon mass balance measurements showed 80.4%, confirming a respectable yield of polyaromatics was obtained. H-ZSM-5 (100)-MW-PS60x calcined with ramp rates of 1 and 7 ^{o}C showed inferior catalytic activity with conversion levels of 28.1 and 20.1% for H-ZSM-5 (100)-MW-PS60-1 and H-ZSM-5 (100)-MW-PS60-0.5 respectively. Despite this, similar yields of DPM were obtained for both catalysts. A slightly larger yield of DBE was produced in H-ZSM-5 (100)-MW-PS60-1 than H-ZSM-5 (100)-MW-PS60-7. This can be ascribed to the larger specific area and total pore volume of H-ZSM-5 (100)-MW-PS60-1. The results of this study show H-ZSM-5 calcined with slower ramp rates displayed superior catalytic performance with porosity having a more significant role in catalytic activity than acidity, as evidence by comparing the catalytic results of H-ZSM-5 (100)-MW-PS60-0.5 and H-ZSM-5 (100)-MW-PS60-7, which had very similar particle sizes and total number of acid

sites with T_{max} position between 264-266 ^{o}C for both catalysts, indicating approximately similar quantities of Brønsted acidity.

4.3.3.5 Effect of templation versus non-templation under identical crystallisation conditions

This section compares the catalytic activity of Friedel-Crafts of benzyl alcohol with benzene using untemplated and hierarchical H-ZSM-5 synthesised under identical conditions. Despite promising results obtained in sections 4.3.1.3-4.3.2.3, it was not apparent that improved catalytic activity was directly due to enhanced porosity generated by the removal of the hard templating agent from the H-ZSM-5 structure. In this study, we investigated the effect of two H-ZSM-5 zeolites with similar physical and chemical properties, with varying external porosity on Friedel-Crafts reaction of benzyl alcohol with benzene. Since untemplated and templated H-ZSM-5 was synthesised at 120 ^{o}C, these two catalysts were chosen for this study to investigate the direct effect of the hard templating agent on catalytic activity. In this study, the untemplated zeolite is denoted as H-ZSM-5 (100)-MW-120, and the untemplated zeolite is denoted as H-ZSM-5 (100)-MW-PS60-120. The results are shown in Figure 4.36.

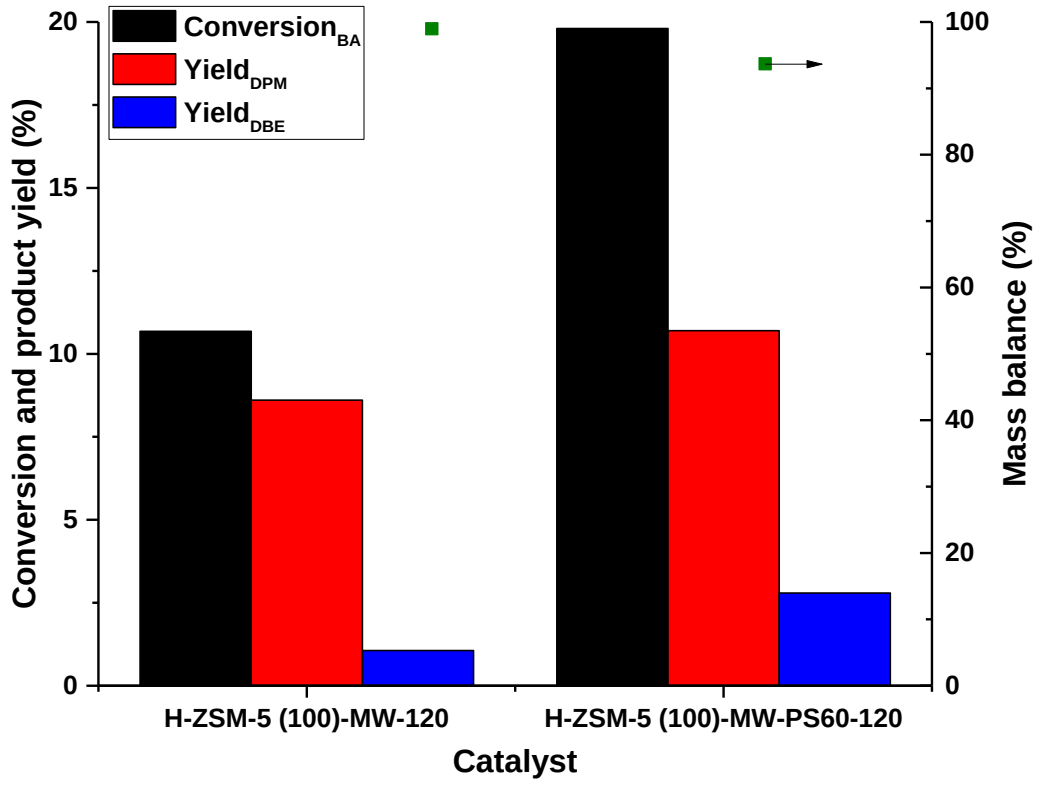

Figure 4.36 Conversion, yield and mass balances obtained for the alkylation of benzene with benzyl alcohol over H-ZSM-5 (100)-MW-120 and H-ZSM-5 (100)-MW-PS60-120.

It was found that hierarchically synthesised H-ZSM-5 synthesised at 120 ^{o}C showed superior catalytic performance than the untemplated H-ZSM-5, synthesised with identical crystallisation conditions, as shown in Figure 4.36. The results showed untemplated H-ZSM-5 displayed conversion of 10.7% with a DPM yield of 7.4%. By comparison, a yield of only 1.8% was obtained for DBE. Mass balance measurements showed 98.5%, which confirmed the presence of polyaromatics in small quantities. The templated zeolite displayed nearly a two-fold increase in conversion (19.8%) with yields of 9.5 and 3.5% obtained for DPM and DBE respectively. The mass balance dropped to 93.2%, confirming the formation of polyaromatics was more pronounced in the templated zeolite due to enhanced porosity. To determine whether improved catalytic activity for the templated zeolite was due to the hard templating agent, the physical and chemical properties of each catalyst needs to be considered. Firstly, XRD studies confirmed highly crystalline structures were obtained independently of the addition of polystyrene (60 nm) to the precursor gel. Surface area measurements showed the untemplated and templated displayed similar surface areas, primarily due to similar particle sizes. However, pore size distribution measurements showed that the templated zeolite displayed mesopores of

width >20 nm, whereas the untemplated zeolite did not show mesoporosity of pore widths > 20 nm. TPD-NH_3 studies confirmed largely similar levels of acid site density with comparable T_{max} values. Therefore, this study confirms that the superior catalytic performance of the templated zeolite can be attributed to enhanced porosity generated from the removal of the hard templating agent by calcination.

4.4 Conclusions

In this investigation, H-ZSM-5 with a SiO_2/Al_2O_3 molar ratio of 100 was synthesised using microwave assisted heating in 6 hours. In addition, hierarchical H-ZSM-5 synthesised by microwave assisted heating in 12 hours or less using polystyrene nanospheres as a hard templating agent was used, generating an optimum surface area of 620 m^2 g^{-1}. This is particularly advantageous due to its tuneable spherical size. Characterisation using XRD, nitrogen sorption and porosity measurements confirmed the microwave synthesis of untemplated H-ZSM-5, with comparable physical and chemical properties as H-ZSM-5 synthesised by conventional heating methods with a specific surface of 363 m^2 g^{-1}. Characterisation of the hierarchical zeolite indicated the presence of mesoporosity, generating slit like pores as shown by SEM measurements. Investigation of the physical properties of hierarchical H-ZSM-5 could be modified by the size of the hard templating agent.

Friedel-Crafts alkylation of benzyl alcohol was used as a probe reaction to compare the effect of porosity. Our study showed that conventional H-ZSM-5 synthesised at 165 ^oC for 6 hours using microwave assisted heated displayed similar catalytic activity than commercial H-ZSM-5, with both zeolites displaying ca 10% of conversion and similar yields attributable to DBE (~5%). The synthetic conditions in the microwave were critical in obtaining hierarchical ZSM-5 and for example, synthesis at 165 ^oC for 12 hours resulted in little mesoporosity and a detrimental effect on catalytic activity. Hierarchical H-ZSM-5, synthesised at 100 ^oC displayed nearly a 3 fold increase in catalytic activity with yields to the desired product increasing from to 10%, nearly a 2 fold increase. Synthesis of conventional and hard templated H-ZSM-5 using identical crystallisation parameters such as temperature yielded a catalyst with comparable surface area, acidity and particle size. However, the templated zeolite displayed mesopores with pore radii >20 nm, with overall mesoporosity increasing by 39%. This effect directly translated into improved catalytic

activity, with the templated zeolite showing nearly 100% greater efficiency in terms of conversion, confirming that polystyrene nanospheres is an extremely effective hard templating agent due to its versatile particle size. Since the synthesis of hierarchical H-ZSM-5 with polystyrene spheres of small particle size or in the microwave have not been studied previously, we can conclude that this work presents a unique opportunity to generate hierarchical H-ZSM-5 zeolites with tuneable porosity depending on the average size of the polystyrene nanospheres and synthetic conditions also applicable to other zeolites.

4.5 Future work

Synthesis of H-ZSM-5 by microwave assisted heating is a fast and alternative method compared to conventional heating methods. However, the work carried out in this chapter was preliminary, and further studies are required. Firstly, our study showed that increasing the average particle size of the hard templating agent from 30 to 60 nm increased the specific surface area from 499 to 580 $m^2\ g^{-1}$, with the total pore volume increasing from 0.48 to 0.62 $cm^3\ g^{-1}$. Further studies need to be carried out, with varying particle sizes to determine the optimum specific surface area and porosity. Further studies are required to show the effect of templating of H-ZSM-5 with varying SiO_2/Al_2O_3 molar ratios. One of the advantages of our hard templating agent is that the particles have a uniform shape, whereas carbonaceous species have non-uniform shape and size. However, the removal of the hard templating agent by calcination is destructive and therefore, non-recoverable. Further studies are required to remove the hard templating agent using an alternative method, so that it could be recovered and regenerated. In terms of analyses of our H-ZSM-5 zeolites synthesised in this chapter, the number of Brønsted and Lewis acid sites were not quantified. As shown in Chapter 3, future work is required to determine the accessibility of the active sites. Despite this, our study has shown the extraordinary effect of polystyrene nanospheres on the generation of mesoporosity for H-ZSM-5. Future work could apply this method to other zeolites, generating zeolites with a very large pore structure.

Chapter 5

Hierarchical H-ZSM-5, H-Beta and H-Y for Diels-Alder Cycloaddition and the Catalytic Production of Renewable Aromatics

5 Hierarchical H-ZSM-5, H-Beta and H-Y for Diels-Alder cycloaddition and the catalytic production of renewable aromatics

5.1 Introduction

Due to diminishing quantities of fossil fuels, lignocellulosic biomass is attracting more attention as a feedstock for platform chemicals due to its large availability and economic factors.[242] One of these platform chemicals obtainable from biomass is *p*-xylene, a precursor in the terephthalic acid synthesis which can be polymerised to produce polyethylene terephthalate (PET).[243] The chemical *p*-xylene is currently produced on an industrial scale from the catalytic reforming of petroleum naphtha which is part of the BTX fraction. Current market demand for *p*-xylene is typically around 34 % of the BTX fraction.[33] Demand for *p*-xylene is growing at a rate 6-8% per year and is currently the third largest chemical produced from petroleum derived naptha.[244] As PET is one of the widely used plastics, its renewable production could significantly decrease its carbon footprint.

Brion et al.[38] found that furan ring compounds could be converted into a six membered ring via a cycloaddition to produce an oxa-norbornene intermediate followed by β elimination (Scheme 5.1). Due to revolution of shale gas in the United States, platform chemicals such as methanol, ethanol, ammonia and propylene can be produced. However, platform chemicals such as BTX will not be produced using shale gas derivatives.[245] Therefore, reliance on alternative routes to *p*-xylene will need to be investigated. Recent studies have shown that 2,5-dimethylfuran (DMF) could act as a potential feedstock for the production of *p*-xylene.[39, 41, 45, 246, 247] The advantage of this route is the production of the pure para isomer of xylene thus removing the necessity to purify *p*-xylene as it is the case in its production from fossil sources. DMF itself can be produced from glucose in a two-step process. Glucose can be converted into 2,5-hydroxymethyfurfural (HMF) which can then be hydrodeoxygenated to produce DMF.[26]

Production of *p*-xylene was reported by the Diels-Alder cycloaddition of DMF with ethylene over different acid catalysts such as zeolite H-Y, γ-alumina, niobic acid, H-ZSM-5 or H-BEA.[41,45] The zeolite H-BEA was shown to be almost an order of magnitude more active than γ-alumina, niobic acid or H-ZSM-5. DFT studies revealed that Brønsted acid sites can significantly decrease the activation barrier of

the oxa-norbornene intermediate dehydration step, while the cycloaddition step proceeds uncatalysed.[39, 248] This was confirmed recently by Wijaya et al.[249] who have shown that increasing Brønsted acid site concentration leads to enhanced *p*-xylene production rate. Additionally, these authors have also reported that polar aprotic solvent such as 1,4-dioxane improves both DMF conversion and *p*-xylene yield attributable to the increased dehydration rate. Still, many experimental and theoretical studies support the hypothesis of Diels-Alder reaction catalysed by Lewis acid which complexes with dienophile and significantly lowers its LUMO energy.[250-254]

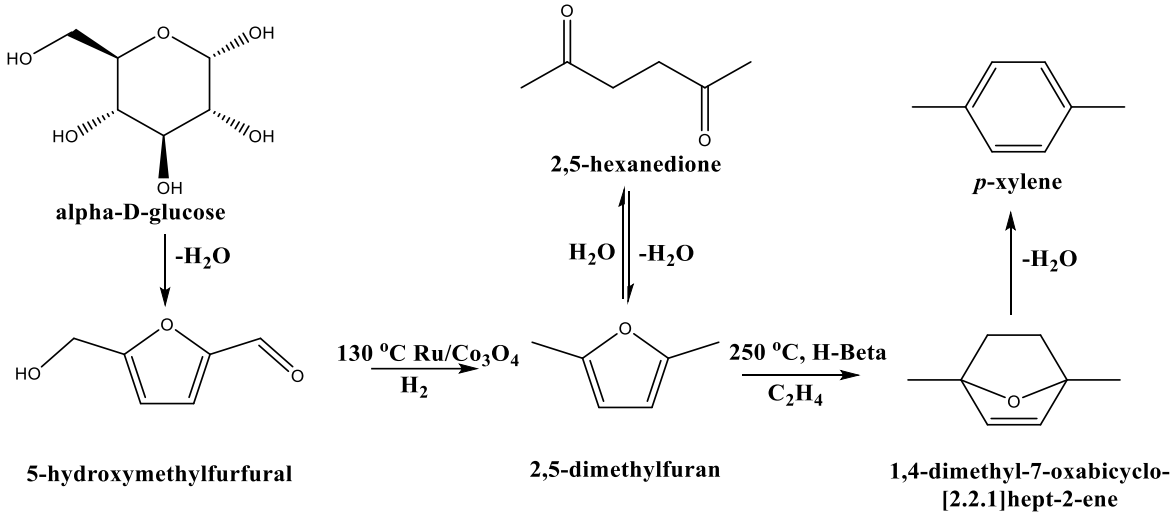

Scheme 5.1 Proposed reaction for the conversion of glucose to *p*-xylene.

It was reported that inducing mesoporosity in zeolites (producing hierarchical zeolites) can alleviate diffusion limitations and significantly increase catalytic activity in a variety of reactions.[255, 256] It has been argued that secondary porosity could also be used to store coke and therefore avoid blockage of the active microporous sites.[255] One of the ways to introduce mesoporosity in zeolites is the extraction of framework Si atoms (desilication).[206] Dean[257] first suggested the idea of alkaline treatment for zeolites to increase performance in the mordenite in the gas-oil reaction and noted that crystallinity was preserved with a 3 times higher conversion compared to the untreated parent zeolite.

Groen et al.[206] found that desilication preserved crystallinity and Brønsted acidity of the parent zeolite.

In this chapter we investigate the effect of increasing the pore size of commercial zeolites H-ZSM-5, H-Beta and H-Y catalysts with varying SiO_2/Al_2O_3 molar ratios by alkaline treatment and how this affects the structural properties of the zeolites as well as how beneficial this can be for the production of renewable *p*-xylene. In addition we investigate the effect of hierarchical zeolites synthesised by a bottom up approach via templating with polystyrene nanospheres on the [4+2] cycloaddition of DMF with ethylene. The modification of commercial and laboratory synthesised zeolites using alkaline treatment can also be found in Chapter 3. The synthesis and characterisation of H-ZSM-5 zeolites using microwave assisted heating are mainly discussed in Chapter 4. The synthesis of conventional H-ZSM-5 and its hierarchical counterpart using polystyrene nanospheres with varying diameters by conventional heating can be found in this chapter.

5.2 Preparation of H-form zeolites.

Commercial H-ZSM-5 (SiO_2/Al_2O_3 = 30 and 80), H-Beta (SiO_2/Al_2O_3 = 25, 38 and 360) and H-Y (SiO_2/Al_2O_3 = 12 and 80) were obtained in the ammonium form. SiO_2/Al_2O_3 represents the molar ratio. Firstly, NH_4-ZSM-5 was calcined using conditions described in section 3.2.1 to produce H-ZSM-5. This was repeated for subsequent calcinations. The parent samples are denoted as zeolite-silica-alumina ratio. For example, the parent H-ZSM-5 with a SiO_2/Al_2O_3 molar ratio equal to 30 is denoted as H-ZSM-5 (30).

5.3 Synthesis of Polystyrene (PS) nanospheres.

Polystyrene (PS) nanospheres were synthesised using the method described in section 4.2.2.

5.4 Synthesis of zeolites using conventional and microwave assisted heating methods

In this section, the synthesis of H-ZSM-5 by conventional heating methods is presented. Prior to the synthesis of H-ZSM-5 by microwave assisted heating (Chapter 4), preliminary

studies were performed to determine the effect of templation using polystyrene nanospheres of average particle sizes 30 and 60 nm on porosity of H-ZSM-5. Preliminary studies were carried out using conventional heating methods. The synthesis parameters and chemical composition of preliminary studies are presented here.

5.4.1 Synthesis of H-ZSM-5 using conventional heating.

The conventional zeolite H-ZSM-5 with varying SiO_2/Al_2O_3 ratios were produced hydrothermally from a precursor gel which contained tetraethoxysilane (TEOS) as the silicon source, 25% in water t-propylammonium hydroxide (TPAOH) as the structure directing agent, aluminium isoproxide (AIP) as the aluminium source and water as the solvent. The solutions were prepared separately based on the following molar ratio compositions: Al_2O_3 :100 SiO_2 : 11.5 TPAOH : 1000 H_2O and Al_2O_3 :180 SiO_2 : 11.5 TPAOH : 1000 H_2O. In a typical synthesis AIP was dissolved in water and TPAOH using a conical flask. The mixture was stirred for approximately 3 hours to allow complete dissolution of AIP. TEOS was slowly added which formed an emulsion mixture. The mixture was stirred overnight at room temperature to ensure complete hydrolysis of TEOS which resulted in a clear homogenous solution. 30 mL of the mixture was placed into a 45 mL Teflon lined stainless steel autoclave (Model 4744, Parr instrument, IL,USA). The autoclave was placed into a preheated oven at 165 ^oC for 72 hours. Once the reaction was complete, the vessel was placed into a fume cupboard and allowed to cool to room temperature. The autoclave was opened and the mixture was filtered under gravity (Whatman grade 1 filter paper) and washed with an abundant amount of distilled water. The solid was dried in an oven overnight at 110 ^oC before being calcined as described in section 3.2.1. At this point a sample was taken for XRD analysis to confirm the MFI structure. The sample was then brought into the proton form by ion exchange with ammonium nitrate (1M) at 80 ^oC for 2 hours under reflux conditions and calcined as described in section 3.2.1 In this section, H-ZSM-5 prepared by conventional hydrothermal synthesis is denoted as zeolite-silica-alumina-ratio-H. For example, H-ZSM-5 with a SiO_2/Al_2O_3 ratio equal to 100 is denoted as H-ZSM-5 (100)-H.

5.4.2 Synthesis of zeolites using microwave assisted heating

In this section, the synthesis of H-ZSM-5, H-Beta and H-Y by microwave assisted heating is discussed. The chemical composition, particularly SiO_2/Al_2O_3 molar ratios and synthesis parameters are presented.

5.4.2.1 H-ZSM-5

H-ZSM-5 zeolite was synthesised using microwave assisted heating. A solution with SiO_2/Al_2O_3 molar ratio equal to 100 was prepared. A more detailed description of the synthesis method can be found in Chapter 3.

5.4.2.2 H-Beta

H-Beta zeolite was synthesised with a gel containing a SiO_2/Al_2O_3 molar ratio equal to 10. The synthesis is discussed in greater detail in Chapter 3.

5.4.2.3 H-Y

H-Y zeolite was synthesised with a gel containing a SiO_2/Al_2O_3 molar ratio equal to 10. The synthesis is discussed in greater detail in Chapter 3.

5.4.3 Synthesis of Hierarchical zeolites by conventional and microwave assisted heating methods

The synthesis of hierarchical H-ZSM-5 synthesised by conventional and microwave assisted heating is presented in this subsection. Strategies for the development of mesoporosity involve top-down strategies such as desilication using sodium hydroxide, and a bottom-up strategy, using a hard templating agent such as polystyrene. Both strategies are presented here, detailing the experimental parameters used for conventional and microwave assisted heating methods.

5.4.3.1 Alkaline treatment of zeolites

A more detailed method for the desilication of zeolites can be found in Chapter 3. The alkaline treated zeolites are denoted as zeolite-silica to alumina ratio-concentration of alkaline treatment. For example, H-ZSM-5 with a SiO_2/Al_2O_3 ratio of 30 desilicated with a 0.2 M solution of sodium hydroxide is denoted as H-ZSM-5 (30.2).

5.4.3.2 Synthesis of hierarchical H-ZSM-5 using conventional heating.

Hierarchical H-ZSM-5 was synthesised using polystyrene nanospheres as a template (synthesis described in section 5.3)**.** A precursor solution gel with Si/Al molar ratio of 50 was used. In a typical synthesis, 30 mL of the precursor solution was placed in a 45 mL Teflon lined stainless steel autoclave. The autoclave was placed into a preheated oven at 100 ^oC and kept there for 72 hours under static conditions. Once the reaction was complete the vessel was placed into a fume cupboard and allowed to cool to room temperature. The autoclave was opened and the mixture was filtered under gravity (Whatman grade 1 filter paper) and washed with an abundant amount of distilled water. The solid was dried in an oven overnight at 50 ^oC before being calcined (section 3.2.1). A small amount of the remaining solid was ground and taken for XRD and FTIR analysis to confirm the removal of polystyrene templating agent. The zeolite was brought into the ammonium form by ion exchange described in 3.2.1. The laboratory synthesised H-ZSM-5 templated with polystyrene nanospheres of size 30 nm is denoted as H-ZSM-5-(SiO_2/Al_2O_3 molar ratio)-H-P30 and H-ZSM-5 templated with polystyrene with an average nanosphere size of 60 nm is denoted as H-ZSM-5-(SiO_2/Al_2O_3 molar ratio)-H-PS60.

5.4.3.3 Synthesis of hierarchical H-ZSM-5 using microwave assisted heating

Hierarchical H-ZSM-5 (100) and H-ZSM-5 (120) was synthesised using microwave assisted heating using polystyrene (30 or 60 nm) as a hard templating agent. A more detailed description of the synthesis is discussed in section 4.2.2.

5.5 The production of renewable *p*-xylene by the [4+2] cycloaddition of DMF with ethylene

In this section, the Diels-Alder cycloaddition of DMF with ethylene is described, with the experimental parameters described. Calculations used to determine conversion, product yield and mass balance are shown.

5.5.1 Blank reaction

A blank experiment was performed without the presence of a catalyst. The reaction was carried out as follows: 37 mL of 2, 5-dimethylfuran (3 M) in hexane was sealed in a 75 mL Parr reactor vessel and purged with nitrogen 3 times before being heated to 180 ^{o}C under stirring (1,100 rpm). As soon as the desired temperature was reached the vessel was pressurised to a total pressure of 40 bar. The reaction was carried out for 20 hours and then quenched in an ice bath for 1 hour. The products were quantified using GC-FID and compared to subsequent catalytic studies.

5.5.2 Catalytic testing

DMF was distilled beforehand to remove heavy contaminants leaving behind a brown residue. Unless stated otherwise, the [4+2] cycloaddition of DMF with ethylene was carried out in a 75 mL closed vessel Parr pressure reactor. In a typical reaction, DMF (1.5-3M), tridecane (0.75 mL), aliphatic solvent and 180 mg of catalyst was charged into the vessel, unless stated otherwise. The vessel was purged 3 times with nitrogen before being depressurised. The mixture was heated to the desired temperature (180-250 ^{o}C) before being pressurised with ethylene to a total pressure of 40-55 bar. The reaction was carried out for 20-40 hours under stirring (1,000 rpm) before being quenched in an ice bath for 1 hour. The spent catalyst was separated from the spend catalyst by centrifugation at 14,000 rpm for 5 minutes and quantified using GC-FID. Conversion, product yields and mass balances were calculated based on the following equations:

$$\text{Conversion}_{\text{DMF}}\ (\%) = \frac{[\text{DMF}]_{\text{initial}} - [\text{DMF}]_{\text{end}}}{[\text{DMF}]\text{initial}}\ \text{x}100$$

$$\text{Yield}_{\text{product}}\ (\%) = \frac{[\text{product}]}{[\text{DMF}]_{\text{initial}}}\ \text{x}\ 100$$

$$\text{Mass balance}\ (\%) = \frac{\sum[\text{known products} + \text{DMF}_{\text{end}}]}{[\text{DMF}]_{\text{initial}}}\ \text{x}\ 100$$

Equation 5.1 Equations used to determine conversion, product yield and mass balance.

5.6 Results and discussion

In this section, the physical and chemical properties of conventional and hierarchical H-ZSM-5 (100) synthesised using conventional heating methods are shown. The catalytic testing results are presented and discussed in detail.

5.6.1 Characterisation of H-ZSM-5 synthesised by conventional heating

The results of the characterisation techniques of conventional and hierarchical H-ZSM-5 synthesised using conventional heating methods are presented and discussed in the following order; XRD and elemental analysis, FT-IR, TGA, nitrogen adsorption-desorption, TPD-NH_3 and solid state NMR and microscopy studies.

5.6.1.1 X-Ray diffraction (XRD) and elemental analysis of H-ZSM-5 prepared by conventional heating

XRD patterns for H-ZSM-5 catalysts synthesised by conventional heating were measured in the 2θ angle range of 5-50º. To save space the 2θ angle range of 5-30º are displayed. Unlike in Chapter 4, crystallinity calculations were based on the relative peak intensity of the [101] peak at 2θ angle at 7.9º. Crystallinity measurements on the untemplated H-ZSM-5 zeolite were not carried out. XRD was only used to determine whether the MFI structure had been formed, and whether the hard templating agent had been removed after the calcination process. XRD diffractograms are shown in Figure 5.1(a-h).

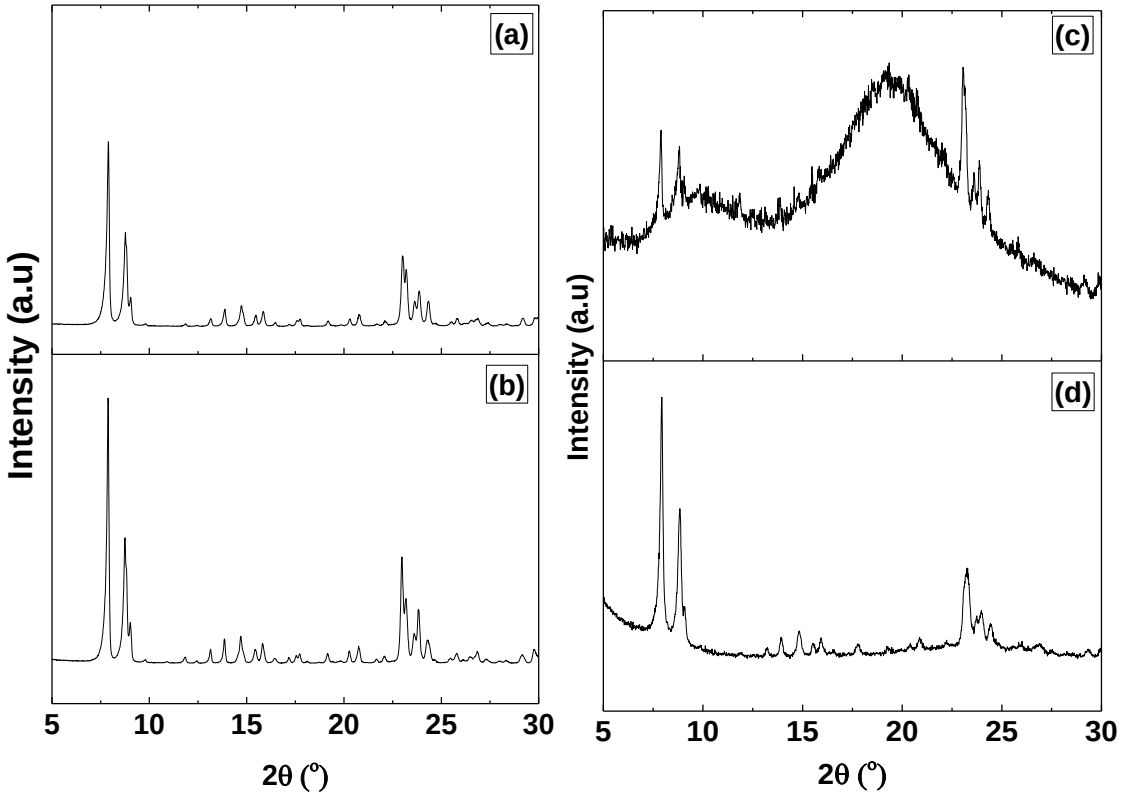
(a)
(b)
(c)
(d)
Intensity (a.u)
Intensity (a.u)
5
10
15
20
25
30
2θ (°)
2θ (°)

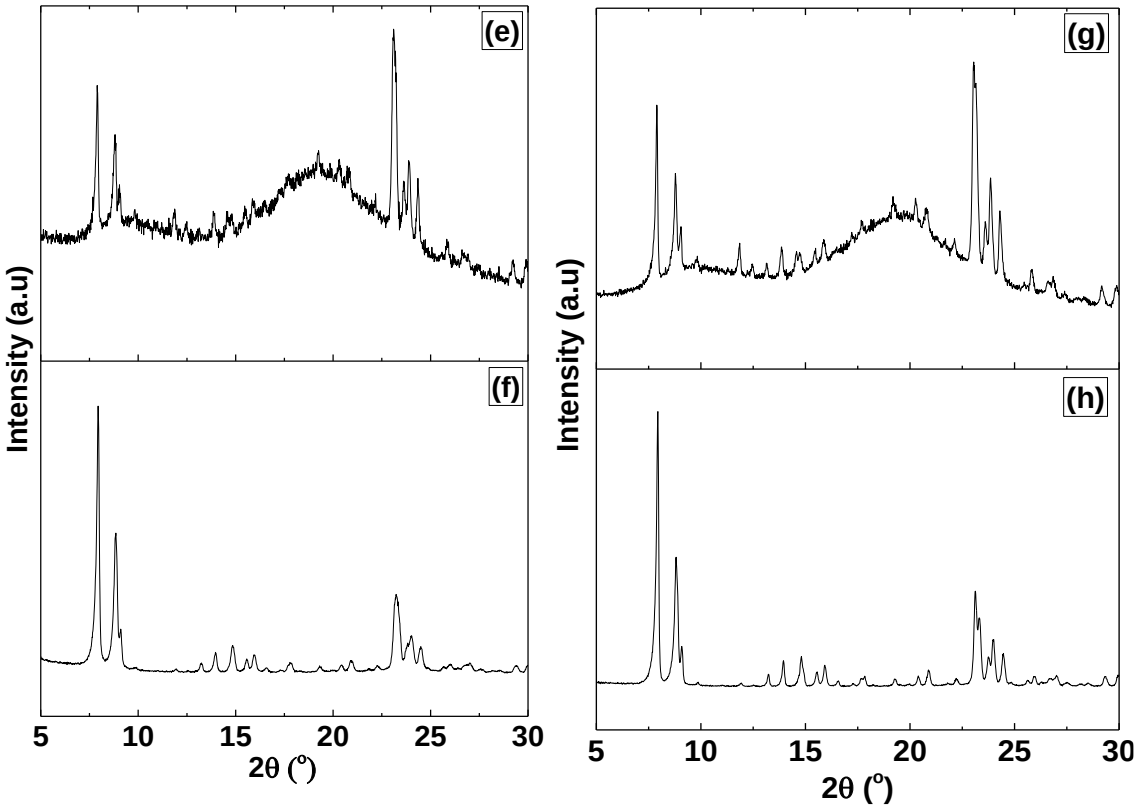

Figure 5.1 XRD patterns of H-ZSM-5 zeolites pre and post calcination; (a) H-ZSM-5 (100)-H, (b) H-ZSM-5 (180)-H, (c) H-ZSM-5 (100)-H-PS30 (pre), (d) H-ZSM-5 (100)-H-PS30 (post), (e) H-ZSM-5 (100)-H-PS60 (pre), (f) H-ZSM-5 (100)-H-PS60 (post), (g) H-ZSM-5 (180)-H-PS30 (pre), (h) H-ZSM-5 (180)-H-PS30 (post).

Figure 5.1 shows the XRD patterns of the templated and untemplated H-ZSM-5 catalysts prepared by conventional heating. The untemplated H-ZSM-5 zeolites displayed patterns typical of the H-ZSM-5 structure with peaks in the 2θ angle regions of; 7.9, 8.8, 23.1° for the peaks associated with the [hkl] planes [101], [020] and [501] respectively. Prior to calcination, the templated H-ZSM-5 zeolites displayed a mixture of a crystalline and an amorphous phase in the 2θ angle region 15-20°, which can be attributed to amorphous polystyrene. After calcination, it can be seen that the highly crystalline H-ZSM-5 phase remains due to the removal of the amorphous polystyrene template. When compared to the untemplated H-HZSM-5 zeolites (not shown) after calcination, the relative intensity of the [101] plane in the templated H-ZSM-5 catalysts were significantly lower. It was found that based on the relative intensity of the [101] plane, H-ZSM-5 (100)-H-PS30 and H-ZSM-5 (100)-HPS60 possessed 30% and 64% crystallinity compared to H-ZSM-5 (100)-H, whereas H-ZSM-5 (180)-H-PS30 possessed 47% crystallinity compared to H-ZSM-5 (180)-H. Similar findings has been reported in the literature.[208, 258] It was shown by Koo et al.[208] that carbon templation of H-ZSM-5 resulted in lower intensity of

templated H-ZSM-5 zeolites compared to untemplated H-ZSM-5 zeolites, due to the formation of disordered mesoporous voids created during the removal of carbon by calcination.

Elemental analysis of untemplated and templated H-ZSM-5 (100)-H and H-ZSM-5 (180)-H zeolites were measured by ICP-OES. The results of the measurements show that the SiO_2/Al_2O_3 molar ratio of H-ZSM-5-(100)-H was 84, which closely matched the theoretical value of 100. The zeolites H-ZSM-5 (100)-H-PS30 and H-ZSM-5 (100)-H-PS60 showed SiO_2/Al_2O_3 molar ratios of 90 and 108 respectively. The zeolite H-ZSM-5 (180)-H and H-ZSM-5 (180)-H-PS30 displayed SiO_2/Al_2O_3 molar ratios of 183 (theoretical value = 180 value) and 191 respectively. Since the templated and untemplated zeolites were prepared using a scaled up mother solution, it is unlikely that the variation in SiO_2/Al_2O_3 molar ratio between the hydrothermally untemplated and templated H-ZSM-5 zeolites is due solely to experimental error of the initial feedstock solution.

5.6.1.2 FT-IR and TGA studies of H-ZSM-5 zeolites prepared by conventional heating

Characterisation of zeolites by FT-IR is one of the most frequently used techniques to determine vibrations of the framework of zeolites. FT-IR can also be used to determine the presence of polystyrene nanospheres. In this study, FT-IR measurements were used to determine the presence of polystyrene (30 nm) before and after calcination of H-ZSM-5 zeolites. The FT-IR spectra for the untemplated H-ZSM-5 zeolites are not shown. FT-IR results of H-ZSM-5(100)-H and H-ZSM-5 (100)-H-PS30 zeolites prior to, and, after calcination, prepared by conventional heating are displayed in Figure 5.2.

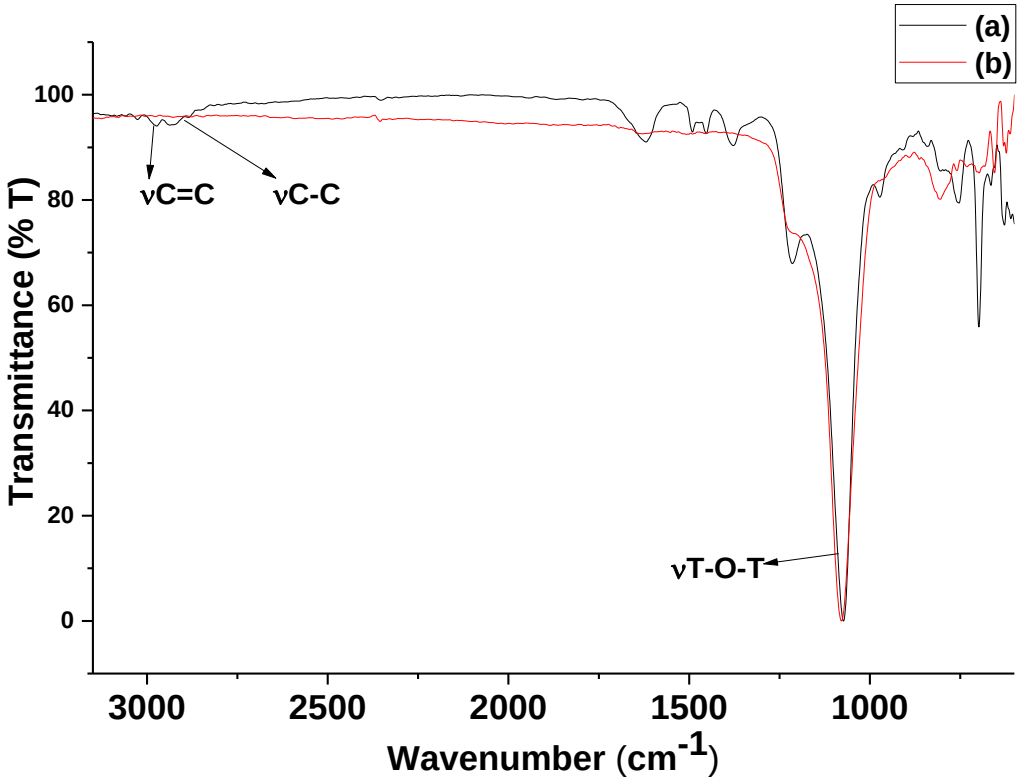

Figure 5.2 FTIR of H-ZSM-5 (100)-H-PS30 (a) before and (b) after calcination at 550 °C.

The FT-IR results show the aromatic *ν*C=H (3030 cm^{-1}), aliphatic *ν*C-H (slightly lower than 3000 cm^{-1}). These peaks strongly indicate the presence of polystyrene. In addition, FT-IR results show that prior to calcination, the presence of the bands at 1080 cm^{-1}, due to the asymmetric stretching vibration of T-O-T (T=Si or Al). The band at 1220 cm^{-1} is strongly indicative of the MFI structure due to the asymmetric stretching vibration of the 5-membered ring. In addition, the FT-IR spectrum shows a band at ~790 cm^{-1}, which is characteristic of the *ν*T-O.[162] Upon calcination, the band at 3030 and ~3000 cm^{-1} disappeared, indicating the removal of the polystyrene template. However, the bands associated with the zeolite structure remained intact.

Thermogravimetric (TGA) profiles were used to determine the thermal stability of the H-ZSM-5 zeolites prepared by conventional heating prior to and after calcination at 550 °C in air. The results are shown in Figure 5.3.

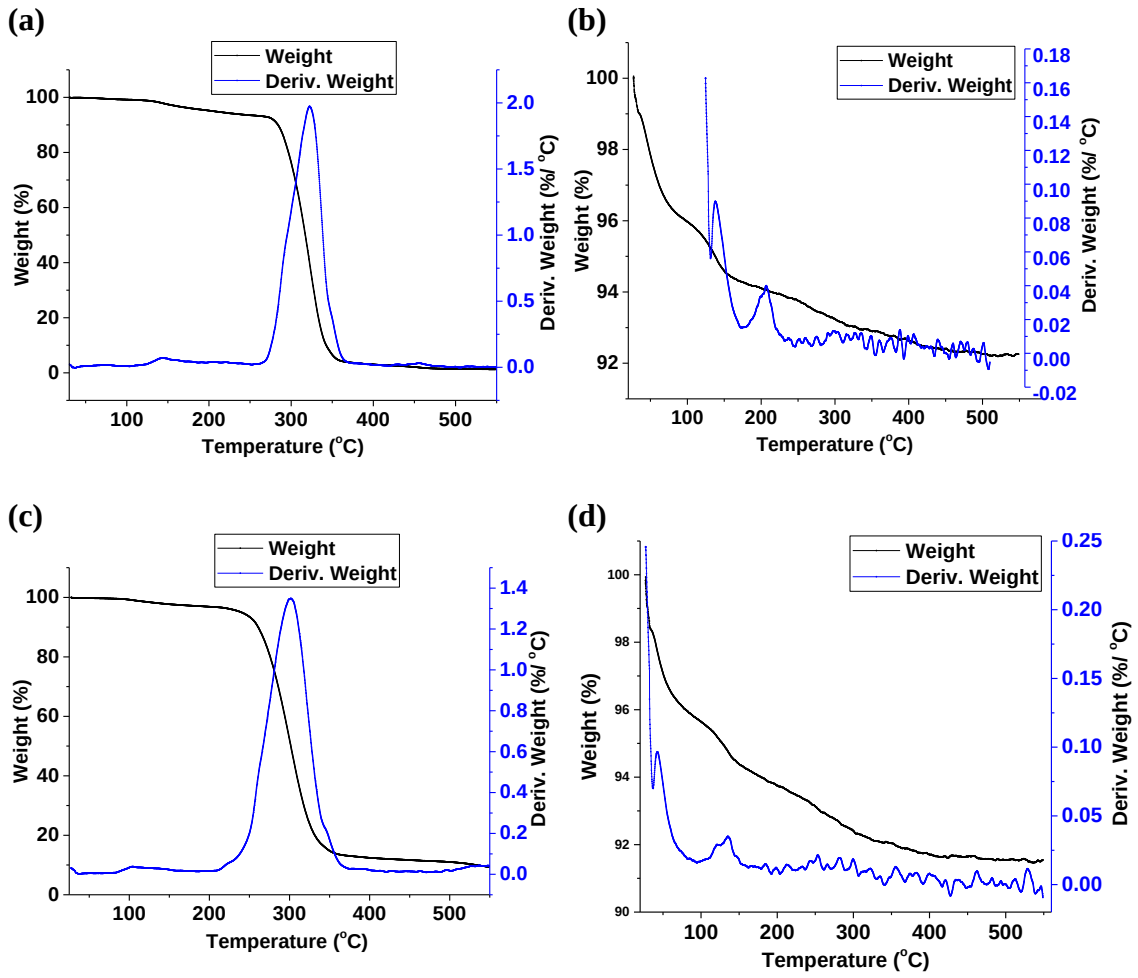

Figure 5.3 Thermogravimetric profiles of PS, H-ZSM-5 (100)-H and H-ZSM-5 (100)-H-PS30 before and after calcination (a) PS (30 nm), (b) H-ZSM-5 (100)-H, (c) H-ZSM-5 (100)-H-PS30 (pre), (d) H-ZSM-5 (100)-H-PS30 (post).

It can be seen from Figure 5.3 (a) the polystyrene template is thermally stable up to approximately 300 ^{o}C, which confirms that high calcination temperatures are required to remove the polystyrene (30 nm) template. Figure 5.3 (b) shows the TGA profile of H-ZSM-5 (100)-H. The profile shows that the zeolite is relatively stable up to 550 ^{o}C, with the overwhelming mass loss occurring at temperatures below 200 ^{o}C, which is due to desorption of physisorbed water on the external surface and within the mesopores. The remaining water loss up to 550 ^{o}C was due to desorption of water from the micropores. Figure 5.3 (c) shows the TGA profile of H-ZSM-5 (100)-H-PS30 prior to calcination. Clearly, the profile shows a similar profile as shown in Figure 5.3 (a), which confirms the complete removal of polystyrene (30 nm) at 300 ^{o}C. In addition, the profile showed that at 550 ^{o}C, only approximately 10% of the original mass was left. The yield obtained after TGA was in excellent agreement when our catalyst was calcined in the muffle furnace,

with a yield of 16% obtained. Figure 5.3 (d) shows the TGA profile of H-ZSM-5 (100)-H-PS30 after calcination. Clearly, the reduced weight loss at approximately 300 ºC can be attributed the absence of polystyrene (30 nm). Therefore, it could be concluded that polystyrene (30 nm) had been completely removed after the calcination step, and the overall weight loss can be attributed to physisorbed water.

5.6.1.3 Surface and porosity measurements of H-ZSM-5 (100)-H and hierarchical H-ZSM-5 zeolites synthesised by conventional heating

The nitrogen isotherms of the untemplated H-ZSM-5 zeolites synthesised by conventional heating showed a combination of type I and IV isotherm, with a high uptake at lower relative pressure with a pronounced hysteresis, confirming the presence of micropores and mesopores. Surface area and porosity measurements for zeolites synthesised by conventional heating are shown below.

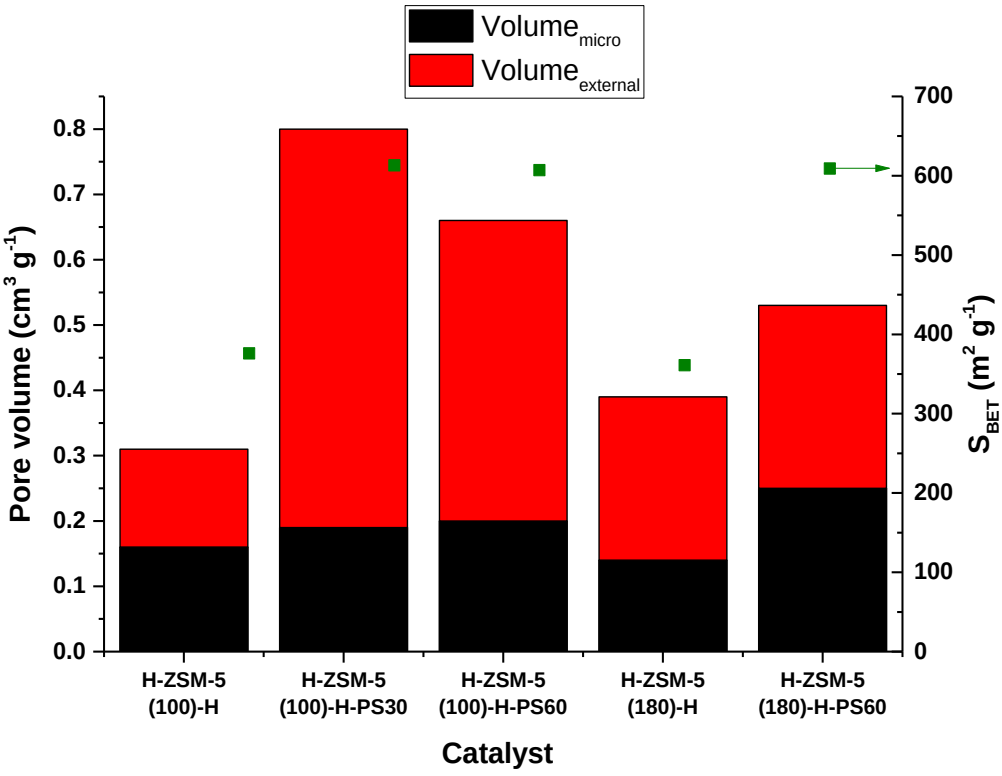

Figure 5.4 Surface area and porosity measurements for untemplated and templated H-ZSM-5 zeolites synthesised using conventional heating.

Figure 5.4 showed all hierarchical H-ZSM-5 zeolites had similar specific surface areas, irrespective of SiO_2/Al_2O_3 molar ratio. Despite the untemplated zeolites displaying similar levels of microporosity, H-ZSM-5 (180)-H displayed higher levels of mesoporosity than H-ZSM-5 (100)-H. Templating H-ZSM-5 with polystyrene (30 nm) increased the specific surface area from 376 m^2 g^{-1} for H-ZSM-5 (100)-H, to 613 m^2 g^{-1} for H-ZSM-5 (100)-H-P30. H-ZSM-5 (180)-H showed a specific surface area of 361 m^2 g^{-1}. This increased to 609 m^2 g^{-1} for H-ZSM-5 (180)-H-PS30. A higher external pore volume was obtained for templated H-ZSM-5 (100)-H zeolites compared to their untemplated counterparts, with an optimum external volume of 0.61 cm^3 g^{-1} obtained for H-ZSM-5 (100)-H templated with polystyrene (30 nm). Substitution of polystyrene (30 nm) to polystyrene (60 nm) did not generate further porosity. This was unexpected, as our results in Chapter 4 showed the external volume was more pronounced when polystyrene (60 nm) was used as a hard templating agent. The BJH adsorption profiles are shown in Figures 5.5-5.6.

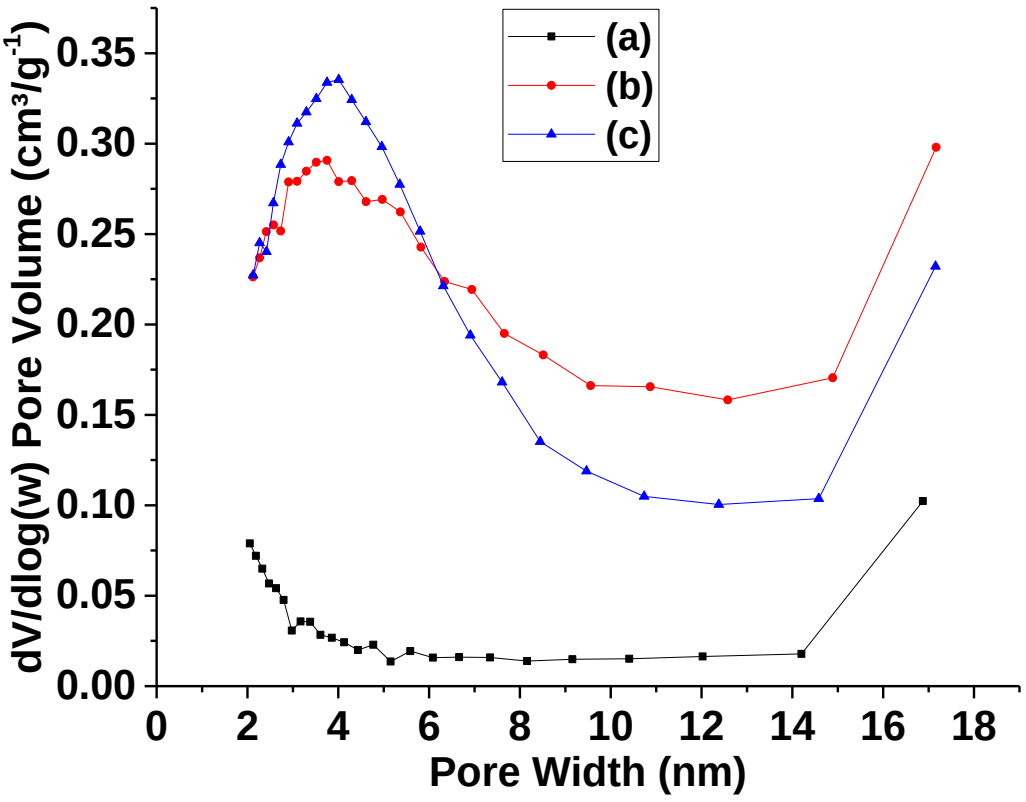

Figure 5.5 Pore size distribution of (a) H-ZSM-5 (100), (b) H-ZSM-5 (100)-H-PS30 and (c) H-ZSM-5 (100)-H.

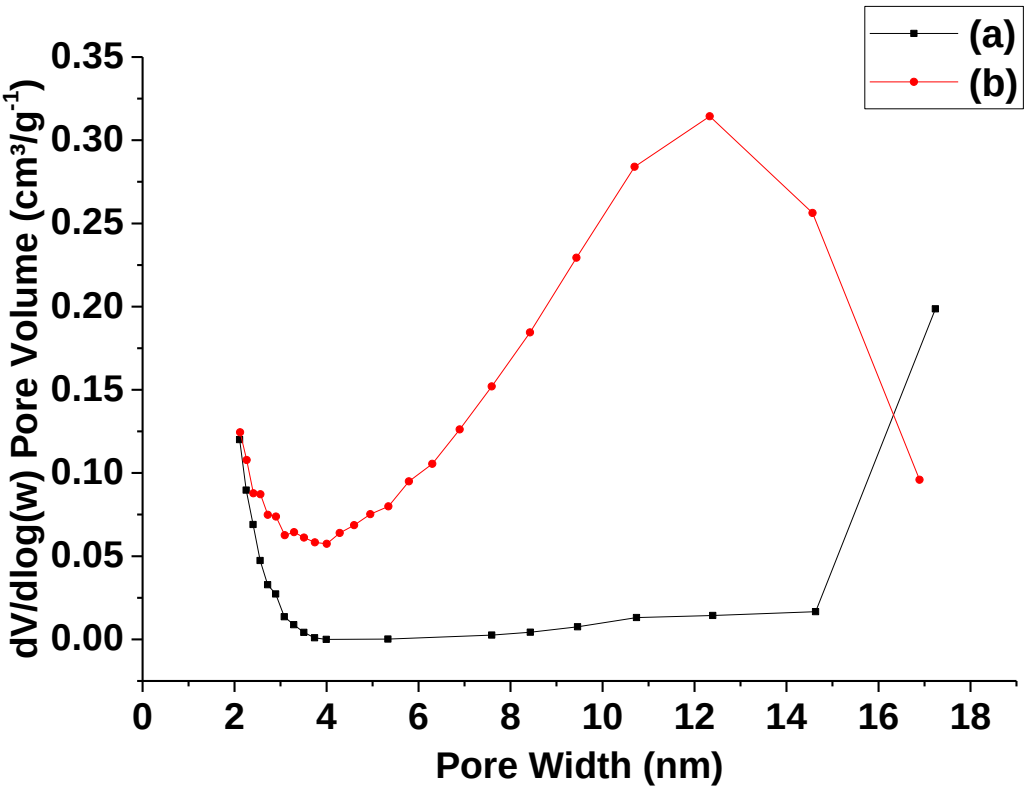

Figure 5.6 Pore size distribution of laboratory synthesised H-ZSM-5 (180) and H-ZSM-5 (180)-H-PS30 prepared by hydrothermal synthesis.

BJH pore size distribution measurements confirmed the generation of mesopores with a sharp peak at around 17 nm, with the peak more pronounced in the case of H-ZSM-5 (180)-H than H-ZSM-5 (100)-H. Templation of H-ZSM-5 (100)-H and H-ZSM-5 (180)-H with polystyrene (30 nm) generated mesopores with a broad distribution, H-ZSM-5 (100)-H-PS30 showing mesoporoes generated mostly in the region of 4 and 17 nm, with H-ZSM-5-(180)-H-PS30 showing mesoporosity in the 14 nm region. Templation of H-ZSM-5 (100)-H with polystyrene (60 nm) increased mesoporosity in the 4 nm region, however, possessed lower mesoporosity in the 17 nm region than H-ZSM-5 (100)-H-PS30.

5.6.1.4 Acidity measurements of H-ZSM-5 zeolites prepared by conventional heating by Temperature programmed desorption (TPD).

Temperature programmed desorption of ammonia was performed on H-ZSM-5 (100)-H, H-ZSM-5 (180)-H and their templated counterparts to determine the effect of crystallisation temperature and templating on acidity. The TPD-NH_3 profiles (see

Appendix) showed one peak with a broad distribution with T_{max} at approximately 350 ^{o}C which can be attributable to strong acid sites.

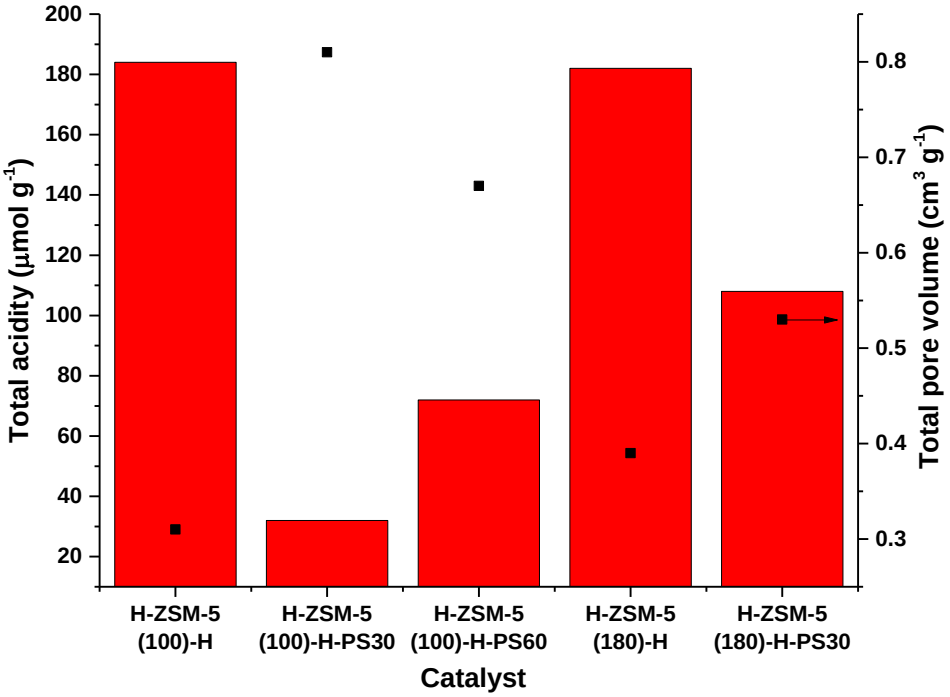

Figure 5.7 Acid site density versus total pore volume measurements for H-ZSM-5 (100)-H and H-ZSM-5 (180)-H zeolites.

The total acid strength of H-ZSM-5 (100)-H was 181 μmol g^{-1}. Templation of H-ZSM-5 (100) with polystyrene nanospheres of 30 and 60 nm in diameter had acid site density values of 32 and 72 μmol g^{-1} respectively, much lower than the untemplated H-ZSM-5 (100)-H zeolite. This can be attributed to the lower crystallinity of the templated zeolites due to the lower crystallisation temperature. Despite varying SiO_2/Al_2O_3 molar ratios the zeolite H-ZSM-5 (180)-H possessed similar acid site density values than the zeolite H-ZSM-5 (100)-H. The templated zeolite, H-ZSM-5 (180)-H-PS30 possessed much lower acid site density than its parent (182 versus 108 μmol g^{-1}), due to the lower amount of aluminium positioned in the tetrahedral position. Clearly, the results displayed in Figure 5.7 show a correlation between acid site density and total pore volume. It can be seen that decreased porosity resulted in enhanced acid site density for all laboratory synthesised H-ZSM-5 zeolites. Similar findings were reported by Zhang et al.[179] who found enhanced

crystallinity and proportion of microporosity reduced the number extra-framework aluminium sites.

5.6.1.5 Solid state NMR of H-ZSM-5 zeolites prepared by conventional heating

The ^{27}Al MAS-NMR spectra for H-ZSM-5 (100)-H and H-ZSM-5 (100)-H-PS30 zeolites are shown in Figure 5.8 (below).

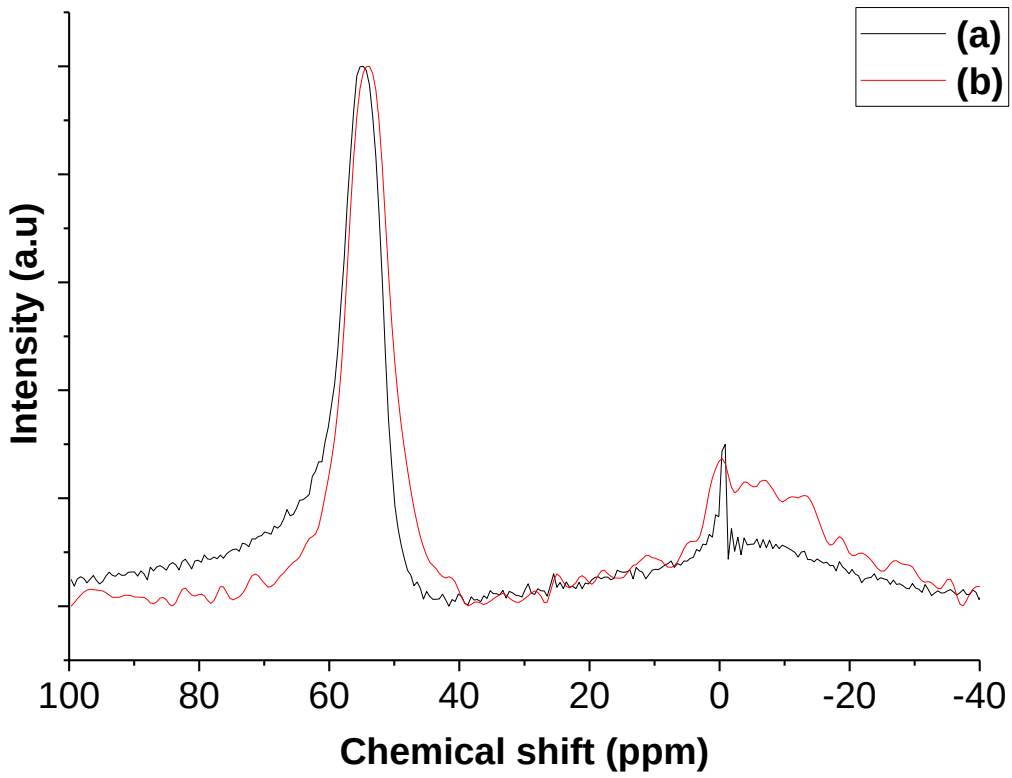

Figure 5.8 ^{27}Al MAS-NMR spectra for H-ZSM-5 (100)-H and H-ZSM-5 (100)-H-PS30.

Clearly, the ^{27}Al MAS-NMR spectra for H-ZSM-5 (100)-H are dominated by the peak at chemical shift ~ 55 ppm (96.8%), which can be attributed due to the presence of tetrahedral aluminium. The presence of the peak at chemical shift 0 ppm, indicated the presence of extra-framework aluminium (3.2%). The spectra showed no evidence of penta-coordinated aluminium present in the structure. The Al_F/Al_{EXT} ratio was 30.3, which indicates that the overwhelming majority of aluminium was located in the framework position. Templation of H-ZSM-5 (100)-H with polystyrene (30 nm) showed a peak at chemical shift 55 ppm (62.7%). The appearance of a slight shoulder at

approximately 45 ppm was found (3.6%), which can be attributed to the presence of penta-coordinated aluminium. It can be seen that the peak at 0 ppm is broad, which indicates that the extra-framework aluminium is unlikely to be homogenous. The Al_F/Al_{EXT} ratio was significantly lower in H-ZSM-5 (100)-H-PS30 than H-ZSM-5 (100)-H (30.3 vs 1.9). However, it is probable that this was due to the lower crystallisation synthesis temperature in the case of H-ZSM-5 (100)-H-PS30, rather than the influence of the PS template.

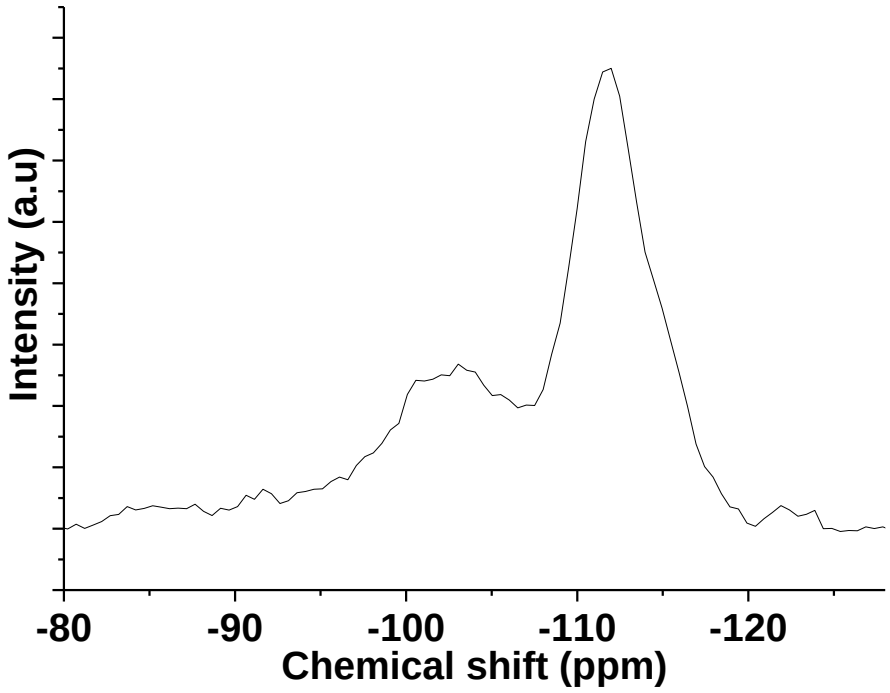

Figure 5.9 ^{29}Si MAS-NMR spectra for H-ZSM-5 (100)-H.

The ^{29}Si MAS-NMR spectra for H-ZSM-5 (100)-H is displayed in

Figure 5.9 showed a highly siliceous material with a predominately $Si(OSi)_4$ environment (68.8%). The peak at chemical shift at approximately -100 ppm confirmed the presence of $Si(OAl)_{1-4}$ environment. The Si/Al_{bulk} ratio (42) was slightly lower than the Si/Al_F ratio (43), confirming the presence of extra-framework aluminium.

5.6.2 The production of renewable *p*-xylene by the [4+2] cycloaddition of DMF with ethylene

The cycloaddition of DMF with ethylene has proven to be an attractive alternative method for the generation of the *p*-xylene, which is used as a precursor to synthesise polyethylene terephthalate (PET). There have been several studies that have shown that zeolites are effective in the development of *p*-xylene from the dehydration of the cycloadduct product 1,4-dimethyl-7-oxabicyclo[2.2.1]hept-2-ene by both Brønsted and Lewis acid sites using zeolites in the liquid phase.[40, 41, 45, 245, 259-261] However, to the best of our knowledge, there have been no studies that have demonstrated the effect of zeolites with increased porosity on conversion of DMF. Our aim was to optimise the yield of *p*-xylene whilst minimising unwanted side products using hierarchical zeolites synthesised in Chapters 3,4 and 5.

5.6.2.1 Blank reaction

The reaction in which no catalyst was used yielded less than 3 % conversion of DMF without the formation of any of the identified products. This confirms that the presence of an acid catalyst is required to dehydrate the cycloadduct product to *p*-xylene.

5.6.2.2 Catalytic activity

In this subsection, the results of preliminary experiments showing the production of renewable *p*-xylene using hierarchical zeolites synthesised by a top-down approach (Chapter 3) and bottom-up approach (Chapter 4) are presented. This subsection describes experimental parameters showing the effect of desilicated and templated zeolites on catalytic conversion, product yield and mass balance. Reaction parameters such as temperature, pressure, solvent, time were studied to determine their effect on the production of renewable *p*-xylene. In addition, reproducibility and recycling experiments were carried out to determine whether our reaction system could generate reproducible data, and whether our catalyst could be recycled and show high yields of *p*-xylene.

5.6.2.2.1 Preliminary experiments of hierarchical H-ZSM-5 prepared by desilication

To show that hierarchical H-ZSM-5 prepared by desilication would have greater catalytic activity than its untreated parent for the [4+2] cycloaddition of DMF with ethylene, preliminary experiments were conducted. Typically, the reaction of DMF and ethylene was carried out in a 45 mL closed pressure vessel (Parr model 4717). DMF (51 mmol), tridecane (1.85 mmol), hexane (125 mmol) and 110 mg of catalyst was charged into the vessel. The vessel was stirred using cross-shaped magnetic stir bar at 1100 rpm, purged with nitrogen 3 times, depressurised and heated to 180 °C using an aluminium block and a hotplate under stirring (1100 RPM). As soon as the desired temperature was reached the vessel was pressurised to a total pressure of 40 bar using ethylene. It must be noted that the initial vapour pressure at 180 ^{o}C prior to addition of ethylene was 10 bar. The reaction was carried out for 20 hours and then quenched in an ice bath for 1 hour. The products were separated from the spend catalyst by centrifugation at 14,000 rpm for 5 minutes and quantified using GC-FID. The preliminary results are shown in Figures 5.10-5.11.

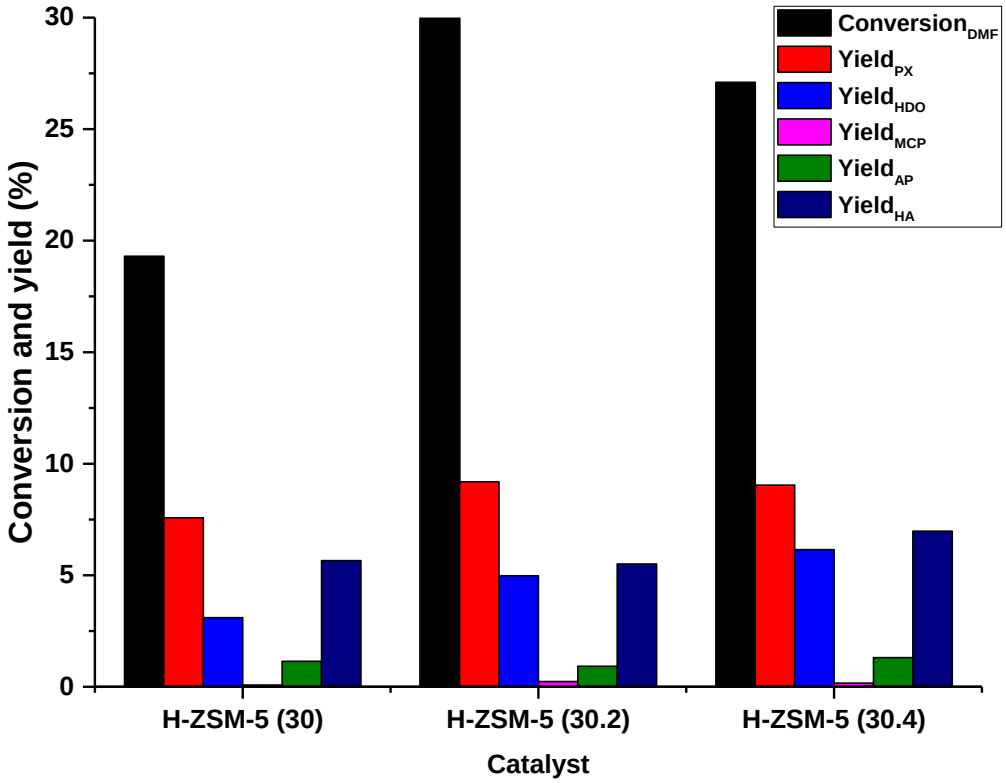

Figure 5.10 Conversion and yields of known products for the Diels-Alder cycloaddition of DMF with ethylene (40 bar) at 180 °C for 20 hours for H-ZSM-5 (30) zeolites.

As can be seen from Figure 5.10, treatment of H-ZSM-5 (30) with sodium hydroxide had a significant effect on conversion and yields obtained for *p*-xylene. In the case of H-ZSM-5 (30) vs H-ZSM-5 (30.2), conversion of DMF increased from 19.3% to 36.0% respectively. The yields obtained for *p*-xylene was 9.2% for H-ZSM-5 (30.2) compared to 7.6% using H-ZSM-5 (30). Despite lower conversion for H-ZSM-5 (30.4) than H-ZSM-5 (30.2), similar yields of *p*-xylene were obtained. It was suggested that this could be caused by the strong adsorption of *p*-xylene on acid sites,[248] which reacts further to alkylated and higher aromatic products and unrecoverable polymerised products (coke).[150] This hypothesis could account for the discrepency for the lower mass balance obtained for H-ZSM-5 (30.2). Quantum mechanics studies by Patet et al.[248] showed that at 250 °C DMF, *p*-xylene and HDO bind more strongly to the active site than ethylene or water.

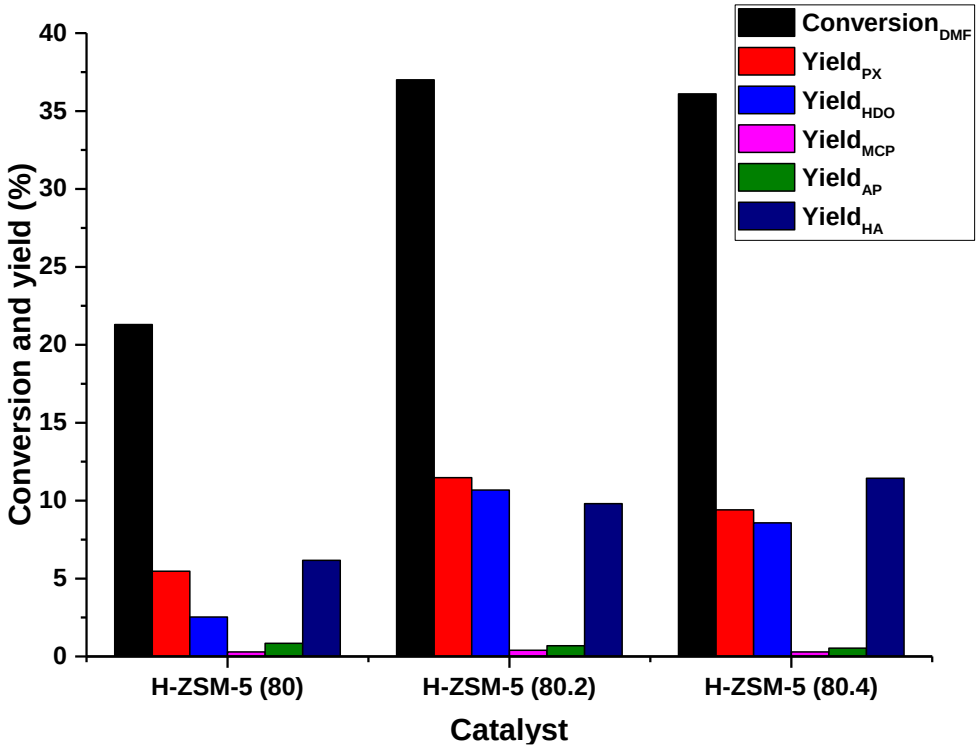

Figure 5.11 Conversion, and yields for known products for the Diels-Alder cycloaddition of DMF with ethylene (40 bar) at 180 °C for 20 hours for H-ZSM-5 (80) zeolites.

The yield of *p*-xylene increased more substantially for alkaline modified H-ZSM-5 (80) zeolites (Figure 5.11) than alkaline modified H-ZSM-5 (30) zeolites. A yield of 5.4% was obtained for H-ZSM-5 (80) at 21.3% conversion. Testing of H-ZSM-5 (80.2) showed 11.5% yield of *p*-xylene at 37.0% conversion. However, catalytic activity for H-ZSM-5 (80.4) was slightly worse than H-ZSM-5 (80.2), with conversion decreasing slightly to 36.1% with a total yield 9.4% for *p*-xylene. The overall mass balances for the H-ZSM-5 (80) zeolites were similar; suggesting variations in yield of *p*-xylene was due to the formation of alkylated or higher aromatics. The results suggest that increased mesoporosity promoted the transformation of DMF to reaction products, with the yield of the desired product increasing in all cases relative to their untreated parent. Trace amounts of 2-methyl-cyclopentenone (MCP) were found in all studies due to the acid catalysed intramolecular aldol reaction of 2,5-hexanedione.

5.6.2.2.2 Effect of desilication of zeolites on catalytic activity

The effect of desilication on H-ZSM-5 (laboratory synthesised), H-Y and H-Beta zeolites on the [4+2] cycloaddition of DMF with ethylene was studied. Testing was carried out using a 75 mL Parr vessel with 37 mL of DMF (3 M) using hexane as a solvent and tridecane as an internal standard. Testing was carried out using 180 mg of catalyst. Testing conditions is described in more detail in section 5.5.2.

Table 5.1 Conversion, product yield and mass balances for the Diels-Alder cycloaddition of DMF with ethylene for commercially untreated and alkaline treated H-ZSM-5, H-Beta and H-Y zeolites.

Catalyst	Conversion (%)	Yield (%)					Mass balance (%)
		PX	HDO	MCP	AP	HA	
H-ZSM-5 (80.2)[a]	33.2	11.2	9.3	0.3	1.4	12.0	101
H-ZSM-5 (80.2)[b]	37.0	11.5	10.7	0.4	0.7	9.8	96.1
H-ZSM-5 (100)[a]	30.9	7.5	3.8	0.1	1.5	11.8	93.8
H-ZSM-5 (100.2)[a]	32.1	10.4	5.6	0.1	1.8	10.6	96.2
H-Beta (10)[a]	31.5	10.4	3.6	0.1	1.4	12.4	96.3
H-Beta (10.2)[a]	37.1	10.5	6.3	0.1	1.4	14.5	95.7
H-Beta (25)[a]	42.9	11.6	11.5	1.0	1.1	11.0	93.2
H-Beta (25.2)[a]	44.3	12.1	12.2	1.3	1.1	13.3	95.6
H-Beta (38)[a]	36.9	10.4	8.9	0.5	1.7	9.8	94.3
H-Beta (38.2)[a]	39.9	10.9	10.1	1.3	1.2	15.0	98.6
H-Beta (360)[a]	30.7	9.1	5.0	0.1	2.1	11.2	96.8
H-Beta (360.2)[a]	40.2	10.4	9.6	0.2	1.7	16.0	97.8
H-Y (10)[a]	24.3	6.6	1.4	0.1	1.9	9.5	95.2
H-Y (10.2)[a]	31.1	7.5	2.9	0.1	1.6	11.4	92.3
H-Y (12)[a]	34.2	9.7	4.6	0.1	2.1	13.9	96.2
H-Y (12.2)[a]	46.7	10.5	13.9	0.3	0.8	17.5	96.2
H-Y (80)[a]	35.6	7.8	5.0	0.1	0.9	16.8	95.0
H-Y (80.2)[a]	40.7	10.3	7.1	0.1	1.3	17.5	95.5

(a)180 mg catalyst, 37.5 mL of 3 M DMF in hexane, 180 ^{o}C, 20 hours, 40 bar total pressure in 75 mL vessel, (b)110 mg catalyst, 22.5 mL of 3 M DMF in hexane, 180 ^{o}C, 20 hours, 40 bar total pressure in 45 mL vessel.

Testing of H-ZSM-5 (80.2) showed conversions of 37.0% with a *p*-xylene yield of 11.5% obtained in the 45 mL vessel. The 75 mL vessel showed conversion of 33.2% with a 11.2% yield of *p*-xylene. This suggests similar results were obtained within an error of 11% irrespective of the size of the vessel and therefore, could be scaled up after taking into account experimental error.

Testing of our laboratory microwave synthesised H-ZSM-5 (100) showed 30.9% conversion, with lower yields of *p*-xylene obtained than for H-ZSM-5 (80). However, the yield of *p*-xylene obtained using H-ZSM-5 (100) was similar to commercial H-ZSM-5 (30). Despite identical specific surface areas of H-ZSM-5 (80) and H-ZSM-5 (100), H-ZSM-5 (80) displayed lower conversion than our laboratory H-ZSM-5 (100) catalyst. This result could be explained by the fact that H-ZSM-5 (100) displayed a higher external volume than the commercial H-ZSM-5 (80) and therefore, enhanced conversion was primarily due to enhanced porosity.

H-Beta and H-Y displayed higher catalytic activity than H-ZSM-5, showing higher yields of *p*-xylene. Unmodified commercial H-Beta with lower SiO_2/Al_2O_3 molar ratios showed higher levels of conversion than unmodified H-Beta zeolites with higher SiO_2/Al_2O_3 molar ratios. Larger yields of *p*-xylene were also obtained for untreated H-Beta zeolites with lower SiO_2/Al_2O_3 molar ratios, with an optimum yield of 11.6% obtained for H-Beta (25). This was an obvious effect of acidity and porosity. Our H-Beta zeolite (SiO_2/Al_2O = 10) displayed higher catalytic activity than H-ZSM-5 despite having a lower specific surface area. Alkaline treatment of H-Beta (10) with 0.2 M NaOH showed superior catalytic performance than its parent with conversion increasing from 31.5% to 37.1%. It is likely that this was due to enhanced porosity and acidity in H-Beta (10.2). The yield of *p*-xylene was largely unchanged due to subsequent reactions of *p*-xylene to higher aromatics. This is supported by the fact that the yield of HDO doubled for H-Beta (10.2), confirming larger yields of *p*-xylene were originally produced for H-Beta (10.2) than H-Beta (10). Comparison of H-Beta (38) and H-Beta (360) showed similar specific surface areas and porosity, confirming conversion is also affected by acidity. Alkaline treatment of H-Beta (25) and H-Beta (38) with 0.2 M NaOH showed slightly higher levels of conversion than their untreated parent, with slightly yields of *p*-xylene obtained for the desilicated H-Beta (25 and 38) samples compared to their parent. Despite amorphisation of H-Beta (360), conversion was significantly higher after alkaline treatment with conversion increasing from 30.7% for H-Beta (360) to 40.2% for H-Beta (360.2), with a

p-xylene yield of 10.4% obtained for H-Beta (360.2) compared to 9.1% for H-Beta (360) under the same reaction conditions. Additionally, higher yields of HDO and higher aromatics were obtained for H-Beta (360.2) compared to H-Beta (360). The parent showed slightly higher yields of alkylated products than H-Beta (360.2). Due to the larger mesoporous network of H-Beta (360.2), it is possible that the alkylated products were converted to higher aromatics.

For comparison, H-Y zeolites were also tested under the same conditions. In this instance two H-Y zeolites with low and high SiO_2/Al_2O_3 molar ratios were chosen and desilicated using the same conditions as described previously for H-ZSM-5 and H-Beta. In addition to this, H-Y zeolite was synthesised by microwave irradiation with a SiO_2/Al_2O_3 molar ratio of 10 and subjected to alkaline treatment. The results in Table 5.1 show that similar levels of conversion were obtained for the commercially obtained H-Y zeolites, despite varying SiO_2/Al_2O_3 molar ratios. H-Y (12) showed slightly larger yields of *p*-xylene than H-Y (80), due to H-Y (12) possessing greater acid site density. Our H-Y zeolite displayed much lower levels of conversion, despite having similar acid site densities, and a larger surface area than H-Y (12). It is probable that the lower activity of H-Y (10) was due to the smaller external pore volume. Despite alkaline treatment having a detrimental effect on the acidity of all the H-Y zeolites, catalytic activity was superior for the desilicated H-Y zeolites compared to their untreated counterparts. Analysis of the specific surface area and porosity measurements of H-Y zeolites showed that alkaline treatment enhanced mesoporosity and catalytic activity in the alkaline modified H-Y zeolites, which can be attributed to the reduction of diffusion limitations.

5.6.2.2.3 Effect of hierarchical H-ZSM-5 prepared by polystyrene templation on catalytic activity

This study investigated the effect of hierarchical H-ZSM-5 zeolites (laboratory synthesised) on the effect of conversion of DMF and yield to *p*-xylene and related products. Testing conditions is described in more detail in section 5.5.2. The results are shown in Figures 5.12-5.15.

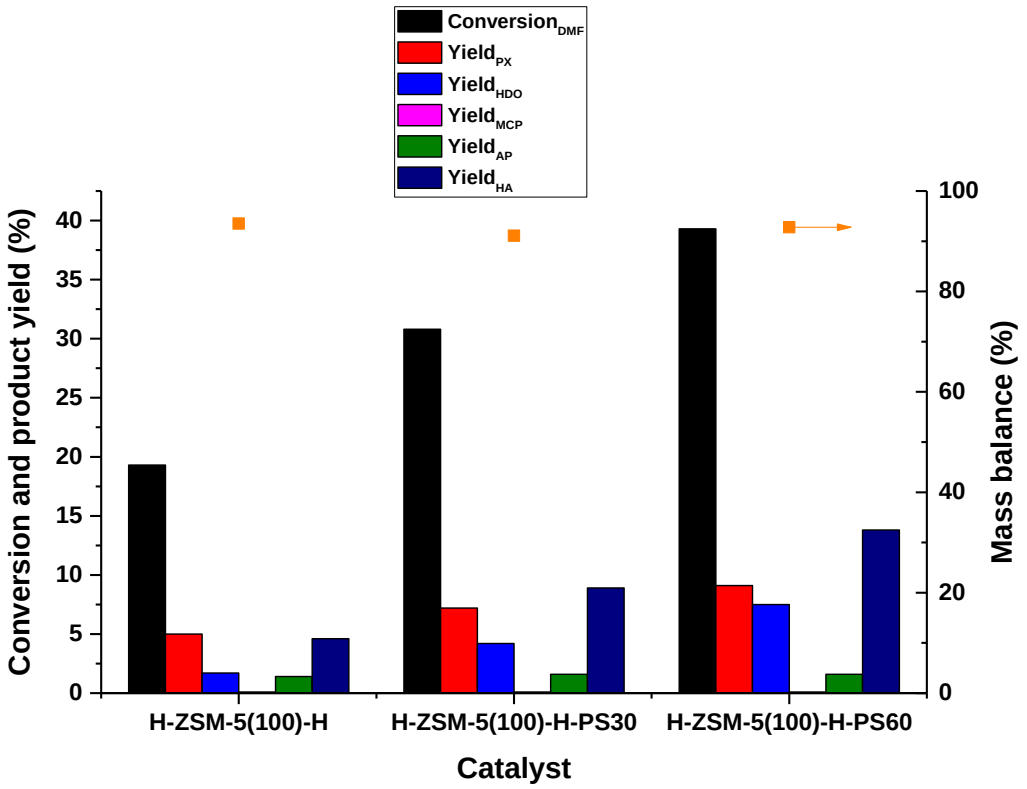

Figure 5.12 Conversion, and yields for known products for the Diels-Alder cycloaddition of DMF with ethylene (40 bar) at 180 °C for 20 hours for conventional and hierarchical H-ZSM-5 (100) synthesised using conventional heating methods.

From Figure 5.12, it can be seen that the hierarchical H-ZSM-5 prepared by hard templation with polystyrene nanospheres, showed greater catalytic activity than their untemplated counterparts. H-ZSM-5 (100)-H showed conversion levels of 19.3%, with a 5.0% yield obtained for *p*-xylene. Templation H-ZSM-5 (100)-H with polystyrene (30 nm) had a dramatic effect on conversion. It can be seen that conversion for H-ZSM-5 (100)-H-PS30 increased to 30.8%. When the size of polystyrene nanospheres was increased further from 30 nm to 60 nm, conversion increased further to 39.3%. In conjunction, the yield of HDO also increased with H-ZSM-5 (100)-templated with polystyrene (60 nm). The yields of MCP and alkylated products remained largely unchanged, irrespective of templation using polystyrene (30 or 60 nm). Worth noting is that the yield of higher aromatics obtained was 4.6% for H-ZSM-5 (100)-H, which increased for the templated H-ZSM-5 zeolites. This can be attributed to enhanced porosity, allowing the bulkier higher aromatics to diffuse out of the larger pores.

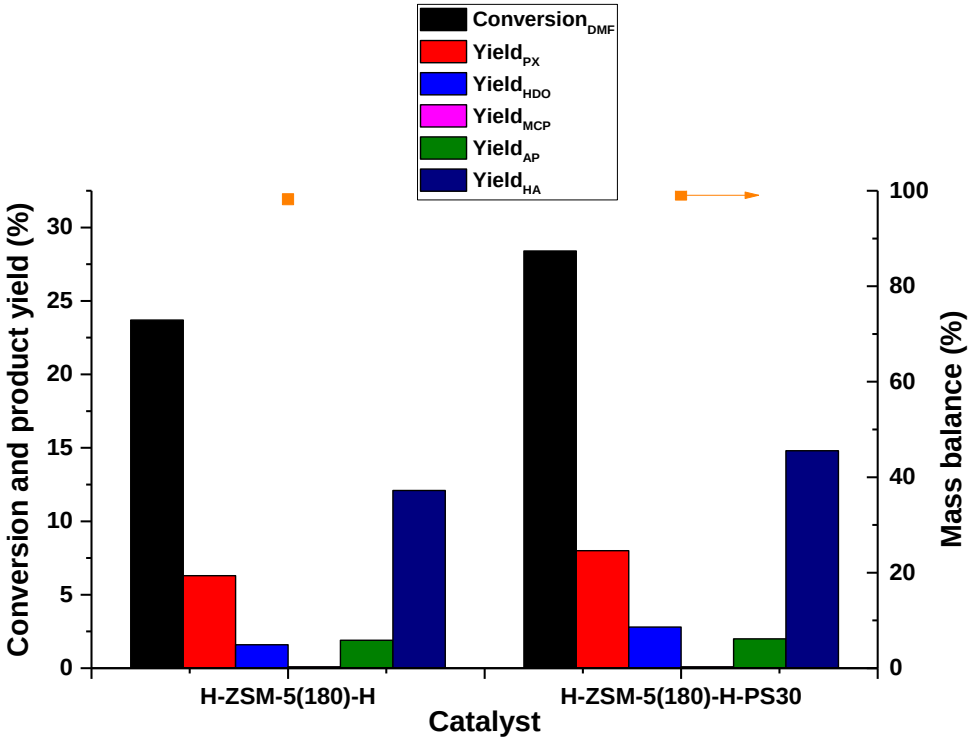

Figure 5.13 Conversion, and yields for known products for the Diels-Alder cycloaddition of DMF with ethylene (40 bar) at 180 ^{o}C for 20 hours for H-ZSM-5 (180)-H and H-ZSM-5 (180)-H-PS30.

H-ZSM-5 (180)-H showed conversion of 23.7% with a 6.3% yield obtained for *p*-xylene, slightly higher values obtained for H-ZSM-5 (100)-H. Since they showed nearly identical acid site density values, this effect cannot primarily be due to acidity. The surface and porosity measurements shown in section 5.6.1.3 showed that H-ZSM-5 (180)-H displayed greater porosity than H-ZSM-5 (100)-H. Therefore, enhanced catalytic activity of H-ZSM-5 (180)-H can be attributed to the enhanced levels of total porosity compared to zeolite H-ZSM-5 (100)-H.

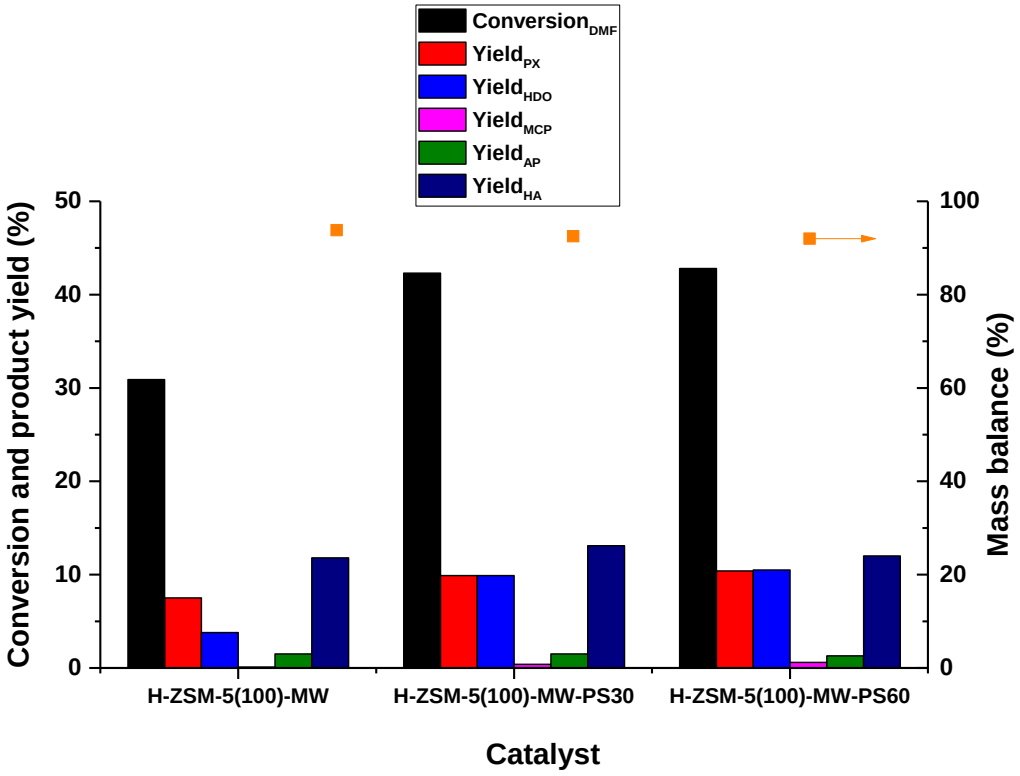

Figure 5.14 Conversion, and yields for known products for the Diels-Alder cycloaddition of DMF with ethylene (40 bar) at 180 °C for 20 hours for H-ZSM-5 (100)-MW, H-ZSM-5 (100)-MW-PS30 and H-ZSM-5 (100)-MW-PS60.

In the case of the hierarchical H-ZSM-5 zeolites synthesised by microwave assisted heating, it can clearly be seen that templation had a similar effect on conversion than in the case of the hierarchical H-ZSM-5 zeolites synthesised by conventional heating. Templation of H-ZSM-5 (100)-MW with polystyrene (30 and 60 nm) showed a dramatic effect on catalytic activity, with conversion increasing to approximately 42% for both templated zeolites, compared to 30.9% for the untemplated H-ZSM-5 (100)-MW zeolite. The yields of *p*-xylene were for higher for the hierarchical samples than the untemplated sample. Increasing the size of polystyrene nanospheres in the precursor gel from 30 nm to 60 nm for H-ZSM-5 synthesised with microwave assisted heating had no effect on catalytic activity. The yields of *p*-xylene and HDO were largely unaffected by the size of polystyrene nanospheres. The full characterisation profile of H-ZSM-5 (100)-MW zeolites can be found in Chapter 4. The untemplated zeolite, synthesised by the microwave assisted heating displayed greater catalytic activity than the untemplated zeolite synthesised by conventional heating. Clearly, enhanced catalytic activity cannot be primarily due to acidity, as the untemplated microwave zeolite showed lower acidity than

the untemplated zeolite synthesised by conventional heating. Comparison of the surface area and porosity measurements showed the untemplated zeolite synthesised by conventional heating displayed larger surface area and porosity than the untemplated H-ZSM-5 synthesised by microwave heating. Taking these two factors into account, it is difficult to ascertain the principal reason that the untemplated microwave H-ZSM-5 zeolite showed superior catalytic activity than the untemplated H-ZSM-5 zeolite synthesised by conventional heating. Since H-ZSM-5-(100)-MW and H-ZSM-5 (100)-MW-PS60 displayed nearly identical levels of acid site density, it is likely that enhanced catalytic activity of the hierarchical H-ZSM-5 catalyst can be attributed to enhanced meso/macroporosity in H-ZSM-5 (100)-MW-PS60, nearly 3 fold larger than H-ZSM-5 (100)-MW.

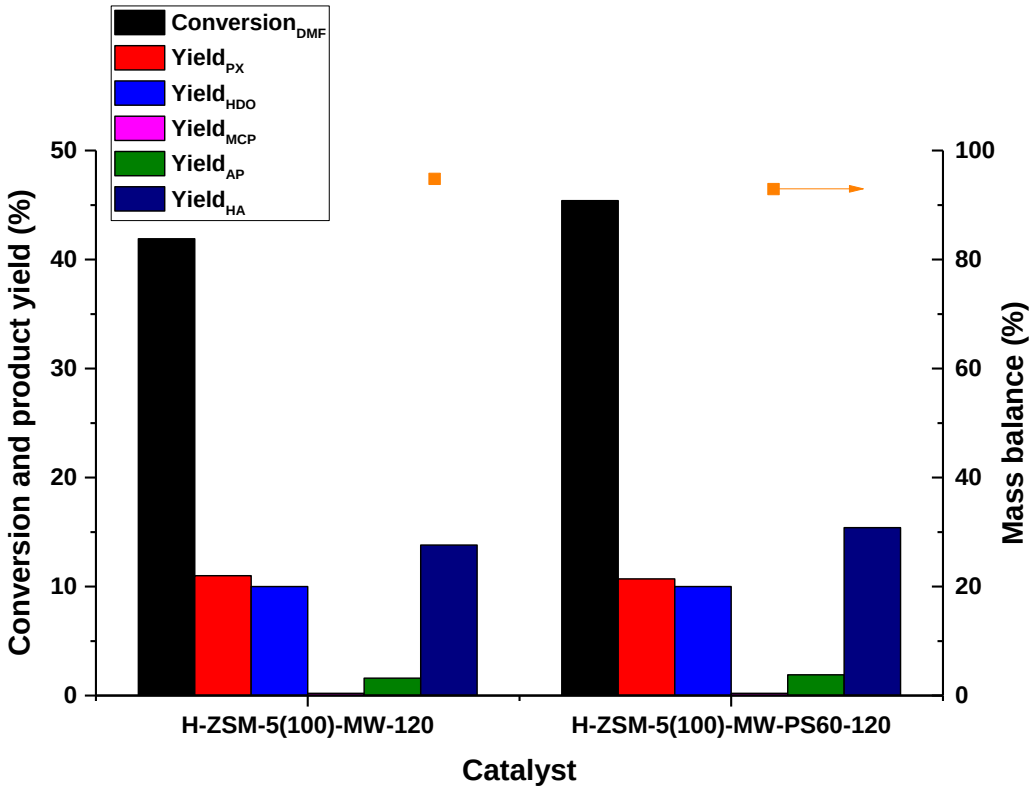

Figure 5.15 Conversion, and yields for known products for the Diels-Alder cycloaddition of DMF with ethylene (40 bar) at 180 ^{o}C for 20 hours for H-ZSM-5 (100)-MW-120 and H-ZSM-5 (100)-MW-PS60-120.

To examine directly the effect of templation on catalytic activity, the zeolites H-ZSM-5 (100)-MW-120 and H-ZSM-5 (100)-MW-PS60-120 were tested. These catalysts were synthesised with identical crystallisation temperatures and time. The results showed that

the templated zeolite displayed superior catalytic activity than its untemplated counterpart, with conversion increasing from 41.9% to 45.4%, with slightly higher yields of *p*-xylene obtained for the untemplated zeolite. This can be attributable to subsequent reactions of *p*-xylene, forming alkylated and higher aromatics. Since both zeolites displayed similar levels of acidity the superior performance of the templated H-ZSM-5 zeolite can be attributed to the enhanced porosity.

5.6.2.2.4 Effect of temperature and pressure on catalytic activity

Since the zeolites H-ZSM-5 (80.2), H-Beta (360.2) and H-Y (80.2) showed greater catalytic activity than their untreated parents, these catalysts were chosen for studies involving higher temperature and pressure. Since higher pressures enhance the rate of reaction in the Diels-Alder reaction,[262] it was decided to increase total pressure of the reaction from 40 bar to 55 bar. This was the maximum pressure that could be obtained from the ethylene cylinder. Additionally, the temperature was increased from 180 ^{o}C to 250 ^{o}C. Firstly, we tested the effect of temperature upon the [4+2] cycloaddition of DMF with ethylene at a total pressure of 40 bar using H-ZSM-5 (80) and H-ZSM-5 (80.2). The reaction was carried out using 3 M DMF in hexane as a solvent, tridecane as an internal standard for 20 hours using 180 mg of catalyst. It must be noted that at 250 ^{o}C, the initial vapour pressure inside the vessel was 30 bar. The vessel was then pressurised to a total pressure of 55 bar.

Table 5.2 The effect of temperature and pressure on the cycloaddition of DMF with ethylene using commercially untreated and hierarchical zeolites.

Catalyst	Conversion (%)	Yield (%)					Mass balance (%)
		PX	HDO	MCP	AP	HA	
H-ZSM-5 (80)[a]	21.3	5.5	2.5	0.3	0.8	6.2	94.0
H-ZSM-5 (80.2)[a]	37.0	11.5	10.7	0.4	0.7	9.8	96.1
H-ZSM-5 (80)[b]	15.5	5.4	1.0	0.1	1.1	3.1	95.1
H-ZSM-5 (80.2)[b]	18.2	7.5	2.2	0.2	2.3	3.1	97.2
H-ZSM-5 (80)[c]	21.1	9.1	1.2	0.1	2.1	4.1	95.7
H-ZSM-5 (80.2)[c]	62.8	30.3	6.0	1.7	5.5	9.1	89.7
H-Beta (360)[c]	63.7	28.2	7.1	1.0	5.9	12.6	91.2
H-Beta (360.2)[c]	79.2	34.1	5.6	2.3	5.9	12.3	80.9
H-Y (80)[c]	42.5	12.2	3.5	0.3	2.6	13.7	89.8
H-Y (80.2)[c]	75.4	35.3	5.4	1.3	6.4	20.0	93.0

(a) 180 mg catalyst, 3 M DMF in hexane, 180 ºC, 20 hours, 40 bar total pressure, (b)180 mg catalyst, 3 M DMF in hexane, 250 ºC, 20 hours, 40 bar total pressure, (c)180 mg catalyst, 3 M DMF in hexane, 250 ºC, 20 hours, 55 bar total pressure.

The results showed that at 250 ºC and a total pressure of 40 bar total, H-ZSM-5 (80 and 80.2) displayed lower levels of conversion than reactions carried out at 180 ºC. At higher temperature, the yield of HDO decreased, with the yield of *p*-xylene unchanged. It is likely that higher temperature inhibits hydrolysis of DMF, therefore suppressing the formation of HDO. At higher temperature the fast diffusivity of *p*-xylene out of the larger pores inhibits condensation and alkylation reactions of the desired product, *p*-xylene to unwanted oligomers and alkylated products. We concluded that higher pressures were required to maximise conversion of DMF to optimise yields of *p*-xylene by the cycloaddition step.

Next, we tested the effect of pressure of ethylene on the [4+2] cycloaddition of DMF using the same zeolites as described above. This time we used a total pressure of 55 bar instead of 40 bar. The results showed that for H-ZSM-5 (80) at 250 ºC, conversion increased from 15.5% at 40 bar, to 21.1% at 55 bar. A yield of 9.1%

was obtained for *p*-xylene at 55 bar, compared to 5.1% at 40 bar. The yield of HDO was largely unaffected by the variation in pressure. However, higher pressures promoted the formation of alkylated products, such as ethyl-*p*-xylene, 1-methyl-4-propylbenzene.[42, 260] and higher aromatics. Next, the alkaline modified zeolite, H-ZSM-5 (80.2) was tested under the same conditions. The results showed that conversion dramatically increased from 21.1% for the untreated zeolite, H-ZSM-5 (80) to 62.8% for H-ZSM-5 (80.2), nearly a 3 fold increase. A 30.3% yield of *p*-xylene was obtained for H-ZSM-5 (80.2), compared to 9.1% for H-ZSM-5 (80). Likewise, only a 1.2% yield of HDO was obtained for H-ZSM-5 (80) compared to 6.0% for H-ZSM-5 (80.2). This was largely due to the enhanced acid site density and porosity of H-ZSM-5 (80.2). It was found that at 250 ^{o}C and 40 bar, lower yields of alkylated and higher aromatic products were produced compared to reactions carried out at 180 ^{o}C and 40 bar. However, at 250 ^{o}C and 55 bar, the yield of alkylated products and higher aromatics increased, especially in the case of H-ZSM-5 (80.2). This largely supports the hypothesis by Patet et al.[248] that products can still be adsorbed on the active sites, even at temperatures as high as 250 ^{o}C.

The same reaction conditions were tested on the commercial H-Beta (360) and H-Y (80) and their alkaline treated counterparts. Generally, the results showed the alkaline treated zeolites enhanced conversion compared to their untreated parents. In the case of H-Beta, the yield of *p*-xylene produced was 28.2% for the parent, whereas H-Beta (360.2) showed a yield of 34.1%. The yield of HDO was more pronounced in the parent. The overall mass balance for H-Beta (360.2) was smaller than in the case of H-Beta (360), suggesting the formation of unidentified oligomers. Alkaline treated H-ZSM-5 (80), H-Beta (360) and H-Y (80) showed increased yields of MCP relative to their untreated parents.

5.6.2.2.5 Effect of concentration of DMF versus catalytic activity

The effect of concentration on conversion and yield obtained for *p*-xylene in the [4+2] cycloaddition of DMF with ethylene was studied with varying concentrations of DMF (1.5-3M) in hexane. Since catalytic activity was enhanced at 250 ^{o}C at a total pressure of 55 bar, it was decided that the effect of concentration would be studied using these reaction conditions. Typically, the reaction was carried out for

20 hours using H-ZSM-5 zeolites with varying SiO_2/Al_2O_3 molar ratios (parent and alkaline treated) using 1.5 M DMF in hexane and compared to the reaction carried out under the same conditions using 3 M of DMF solution. The effect of concentration results are displayed in Table 5.3.

Table 5.3 The effect of concentration on the cycloaddition of DMF with ethylene using commercially untreated and hierarchical H-ZSM-5 zeolites. Reaction conditions; 180 mg catalyst, 250 ^{oC}, 20 hours, 55 bar total pressure.

Catalyst	$[DMF]_{initial}$ (M)	Conversion (%)	Yield (%)			Mass balance (%)
			PX	HDO	Others[a]	
H-ZSM-5 (80)	3	21.1	9.1	1.2	6.4	95.7
H-ZSM-5 (80.2)	3	62.8	30.3	6.0	16.2	89.7
H-ZSM-5 (30)	1.5	61.3	37.7	0.5	15.4	93.3
H-ZSM-5 (30.2)	1.5	48.4	24.1	3.8	11.6	91.0
H-ZSM-5 (80)	1.5	38.2	19.9	0.6	10.5	92.8
H-ZSM-5 (80.2)	1.5	25.5	9.7	1.5	5.1	90.7

(a) others include MCP, alkylated and higher aromatics

The results in Table 5.3 showed that varying the initial concentration of DMF from 3 M to 1.5 M using H-ZSM-5 (80) enhanced catalytic activity. An initial concentration of 3 M of DMF showed 21.1% conversion. Decreasing the initial concentration to 1.5 M increased conversion to 38.2%. Higher yields of *p*-xylene were obtained for reactions carried out when an initial concentration of 1.5 M DMF was used. Despite higher conversion, lower yields of HDO were obtained for reactions carried out with 1.5 M DMF. Contrary to our predictions, it was found that when all alkaline treated H-ZSM-5 zeolites were tested at lower initial concentration of DMF at 250 ^{o}C and 55 bar, conversion was significantly lower compared to the results obtained for untreated H-ZSM-5 catalysts under the same reaction conditions. It is worth noting that higher yields of HDO were obtained for the alkaline treated H-ZSM-5 catalysts compared to their untreated parent. Since HDO can be formed by acid catalysed hydrolysis of DMF, it is likely that at higher temperatures, DMF was re-formed by the acid catalysed dehydration of HDO. This is supported by TPD studies which confirm that alkaline treated H-ZSM-5 zeolites

displayed higher acid site density than their untreated parent. It is also likely that mass transport limitations were influential as shown in studies carried out Chapter 3.

5.6.2.2.6 Effect of aliphatic solvent versus catalytic activity

The effect of varying the aliphatic solvent on conversion in the [4+2] cycloaddition of DMF with ethylene was studied. The reaction was carried out using 1.5 M of DMF solution with 180 mg H-ZSM-5 (30) for 20 hours at a total pressure of 40 bar. It must be noted that the initial vapour pressure of the mixtures at 180 ^{o}C was as follows; 11 bar for hexane, 3.2 bar for octane and 1.3 bar for dodecane. The vessels were then pressurised to a total pressure of 40 bar.

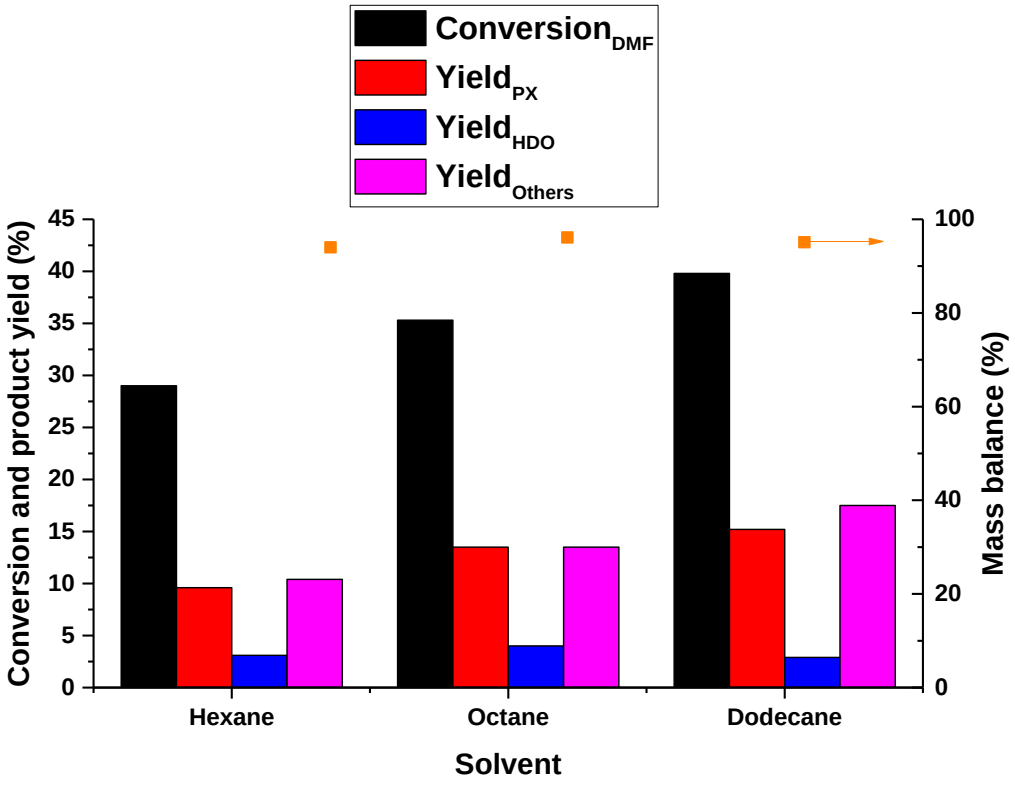

Figure 5.16 Conversion, and yields for known products for the Diels-Alder cycloaddition of DMF with ethylene (40 bar) at 180 ^{o}C for 20 hours for H-ZSM-5 (30) using various aliphatic solvents.

The results show that there was a correlation between the boiling point of the aliphatic solvent and conversion of DMF. As shown in Figure 5.16, it can be seen that conversion was the lowest for the reaction carried out when hexane was used as a solvent, producing the lowest yield of *p*-xylene. This was unsurprising, since the vessel containing hexane

had the highest initial vapour pressure. Therefore, the amount of ethylene added was significantly lower than the vessels containing octane and dodecane under the same reaction temperature. Higher yields of *p*-xylene were obtained when hexane was substituted to aliphatic solvents with higher boiling points, with the highest yield being obtained when dodecane was used. There appeared to be no clear trend in the yield of HDO produced with varying solvents.

5.6.2.2.7 Effect of reaction time on the formation of *p*-xylene

In this subsection, the effect of reaction time on catalytic activity. The aim of this study was to investigate whether increasing the reaction time from 20 hours to 40 hours would have a dramatic effect on the conversion of DMF and enhanced *p*-xylene yield. This study was carried out using unmodified H-ZSM-5 (30) due to its large microporous network. The reaction was carried out using conditions as described in section 5.6.2.2.1.

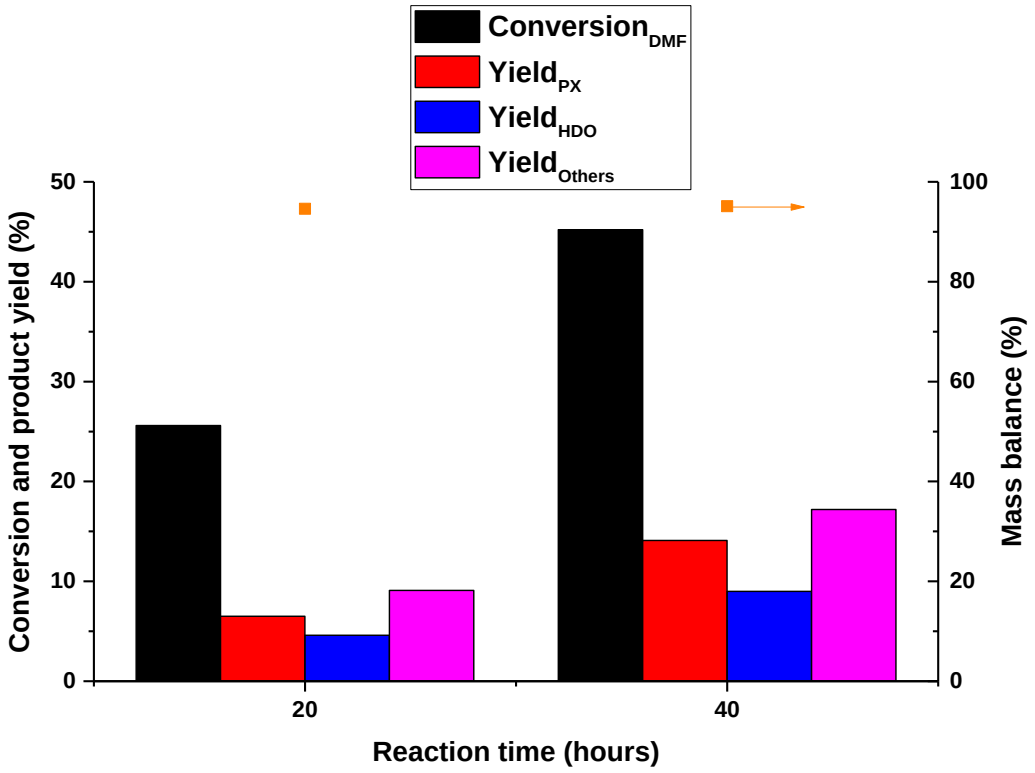

Figure 5.17 Conversion, and yields for known products for the Diels-Alder cycloaddition of DMF with ethylene (40 bar) at 180 °C for 20/40 hours for H-ZSM-5 (30).

The reaction carried out for 20 hours showed conversion of 25.6%, resulting in a *p*-xylene yield of 6.5%. When the reaction time was increased from 20 hours to 40 hours, conversion of DMF increased from 25.6% to 45.2%. This resulted in a 14.1% yield of *p*-xylene being generated. The dramatic increase in conversion and yield being obtained for *p*-xylene also translated in a higher yield being obtained for HDO at longer reaction times. This was hardly surprising due to the increased yield of *p*-xylene. Clearly, these results were due to the effect of reaction time. As can be seen from Figure 5.17 the overall carbon mass balance remained largely unchanged, largely suggesting the formation of unidentified oligomers did not occur. It is probable that higher temperatures and pressures are required to suppress the formation of HDO and therefore, increase yields of *p*-xylene.

5.6.2.2.8 Maximising conversion and yield of *p*-xylene

Since conversion of DMF was higher when dodecane was used as a solvent, this solvent was used for subsequent studies to maximise conversion of DMF and *p*-xylene yield over a range of commercially untreated and alkaline treated zeolites, synthesised by desilication. The study was carried out using temperatures ranging from 200-250 ^{o}C. The initial concentration of DMF used in this study was 1.5 M. H-ZSM-5 (30) and H-ZSM-5 (80) and their alkaline treated counterparts were tested at 250 ^{o}C. The results are displayed in Figures 5.18-5.22.

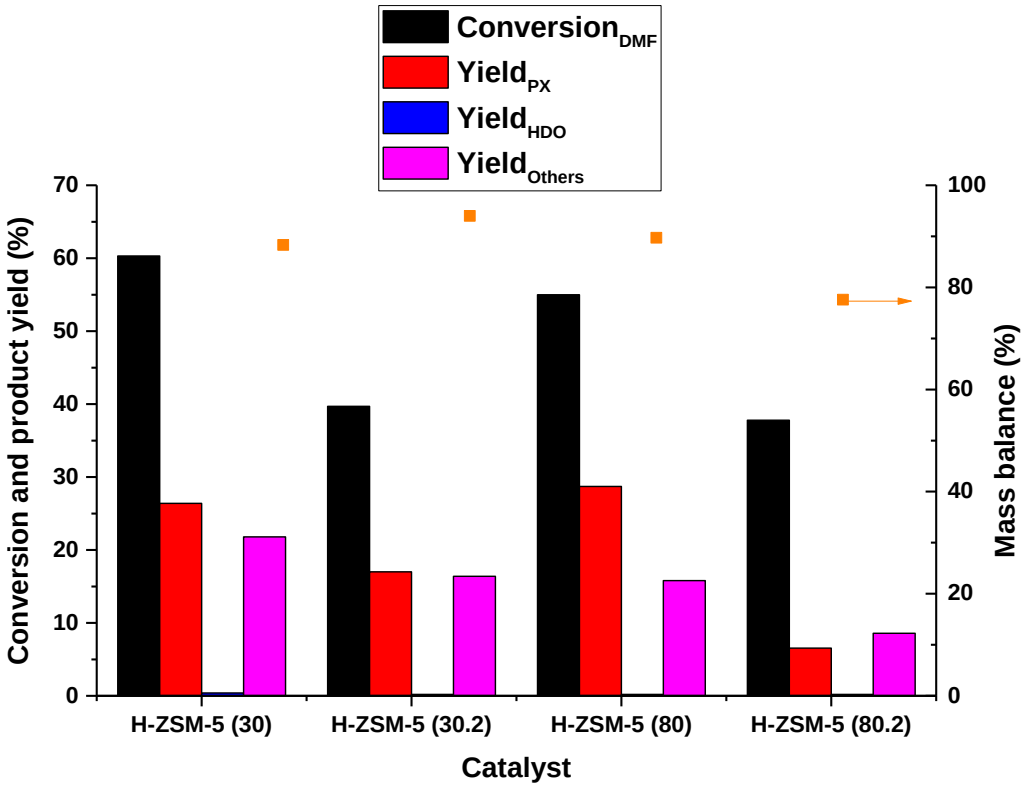

Figure 5.18 Conversion, and yields for known products for the Diels-Alder cycloaddition of DMF (1.5 M) with ethylene (55 bar) at 250 °C for 20 hours for H-ZSM-5 zeolites.

Similar to the studies carried out in section 5.6.2.2.5 when hexane was used as a solvent, alkaline treated H-ZSM-5 zeolites displayed inferior catalytic activity than their untreated parent at 250 °C using a concentration of 1.5 M. Owing to the insignificant yields of HDO, it is highly unlikely that catalytic activity was significantly lower in the desilicated samples due to the acid catalysed dehydration of HDO. It is possible the reduction in catalytic activity is related to the mass transport phenomenon, due to faster diffusivity of DMF from the pores at elevated temperatures. The yields of *p*-xylene are shown to be considerably higher in untreated H-ZSM-5 zeolites, likely caused by the decrease in concentration of Brønsted acid sites in H-ZSM-5 (30.2 and 80.2) compared to H-ZSM-5 (30 and 80) respectively. When comparing H-ZSM-5 (80) and H-ZSM-5 (80.2), the yield of *p*-xylene decreased from 28.7% for the commercially unmodified H-ZSM-5 catalyst, to 6.4% for H-ZSM-5 (80.2).

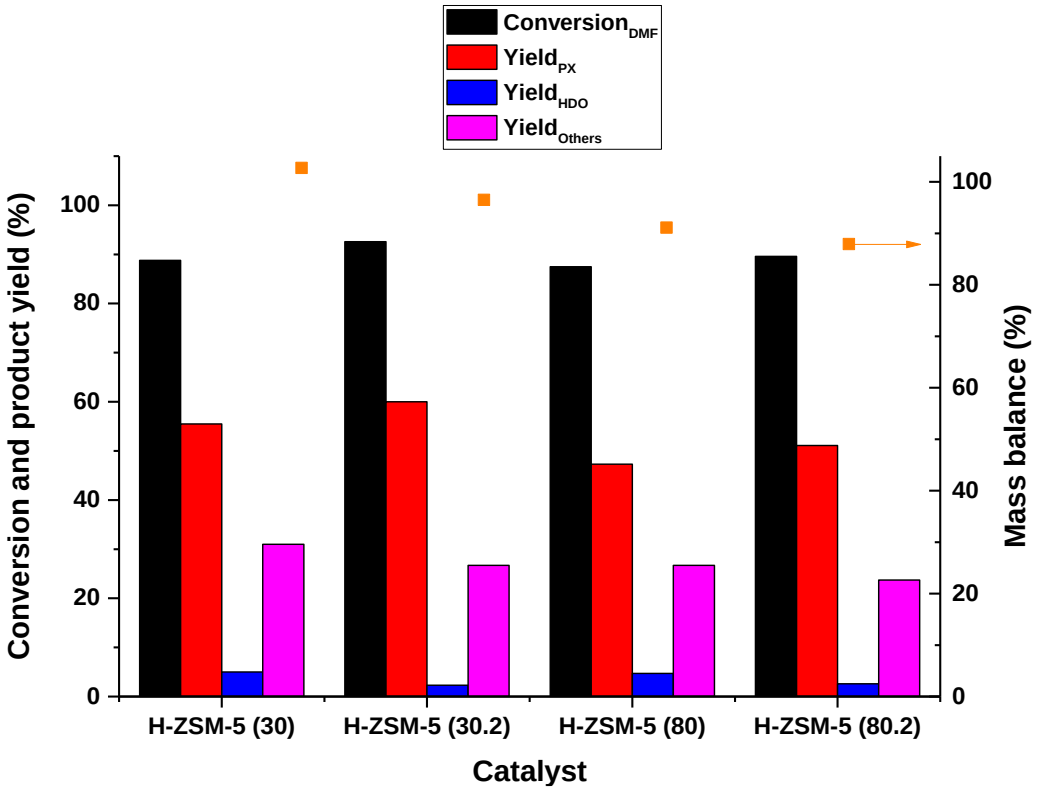

Figure 5.19 Conversion, and yields for known products for the Diels-Alder cycloaddition of DMF (1.5 M) with ethylene (55 bar) at 220 °C for 20 hours for H-ZSM-5 zeolites.

When the reactions were carried out at 220 °C, conversion for the unmodified H-ZSM-5 catalysts were significantly enhanced than those carried out at 250 °C. Comparison of H-ZSM-5 (30) and H-ZSM-5 (80) showed similar conversions, with H-ZSM-5 (30) showing higher yields of *p*-xylene than H-ZSM-5 (80). This was unsurprising, largely owing to the larger concentration of Brønsted acid sites in H-ZSM-5 (30) than H-ZSM-5 (80). Despite this, the yield of HDO was similar in both H-ZSM-5 (30) and H-ZSM-5 (80). The desilicated H-ZSM-5 zeolites showed only slightly higher activity than their parent zeolites. Despite this, the yields of *p*-xylene enhanced. The study showed that at 220 °C, alkaline treated H-ZSM-5 zeolites displayed lower yields of HDO due to the reduction in the concentration of Brønsted acid sites for desilicated H-ZSM-5 zeolites. This confirmed that hydrolysis of DMF is correlated to the number of Brønsted acid sites available.

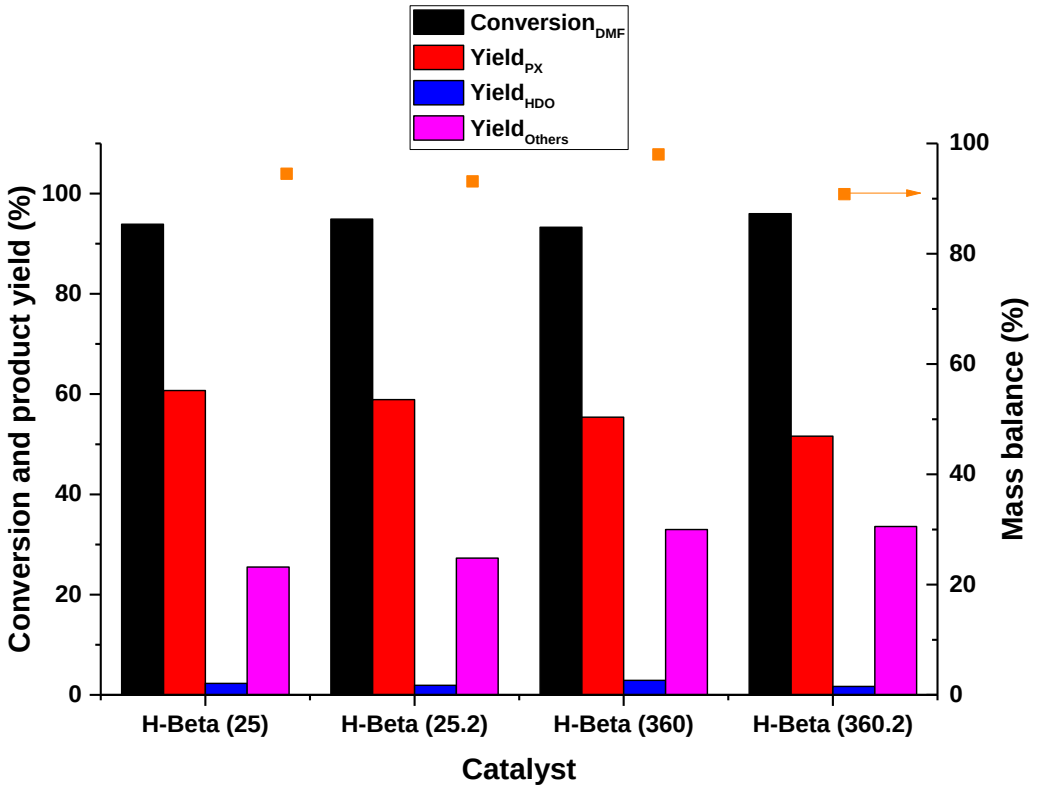

Figure 5.20 Conversion, and yields for known products for the Diels-Alder cycloaddition of DMF (1.5 M) with ethylene (55 bar) at 220 °C for 20 hours for H-Beta zeolites.

Commercial H-Beta with varying SiO_2/Al_2O_3 molar ratios and their desilicated counterparts were tested at 220 °C. Likewise, Figure 5.20 shows modification of H-Beta showed slightly improved catalytic activity compared to their parent. Despite the parent H-Beta zeolites possessing varying SiO_2/Al_2O_3 molar ratios, they displayed similar levels of conversion, with H-Beta (25) showing 93.9% conversion and H-Beta (360) 93.3% conversion. Despite similar levels of conversion, H-Beta (25) showed a *p*-xylene yield of 60.7%, whereas a *p*-xylene yield of 55.4% was obtained for H-Beta (360). Clearly, this was a direct consequence of the enhanced acid site density in H-Beta (25). It would have been expected that a higher yield of *p*-xylene would have translated to a higher yield of HDO. However, this was not the case even though H-Beta (360) possessed lower concentration of acid sites than H-Beta (25). From our results, it was established that a yield of 3.5% of MCP was produced for H-Beta (25), whereas a yield of only 1.0% was produced for H-Beta (360). Therefore, the reduced yield of HDO for H-Beta (25) can be attributed by the formation of MCP by the acid catalysed intramolecular aldol reaction of HDO.

Previous studies have shown the most promising *p*-xylene yields were obtained using H-Beta zeolites with an initial SiO_2/Al_2O_3 molar ratio of 25, with yields of 90-97% obtained.[45, 263] Despite similar levels of conversion compared to the literature, our study showed lower *p*-xylene yields. It is possible that this was due to the lower temperature facilitating alkylated products and oligomers in our study which reduced the *p*-xylene yield. In addition, our study was carried out using a batch reactor system compared to a semi-continuous system.

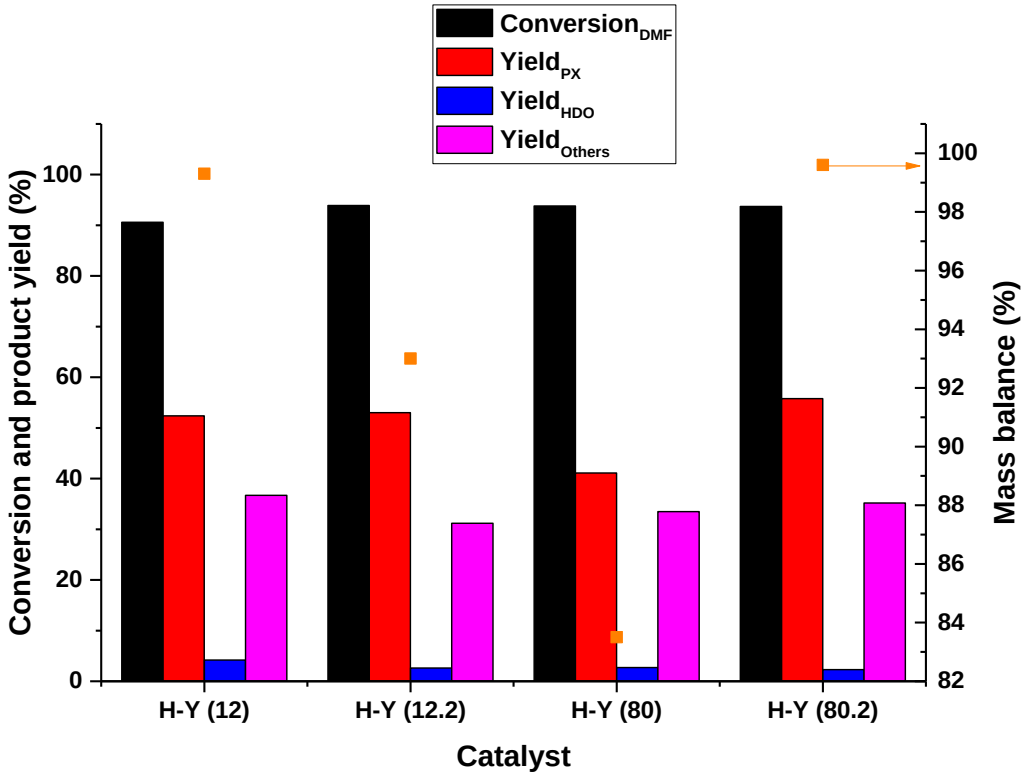

Figure 5.21 Conversion, and yields for known products for the Diels-Alder cycloaddition of DMF (1.5 M) with ethylene (55 bar) at 220 °C for 20 hours for H-Y zeolites.

Figure 5.21 shows H-Y (12 and 80) at 220 °C showed 90.6 and 93.8% conversion respectively. As in the case of H-Beta zeolites, H-Y (12) produced higher yields of *p*-xylene than H-Y (80). Since H-Y (12 and 80) had very similar total pore volumes (see Chapter 3), it is clear that larger yields of *p*-xylene were obtained due to the larger acid site density of H-Y (12). Similar to H-Beta, larger yields of HDO were produced in zeolites with lower SiO_2/Al_2O_3 molar ratios, with H-Y (12) showing a 4.2% yield of HDO compared to 2.7% for H-Y (80). Alkaline treatment of both H-Y (12 and 80) with 0.2 M NaOH resulted in slightly higher catalytic activity in terms of conversion. The yield of *p*-

xylene increased only slightly for after desilication of H-Y (12). However, desilication of H-Y (80) showed larger yields of *p*-xylene obtained compared to the unmodified parent, with the parent showing 41.1% yield of *p*-xylene compared to 55.8% obtained for H-Y (80.2). Despite this, the carbon mass balance for H-Y (80) was close 83.5%, indicating the formation of unwanted and uncharacterised products.

Next, we decided to test whether reducing the temperature from 220 ºC to 200 ºC would have a significant impact on the conversion of DMF and yield to *p*-xylene using H-ZSM-5 (30) and H-ZSM-5 (30.2).

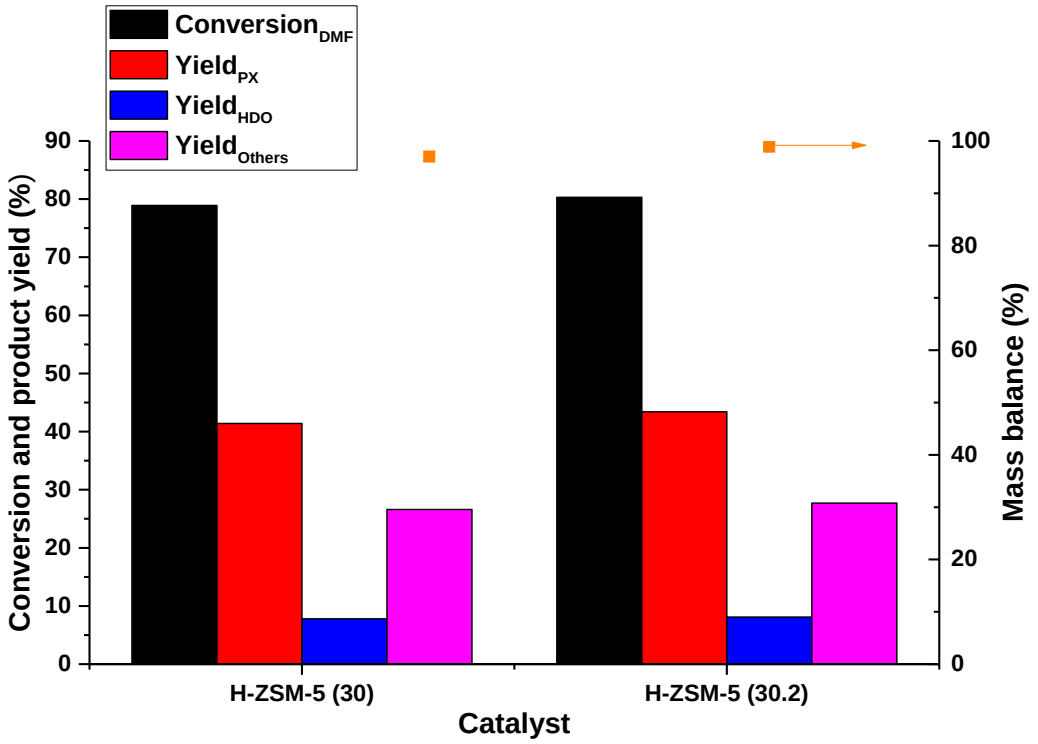

Figure 5.22 Conversion, and yields for known products for the Diels-Alder cycloaddition of DMF (1.5 M) with ethylene (55 bar) at 200 ºC for 20 hours for H-ZSM-5 (30 and 30.2).

Figure 5.22 showed that comparison of the parent H-ZSM-5 (30) catalyst, conversion was significantly reduced at lower temperatures, with the yield of *p*-xylene decreasing in accordance. Interestingly, it was found that reactions carried out at 220 ºC displayed improved yields of HDO which confirms there is an inverse proportional relationship between temperature and yield of HDO produced. It is clear that higher temperatures favours acid catalysed dehydration of HDO as opposed to acid catalysed hydrolysis of DMF. When we compared H-ZSM-5 (30) to H-ZSM-5 (30.2), we could see that conversion of DMF was slightly enhanced

from 78.9% for the zeolite, H-ZSM-5 (30) to 80.3% for H-ZSM-5 (30.2), with H-ZSM-5 (30.2) obtaining a slightly higher yield of *p*-xylene than its unmodified parent. The slight increase of yield of HDO for H-ZSM-5 (30.2) is a direct consequence of enhanced yield of *p*-xylene.

5.6.2.2.9 Conversion of 2,5-hexanedione to *p*-xylene

Due to the unexpected results obtained in section 5.6.2.2.5, where the alkaline treated zeolites displayed worse catalytic activity than their unmodified parent, the production of DMF and *p*-xylene was investigated using HDO as the initial substrate. The reaction was carried out using 1.5 M HDO using acetonitrile (ACN) as a solvent at 220 ^{o}C with 0.12 g of H-Beta (25) as the catalyst. The concentration of the products was determined using the calibration curve with hexane as the solvent. 1 μL was taken from the stock solution and injected into the GC and used as the blank. Prior to heating, the reaction vessel was pressurised to 10 bar using ethylene and then heated to 220 ^{o}C. The vessel was pressurised to 50 bar. The reaction was carried out for 8 hours.

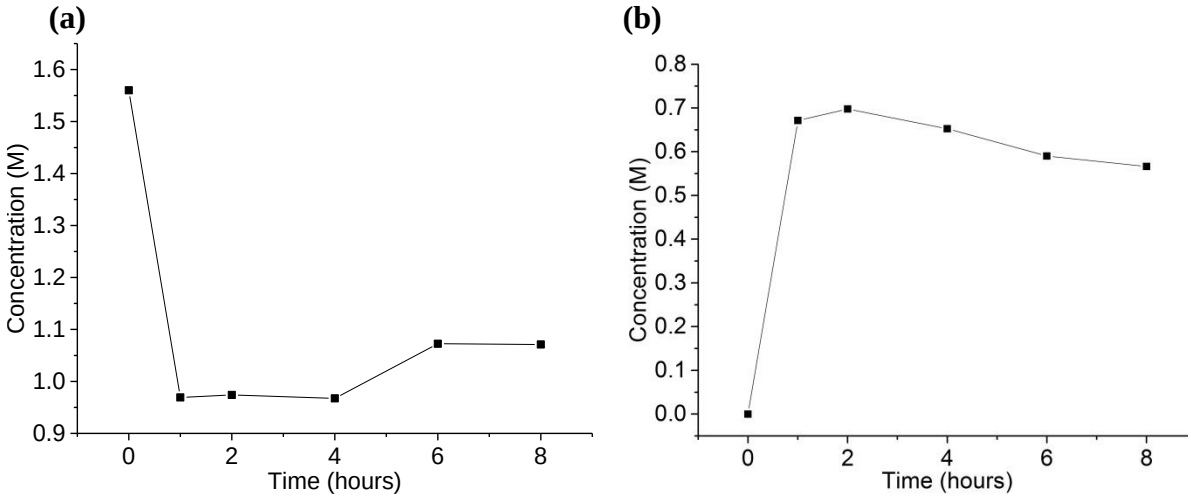

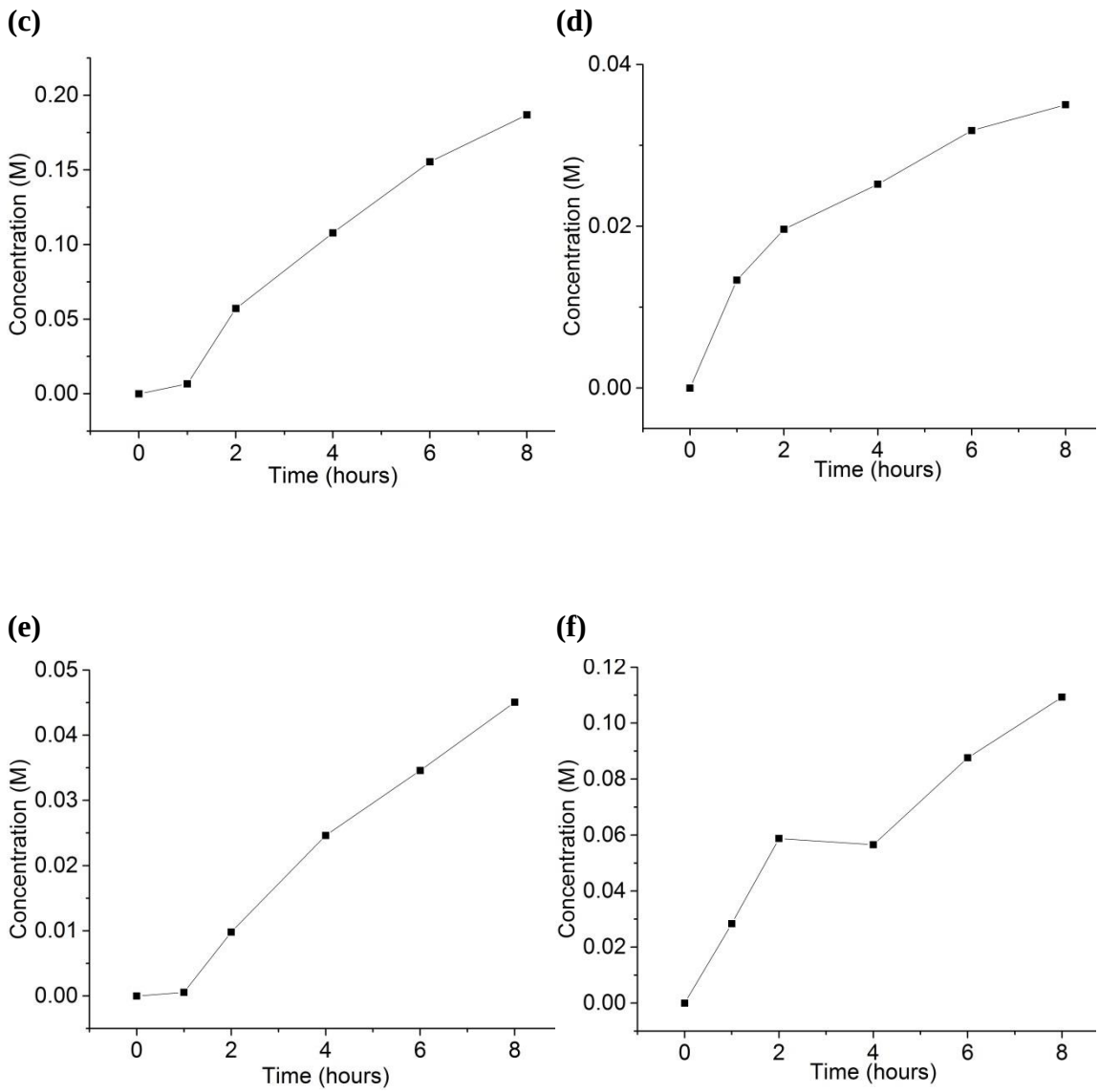

Figure 5.23 Concentration of products as a function of time for the reaction of HDO over H-Beta (25) at 220 °C, 55 bar, 8 hours (a) HDO, (b) DMF, (c) PX, (d) MCP, (e) AP, (f) HA.

The reaction profile showed after one hour that the concentration of HDO decreased from 1.6 M to 1.0 M, while the concentration of DMF was approximately 0.7 M, due to the Brønsted acid catalysed dehydration of HDO. The formation of *p*-xylene was clearly due consumption of DMF reacting with ethylene. It can be seen from the results that the formation of HDO is enhanced after 4 hours due to Brønsted acid catalysed hydrolysis of DMF. It can clearly be seen that the formation of higher aromatics is more pronounced after 2 hours and continued to increase with increasing formation of *p*-xylene due to undesired condensation reactions of *p*-xylene.

5.6.2.2.10 Time online studies of DMF to *p*-xylene and related products

In this study, kinetic studies were carried out using 0.12g of H-ZSM-5 (30), 30 mL of 3 M of DMF dissolved in octane at 250 ^{o}C (controlled by a 4848B Parr unit) for 24 hours under stirring (1,100 rpm). The reaction was carried out using a 50 mL bench-top reactor (Parr model 4597) equipped with an auto sampling valve. Samples were taken at time intervals (1,2,3,4, 18, 20 and 24 hours). The reaction vessel was pressurised to 50 bar after each sample was taken.

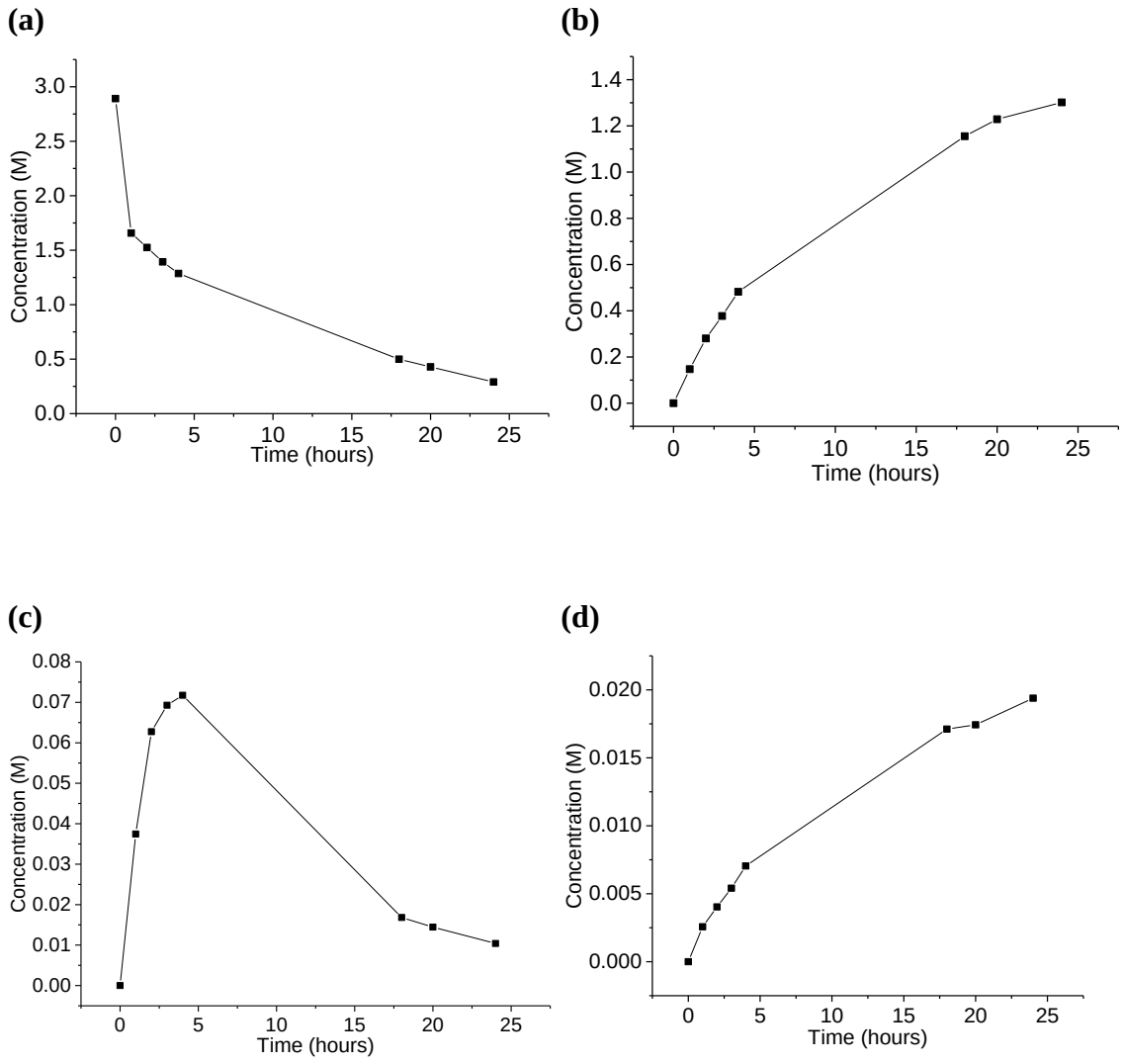

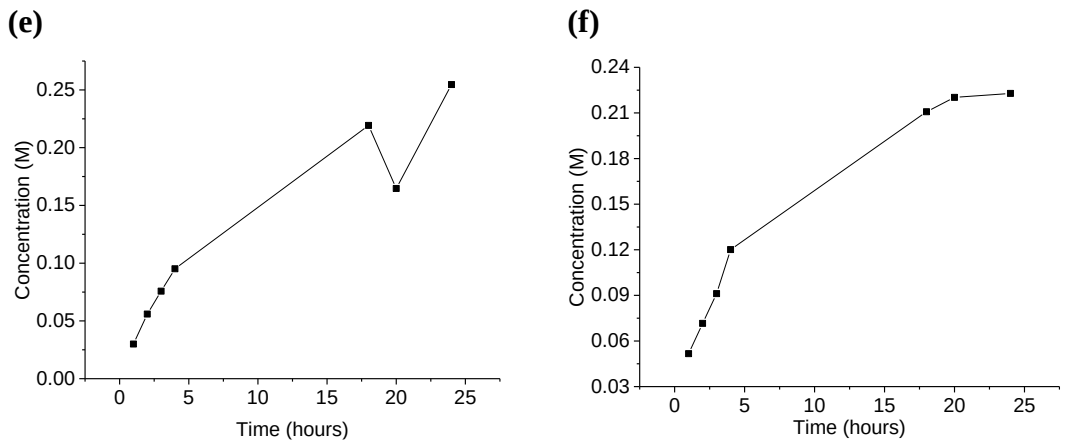

Figure 5.24 Concentration of products as a function of time for the reaction of DMF over H-ZSM-5 (30) at 250 °C, 55 bar, 24 hours (a) DMF, (b) PX, (c) HDO, (d), MCP, (e) AP, (f) HA.

Time online studies for the reaction of DMF and ethylene showed that after 4 hours, the concentration of DMF decreased from 2.89 M to 1.3 M due to the formation of the cycloadduct product. The final concentration of DMF after 24 hours was 0.3 M. The rate of reaction slowed probably to catalyst deactivation due to pore blocking. The concentration of *p*-xylene was 0.5 M after four hours due to dehydration of the cycloadduct product. After 24 hours, the concentration of *p*-xylene was 1.3 M, which confirms the rate of formation of *p*-xylene was faster within the first 4 hours of reaction. Figure 5.24 (c) shows the concentration of HDO after the initial 4 hours was 0.07 M. However, the concentration of HDO started to decrease after 4 hours, likely due to the re-formation of DMF due to acid catalysed dehydration and intramolecular aldol reaction of HDO.

5.6.2.2.11 Reproducibility and Recycling Studies

One of the most important features of a solid acid catalyst is its ability to show reproducible results and, more importantly, is able to show that it can be regenerated after catalytic tests and produce reproducible data. This study investigated both of these parameters. The reaction conditions were carefully chosen to show moderate conversion with considerable amounts of *p*-xylene and higher aromatics produced. All reactions were carried out in series. Typically, 37 mL of DMF (1.5 M) in dodecane with 180 mg of H-ZSM-5 (30) was added to a 75 mL stainless steel vessel and purged with nitrogen. The vessel was heated to 220 °C and pressurised to a total pressure of 55 bar with ethylene. The reaction was carried out for 2 hours. After the reaction was allowed to cool, the spent

catalyst were filtered and washed with cold ethanol and dried in an oven overnight at 110 ^{o}C. The resulting brown catalyst clearly indicated that the catalyst had been deactivated after 2 hours due to coking. The spent catalyst was then calcined as described in section 3.2.1 to remove the carbonaceous species from the catalyst. After calcination, the catalyst had turned from brown to white, clearly indicating the removal of all carbonaceous species deposited on the external and internal surface. After the end of the third cycle, the calcined catalyst was characterised by TPD to determine the change in acidity after multiple calcination steps, XRD to determine any significant change in crystallinity and surface area and porosity measurements. For the purpose of this study, only conversion and yield of *p*-xylene obtained is discussed. The results of the catalytic testing are shown in Table 5.4 (below).

Table 5.4 Reproducibilty and recycling studies using H-ZSM-5 (30). Reaction conditions; 180 mg catalyst, 1.5 M DMF, 220 ^{o}C, 2 hours, 55 bar total pressure.

Regeneration number	S_{BET} (m^2 g^{-1})[a]	V_{total} (cm^3 g^{-1})[b]	Conversion (%)	Yield PX (%)	Mass balance (%)
0	344	0.25	29.1	11.3	96.8
0	344	0.25	31.7	12.5	96.0
0	344	0.25	33.0	12.2	94.7
1	n/a	n/a	31.1	11.7	95.1
1	n/a	n/a	30.6	11.6	95.4
2	362	0.26	21.5	7.1	96.3

(a) determined by BET method, (b) determined by single point adsorption (P/P_o = 0.99).

The results show that during the first cycle, conversion of DMF was 29.1%, 31.7% and 33.0% with yields of 11.3%, 12.5% and 12.2% obtained for *p*-xylene. This clearly shows that the catalyst generates reproducible data after taking into account experimental error. During the second cycle, it was found that conversion and yield of to *p*-xylene was largely unchanged compared to the first cycle, demonstrating the catalyst's excellent regeneration properties. During the third cycle, conversion decreased to 21.5% with a yield of 7.1% obtained for *p*-xylene. TPD studies showed that after the third cycle, the total number of acid sites of H-ZSM-5 (30) decreased from 581 μmol g^{-1} for the fresh catalyst to 323 μmol g^{-1} for the spent catalyst, largely due to dehydroxylation. XRD patterns (not shown here) showed that the regeneration of the catalyst by calcination did not result in the loss of crystallinity. Surface area and porosity measurements conducted on the catalyst prior to

the first cycle and after the third cycle showed that the surface area and total porosity remained unchanged, which indicates that all the carbonaceous products had been removed after calcination at 550 ^{o}C. This shows that the decrease in activity in the last cycle cannot be due to pore blockage from previous tests and loss of crystallinity. Therefore, loss of activity after the 2nd regeneration was primarily due to the loss of acidity by dehydroxylation.

5.6.2.2.12 Effect of pressurisation at room temperature versus elevated temperature

The overwhelming majority of our experiments focused on the work carried out by the group of Dauenhauer[41, 45, 245] which subsequently pressurised their system at the final temperature. The principal reason for this was to monitor precisely the time of t_0. More recently, there have been studies which have been carried out with pressurisation of the vessel at room temperature.[42, 44, 264] However, to the best of our knowledge, there is no study which determines whether conversion is affected by the addition of ethylene at room temperature, or at elevated temperature. The main target of this study was to determine whether pressurising the system at room temperature or at the desired reaction temperature would influence the conversion, and therefore, yield to the desired product, *p*-xylene. The reaction was carried out as follows; in vessel I, DMF (1 M) in hexane and 180 mg commercially unmodified H-ZSM-5 (30) was added to a 75 mL stainless steel vessel. The vessel was heated to 180 ^{o}C and then pressurised to a total pressure of 40 bar using ethylene. In vessel II; the vessel was pressurised at room temperature with ethylene and heated to 180 ^{o}C. The corresponding pressure at 180 ^{o}C was 40 bar. The reactions in vessels I and II were carried out for 20 hours.

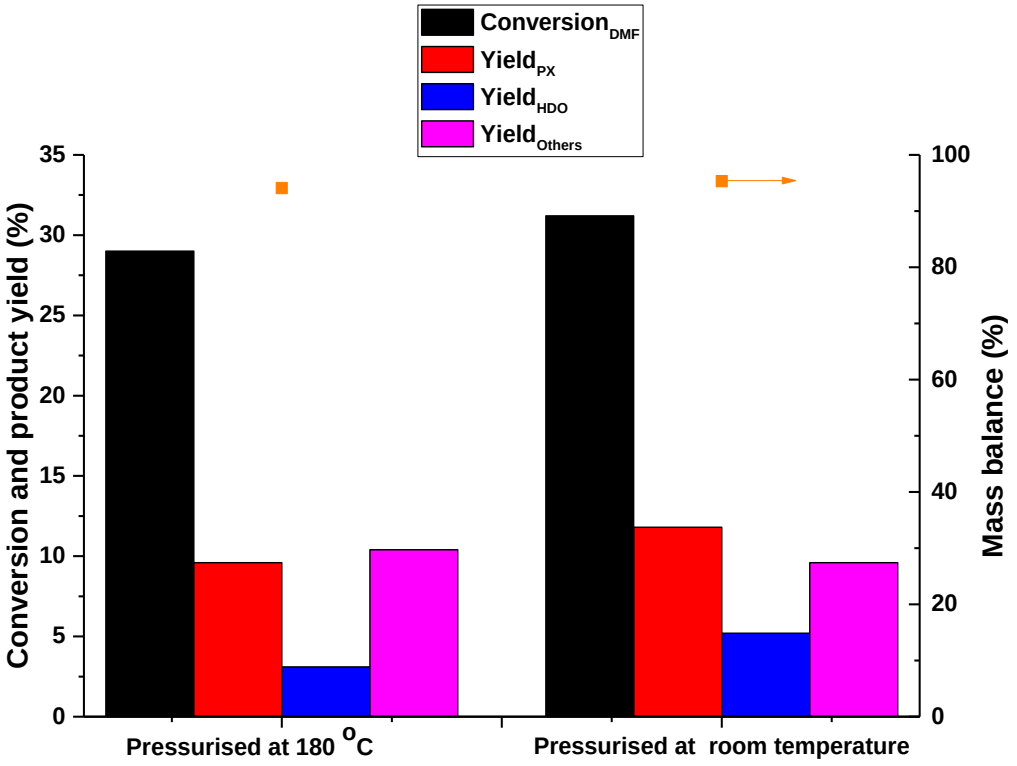

Figure 5.25 The effect of pressurisation at elevated pressure and room temperature on conversion, and yields for known products for the Diels-Alder cycloaddition of DMF (1 M) with ethylene at 180 °C for 20 hours for H-ZSM-5 (30).

The conversion of DMF over the zeolite H-ZSM-5 (30), pressurised at 180 °C is 29.0% with 9.6% yield of *p*-xylene obtained. When ethylene was added at room temperature, the conversion of DMF was similar to that carried out when the vessel was pressurised at the desired temperature. The yield of *p*-xylene increased only slightly to 11.8%. This translated into improved yield of HDO when the vessel was pressurised at room temperature. Interesting to note is that pressurising the vessel at the desired temperature showed slightly higher yields of MCP, alkylated and higher aromatics. Despite pressurising the vessel at the desired temperature resulted in slightly lower conversion, it can also be seen that a slightly lower mass balance was obtained. This strongly suggests the formation of uncalibrated products.

5.6.2.2.13 Effect of the calcination temperature on catalytic activity

In an effort to understand the effect of acidity of catalytic activity, the [4+2] reaction of DMF with ethylene, H-ZSM-5 (30) with varying acidity was investigated. The reaction

was carried out using DMF (1.5 M) in hexane at 180 ºC with a total pressure of 40 bar. The reaction was carried out for 20 hours. Commercially obtained H-ZSM-5 (30) zeolites in the ammonium form were calcined at temperatures 550-750 ºC for 6 hours with a heating ramp of 1ºC min^{-1}. After calcination, the acid site density of each catalyst was determined using TPD-NH_3. Surface area and porosity measurements were not conducted. It was assumed that surface area and porosity was largely unaffected with varying calcination temperatures.

Table 5.5 The effect of calcination temperature on the conversion of DMF and yield to *p*-xylene using H-ZSM-5 (30). Reaction conditions; 180 mg catalyst, 1.5 M DMF, 180 ºC, 40 bar, 20 hours.

Calcination temperature (ºC)	Total acid sites (μmol g^{-1})	Conversion (%)	Yield (%)			Mass balance (%)
			PX	HDO	Others[a]	
550	581	29.0	9.6	3.1	10.4	94.1
650	524	31.7	10.3	5.3	9.7	93.6
750	460	33.7	11.1	5.6	10.1	93.1

(a) others include MCP, alkylated and higher aromatics.

Table 5.5 shows acid site density decreased from 581 μmol g^{-1} for H-ZSM-5 (30) calcined at 550 ºC to 524 and 460 μmol g^{-1} to H-ZSM-5 (30) zeolites calcined at 650 and 750 ºC respectively, due to dehydroxylation. At this stage, it is difficult to ascertain the slight increase in catalytic activity with H-ZSM-5 (30) zeolites with lower acidity without considering experimental error. With the assumption that increased calcination temperature had no effect on the resulting porosity, it could be possible that despite varying acid concentrations, that the very similar catalytic activities could be due to inaccessibility of the acid sites. Therefore, studies with large probe molecules such as collidine are required to quantify accessibility of the acid sites.

5.7 Conclusions

In this study, H-ZSM-5 zeolites were synthesised using conventional heating with comparable properties of H-ZSM-5 obtained from the manufacturer, Zeolyst

International. FT-IR studies showed that the laboratory synthesised H-ZSM-5 (100)-H and H-ZSM-5 (180)-H zeolites by conventional heating displayed the stretching bands typical for H-ZSM-5 zeolite. ICP-OES measurements of H-ZSM-5 (100)-H and H-ZSM-5 (180)-H closely matched the SiO_2/Al_2O_3 molar ratio of the precursor solution. TPD-NH_3 showed H-ZSM-5 (100)-H and H-ZSM (180)-H displayed total acidities of 181 and 182 μ mol g^{-1} respectively. Solid state NMR studies showed H-ZSM-5 (100) possessed aluminium atoms predominately located in the framework position (96.8%), with ^{29}Si MAS-NMR studies showing a highly siliceous zeolite had been synthesised with 68.8% of the structure being Si-O-Si in nature. ^{27}Al and ^{29}Si-MAS NMR studies confirmed the presence of extra-framework aluminium. Surface area and porosity measurements by nitrogen sorption confirmed that the laboratory synthesised H-ZSM-5 (100)-H and H-ZSM-5 (180)-H were porous, with specific surface and porosity comparable to the commercially obtained H-ZSM-5 zeolites. Untemplated H-ZSM-5 (100) synthesised using conventional (Chapter 5) and microwave assisted heating (Chapter 4) showed similar specific surface areas (376 m^2 g^{-1} and 363 m^2 g^{-1} respectively).

The addition of polystyrene nanospheres (30 and 60 nm) to the precursor gel generated H-ZSM-5 catalysts with enhanced specific surface area and porosity compared to their untemplated counterparts with specific surface areas greater than 600 m^2 g^{-1} for templated H-ZSM-5 compared to $\leq$ 376 m^2 g^{-1} for untemplated H-ZSM-5. However, due to the poor crystallinity obtained with the lower crystallisation temperature utilised in the templated synthesis, the acidities of the resulting materials were lower than those synthesised at higher temperatures. Chemical analysis of the hierarchical H-ZSM-5 zeolites prepared using polystyrene nanospheres showed SiO_2/Al_2O_3 molar ratios slightly higher than their untemplated counterparts. ^{27}Al NMR studies conducted on H-ZSM-5 (100)-H-PS30 zeolites showed that 62.7% of the aluminium species was located in the framework position.

Studies confirmed that the zeolite showed appreciable reproducibility and regeneration capabilities after calcination at 550 ^oC. We have also demonstrated that hierarchical zeolites prepared by a top down approach and a bottom up

approach, can be beneficial in the cycloaddition of DMF with ethylene reaction compared to their unmodified parent. Desilication increased conversion by 51% in the case of H-ZSM-5 (30.2) compared to its untreated parent, H-ZSM-5 (30). Also, elevated temperatures and increased ethylene pressure were able to significantly enhance conversion and aromatic yield. Catalytic studies carried out at 250 ^{o}C and 55 bar showed enhanced yields of *p*-xylene, with the suppression of the unwanted side product 2,-5-hexanedione. Our study showed that desilication of zeolites using sodium hydroxide showed conversion increased nearly 3 fold for H-ZSM-5 (80.2) compared to H-ZSM-5 (80), with H-ZSM-5 (80.2) showing 62.8% conversion and a 30.3% yield of *p*-xylene, compared to 21.1% conversion and 9.1% yield of *p*-xylene obtained for H-ZSM-5 (80). Studies of templated H-ZSM-5 showed increased catalytic activity compared to the untemplated H-ZSM-5 catalyst, with H-ZSM-5 (100)-MW-PS60 displaying 42.8% conversion compared to 30.9% conversion for H-ZSM-5 (100)-MW. Templation of H-ZSM-5 with a SiO_2/Al_2O_3 molar ratio of 100 with polystyrene (60 nm) generally resulted in ca. 9-10% yields of *p*-xylene, compared to 5-7.5% yields of *p*-xylene produced for untemplated H-ZSM-5. Overall, it could be concluded that the generation of mesoporosity in the zeolites reported in this study is highly advantageous for catalytic conversion of DMF to renewable *p*-xylene.

5.8 Future work

Our study has shown that increased porosity can generate higher yields of renewable *p*-xylene from DMF compared to less porous zeolites. To the best of our knowledge, there does not appear to be a study that shows a 100% yield of *p*-xylene produced in the cycloaddition of DMF with ethylene in the liquid phase using zeolites. This is largely due to unwanted side reactions forming oligomers. Although we have shown that higher temperatures can reduce the formation of HDO, further studies are still required to completely suppress the formation of HDO. It must be remembered that HDO is formed due to acid catalysed hydrolysis of DMF. Therefore, further studies are required to trap the water molecules produced from the dehydration of the cycloadduct product. In addition, it is not clear what role water plays in the formation of the higher aromatics. Future studies are required to separate and identify the higher aromatics produced. Do et al.[265] obtained a product distribution of some of the higher aromatics. However,

subsequent studies have never attempted to quantify the higher aromatics. They are generally disregarded and classed as “unidentified products”. A new study has shown that ethanol could be used as a substitute to ethylene to generate renewable *p*-xylene from DMF.[266] This would be extremely advantageous since ethanol is significantly cheaper than ethylene.

Chapter 6

Conclusions and Outlook

6 Conclusions and Outlook

There were three main objectives of the work carried out in this thesis. The first was the development of zeolites with larger pore volumes than their parent using a top down approach, such as treatment of conventional H-ZSM-5, H-Beta and H-Y with 0.2 or 0.4 M sodium hydroxide solution to remove silicon from the structure, generating mesoporosity.

The second objective was using a hard template to produce hierarchical zeolites directly in one step in the microwave. When our work began, most studies were limited to templation of ZSM-5 using carbonaceous species, and these materials do not have a well-defined shape or size. Our focus has been driven towards the use of polystyrene as a hard templating agent as its application was limited, with the majority of the studies focused on templation of silicalite-1 or using too large PS nanoparticles of 280 nm.

The final objective of the work carried out in this thesis was the catalytic testing of hierarchical H-ZSM-5, H-Beta and H-Y, synthesised by post synthesis treatment using 0.2 or 0.4 M NaOH and microwave synthesised hierarchical H-ZSM-5, H-Beta and H-Y prepared by templation or by 0.2 NaOH on the Diels-Alder cycloaddition reaction of 2,5-dimethylfuran with ethylene. The primary objective was achieving higher yields of aromatics, especially *p*-xylene compared to conventional H-ZSM-5, H-Beta and H-Y. A summary of conclusions Chapters 3-5 are summarised below.

In Chapter 3, XRD studies showed that for H-ZSM-5, crystallinity was generally preserved after alkaline treatment with 0.2 M NaOH. Surface area measurements showed that alkaline treatment generally increased the total pore volume, with one example from 0.25 cm^3 g^{-1} for the parent to 0.73 cm^3 g^{-1} for the desilicated sample. Acidity measurements showed that alkaline treatment resulted in an increase in acid site density for H-ZSM-5, whereas alkaline treatment of H-Beta and H-Y resulted in a decrease in acid site density.

Testing of hierarchical zeolites in the Friedel-Crafts Alkylation of benzyl alcohol with benzene showed that increasing the initial concentration of benzyl alcohol from 0.14 M to 0.42 M showed that desilicated H-Y had greater catalytic activity than its untreated parent.

In Chapter 4, conventional H-ZSM-5 was synthesised in 6 hours using microwave assisted heating, compared to days when using conventional heating methods. Hierarchical H-ZSM-5 using polystyrene as a hard templating agent was synthesised using microwave assisted heating in 12 hours or less. Surface area and porosity measurements showed that conventional H-ZSM-5 had a surface area comparable to the surface area of H-ZSM-5 supplied by a manufacturer (363 m^2 g^{-1} and 376 m^2 g^{-1} respectively). Surface area and porosity measurements for hierarchical H-ZSM-5 showed higher surface areas and porosity measurements compared to the conventional zeolite, with an optimum specific surface of 620 m^2 g^{-1} obtained. Conventional and hierarchical H-ZSM-5 were synthesised with similar total acidities (88 µmol g^{-1} for the conventional H-ZSM-5 versus 97 µmol g^{-1} for hierarchical H-ZSM-5) and differing external pore volumes (0.23 cm^3 g^{-1} for conventional H-ZSM-5 versus 0.32 cm^3 g^{-1} for hierarchical H-ZSM-5).

Templated zeolites showed greater catalytic activity in the Friedel-Crafts Alkylation than their untemplated counterparts, confirming that polystyrene nanospheres is an extremely effective hard templating agent due to its versatile particle size.

In Chapter 5, the focus of this study was to determine whether hierarchical zeolites would show greater yields of aromatics, especially renewable *p*-xylene.

We found that hierarchical zeolites prepared by top-down and bottom-up approaches generally showed higher yields to *p*-xylene, with one example including hierarchical H-ZSM-5, prepared by microwave assisted heating resulting in 33% larger yields of *p*-xylene obtained compared to untemplated H-ZSM-5.

Overall, we conclude that hierarchical zeolites, prepared by both desilication and templation is beneficial for increasing yields of *p*-xylene. The synthesis of hierarchical H-ZSM-5 using polystyrene as a hard templating agent is still a relatively unexplored field, especially using microwave assisted heating. In this study, we have demonstrated that templating of H-ZSM-5 using microwave assisted heating can lead to fast synthesis times compared to conventional heating methods and it is very efficient to producing hierarchical zeolites by templation. It is clear that optimisation studies are required to generate higher mesoporosity with stronger acidity. We can conclude that this method could be applied to various zeolites such as H-Beta and H-Y. Hierarchical H-ZSM-5, H-Beta and H-Y with

varying acidities and mesoporosity could have wider industrial applications such as the Mobil process.

Chapter 7

Appendix

7 Appendix

7.1 Nitrogen adsorption-desorption isotherms

7.1.1 Chapter 3

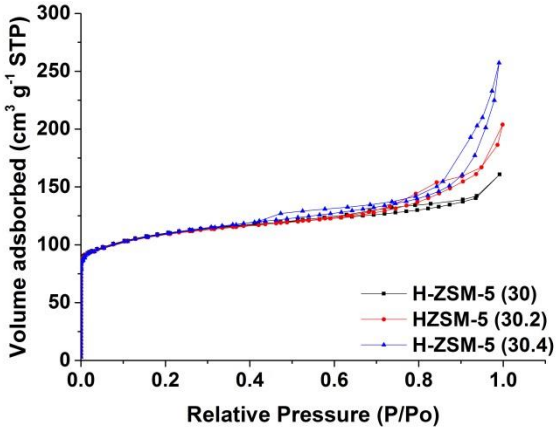

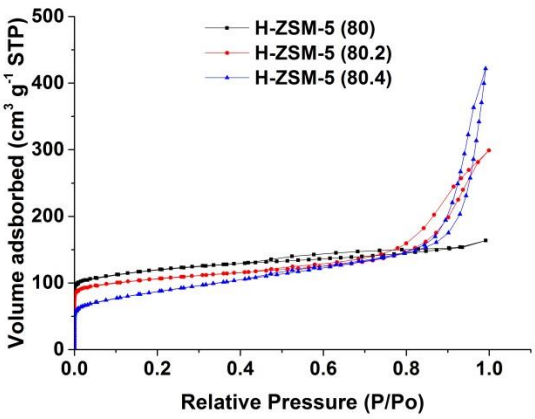

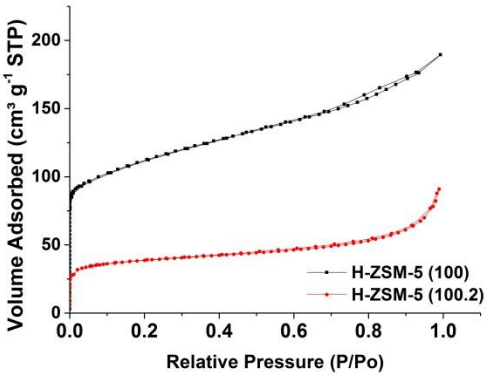

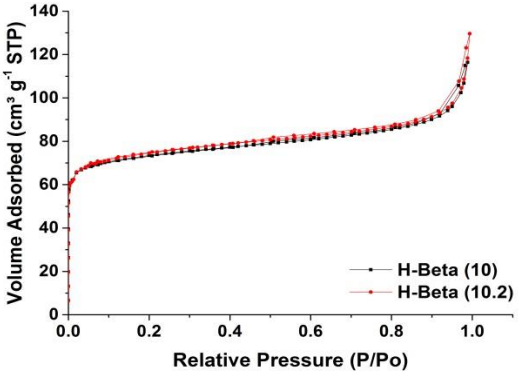

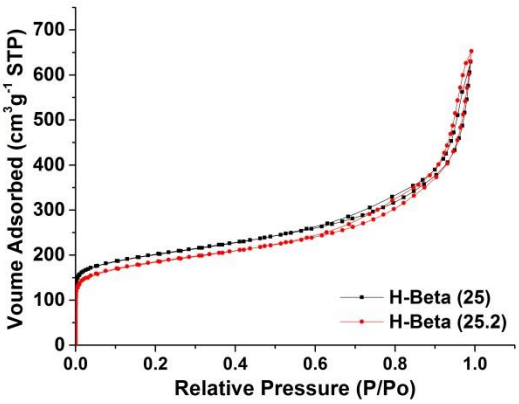

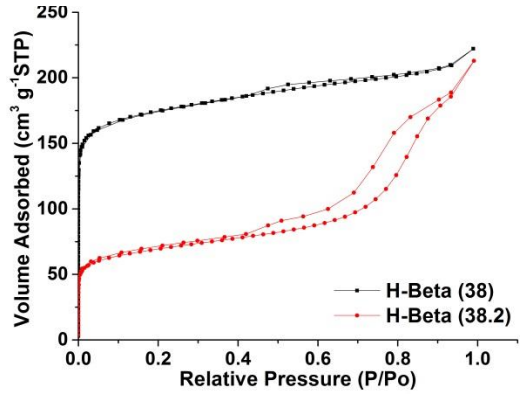

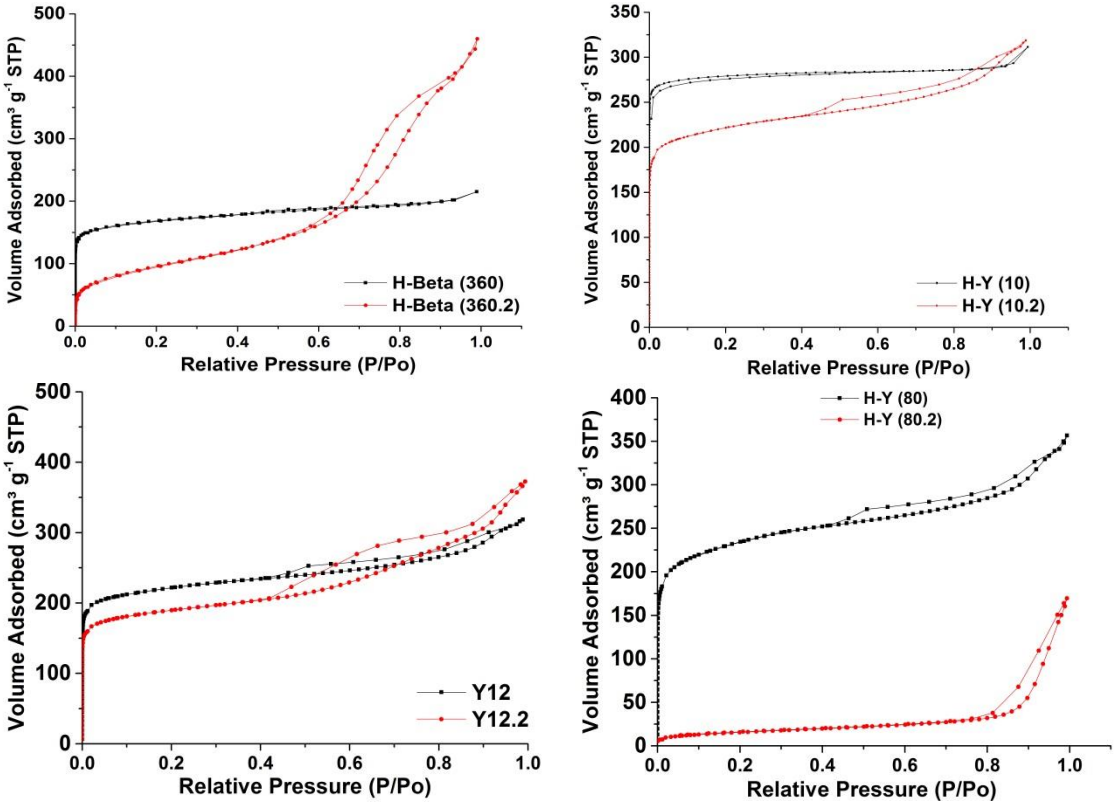

Figure 7.1 Nitrogen adsorption-desorption isotherms of zeolites from Chapter 3.

7.1.2 Chapter 4

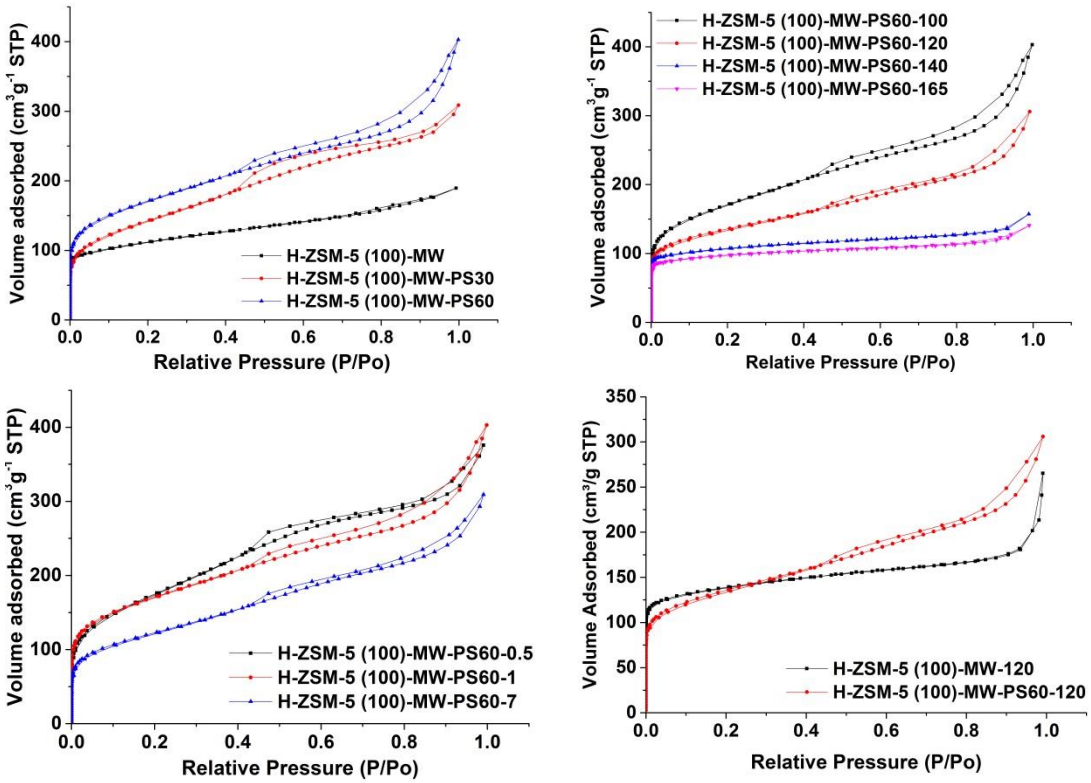

Figure 7.2 Nitrogen adsorption-desorption isotherms of zeolites from Chapter 4.

7.1.3 Chapter 5

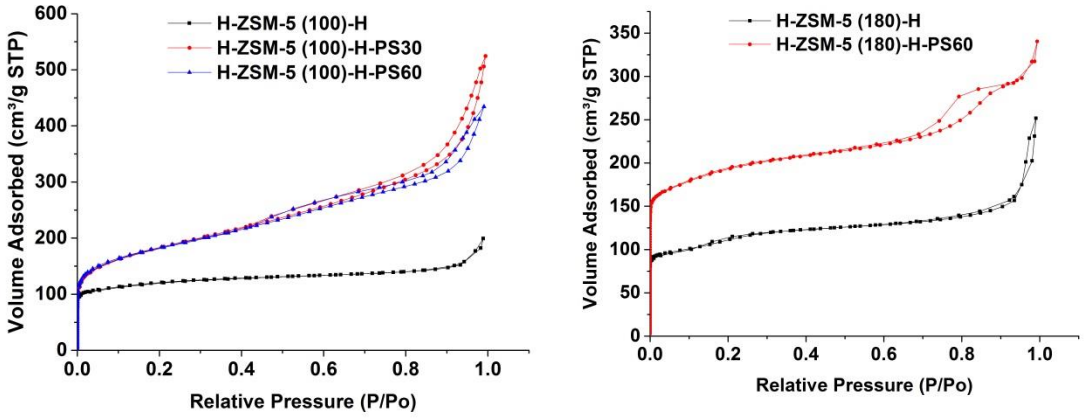

Figure 7.3 Nitrogen adsorption-desorption isotherms of zeolites from Chapter 5.

7.2 Temperature programmed desorption

7.2.1 Chapter 3

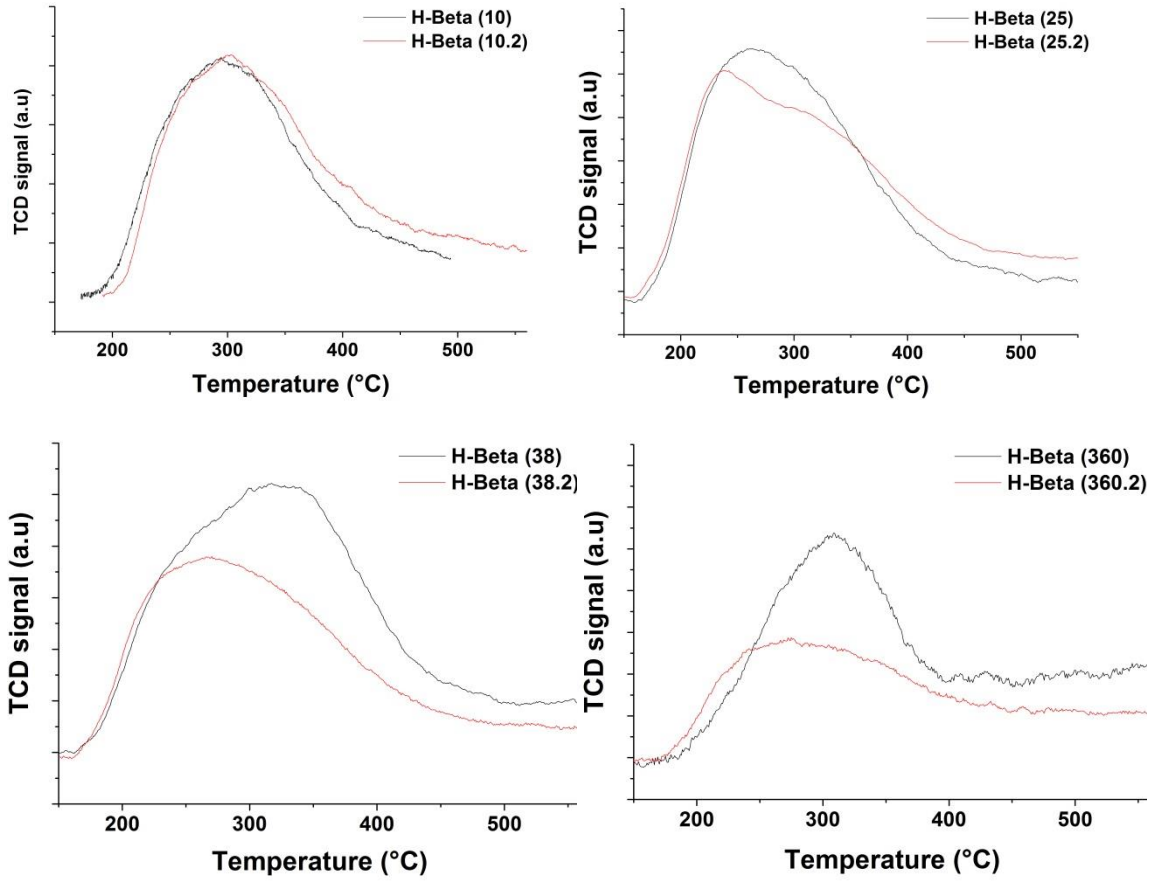

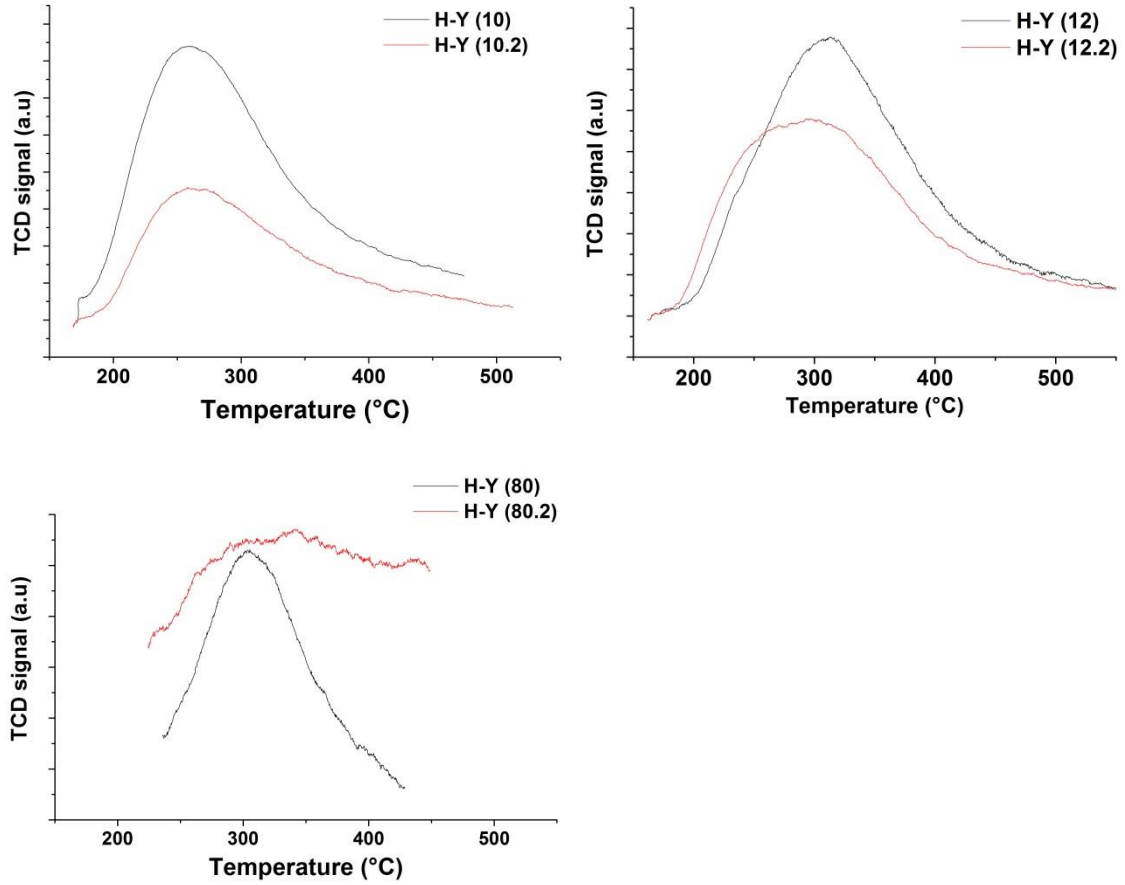

Figure 7.4 Temperature programmed desorption profiles of zeolites from Chapter 3.

7.2.2 Chapter 5

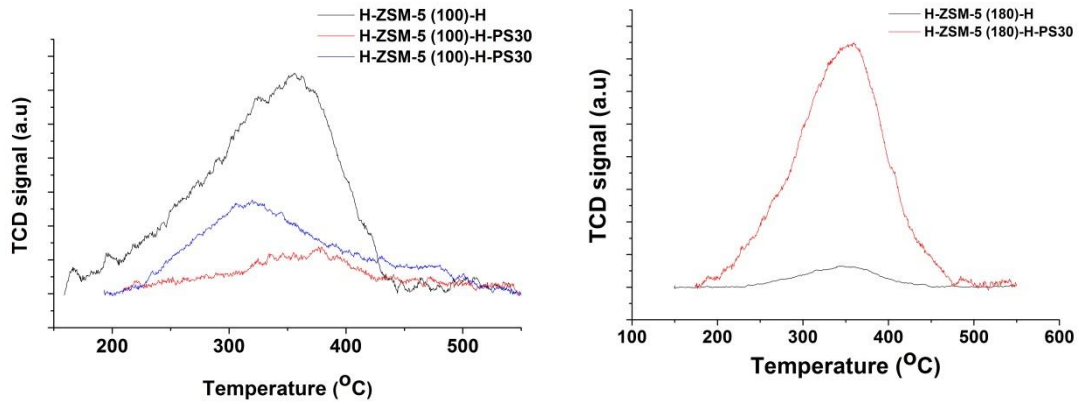

Figure 7.5 Temperature programmed desorption profiles of zeolites from Chapter 5.

7.3 Scanning Electron Micropscopy

7.3.1 Chapter 3

(a)

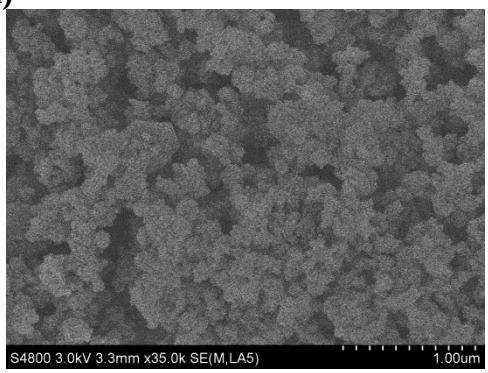

(b)

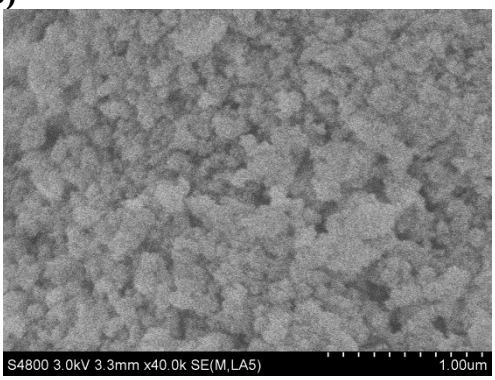

(c)

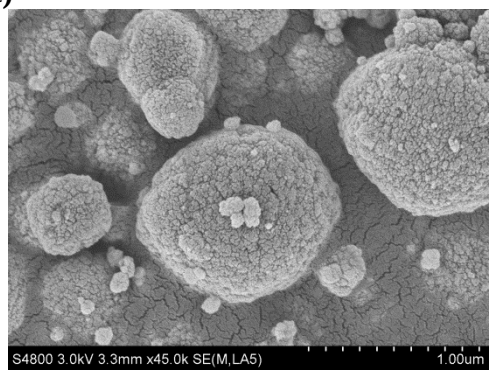

(d)

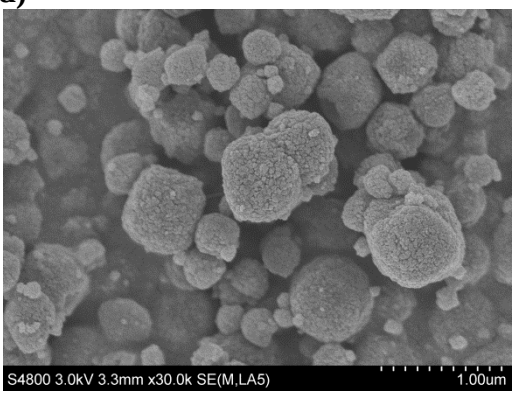

(e)

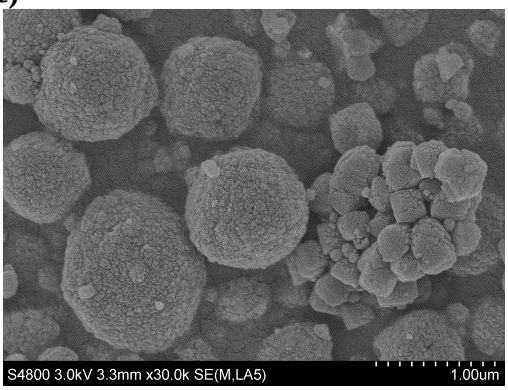

(f)

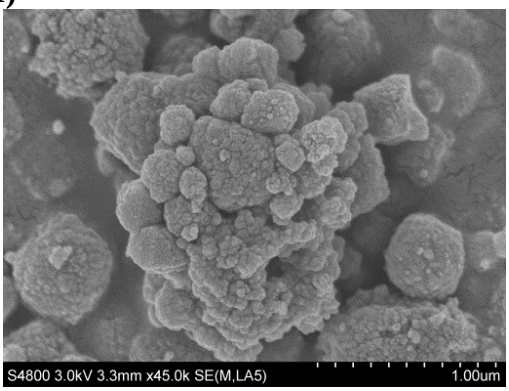

(g) **(h)**

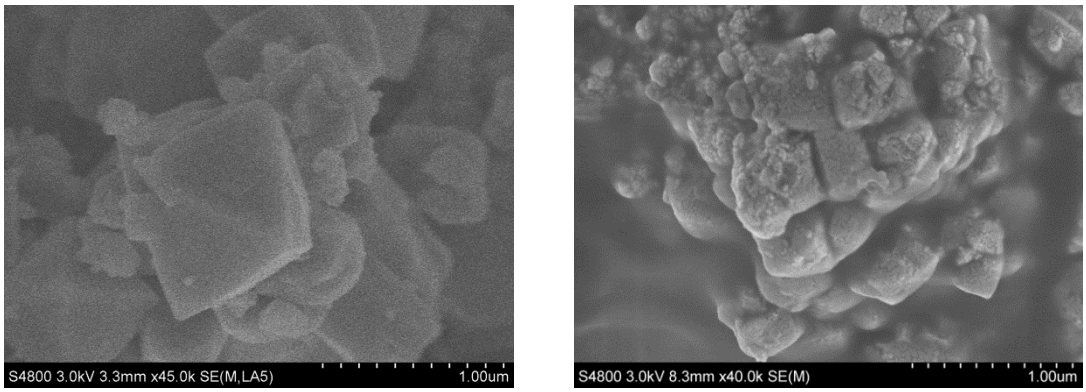

Figure 7.6 SEM images of (a) H-Beta (25), (b) H-Beta (25.2), (c) H-Beta (38), (d) H-Beta (38.2), (e) H-Beta (360), (f) H-Beta (360.2), (g) H-Y (10) and (h) H-Y (10.2).

7.4 Calibration curves

7.4.1 Calibration curves used for the Friedel-Crafts alkylation reaction

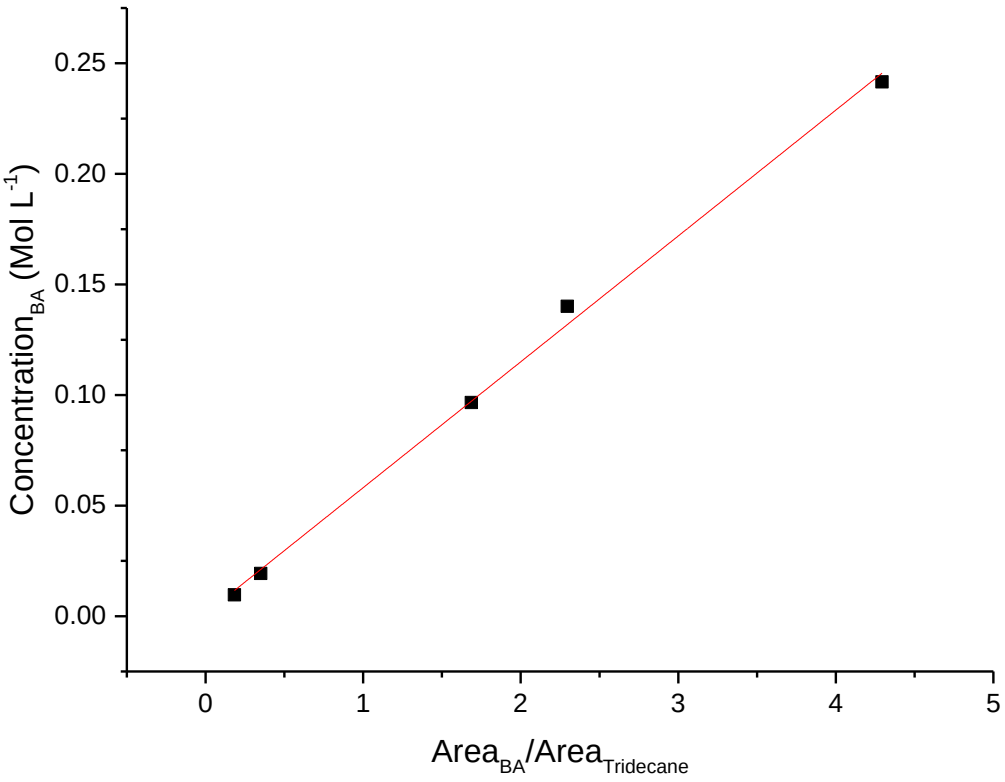

Figure 7.7 Calibration curve profile of Benzyl alcohol.

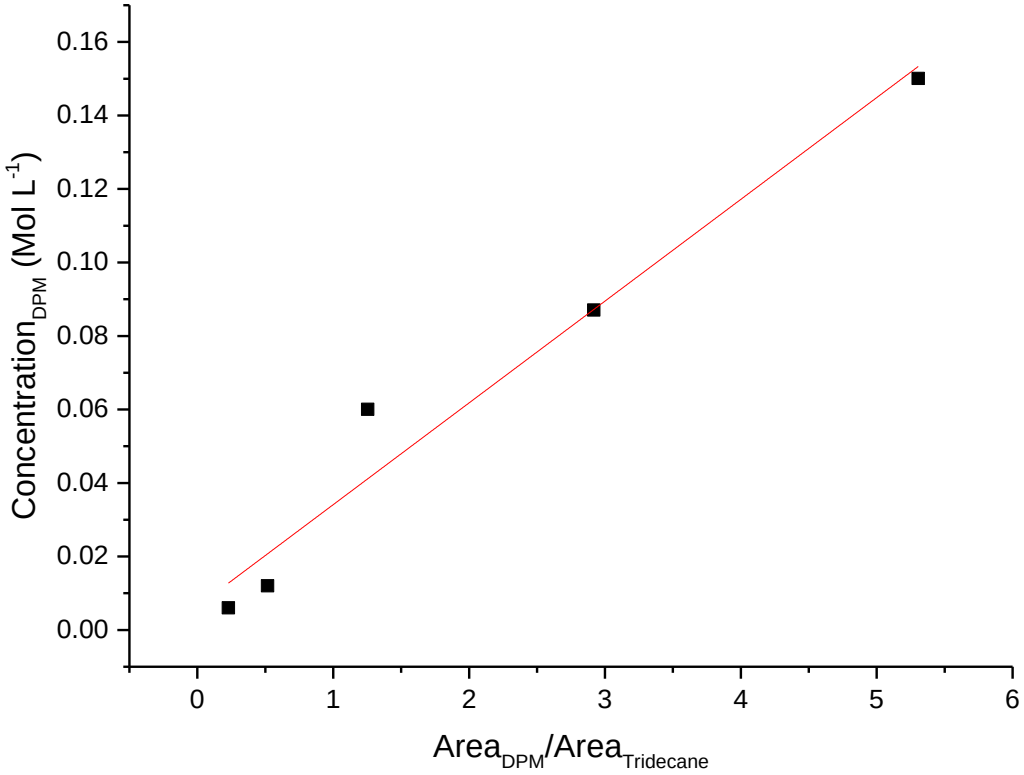

Figure 7.8 Calibration curve profile of Diphenylmethane.

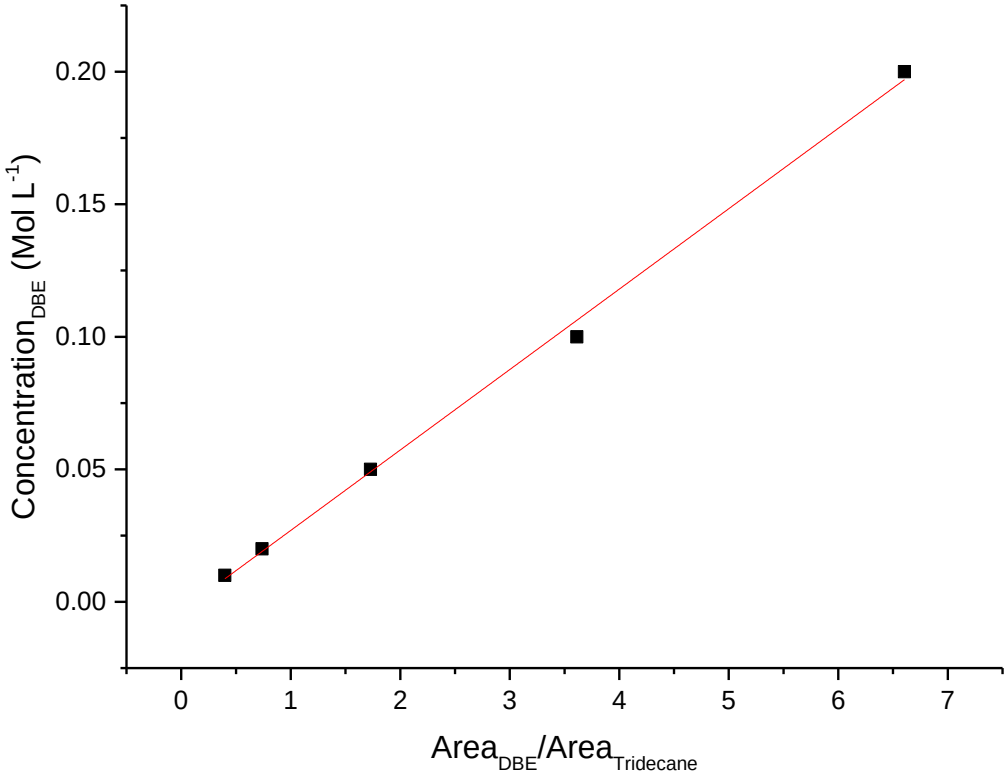

Figure 7.9 Calibration curve profile of Dibenzyl ether.

7.4.2 Calibration curves used for the Diels-Alder Cycloaddition reaction

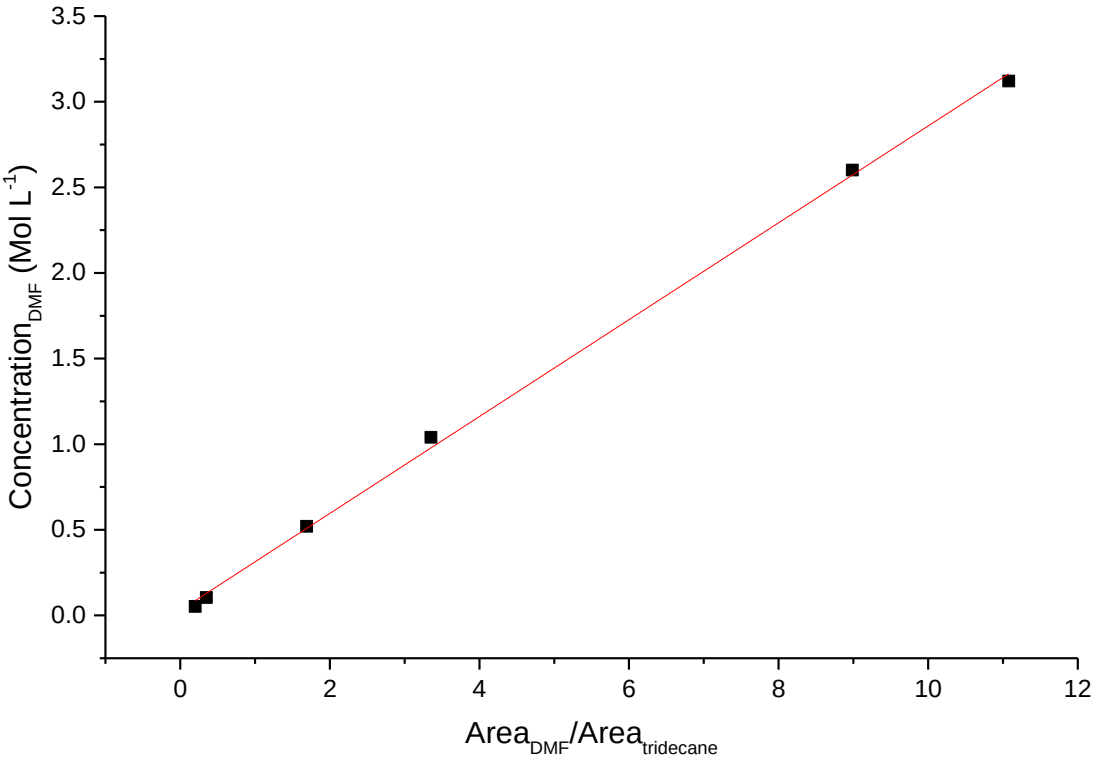

Figure 7.10 Calibration curve profile of 2,5-dimethylfuran.

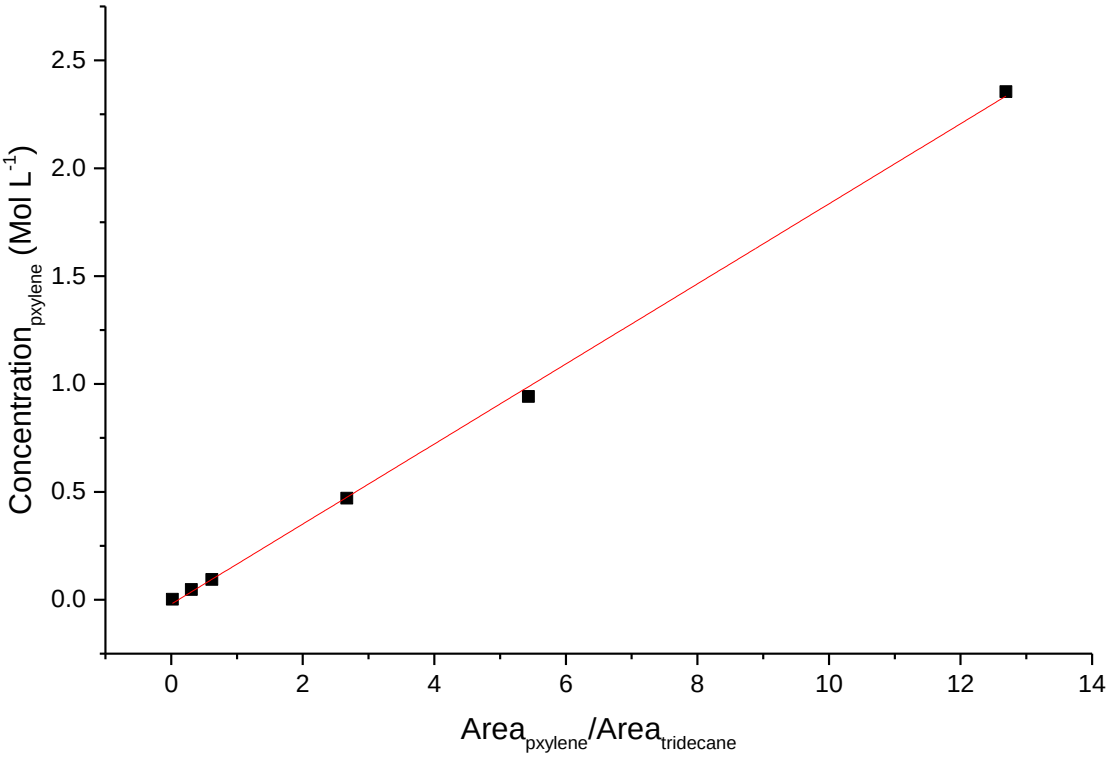

Figure 7.11 Calibration curve profile of *p*-xylene.

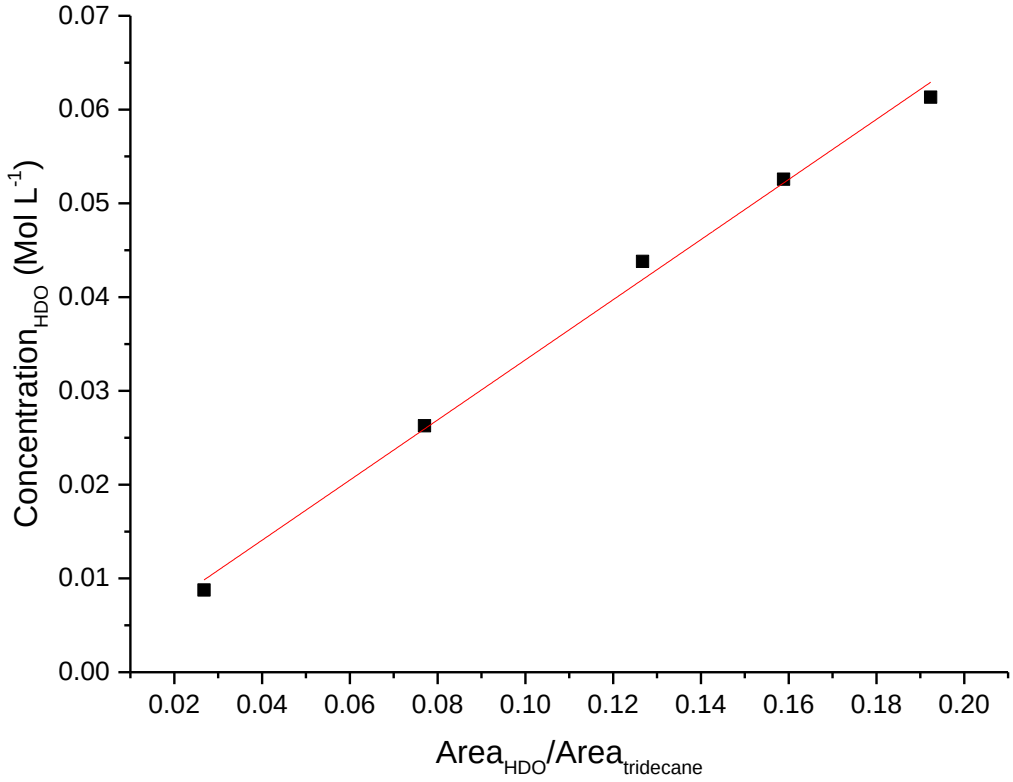

Figure 7.12 Calibration curve profile of 2,5-hexanedione.

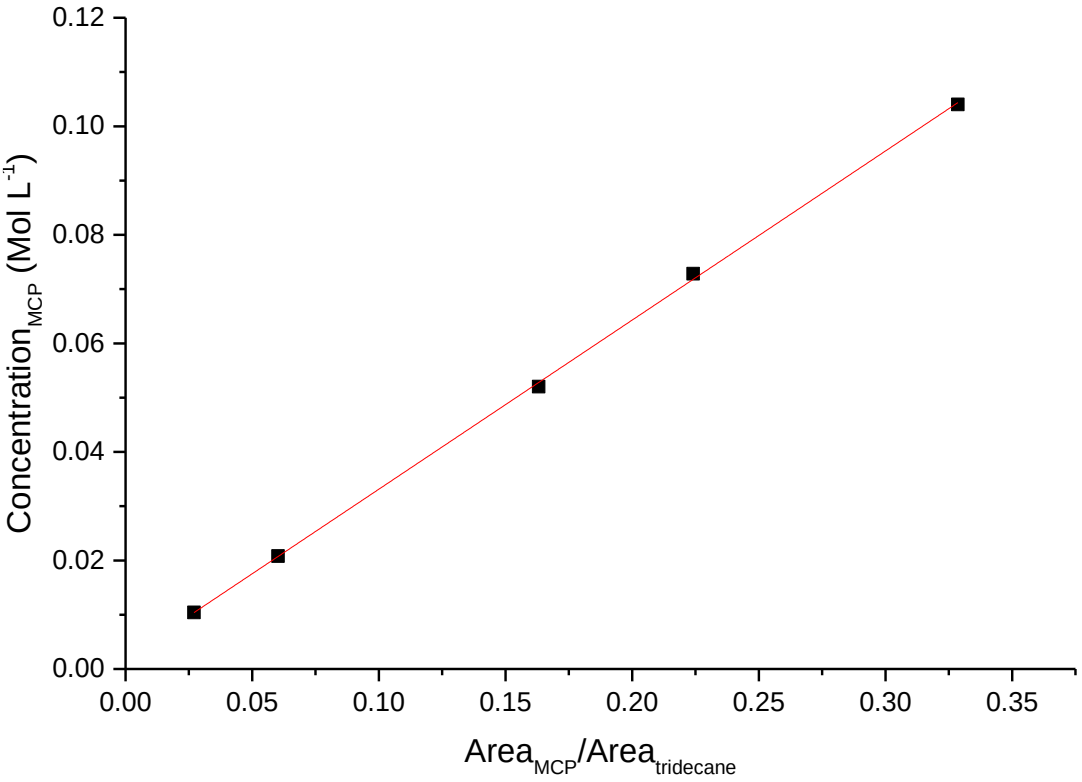

Figure 7.13 Calibration profile of 2-methyl-cyclopentenone.

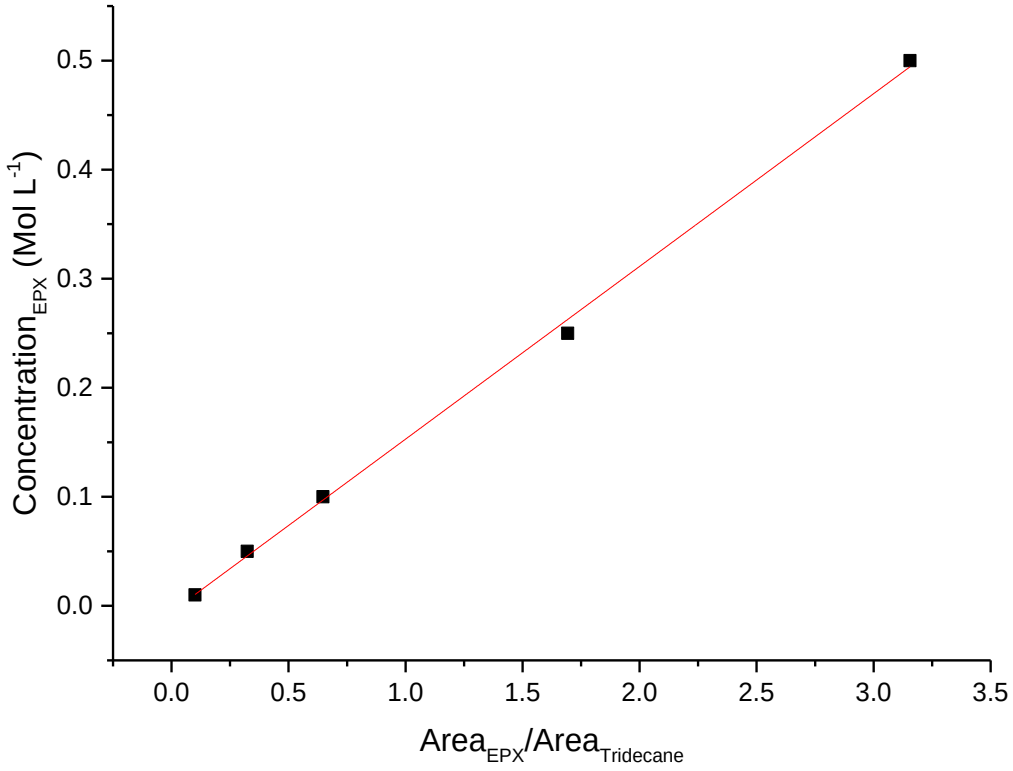

Figure 7.14 Calibration profile of 2-ethyl-*p*-xylene.

8 References

1. J. N. Chheda, G. W. Huber and J. A. Dumesic, *Angew Chem Int Edit*, 2007, **46**, 7164-7183.
2. F. Z. Alvise Perosa, *Methods and Reagents for Green Chemistry: An Introduction*, 2007, 203.
3. P. Maki-Arvela, T. Salmi, B. Holmbom, S. Willfor and D. Y. Murzin, *Chem Rev*, 2011, **111**, 5638-5666.
4. R. A. Sheldon, *Green Chemistry*, 2014, **16**, 950-963.
5. J. A. Melero, J. Iglesias and A. Garcia, *Energy & Environmental Science*, 2012, **5**, 7393-7420.
6. S. Deguchi, K. Tsujii and K. Horikoshi, *Chem Commun*, 2006, DOI: 10.1039/b605812d, 3293-3295.
7. A. Mukherjee, M. J. Dumont and V. Raghauan, *Biomass Bioenerg*, 2015, **72**, 143-183.
8. A. Corma, S. Iborra and A. Velty, *Chem Rev*, 2007, **107**, 2411-2502.
9. B. A. Fachri, R. M. Abdilla, H. H. van de Bovenkamp, C. B. Rasrendra and H. J. Heeres, *Acs Sustain Chem Eng*, 2015, **3**, 3024-3034.
10. J. C. Serrano-Ruiz, R. Luque and A. Sepulveda-Escribano, *Chemical Society Reviews*, 2011, **40**, 5266-5281.
11. D. W. Harris and M. S. Feather, *J Org Chem*, 1974, **39**, 724-725.
12. B. F. M. Kuster and H. M. G. Temmink, *Carbohyd Res*, 1977, **54**, 185-191.
13. C. J. Moye and R. J. Goldsack, *J Appl Chem*, 1966, **16**, 206-+.
14. M. J. Antal, W. S. L. Mok and G. N. Richards, *Carbohyd Res*, 1990, **199**, 91-109.
15. M. Bicker, J. Hirth and H. Vogel, *Green Chemistry*, 2003, **5**, 280-284.
16. Y. Roman-Leshkov, J. N. Chheda and J. A. Dumesic, *Science*, 2006, **312**, 1933-1937.
17. B. F. M. Kuster, *Starch-Starke*, 1990, **42**, 314-321.
18. H. E. Van Dam, A. P. G. Kieboom and H. Van Bekkum, *Starch-Starke*, 1986, **38**, 95-101.
19. P. Rivalier, J. Duhamet, C. Moreau and R. Durand, *Catalysis Today*, 1995, **24**, 165-171.
20. Y. Qian, L. F. Zhu, Y. Wang and X. C. Lu, *Renew Sust Energ Rev*, 2015, **41**, 633-646.
21. W. Coyle, *U.S Department of Agriculture, Economic Research Rev.*, 2010, **8**.
22. B. Saha and M. M. Abu-Omar, *Chemsuschem*, 2015, **8**, 1133-1142.
23. D. J. S. M.T. Barlow, D.G Steward, *British Petroleum patent UP0082689*, 1983.
24. X. L. Tong, Y. Ma and Y. D. Li, *Appl Catal a-Gen*, 2010, **385**, 1-13.
25. M. Fromowitz, J. Shuga, A. Wlassowsky, Z. Y. Ji, M. North, C. D. Vulpe, M. T. Smith and L. P. Zhang, *Environ Mol Mutagen*, 2012, **53**, 488-491.
26. Y. Roman-Leshkov, C. J. Barrett, Z. Y. Liu and J. A. Dumesic, *Nature*, 2007, **447**, 982-U985.
27. T. Thananatthanachon and T. B. Rauchfuss, *Angew Chem Int Edit*, 2010, **49**, 6616-6618.
28. P. P. A. Maneffa, J.A. Lopez-Sanchez, *Chemsuschem*, 2016, **9**, 2736-2748.
29. Y. T. Cheng and G. W. Huber, *ACS Catal.*, 2011, **1**, 611-628.
30. T. R. Carlson, Y. T. Cheng, J. Jae and G. W. Huber, *Energy & Environmental Science*, 2011, **4**, 145-161.

31. T. R. Carlson, G. A. Tompsett, W. C. Conner and G. W. Huber, *Top Catal*, 2009, **52**, 241-252.
32. H. Y. Zhang, Y. T. Cheng, T. P. Vispute, R. Xiao and G. W. Huber, *Energy & Environmental Science*, 2011, **4**, 2297-2307.
33. Y. T. Cheng and G. W. Huber, *Green Chemistry*, 2012, **14**, 3114-3125.
34. Y. T. Cheng, Z. P. Wang, C. J. Gilbert, W. Fan and G. W. Huber, *Angew Chem Int Edit*, 2012, **51**, 11097-11100.
35. F. H. Isikgor and C. R. Becer, *Polym Chem-Uk*, 2015, **6**, 4497-4559.
36. J. F. Pang, M. Y. Zheng, R. Y. Sun, A. Q. Wang, X. D. Wang and T. Zhang, *Green Chemistry*, 2016, **18**, 342-359.
37. O. Diels and K. Alder, *Ber Dtsch Chem Ges*, 1927, **60**, 716-723.
38. F. Brion, *Tetrahedron Letters*, 1982, **23**, 5299-5302.
39. N. Nikbin, P. T. Do, S. Caratzoulas, R. F. Lobo, P. J. Dauenhauer and D. G. Vlachos, *Journal of Catalysis*, 2013, **297**, 35-43.
40. N. Nikbin, P. T. Do, S. Caratzoulas, R. F. Lobo, P. J. Dauenhauer and D. G. Vlachos, *Journal of Catalysis*, 2013, **297**, 35-43.
41. C. L. Williams, C. C. Chang, P. Do, N. Nikbin, S. Caratzoulas, D. G. Vlachos, R. F. Lobo, W. Fan and P. J. Dauenhauer, *Acs Catal*, 2012, **2**, 935-939.
42. Y. P. Wijaya, D. J. Suh and J. Jae, *Catal Commun*, 2015, **70**, 12-16.
43. J. Yu, S. Zhu, P. J. Dauenhauer, H. J. Cho, W. Fan and R. J. Gorte, *Catal Sci Technol*, 2016, DOI: 10.1039/c6cy00501b.
44. D. Wang, C. M. Osmundsen, E. Taarning and J. A. Dumesic, *Chemcatchem*, 2013, **5**, 2044-2050.
45. C. C. Chang, S. K. Green, C. L. Williams, P. J. Dauenhauer and W. Fan, *Green Chemistry*, 2014, **16**, 585-588.
46. T. A. Branvold, *US Patent 20100331568 A1*, 2010.
47. D. C. Rideout and R. Breslow, *Journal of the American Chemical Society*, 1980, **102**, 7816-7817.
48. R. Breslow and T. Guo, *Journal of the American Chemical Society*, 1988, **110**, 5613-5617.
49. R. Hake, G. Mclendon, A. Corin and D. Holzschu, *Journal of the American Chemical Society*, 1992, **114**, 5442-5443.
50. Kraihanz.Cs and M. L. Losee, *Journal of the American Chemical Society*, 1968, **90**, 4701-&.
51. Y. Tsuda, T. Ohshima, T. Sano and J. Toda, *Heterocycles*, 1982, **19**, 2027-2032.
52. V. Froidevaux, M. Borne, E. Laborbe, R. Auvergne, A. Gandini and B. Boutevin, *Rsc Adv*, 2015, **5**, 37742-37754.
53. D. Fuoco, *Nanomaterials*, 2012, **2**, 79-91.
54. S. M. Campbell, D. M. Bibby, J. M. Coddington and R. F. Howe, *Journal of Catalysis*, 1996, **161**, 350-358.
55. X. H. Gao, Z. C. Tang, D. Ji and H. T. Zhang, *Catal Commun*, 2009, **10**, 1787-1790.
56. S. R. Zheng, A. Jentys and J. A. Lercher, *Journal of Catalysis*, 2006, **241**, 304-311.
57. I. Z. Database.
58. G. Bellussi, *Stud Surf Sci Catal*, 2004, **154**, 53-65.
59. B. Yilmaz and U. Muller, *Top Catal*, 2009, **52**, 888-895.
60. U. S. D. o. t. Interior, *Mineral Commodity Summaries*, 2015, 187.
61. W.-C. Yang, *Handbook of Fluidization and Fluid Particle Systems. CRC Press*, 2003.
62. E. Izci and A. Izci, *Turk J Chem*, 2007, **31**, 523-530.

63. W. H. Baur, *Acta Crystallogr B*, 1980, **36**, 2198-2202.
64. W. H. Baur, *Acta Crystallogr B*, 1978, **34**, 1751-1756.
65. R. T. Downs, G. V. Gibbs, K. L. Bartelmehs and M. B. Boisen, *Am Mineral*, 1992, **77**, 751-757.
66. J. J. Pluth and J. V. Smith, *Journal of the American Chemical Society*, 1980, **102**, 4704-4708.
67. S. L. Qiu, W. Q. Pang, H. Kessler and J. L. Guth, *Zeolites*, 1989, **9**, 440-444.
68. Grant, *US4406822 A*, 1983.
69. H. Lermer, M. Draeger, J. Steffen and K. K. Unger, *Zeolites*, 1985, **5**, 131-134.
70. R. Caicedo-Realpe and J. Perez-Ramirez, *Micropor Mesopor Mat*, 2010, **128**, 91-100.
71. D. Karami and S. Rohani, *Ind Eng Chem Res*, 2009, **48**, 4837-4843.
72. J. Perezpariente, J. A. Martens and P. A. Jacobs, *Zeolites*, 1988, **8**, 46-53.
73. Z. Z. Jiangyin Lu, Chunming Xu, Aijun Duan and Pu Zhang, *Journal of Natural Gas Chemistry*, 2005, **14**, 213-220.
74. M. Stocker, *Micropor Mesopor Mat*, 2005, **82**, 257-292.
75. P. B. Weisz and V. J. Frilette, *J Phys Chem-Us*, 1960, **64**, 382-382.
76. R. Rinaldi and F. Schuth, *Energy & Environmental Science*, 2009, **2**, 610-626.
77. S. M. Csicsery, *Zeolites*, 1984, **4**, 202-213.
78. R. J. A. a. G. R. Landolt, *US patent 3,702,886*, 1972.
79. G. T. Kokotailo, S. L. Lawton, D. H. Olson, D. H. Olson and W. M. Meier, *Nature*, 1978, **272**, 437-438.
80. D. G. Hay and H. Jaeger, *J Chem Soc Chem Comm*, 1984, 1433-1433.
81. R. M. Mohamed, H. M. Aly, M. F. El-Shahat and I. A. Ibrahim, *Micropor Mesopor Mat*, 2005, **79**, 7-12.
82. A. A. Ismail, R. M. Mohamed, O. A. Fouad and I. A. Ibrahim, *Cryst Res Technol*, 2006, **41**, 145-149.
83. Z. Z. Jiangyin Lu, Chunming Xu, Aijun Duan, Pu Zhang, *Journal of Natural Gas Chemistry*, 2005, **14**, 213-220.
84. R. L. Wadlinger, Kerr, G.T. and Rosinski, E.J., *US patent 3,308,069*, 1967.
85. R. La-Pierre., *Euro. Patent 94827*, 1983.
86. N. Chen and T. Huang, *US Patent 4672049*, 1986.
87. S. M. Oleck and R. C. Wilson, *US Patent 4568655*, 1986.
88. A. Corma, M. Moliner, A. Cantin, M. J. Diaz-Cabanas, J. L. Lorda, D. L. Zhang, J. L. Sun, K. Jansson, S. Hovmoller and X. D. Zou, *Chem Mater*, 2008, **20**, 3218-3223.
89. J. M. Newsam, M. M. J. Treacy, W. T. Koetsier and C. B. Degruyter, *P Roy Soc Lond a Mat*, 1988, **420**, 375-&.
90. J. B. Higgins, R. B. Lapierre, J. L. Schlenker, A. C. Rohrman, J. D. Wood, G. T. Kerr and W. J. Rohrbaugh, *Zeolites*, 1988, **8**, 446-452.
91. D. W. Breck, *US Patent*, 1964, **3130007**.
92. R. Milton, *US Patent*, 1959, **2882244 A**.
93. I. H. Abd El Maksod, E. A. Elzaharany, S. A. Kosa and E. Z. Hegazy, *Micropor Mesopor Mat*, 2016, **224**, 89-94.
94. E. T. C. Vogt and B. M. Weckhuysen, *Chemical Society Reviews*, 2015, **44**, 7342-7370.
95. T. Maesen and B. Marcus, *Introduction to Zeolite Science and Practice, 2nd ed.*, 2001, **137**.
96. P. Blonski, A. Birczynski, Z. T. Lalowicz, J. Datka and Z. Lodziana, *J Phys Chem C*, 2015, **119**, 19548-19557.

97. M. Treacy and J. Higgins, *Structural Commision of the International Zeolite Assocation Fourth Revised Edition, Elsevier*, 2001.
98. P. D. Chu, F.G; Vartuli, J.C. , *U.S Patent 4778666*, 1988.
99. A. Arafat, J. C. Jansen, A. R. Ebaid and H. Van Bekkum, *Zeolites*, 1993, **13**, 162-165.
100. O. G. Somani, A. L. Choudhari, B. S. Rao and S. P. Mirajkar, *Mater Chem Phys*, 2003, **82**, 538-545.
101. M. Tatlier, K. Baris, C. B. Tokay and A. Erdem-Senatalar, *J Cryst Growth*, 2007, **306**, 146-151.
102. X. H. Xu, W. H. Yang, J. Liu and L. W. Lin, *Sep Purif Technol*, 2001, **25**, 241-249.
103. C. B. M. M. Stenzel, J.; Schertlen, R.; Venot, Y.; Wiesbeck,W.A., *Microwave Power Electro. Energy*, 2001, **36**, 155.
104. I. Girnus, K. Jancke, R. Vetter, J. Richtermendau and J. Caro, *Zeolites*, 1995, **15**, 33-39.
105. J. C. Jansen, A. Arafat and H. Van Bekkum, *Abstr Pap Am Chem S*, 1991, **202**, 80-Petr.
106. P. M. Slangen, J. C. Jansen and H. Van Bekkum, *Microporous Mater*, 1997, **9**, 259-265.
107. Y. S. Li and W. S. Yang, *J Membrane Sci*, 2008, **316**, 3-17.
108. H. Jin, M. B. Ansari and S. E. Park, *Chem Commun*, 2011, **47**, 7482-7484.
109. Z. Hasan, J. W. Jun, C. U. Kim, K. E. Jeong, S. Y. Jeong and S. H. Jhung, *Mater Res Bull*, 2015, **61**, 469-474.
110. D. P. Serrano, J. M. Escola and P. Pizarro, *Chemical Society Reviews*, 2013, **42**, 4004-4035.
111. M. Ogura, S. Y. Shinomiya, J. Tateno, Y. Nara, E. Kikuchi and H. Matsukata, *Chem Lett*, 2000, DOI: Doi 10.1246/Cl.2000.882, 882-883.
112. B. Sulikowski, *J Phys Chem-Us*, 1993, **97**, 1420-1425.
113. K. Na, C. Jo, J. Kim, K. Cho, J. Jung, Y. Seo, R. J. Messinger, B. F. Chmelka and R. Ryoo, *Science*, 2011, **333**, 328-332.
114. C. Madsen and C. J. H. Jacobsen, *Chem Commun*, 1999, DOI: Doi 10.1039/A901228a, 673-674.
115. L. Xu, S. J. Wu, J. Q. Guan, H. S. Wang, Y. Y. Ma, K. Song, H. Y. Xu, H. J. Xing, C. Xu, Z. Q. Wang and Q. B. Kan, *Catal Commun*, 2008, **9**, 1272-1276.
116. D. P. Serrano, J. M. Escola and P. Pizarro, *Chemical Society Reviews*, 2013.
117. K. Malek and M. O. Coppens, *J Chem Phys*, 2003, **119**, 2801-2811.
118. J. C. Groen, L. A. A. Peffer, J. A. Moulijn and J. Perez-Ramirez, *Chem-Eur J*, 2005, **11**, 4983-4994.
119. D. A. Young, *US Patent* 1967, **3326797**.
120. D. H. Rosback and R. W. Neuzil, *US Patent* 1977, **4048111**.
121. A. J. Rein, D. D. Saperstein and S. H. Pines, *US Patent*, 1979, **4134965**.
122. R. M. Dessau, E. W. Valyocsik and N. H. Goeke, *Zeolites*, 1992, **12**, 776-779.
123. A. Cizmek, B. Subotic, I. Smit, A. Tonejc, R. Aiello, F. Crea and A. Nastro, *Microporous Mater*, 1997, **8**, 159-169.
124. A. R. R. Le Van Mao, S. Xiao, J. Yao and V. Semmer, *J. Mater.Chem.*, 1995, **5**, 533.
125. J. C. Groen, J. Perez-Ramirez and L. A. A. Peffer, *Chem Lett*, 2002, DOI: DOI 10.1246/cl.2002.94, 94-95.
126. J. C. Groen, L. A. A. Peffer and J. Perez-Ramirez, *Micropor Mesopor Mat*, 2003, **60**, 1-17.
127. T. Suzuki and T. Okuhara, *Micropor Mesopor Mat*, 2001, **43**, 83-89.

128. L. L. Su, L. Liu, J. Q. Zhuang, H. X. Wang, Y. G. Li, W. J. Shen, Y. D. Xu and X. H. Bao, *Catal Lett*, 2003, **91**, 155-167.
129. J. C. Groen, J. A. Moulijn and J. Perez-Ramirez, *J Mater Chem*, 2006, **16**, 2121-2131.
130. S. Svelle, L. Sommer, K. Barbera, P. N. R. Vennestrom, U. Olsbye, K. P. Lillerud, S. Bordiga, Y. H. Pan and P. Beato, *Catalysis Today*, 2011, **168**, 38-47.
131. D. P. Serrano, J. Aguado, J. M. Escola, J. M. Rodriguez and A. Peral, *Chem Mater*, 2006, **18**, 2462-2464.
132. M. Choi, H. S. Cho, R. Srivastava, C. Venkatesan, D. H. Choi and R. Ryoo, *Nat Mater*, 2006, **5**, 718-723.
133. H. Wang and T. J. Pinnavaia, *Angew Chem Int Edit*, 2006, **45**, 7603-7606.
134. F. J. Liu, T. Willhammar, L. Wang, L. F. Zhu, Q. Sun, X. J. Meng, W. Carrillo-Cabrera, X. D. Zou and F. S. Xiao, *Journal of the American Chemical Society*, 2012, **134**, 4557-4560.
135. M. Choi, K. Na, J. Kim, Y. Sakamoto, O. Terasaki and R. Ryoo, *Nature*, 2009, **461**, 246-U120.
136. K. Na, W. Park, Y. Seo and R. Ryoo, *Chem Mater*, 2011, **23**, 1273-1279.
137. I. Schmidt, C. Madsen and C. J. H. Jacobsen, *Inorg Chem*, 2000, **39**, 2279-2283.
138. C. J. H. Jacobsen, C. Madsen, T. V. W. Janssens, H. J. Jakobsen and J. Skibsted, *Micropor Mesopor Mat*, 2000, **39**, 393-401.
139. B. T. Holland, L. Abrams and A. Stein, *J Am Chem Soc*, 1999, **121**, 4308-4309.
140. B. T. Holland, C. F. Blanford, T. Do and A. Stein, *Chem Mater*, 1999, **11**, 795-805.
141. P. A. Jacobs, H. K. Beyer and J. Valyon, *Zeolites*, 1981, **1**, 161-168.
142. R. Anand, R. Maheswari, K. U. Gore and B. B. Tope, *J Mol Catal a-Chem*, 2003, **193**, 251-257.
143. M. S. Holm, E. Taarning, K. Egeblad and C. H. Christensen, *Catalysis Today*, 2011, **168**, 3-16.
144. S. van Donk, A. H. Janssen, J. H. Bitter and K. P. de Jong, *Catal Rev*, 2003, **45**, 297-319.
145. J. Cejka and S. Mintova, *Catal Rev*, 2007, **49**, 457-509.
146. J. Perez-Ramirez, C. H. Christensen, K. Egeblad, C. H. Christensen and J. C. Groen, *Chemical Society Reviews*, 2008, **37**, 2530-2542.
147. Y. Y. Sun and R. Prins, *Appl Catal a-Gen*, 2008, **336**, 11-16.
148. X. F. Li, R. Prins and J. A. van Bokhoven, *Journal of Catalysis*, 2009, **262**, 257-265.
149. H. Jin, M. B. Ansari, E. Y. Jeong and S. E. Park, *Journal of Catalysis*, 2012, **291**, 55-62.
150. P. T. M. Do, J. R. McAtee, D. A. Watson and R. F. Lobo, *ACS Catal.*, 2013, **3**, 41-46.
151. G. A. Olah, *Wiley-Interscience, New York.*, 1963.
152. I. Iovel, K. Mertins, J. Kischel, A. Zapf and M. Beller, *Angew Chem Int Edit*, 2005, **44**, 3913-3917.
153. N. B. R. Commandeur, P. Jay, J. Kervenal, *European Patent 0422 986*, 1991.
154. J. C. Groen, W. D. Zhu, S. Brouwer, S. J. Huynink, F. Kapteijn, J. A. Moulijn and J. Perez-Ramirez, *Journal of the American Chemical Society*, 2007, **129**, 355-360.
155. D. Verboekend and J. Perez-Ramirez, *Catal Sci Technol*, 2011, **1**, 879-890.
156. J. C. Groen, J. C. Jansen, J. A. Moulijn and J. Perez-Ramirez, *J Phys Chem B*, 2004, **108**, 13062-13065.
157. J. C. Groen, S. Abello, L. A. Villaescusa and J. Perez-Ramirez, *Micropor Mesopor Mat*, 2008, **114**, 93-102.

158. J. C. Groen, L. A. A. Peffer, J. A. Moulijn and J. Perez-Ramirez, *Micropor Mesopor Mat*, 2004, **69**, 29-34.
159. D. S. Kim, J. S. Chang, J. S. Hwang, S. E. Park and J. M. Kim, *Micropor Mesopor Mat*, 2004, **68**, 77-82.
160. H. Karge and H. Robson, *Verified syntheses of zeolitic materials*, 1992.
161. J. Xing, L. Song, C. Zhang, M. D. Zhou, L. Yue and X. B. Li, *Catalysis Today*, 2015, **258**, 90-95.
162. T. S. Frantz, W. A. Ruiz, C. A. da Rosa and V. B. Mortola, *Micropor Mesopor Mat*, 2016, **222**, 209-217.
163. L. P. Jens Weitkamp, *Catalysis and Zeolites: Fundamentals and Applications*, 1999, 127.
164. Y. Wang, Y. Y. Sun, C. Lancelot, C. Lamonier, J. C. Morin, B. Revel, L. Delevoye and A. Rives, *Micropor Mesopor Mat*, 2015, **206**, 42-51.
165. V. Rac, V. Rakic, Z. Miladinovic, D. Stosic and A. Auroux, *Thermochim Acta*, 2013, **567**, 73-78.
166. B. Gil, L. Mokrzycki, B. Sulikowski, Z. Olejniczak and S. Walas, *Catalysis Today*, 2010, **152**, 24-32.
167. S. Y. Huang, P. Z. Chen, B. Yan, S. P. Wang, Y. L. Shen and X. B. Ma, *Ind Eng Chem Res*, 2013, **52**, 6349-6356.
168. T. C. Keller, J. Arras, S. Wershofen and J. Perez-Ramirez, *ACS Catal.*, 2015, **5**, 734-743.
169. J. R. Garcia, M. Falco and U. Sedran, *Top Catal*, 2016, **59**, 268-277.
170. J. E. S. S. Lowell, Martin A. Thomas, Matthias Thommes, *Characterization of Porous Solids and Powders: Surface Area, Pore Size and Density*, 2004, 145.
171. A. G. Popov, V. S. Pavlov and I. I. Ivanova, *Journal of Catalysis*, 2016, **335**, 155-164.
172. Y. Zhao, B. Shen and H. Sun, *Rsc Adv*, 2016, **6**, 93086-93093.
173. E. Epelde, J. I. Santos, P. Florian, A. T. Aguayo, A. G. Gayubo, J. Bilbao and P. Castano, *Appl Catal a-Gen*, 2015, **505**, 105-115.
174. L. Rodriguez-Gonzalez, F. Hermes, M. Bertmer, E. Rodriguez-Castellon, A. Jimenez-Lopez and U. Simon, *Appl Catal a-Gen*, 2007, **328**, 174-182.
175. J. C. Groen, J. A. Moulijn and J. Pérez-Ramírez, *Micropor Mesopor Mat*, 2005, **87**, 153-161.
176. K. Zhang, S. Fernandez, S. Kobaslija, T. Pilyugina, J. O'Brien, J. A. Lawrence and M. L. Ostraat, *Ind Eng Chem Res*, 2016, **55**, 8567-8575.
177. J. Perez-Ramirez, S. Abello, A. Bonilla and J. C. Groen, *Adv Funct Mater*, 2009, **19**, 164-172.
178. Y. H. Wu, F. P. Tian, J. Liu, D. Song, C. Y. Jia and Y. Y. Chen, *Micropor Mesopor Mat*, 2012, **162**, 168-174.
179. Q. Zhang, H. H. Yang and W. Yan, *Rsc Adv*, 2014, **4**, 56938-56944.
180. G. Sunita, B. M. Devassy, A. Vinu, D. P. Sawant, V. V. Balasubramanian and S. B. Halligudi, *Catal Commun*, 2008, **9**, 696-702.
181. M. L. Gou, R. J. Wang, Q. W. Qiao and X. X. Yang, *Micropor Mesopor Mat*, 2015, **206**, 170-176.
182. C. Fernandez, I. Stan, J. P. Gilson, K. Thomas, A. Vicente, A. Bonilla and J. Perez-Ramirez, *Chem-Eur J*, 2010, **16**, 6224-6233.
183. J. Jiao, S. S. Ray, W. Wang, J. Weitkamp and M. Hunger, *Z Anorg Allg Chem*, 2005, **631**, 484-490.
184. P. Wu, T. Komatsu and T. Yashima, *J Chem Soc Faraday T*, 1996, **92**, 861-870.
185. A. C. Jiri Cejka, Stacey Zones, *Zeolites and Catalysis: Synthesis, Reactions and Applications p497*.

186. K. Sadowska, K. Gora-Marek, M. Drozdek, P. Kustrowski, J. Datka, J. M. Triguero and F. Rey, *Micropor Mesopor Mat*, 2013, **168**, 195-205.
187. W. C. Yoo, X. Y. Zhang, M. Tsapatsis and A. Stein, *Micropor Mesopor Mat*, 2012, **149**, 147-157.
188. K. Sadowska, A. Wach, Z. Olejniczak, P. Kustrowski and J. Datka, *Micropor Mesopor Mat*, 2013, **167**, 82-88.
189. J. Liang, W. Xia, J. L. Sun, J. Su, M. F. Dou, R. Q. Zou, F. H. Liao, Y. X. Wang and J. H. Lin, *Chem Sci*, 2016, **7**, 3025-3030.
190. A. Chica, K. G. Strohmaier and E. Iglesia, *Appl Catal B-Environ*, 2005, **60**, 223-232.
191. Q. Q. Zhang, W. X. Ming, J. H. Ma, J. L. Zhang, P. Wang and R. F. Li, *J Mater Chem A*, 2014, **2**, 8712-8718.
192. J. Shi, Y. D. Wang, W. M. Yang, Y. Tang and Z. K. Xie, *Chemical Society Reviews*, 2015, **44**, 8877-8903.
193. S. Sklenak, J. Dedecek, C. Li, B. Wichterlova, V. Gabova, M. Sierka and J. Sauer, *Physical Chemistry Chemical Physics*, 2009, **11**, 1237-1247.
194. M. Sawa, M. Niwa and Y. Murakami, *Zeolites*, 1990, **10**, 532-538.
195. B. Burger, K. Haas-Santo, M. Hunger and J. Weitkamp, *Chem Eng Technol*, 2000, **23**, 322.
196. M. S. Holm, S. Svelle, F. Joensen, P. Beato, C. H. Christensen, S. Bordiga and M. Bjorgen, *Appl Catal a-Gen*, 2009, **356**, 23-30.
197. N. Candu, M. Florea, S. M. Coman and V. I. Parvulescu, *Appl Catal a-Gen*, 2011, **393**, 206-214.
198. K. Mlekodaj, K. Tarach, J. Datka, K. Gora-Marek and W. Makowski, *Micropor Mesopor Mat*, 2014, **183**, 54-61.
199. F. Thibault-Starzyk, I. Stan, S. Abello, A. Bonilla, K. Thomas, C. Fernandez, J. P. Gilson and J. Perez-Ramirez, *Journal of Catalysis*, 2009, **264**, 11-14.
200. D. Tzoulaki, A. Jentys, J. Perez-Ramirez, K. Egeblad and J. A. Lercher, *Catalysis Today*, 2012, **198**, 3-11.
201. J. C. Groen, W. Zhu, S. Brouwer, S. J. Huynink, F. Kapteijn, J. A. Moulijn and J. Perez-Ramirez, *J Am Chem Soc*, 2007, **129**, 355-360.
202. M. Ansari, A. Aroujalian, A. Raisi, B. Dabir and M. Fathizadeh, *Adv Powder Technol*, 2014, **25**, 722-727.
203. P. Chu, F. Dwyer and J. Vartuli, *US Patent*, 1988, **4778666 A**.
204. M. Muller, G. Harvey and R. Prins, *Micropor Mesopor Mat*, 2000, **34**, 135-147.
205. Y. Wang, T. Yokoi, S. Namba and T. Tatsumi, *Catalysts*, 2016, **6**.
206. J. C. Groen, L. A. A. Peffer, J. A. Moulijn and J. Perez-Ramirez, *Colloid Surface A*, 2004, **241**, 53-58.
207. S. Abello, A. Bonilla and J. Perez-Ramirez, *Appl Catal a-Gen*, 2009, **364**, 191-198.
208. J. B. Koo, N. Jiang, S. Saravanamurugan, M. Bejblova, Z. Musilova, J. Cejka and S. E. Park, *Journal of Catalysis*, 2010, **276**, 327-334.
209. X. L. Wang, H. M. Zhang, J. L. Zhang, H. F. Xu, X. B. Zhu, J. Chen and B. L. Yi, *J Power Sources*, 2006, **162**, 474-479.
210. K. A. Sashkina, V. S. Labko, N. A. Rudina, V. N. Parmon and E. V. Parkhomchuk, *Journal of Catalysis*, 2013, **299**, 44-52.
211. E. V. Parkhomchuk, K. A. Sashkina and V. N. Parmon, *Petrol Chem+*, 2016, **56**, 197-204.
212. G. W. He and Q. M. Pan, *Macromol Rapid Comm*, 2004, **25**, 1545-1548.
213. G. M. L. Donald L Pavia, George S. Kriz and James R. Vyvyan, 2009, 43.

214. N. A. Yusof, N. D. Zakaria, N. A. M. Maamor, A. H. Abdullah and M. J. Haron, *Int J Mol Sci*, 2013, **14**, 3993-4004.
215. B. C. Smith, *Infrared Spectral Interpretation: A Systematic Approach*, 1998, 22.
216. R. V. K. Kelothu Suresh, G. Pugazhenthi, *Journal of Science: Advanced Materials and Devices*, 2016, **1**, 351-361.
217. S. Kulprathipanja, *Zeolites in Industrial Separation and Catalysis*, 2010, 94.
218. H. Pushparaj, G. Mani, P. Muthiahpillai, M. Velayutham, Y. K. Park, W. C. Choi and H. T. Jang, *Chinese J Catal*, 2013, **34**, 294-304.
219. Y. C. Zhang, K. K. Zhu, X. G. Zhou and W. K. Yuan, *New J Chem*, 2014, **38**, 5808-5816.
220. B. Zhang, Y. H. Zhang, Y. Y. Hu, Z. P. Shi, A. Azhati, S. H. Xie, H. Y. He and Y. Tang, *Chem Mater*, 2016, **28**, 2757-2767.
221. G. Leofanti, M. Padovan, G. Tozzola and B. Venturelli, *Catalysis Today*, 1998, **41**, 207-219.
222. M. Firoozi, M. Baghalha and M. Asadi, *Catal Commun*, 2009, **10**, 1582-1585.
223. Q. Li, D. Creaser and J. Sterte, *Micropor Mesopor Mat*, 1999, **31**, 141-150.
224. F. Schmidt, C. Hoffmann, F. Giordanino, S. Bordiga, P. Simon, W. Carrillo-Cabrera and S. Kaskel, *Journal of Catalysis*, 2013, **307**, 238-245.
225. T. Meng, D. S. Mao, Q. S. Guo and G. Z. Lu, *Catal Commun*, 2012, **21**, 52-57.
226. S. Kulprathipanja, *Zeolites in Industrial Separation and Catalysis*, 2010, 146.
227. Z. Y. Liu, D. Wu, S. Ren, X. Q. Chen, M. H. Qiu, G. J. Liu, G. F. Zeng and Y. H. Sun, *Rsc Adv*, 2016, **6**, 15816-15820.
228. Q. Y. Wang, S. T. Xu, J. R. Chen, Y. X. Wei, J. Z. Li, D. Fan, Z. X. Yu, Y. Qi, Y. L. He, S. L. Xu, C. Y. Yuan, Y. Zhou, J. B. Wang, M. Z. Zhang, B. L. Su and Z. M. Liu, *Rsc Adv*, 2014, **4**, 21479-21491.
229. D. P. Serrano, R. A. Garcia, M. Linares and B. Gil, *Catalysis Today*, 2012, **179**, 91-101.
230. J. E. S. S. Lowell, Martin A. Thomas, Matthias Thommes, *Characterization of Porous Solids and Powders: Surface Area, Pore Size and Density*, 2004, 44.
231. A. Petushkov, S. Yoon and S. C. Larsen, *Micropor Mesopor Mat*, 2011, **137**, 92-100.
232. K. S. Triantafyllidis, L. Nalbandian, P. N. Trikalitis, A. K. Ladavos, T. Mavromoustakos and C. P. Nicolaides, *Micropor Mesopor Mat*, 2004, **75**, 89-100.
233. J. Aguado, D. P. Serrano, J. M. Escola and J. M. Rodriguez, *Micropor Mesopor Mat*, 2004, **75**, 41-49.
234. P. L. Tan, Y. L. Leung, S. Y. Lai and C. T. Au, *Appl Catal a-Gen*, 2002, **228**, 115-125.
235. K. L. Javier García-Martínez, *Mesoporous Zeolites: Preparation, Characterization and Applications*, 2015, 473.
236. J. P. Thielemann, F. Girgsdies, R. Schlogl and C. Hess, *Beilstein J Nanotech*, 2011, **2**, 110-118.
237. I. Melian-Cabrera, F. Kapteijn and J. A. Moulijn, *Chem Commun*, 2005, DOI: 10.1039/b502167g, 2744-2746.
238. Y. S. Tao, H. Kanoh, L. Abrams and K. Kaneko, *Chem Rev*, 2006, **106**, 896-910.
239. L. F. Wang, C. Y. Yin, Z. C. Shan, S. Liu, Y. C. Du and F. S. Xiao, *Colloid Surface A*, 2009, **340**, 126-130.
240. H. X. Tao, H. Yang, X. H. Liu, J. W. Ren, Y. Q. Wang and G. Z. Lu, *Chem Eng J*, 2013, **225**, 686-694.
241. P. Q. Zhang, X. W. Guo, H. C. Guo and X. S. Wang, *J Mol Catal a-Chem*, 2007, **261**, 139-146.
242. Z. Lin, M. Ierapetritou and V. Nikolakis, *AIChE*, 2013, **59**, 2079-2087.

243. T. W. Lyons, D. Guironnet, M. Findlater and M. Brookhart, *Journal of the American Chemical Society*, 2012, **134**, 15708-15711.
244. C. C. Chang, H. J. Cho, J. Y. Yu, R. J. Gorte, J. Gulbinski, P. Dauenhauer and W. Fan, *Green Chemistry*, 2016, **18**, 1368-1376.
245. C. L. Williams, K. P. Vinter, C. C. Chang, R. C. Xiong, S. K. Green, S. I. Sandler, D. G. Vlachos, W. Fan and P. J. Dauenhauer, *Catal Sci Technol*, 2016, **6**, 178-187.
246. K. An, N. Musselwhite, G. Kennedy, V. V. Pushkarev, L. Robert Baker and G. A. Somorjai, *J. Colloid Interface Sci.*, 2013, **392**, 122-128.
247. M. Shiramizu and F. D. Toste, *Chem-Eur J*, 2011, **17**, 12452-12457.
248. R. E. Patet, N. Nikbin, C. L. Williams, S. K. Green, C. C. Chang, W. Fan, S. Caratzoulas, P. J. Dauenhauer and D. G. Vlachos, *ACS Catal.*, 2015, **5**, 2367-2375.
249. Y. P. Wijaya, D. J. Suh and J. Jae, *Catal Commun*, 2015, **70**, 12-16.
250. K. N. Houk and R. W. Strozier, *Journal of the American Chemical Society*, 1973, **95**, 4094-4096.
251. D. M. Birney and K. N. Houk, *Journal of the American Chemical Society*, 1990, **112**, 4127-4133.
252. T. A. Eggelte, H. de Koning and H. O. Huisman, *Tetrahedron*, 1973, **29**, 2491-2493.
253. S. Otto, G. Boccaletti and J. B. F. N. Engberts, *Journal of the American Chemical Society*, 1998, **120**, 4238-4239.
254. S. Otto and J. B. F. N. Engberts, *Journal of the American Chemical Society*, 1999, **121**, 6798-6806.
255. J. Kim, M. Choi and R. Ryoo, *Journal of Catalysis*, 2010, **269**, 219-228.
256. M. Moliner, C. Martínez and A. Corma *Angew. Chem. Int. Ed.*, 2015, **54**, 3560-3579.
257. A. Y. Dean, *Journal*, 1967.
258. J. Zhao, Y. C. Yin, Y. Li, W. Y. Chen and B. J. Liu, *Chem Eng J*, 2016, **284**, 405-411.
259. J. Y. Yu, S. Y. Zhu, P. J. Dauenhauer, H. J. Cho, W. Fan and R. J. Gorte, *Catal Sci Technol*, 2016, **6**, 5729-5736.
260. R. C. Xiong, S. I. Sandler, D. G. Vlachos and P. J. Dauenhauer, *Green Chemistry*, 2014, **16**, 4086-4091.
261. P. J. Dauenhauer, W. Fan, R. Lobo, D. G. Vlachos and S. Caratzoulas, *Abstr Pap Am Chem S*, 2013, **246**.
262. K. Afarinkia, V. Vinader, T. D. Nelson and G. H. Posner, *Tetrahedron*, 1992, **48**, 9111-9171.
263. Hong Je Cho, Limin Ren, Vivek Vattipalli, Yu-Hao Yeh, Nicholas Gould, Bingjun Xu, Raymond J. Gorte, Raul Lobo, Paul J. Dauenhauer, Michael Tsapatsis and W. Fan, *Chemcatchem*, 2017, **9**, 398-402.
264. T. W. Kim, S. Y. Kim, J. C. Kim, Y. Kim, R. Ryoo and C. U. Kim, *Appl Catal B-Environ*, 2016, **185**, 100-109.
265. P. T. Do, J. R. McAtee, D. A. Watson and R. F. Lobo, *ACS Catal*, 2013, **3**, 41-46.
266. I. F. Teixeira, B. T. Lo, P. Kostetskyy, M. Stamatakis, L. Ye, C. C. Tang, G. Mpourmpakis and S. C. Tsang, *Angew Chem Int Ed Engl*, 2016, **55**, 13061-13066.